

**Design and Synthesis of Novel π -conjugated Molecules and
Polymers based on Naphthalene and Perylene Diimides and
their Application in Organic Electronics**

Thesis Submitted to AcSIR for the Award of
the Degree of

DOCTOR OF PHILOSOPHY
In Chemical Sciences



By

NAGESH B. KOLHE

Registration Number: 10CC11J26105

Under the Guidance of

Dr. S. K. ASHA

Polymer Science and Engineering Division


CSIR-NATIONAL CHEMICAL LABORATORY

PUNE – 411008, INDIA

March 2015

Certificate

This is to certify that the work incorporated in this Ph.D. thesis entitled “**Design and Synthesis of Novel π -conjugated Molecules and Polymers based on Naphthalene and Perylene Diimides and their Application in Organic Electronics**” submitted by **Mr. Nagesh B. Kolhe** to Academy of Scientific and Innovative Research (AcSIR) in fulfillment of the requirements for the award of the Degree of **Doctor of Philosophy in Chemical Sciences**, embodies original research work under my supervision. I further certify that this work has not been submitted to any other University or Institution in part or full for the award of any degree or diploma. Research material obtained from other sources has been duly acknowledged in the thesis. Any text, illustration, table etc., used in the thesis from other sources, have been duly cited and acknowledged.



Research Student

Mr. Nagesh B. Kolhe



Research Guide

Dr. S. K. Asha
Dr. Asha S. K.
Senior Scientist
Scientist, Polymer Science & Engineering Division
राष्ट्रीय रासायनिक प्रयोगशाला
NATIONAL CHEMICAL LABORATORY
पुणे / PUNE - 411 008.

Dedicated to

My Beloved Mother.....

ACKNOWLEDGEMENTS

The process of earning a doctorate and writing a dissertation is long and arduous and it is certainly not done singlehandedly. So, I am using this opportunity to express my gratitude to everyone who helped and supported me throughout the course of my research.

Firstly, I would like to express my special appreciation and thanks to my research supervisor Dr. S. K. Asha for her valuable guidance and scholarly inputs. I have enjoyed the opportunity to watch and learn from her knowledge and experience. Her enthusiasm, encouragement and faith in me throughout have been extremely helpful. She always knew where to look for answers to obstacle while leading me to right source, theory and perspective. Your advice on both research as well as on my personal life have been priceless. She is the one who moulded me in to a good researcher. Myself and my family is obliged to you madam.

I would like to thank Dr. M. Jayakannan for his scientific advice and knowledge and many insightful discussions and suggestions that helped me a lot in the practical handling of polymers in the lab.

My sincere thank to Prof. K. S. Narayan (JNCASR- Bangalore) for his active collaboration which helped me to understand my system in better way and gave fruitful results. Without this opportunity, we are not able to know the semiconducting properties of these polymers.

I am also grateful to Dr. K. Krishnamoorthy and Dr. R. Nandini Devi for their valuable scientific teaching and discussion during progress of my work.

I express warm thanks to my DAC members Dr. S. P. Chavan, Dr. K. Krishnamoorthy, Dr. J. Nithyanandhan whose contribution in stimulating suggestions and encouragement, helped me to coordinate my work.

I also want to thank Dr. S. Sivaram (former director CSIR – NCL) for helping me with the fundamentals of polymer science. His lectures on polymer chemistry during my coursework helped me a lot in understanding the basics of the subject.

My sincere gratitude to Dr. S. Sourav Pal (director CSIR – NCL) for giving a fantastic infrastructure to do better research.

A special thanks to Dr. Prakash Wadagoankar, Prof Ramakrishnan (IISc Bangalore), Dr. Ashish Lele (Head of Polymer Science and Engineering Division), Dr.

Rahul Banerjee, Dr. Sayam Sen Gupta, Dr. Sarika Bhattacharyya, , Dr. Ramesh C., Dr. K. Guruswamy, Dr. Satish Oagale, Dr. P. A. Joy, Dr. Avdhani, Dr. Ashitosh Ambade who have been very kind to extend their help at various phases of my research, whenever I approached them. I also acknowledge the financial support of CSIR, New Delhi

I extend my thanks to Mrs. Deepa Dhoble, Mrs. Anuya Nisal, Mr. Saroj Kumar Jha and Mrs. Poorvi Purohit for their kind help in giving training for the divisional instrumental facility.

I wish to thank Mr. Shamal K. Menon for helping me in GPC measurements. I would also like to thank Mrs. B. Santhakumari, Mr. Ketan and Mrs. pooja, Usha for helping me lot in various characterization of my samples.

I also want to thank my all seniors and colleagues who have offered unconditional support and help during my Ph.D. study. My lab seniors Dr. Deepak Vishnu, Dr. Anilkumar, Dr. Jinish, Dr. Rekha, Dr. Balamurugan, Dr. Mahima, and Dr. Kaushal for their valuable advice and help in lab practices which I greatly acknowledge. I can never forget the assist and helpful advices from my seniors Dr. Nagesh K., Dr. Ankush B., Dr. Praksah S., Dr. Dhanaraj, Dr. Mangesh, Dr. Pankaj, Dr. Arun, Dr. Pandurang, Dr. Hari

A special thanks goes to all my labmates and friends from CSIR-NCL and IISER Pune, Chinmay, Shekhar, Dr. Nisha, Senthil, Prajitha, Saibal, Swapnil, Sandeep, Sarabjot, Ghanashyam, Bavitha, Jeena, Nithin, Vinay, Smita, Pramod, Ananthraj, Babu, Moumita, Bhagyashree, Narsimha, Rajendra, Nilesh, Sonashree, Maitri and Mehak for sharing their truthful and illuminating views on a number of issues related to my work. I would like to thank all my beloved friends Dr. Maroti Pawar, Dr. Dhiraj M., Dr. Chandrashekhara M., Dr. Gajdatta C., Dr. Digambar, Dr. Pradeep, Dr. Jayasree, Dr. Basab , Anil valekar, Samadhan Lomate, Majid (Bhai) Manik Bhosale , Avinash pawade, Sharad Parwe, Vaibhav Bhosale, Jaikumar Bhosale, Sachin Sangle, Shrikant, Vilas Kadam, Nagnath Patil, Ramprasad Ghatul, Ashish C., Manoj, Satej, Rajshree, Chayanika, Arul, Chini, Soumya, Jaya, Nagendra, Anil Naidu, Umakant Navaghare, Mohan Lonikar, Sandeep J., Vaibhav Mohale , Tukaram, Bhausahab, Atul, Govind, Dnyaneshwar, Arun, , and Leena.

I owe a lot to my mother, father, and mother-in-law, father-in-law who encouraged and helped me at every stage of my personal and academic life, and longed to see this achievement come true. My sincere thank to my beloved brothers

Santosh and Sushil for their endless support. I also thank to my Bhabi Ashwini and nephew Swaraj. I would like to express my deepest appreciation to my better half Mrs. Swati for her love, kindness, support which she has shown during past two years, it has taken me to finalize this thesis and to our dearest son Shreeyansh, who completes our life in every way. He put me on life' pedestal and the view of life from here is fantastic. Thanks dear.

I am very much indebted to my whole family..... Who supported me in every possible way to see the completion of this research work. I also thank my brothers-in-law and their families, sisters- in- law and their families for their good wishes.

Above all, I owe it all to Almighty God for granting me the wisdom, health and strength to undertake this research task and enabling me to its completion.

Nagesh Kolhe

TABLE OF CONTENTS

Abbreviation	i-ii
Preface	iii-vii
<i>Chapter 1 : Introduction</i>	<i>1-56</i>
1.1 Introduction to Organic Electronics	2
1.1.1. Overview	2
1.1.2. Challenges and Opportunities Using Organic Electronics	4
1.1.3. Charge Transport in Organic Semiconductor	6
1.2 Organic Semiconductor Devices	9
1.2.1 Organic Light Emitting Diode (OLED)	9
1.2.2 Organic Photovoltaics (OPV)	11
1.2.3 Organic Field Effect Transistor (OFET)	13
1.3 Types of Organic Semiconductor	17
1.3.1 <i>p</i> -Types Organic Semiconductor	19
1.3.2 <i>n</i> -Types Organic Semiconductor	20
1.3.3 Ambipolar Organic Semiconductor	22
1.4 Basic Tools Used In the Characterization of Organic Semiconductor	23
1.4.1 Techniques to Measure Charge Carrier Mobility (μ)	23
1.4.2 X-ray Diffraction and Microscopic Technique	26
1.4.3 UV-visible Absorption and Fluorescence Spectroscopy	27
1.4.4 Cyclic Voltammetry	28
1.5 Naphthalene and Perylenediimide based Semiconducting Materials	29
1.5.1 Synthesis	30
1.5.2 Optical and Electrochemical Properties	35
1.5.3 Small Molecule Based Semiconductors	38
1.5.4 Polymeric Semiconductor	41
1.6 Aim of the Thesis	44
1.7 References	47
<i>Chapter 2 : Structure Engineering of Naphthalenediimide Small Molecules: Effect of Self-assembly on Charge Transport Properties</i>	<i>57-97</i>
2.1 Introduction	58
2.2 Experimental Section	62
2.2.1 Materials	62
2.2.2 Instrumentation Details	62

2.2.3 Device Fabrication (OFET)	63
2.2.4 Synthesis	64
2.3 Results and Discussion	68
2.3.1 Synthesis and Characterization	68
2.3.2 Optical and Electrochemical Properties	74
2.3.3 Bulk Organization	80
2.3.4 Device Characteristics (OFET)	87
2.3.5 Conclusions	94
2.4 References	95
Chapter 3 : Synthesis of Electron Deficient Donor-Acceptor Poly (benzobisoxazole-co-imides) Containing Naphthalene or/and Perylene	98-138
3.1 Introduction	99
3.2 Experimental Section	102
3.2.1 Material	102
3.2.2 Instrumentation Details	102
3.2.3 Device Fabrication (OFET)	103
3.2.4 Synthesis	104
3.3 Results and Discussion	109
3.3.1 Synthesis and Characterization	109
3.3.2 Liquid Crystalline Phases	116
3.3.3 Wide Angle X-ray Diffraction	118
3.3.4 Photophysical Studies	119
3.3.5 Electrochemical Properties	127
3.3.6 Device Characteristics (OFET)	129
3.3.7 Conclusions	135
3.4 References	136
Chapter 4 : Core Substituted Naphthalenediimide Copolymers for Ambipolar OFETs: Effect of Varying Donor Strength on Optical, Electrochemical and Semiconducting Properties	139-179
4.1 Introduction	140
4.2 Experimental Section	144
4.2.1 Material	144
4.2.2 Instrumentation Details	144
4.2.3 Device Fabrication (OFET)	145
4.2.4 Synthesis	146

4.3 Results and Discussion	153
4.3.1 Synthesis and Characterization	153
4.3.2 Photophysical Properties	163
4.3.3 Electrochemistry	166
4.3.4 Computational Studies	168
4.3.5 Thin-Film Morphology	171
4.3.6 Device Characteristics (OFET)	172
4.3.7 Conclusions	176
4.4 References	177
<i>Chapter 5 : Side chain Engineering of Core Substituted Naphthalenediimide Copolymer: Effect on Semiconducting Properties</i>	180-206
5.1 Introduction	181
5.2 Experimental Section	184
5.2.1 Material	184
5.2.2 Instrumentation Details	184
5.2.3 Device Fabrication (OFET)	185
5.2.4 Synthesis	185
5.3 Results and Discussion	190
5.3.1 Synthesis and Characterization	190
5.3.2 Optical and Electrochemical Properties	197
5.3.3 Thin-Film Morphology	176
5.3.4 Device Characteristics (OFET)	201
5.3.5 Conclusions	204
5.4 References	205
<i>Chapter 6 : Summary and Conclusions</i>	207-211
<i>Publication and Symposia</i>	212-213

List of Abbreviations

Abbreviations	Expansion
ATR	Attenuated total reflectance
CHCl ₃	Chloroform
CDCl ₃	Deuterated chloroform
O-DCB	1,2 –Dichlorobenzene
CH ₃ CN	Acetonitrile
DCM	Dichloromethane
DMAc	N,N-Dimethylacetamide
DMF	N,N-Dimethylformamide
DMSO-d ₆	Deuterated dimethyl sulfoxide
DSC	Differential scanning calorimetry
TGA	Thermo gravimetric Analysis
DFT	Density functional theory
dL	Deciliter
EtOAc	Ethyl acetate
FT-IR	Fourier transform infrared
GPC	Gel permeation chromatography
g	Gram
HCl	Hydrochloric acid
H ₂ SO ₄	Sulfuric acid
ITO	Indium tin oxide
KJ	Kilojoule
K ₂ CO ₃	Potassium carbonate
KI	Potassium iodide
LC	Liquid crystal
LCPs	Liquid crystalline polymers
MALDI-TOF	Matrix-assisted laser desorption ionization-time of flight
mg	Milligram
mL	Milliliter
μL	Micro liter
mmol	Milli mole
MHz	Megahertz
M _n	Number average molecular weight
M _w	Weight average molecular weight
NMR	Nuclear magnetic resonance
N ₂	Nitrogen
nm	Nanometer
η _{inh}	Inherent viscosity
OD	Optical density
PDI	Polydispersity index
ppm	Part per million
PLM	Polarized light microscope
RI	Refractive index
SEM	Scanning electron microscope
TEM	Transmission electron microscopy
AFM	Atomic force microscopy
SEC	Size exclusion chromatography

SiO ₂	Silicon dioxide
THF	Tetrahydrofuran
TFA	Trifluoroacetic acid
T _m	Melting temperature
T _g	Glass transition temperature
T _c	Crystallization temperature
T _D	Decomposition temperature
UV	Ultraviolet
FL	Fluorescence
VTXRD	Variable temperature X-ray diffraction
WXRD	Wide angle X-ray diffraction
OFET	Organic field effect transistor
OLED	Organic light emitting diode
OPV	Organic photovoltaic
SAM	Surface assemble monolayer
RCA	Radio corporation of America
Au	Gold
Ag	Silver
Al	Aluminum
HMDS	Hexamethylenedisilazane
SCLC	Space charge limited current
ZnO	Zinc oxide
V	Volt
eV	Electron volt
n-Bu ₄ PF ₆	Tetrabutyl ammonium hexafluorophosphate
E _g (opt)	Optical band gap
E _g (ele)	Electronic band gap
HOMO	Highest occupied molecular orbital
LUMO	Lowest occupied molecular orbital
PCE	Power conversion efficiency
J _{sc}	Current density
Å	Angstrom
cm	Centimeter
s	Second
λ	Wavelength
V _{oc}	Open circuit voltage
F.F.	Fill factor

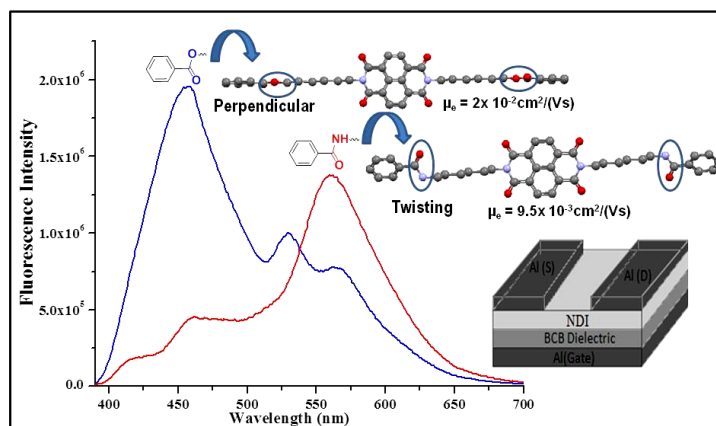
PREFACE

Organic semiconducting material based on the π - conjugated small molecules and polymers have proved to be promising for application in the optoelectronic devices such as organic field effect transistor (OFETs), light emitting diode (OLEDs), and solar cells due to their unique properties like low fabrication cost, lightweight, flexibility and solution-processability. They are widely classified as electron (n-type), hole (p-type) and electron-hole (ambipolar) transporting material, depending upon the intrinsic ability of material to transport the charges. Among the various parameters which decide the high efficiency of optoelectronic devices, one common characteristic is the intrinsic charge carrier mobility and hence the performance of organic semiconductors is often judged by their high charge carrier mobility. Although the majority of materials reported are p-type with high performance parameters in terms of hole mobility and air stability, the scenario for n-type and ambipolar materials are also improving steadily, due to accomplishment of rational molecular design and solution processable polymeric semiconductors. Among the non-fullerene type electron deficient material, naphthalene and perylenediimide (NDI and PDI) containing small molecules and polymers are promising candidates as they showed outstanding optical and semiconducting properties. These versatile building blocks could be utilized to construct the potential n-type material with unique combination of desired properties such as strong absorption in visible region, high electron affinity and excellent thermal and photostabilities. Furthermore, they showed fantastic self-assembling properties via extensive π - π stacking interaction which leads to strong electronic coupling.

The objective of the present thesis work was to design and synthesize NDI based materials (small molecules and polymers) and to study their transport characteristics in device like OFETs. The major focus of this dissertation includes the detailed studies of structure-property relationship in NDI based conjugated polymers for which the synthesis of a variety of novel polymers was targeted by using donor-acceptor design strategy. This thesis has been divided into six chapters. The **Chapter 1** gives a brief introduction to the field of organic electronics. A short overview on the charge transport mechanism, challenges and opportunities, types of organic semiconductors, optoelectronic devices, characterization tools and application of organic semiconductors are discussed. Specific attention is paid to the naphthalene and perylenediimide based semiconducting material viz., small molecules and polymers with up to date literature survey on their synthetic approaches, optical,

electrochemical and semiconducting properties. Finally, the outline and aim of thesis is given.

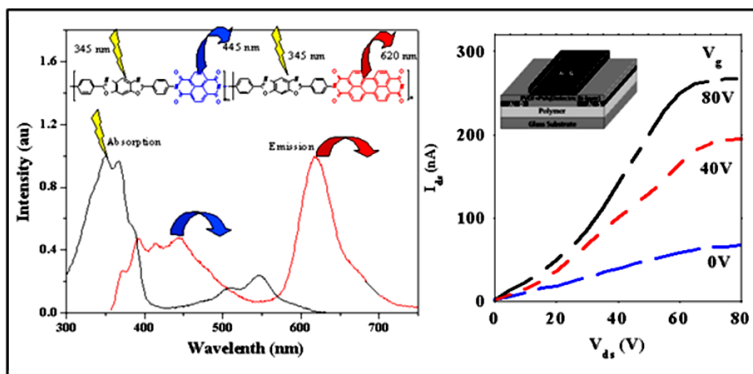
Chapter 2 describes the fundamental understanding of charge transport in self-assembled NDI molecules. This was achieved by designing two series of naphthalenediimide (NDI) derivatives by varying the functional group through either ester (NDI-E) or an amide (NDI-A) linkage. Solution processed thin films of these molecules exhibited n-type charge transport characteristics in a bottom gate top contact organic field effect transistor (OFET)



geometry. The amide derivatives showed evidence of self-organization due to intermolecular hydrogen bonding with observation of red shifted aggregate emission in solution as well as solid state. Variable temperature FT-IR studies in the solid state confirmed the existence of strong hydrogen bonding. However, contrary to expectations, the NDI ester derivatives showed better device efficiency with electron mobilities in the range $8.5 \times 10^{-3} \text{ cm}^2 \text{ V}^{-1} \text{ s}^{-1}$ to $2 \times 10^{-2} \text{ cm}^2 \text{ V}^{-1} \text{ s}^{-1}$ and on off ratio $\sim 10^4$ compared to amides. The thin-film crystallinity and morphology of NDI molecules were examined through X-ray diffraction and atomic force microscopy (AFM). The correlation of crystallinity, hydrogen bonding and charge carrier mobility was studied using energy minimized structure from density functional theory (DFT). The higher electron mobility of ester linked NDI derivatives over the amide linked ones was attributed to the freedom in charge transport pathways offered by a three dimensional crystalline organization in the ester compared to the restricted directional hydrogen bonding interaction in the amide derivatives.

Chapter 3 explored the synthesis of novel electron deficient poly (benzobisoxazole-co-imide) containing naphthalene or /and perylenediimide building blocks and studied their semiconducting properties in OFET device. Because of the extremely rigid nature of the polymers, they exhibited solubility only in strong protic acid such as methane sulfonic acid (MSA). Photoinduced energy transfer and charge separation

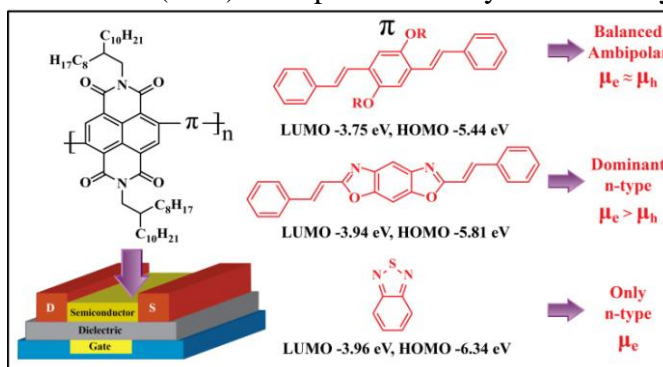
was studied in MSA solution via absorption, excitation and steady state fluorescence studies. Excitation of the benzobisoxazole moiety resulted in enhanced emission from the perylene-3,4,9,10-tetracarboxylic diimide unit as a result of FRET (Förster Resonance Energy Transfer).



The influence of the imide substitution into the linear chain of Poly (benzobisoxazole) PBO on its solid state packing was examined by wide angle X-ray diffraction (WXR) analysis. Top

gate, top contact field effect transistors (FET) based on thermally annealed polymer films were fabricated and studied. The polymers showed n-type charge transport and current modulation with on/off ratio greater than 10^2 . The maximum electron mobility of $2 \times 10^{-3} \text{ cm}^2 \text{ V}^{-1} \text{ s}^{-1}$ was observed for random copolymer which contained both perylene and naphthalenediimide units along with bisoxazole. Although, these novel polymers exhibited promising n-type behavior the inherent poor solubility in common organic solvent limited their use for the device application and led to search for alternate design strategy to accomplish solution-processable polymer.

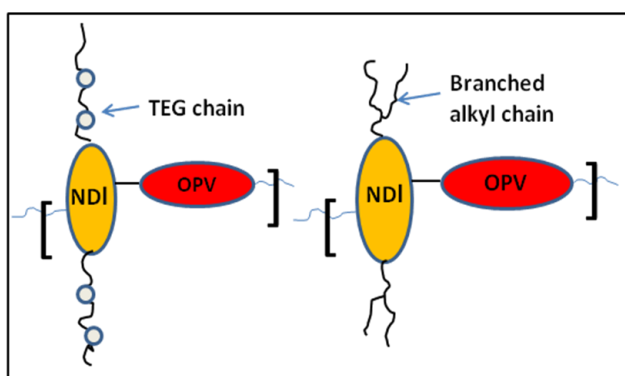
Chapter 4 illustrates the design and synthesis of solution-processable core-substituted NDI copolymers by substituting imide nitrogen atom of NDI with long branched alkyl chain (2-octyldodecyl). A series of alternating and random donor (D) - acceptor (A) copolymers based on naphthalenediimide (NDI) acceptor were synthesized by systematically varying the different donors from oligo (phenylenevinylene) (OPV) NDI-*alt*-OPV to benzobisoxazole (BBO) NDI-*alt*-BBO to benzothiadiazole (BT) NDI-*alt*-BT. The effect of



the varying donor strength of OPV, BBO and BT on the photophysical, electrochemical and semiconducting properties of the polymers was investigated. Absorption and emission spectrum recorded for dilute chloroform solution and thin

film showed increased intramolecular charge transfer for NDI-*alt*-OPV polymer compared to NDI-*alt*-BBO and NDI-*alt*-BT polymer. Cyclic voltammetry studies along with DFT (density functional theory) studies at B3LYP /6-31g* level gave insight into the energy level (HOMO/LUMO) and molecular orientation of donor and acceptor along the polymer backbone. NDI-*alt*-OPV polymer exhibited rigid coplanar structure with extended π - conjugation which induced backbone planarity and crystallinity to the polymer. The inherent poor solubility of the NDI-*alt*-BBO prevented further device characterization of this polymer. Random copolymer having maximum 30% incorporation of BBO comonomer in NDI-*r*-OPV/BBO was found to be soluble for further characterization. Compared to NDI-*alt*-OPV lowering of both energy levels LUMO (~ 0.2 eV) and HOMO (~ 0.9 eV) was observed for other polymers. Bottom gate-top contact organic field effect transistors (OFETs) of NDI-*alt*-OPV exhibited balanced ambipolar charge transport with average electron and hole mobility of $3.09 \times 10^{-3} \text{ cm}^2 \text{ V}^{-1} \text{ s}^{-1}$ and $2.1 \times 10^{-3} \text{ cm}^2 \text{ V}^{-1} \text{ s}^{-1}$ respectively. On the other hand, the random copolymer incorporating both OPV and BBO units NDI-*r*-OPV/BBO showed dominant n-type charge transport with moderate $4 \times 10^{-4} \text{ cm}^2 \text{ V}^{-1} \text{ s}^{-1}$ average electron mobility and NDI- *alt*-BT showed only n-type charge transport with electron mobility of $1.59 \times 10^{-3} \text{ cm}^2 \text{ V}^{-1} \text{ s}^{-1}$. The present work thus highlights the structure property relationship and the electronic tunability required in this class of NDI based polymers to produce ambipolar transistors.

Chapter 5 demonstrates the influence of side chain modification at the imide nitrogen of core substituted NDI polymer on molecular packing and charge carrier transport properties. Two naphthalenediimide-oligo(phenylenevinylene) based donor-acceptor



copolymers were synthesized by varying the side chain on NDI unit from hydrophilic linear triethylene glycol in P1 to hydrophobic branched 2-octyldodecyl in P2 and OPV had identical 2-octyldodecyl chain in both the polymers. Both

polymers exhibited identical UV-visible absorption spectra as well as HOMO and LUMO energy levels as observed from cyclic voltammetry. Molecular packing and crystalline nature of polymers were studied by thin film X-ray diffraction analysis

which suggested that thermal annealing had a huge impact on the crystallinity as well as molecular orientation of polymer on thin film. Thermally annealed thin films of P1 showed huge decrease in the SCLC electron mobility ($\sim 10^{-9} \text{ cm}^2 \text{ V}^{-1} \text{ s}^{-1}$) compared to as-spun thin film mobility ($\sim 10^{-5} \text{ cm}^2 \text{ V}^{-1} \text{ s}^{-1}$) which suggested their predominant edge-on orientation on thin film. On the other hand, alkyl chain containing polymer P1 did not show significant change in the mobility after thermal annealing which confirmed that texture formed during active layer deposition was retained with majority of face-on arrangement. The lowering of the bulk electron mobility of P1 was substantiated by all-polymer BHJ solar cell data which exhibited relatively lower current density and PCE ($J_{\text{sc}} = 0.23 \text{ mA cm}^{-2}$ and PCE = 0.050 %) for P1 compared to P2 ($J_{\text{sc}} = 0.53 \text{ mA cm}^{-2}$ and PCE = 0.067 %).

The **Chapter 6** summarizes the overall outcome of the research work carried out in the present Ph.D. thesis.

Chapter 1

Introduction

1.1 Introduction to Organic Electronics

1.1.1. Overview

It is exciting to consider what would happen if organic molecules made up of hydrocarbons as the major backbone were able to exhibit electronic behavior and one could tailor make materials with predefined electronic properties using them. Most certainly, it would give birth to a new area of electronics. That was exactly what happened in the 20th century and the term “Molecular electronics” was introduced for the first time by C. H. Lewis in the conference organized by US air force, although the term originally referred to a new strategy for fabrication of electronic components.¹ The concept of molecular electronics was started at IBM in 1974 where Avi Aviram, a synthetic chemist was doing his doctoral study under the supervision of Ratner. They demonstrated current rectification in the organic molecular system and showed that a modified charge-transfer salt could operate as a traditional diode.² This was probably the first proposal to use single molecule as an electronic component but it did not create much impact on the scientific community. The major breakthrough came out in 1977 when the polymer chemist Hideki Shirakawa, an inorganic chemist Alan MacDiarmid and a physicist Alan Heeger presented their discovery of the simplest conducting polymer.³ It was observed that a thin film of polyacetylene could be oxidized with iodine (or any other halogen) which turned it from insulator to semiconductor to highly conductive material, depending upon the concentration of the dopant. This work reinforced the emerging concept that organic materials could act like semiconductor or metallic conductor. This discovery of conducting polyacetylene was recognized by the award of Nobel Prize in the year 2000. After this many researchers including synthetic chemists pursued their interest in design and synthesis of structurally new conjugated polymers (conducting and semiconducting) which has driven many advances in materials science, electronic theory and technological applications. For Instance, Burroughes *et al.* demonstrated the first polymer light emitting diode using an emissive layer of poly (phenylenevinylene).⁴ Two years later Saraciftci *et al.* reported evidence for photoinduced electron transfer from excited state of conducting polymer to fullerene C₆₀.⁵ Subsequently, the photoluminescence quenching of polymer by interaction with C₆₀ confirmed the charge-separated states in composite film which is the prerequisite of polymer/plastic solar cell. Inspired from these discoveries, many photonic application based on optoelectronic and

semiconducting polymer have been introduced. A few of these devices are field-effect transistors (FET),⁶ photovoltaic devices (PV),⁷ polymeric light emitting diodes (PLEDs),⁸ photodetectors,⁹ sensors,¹⁰ solution¹¹ and solid state lasers¹² etc. The milestone of conducting polymer was recently showcased by Heeger, where he categorized the conducting polymers into various generations.¹³ According to Heeger the first generation of conducting polymers include the early work on polyacetylene, the second generation was more specific and focused on soluble and processable polymers and copolymers which included soluble poly (alkylthiophene) and poly (phenylenevinylene). **Chart 1.1** shows the molecular structures of some of the more important first and second generation semiconducting polymers. Third and recent generation have more complex molecular structures with more atoms in the repeating unit. For the past few years more attention has been paid to the design of copolymers having both electron rich and electron deficient component together in the backbone which has created the ever-growing class of donor-acceptor copolymer. Tunable electronic and optical properties could be achieved by using this design strategy; for example the bithiophene–acceptor co-polymers pioneered by Konarka¹⁴ and the polycarbazole–acceptor co-polymers pioneered by Leclerc and colleagues¹⁵.

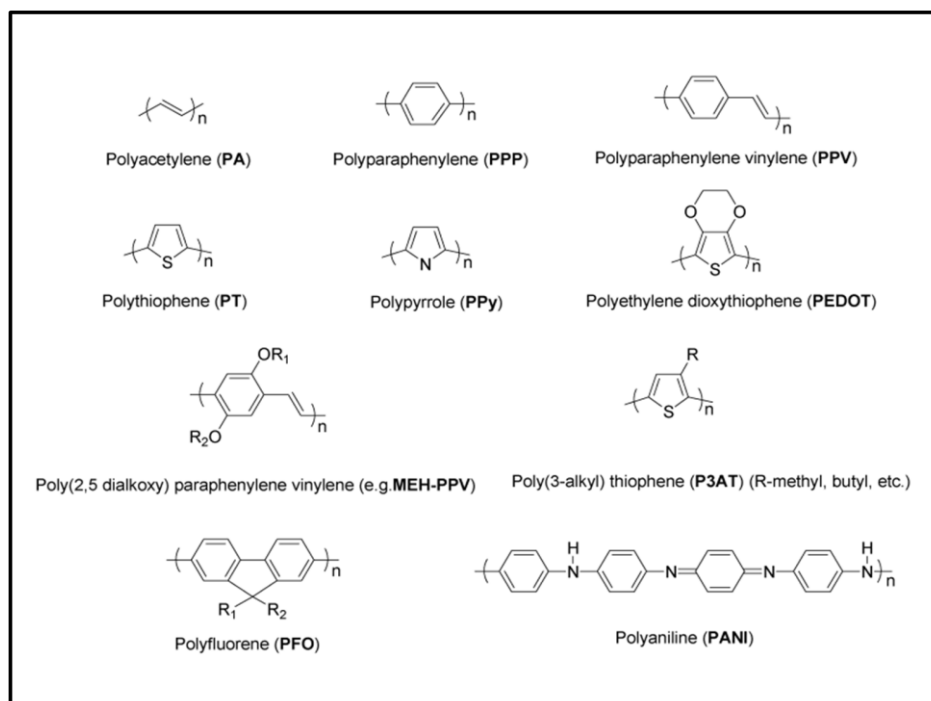


Chart 1.1 Molecular structures of some important first and second generation semiconducting polymers. (Adapted from Ref¹³)

Ching W. Tang is widely considered as the father of organic electronics due to his efforts to build the first organic solar cell and organic light emitting diode (OLED) at Kodak in 1980.¹⁶ He was able to fabricate both devices (solar cell and OLED) using one structure of organic heterojunction - a bilayer structure of an electron donor and an electron acceptor.¹⁷ Even though solar cell performance (PCE, 1%) was lower compared to conventional inorganic solar cells, Tang's insights released a torrent of activities in academia and eventually sparked industrial interest. Sometime later Koezuka and coworkers reported the first organic field effect transistor in 1987 based on a conjugated polythiophene, thus avoiding the use of expensive metal oxide semiconductor.¹⁸

1.1.2. Challenges and Opportunities Using Organic Electronics

Today organic/polymer/plastic electronic has not remained solely as an academic interest but also created huge impact in industry due to their unique physical properties and ease of processability. Additionally, organic electronics can provide promising technological opportunities such as large area fabrication, low cost, lightweight, low temperature processing and flexible electronics applications.¹⁹ On the other hand, the conventional inorganic semiconductor such as silicon requires very harsh processing condition and handling equipment, sophisticated wafer processing, high-resolution lithography tools, wafer testing equipment, clean-room environment, and costly chemical distribution and disposal facilities.²⁰ Forthcoming opportunities in the field of organic electronics are because of their unique features such as

- a) Synthetic tuneability: It is possible to synthesize desired organic molecule or polymer with predefined electronic and physical properties using a variety of available synthetic methodologies.
- b) Processability: The fabrication of organic semiconductor can be achieved by relatively simple and cost-effective techniques such as solution spin coating, drop casting, ink-jet printing, screen printing and low temperature vacuum deposition which do not require high-end clean room laboratories.
- c) Self-assembly: Molecular structures can be controlled on smaller length scales by using organic molecules or polymers which could result in a variety of self assembled structure.

Figure 1.1 shows broad ranges of application that can be achieved using organic electronics. Some of the potential applications include light-emitting diodes

(LEDs),^{8a-8b-8c} thin film transistors (TFTs),²¹ photovoltaic devices (PVDs),²² sensors,^{10a} electrochromism devices (ECDs)²³ and radio-frequency identification (RF-ID) tags.²⁴ Because of their high performance and inexpensive fabrication on flexible substrate, the electronic devices based on OLEDs are already commercialized in the market. Currently, several corporate sectors are putting their effort in R&D for making OTFT-driven large area displays. For instance, in 2007 Sony demonstrated a 2.5 inch active-matrix LED display that was driven by OTFTs.²⁵ High resolution active-matrix liquid crystal display (AMLCD) with an OTFT-driven backplane fabricated using solution processing was presented by LG Philips' LCD division.²⁵ Samsung Electronics reported an active-matrix display using printed OTFTs.²⁵

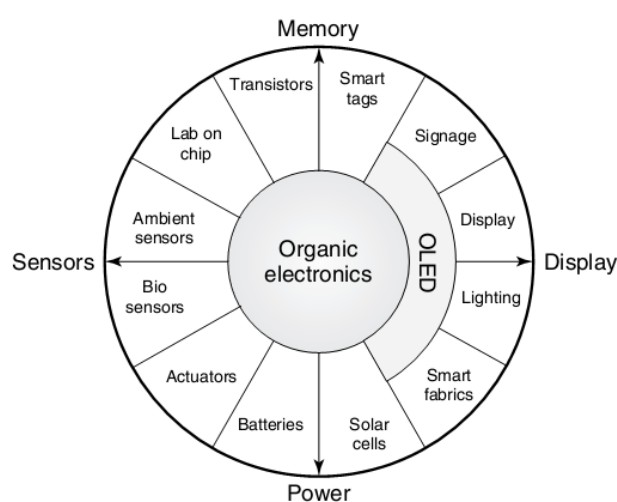


Figure 1.1 Broad range of application that can be achieved using organic electronics (Adapted from Ref²⁵)

However, currently the field of organic electronics is facing several technological challenges and it still remains at an early stage of commercialization. Particularly, the organic thin film transistors (OTFTs) are still facing several shortcomings such as low charge carrier mobility, relatively higher operating voltage, high contact resistance, device reliability issue and insufficient robust patterning technique and fabrication process. **Figure 1.2** shows general comparison of cost and performance between silicon technology and organic semiconductor technology. In general the electrical performance of organic semiconductor is lower than silicon. The organic semiconductor is not expected to compete with silicon because silicon technology is aimed for high-end, high performance and high processing power electronic products. On the other hand, organic semiconductor technology is aimed for lower end, cost-effective disposable electronics products.

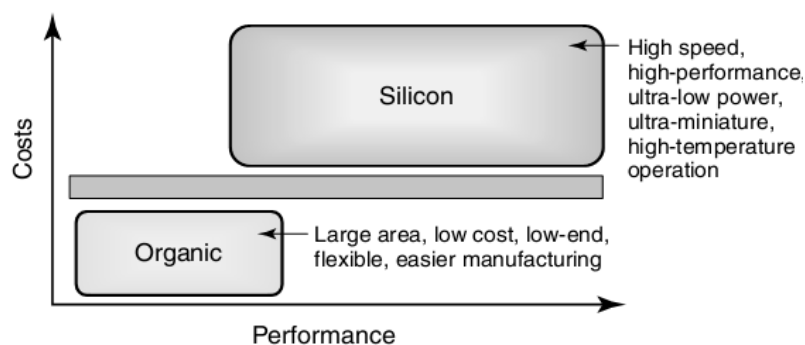


Figure 1.2 Comparison of cost versus performance between silicon and organic semiconductor (Adapted from Ref²⁵)

1.1.3. Charge Transport in Organic Semiconductor

Charge transport or conduction may be defined as the flow of charges through a material upon application of external electric field; there are different mechanisms of charge transport depending upon the nature of material. The conduction in inorganic material can be explained using band theory of solid which was initially developed by Bloch in 1928 to determine the electronic structure of metallic and inorganic semiconductors.²⁶

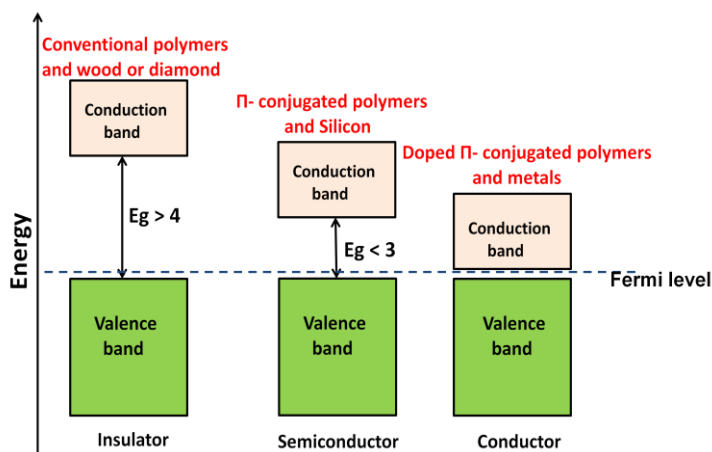


Figure 1.3 Band structures (energy level) of insulator, semiconductor and conductor.

According to band theory, the solids are divided into three categories, conductor, semiconductor and insulator depending on the availability of electrons in valence band (VB) and conduction band (CB) (**Figure 1.3**). At temperature 0 Kelvin, the valence band of a material is filled by all available electrons within the atoms of that material. The highest occupied molecular orbital of valence band is known as HOMO and lowest unoccupied molecular orbital of conduction band is known as LUMO. The

energy difference between HOMO and LUMO is termed as band gap or energy gap (E_g). In insulator, there is a large forbidden gap ($E_g > 4$) existing between the energies of the valence electron and conduction band, so that insulators are unable to conduct charges or electricity. On the other hand, there is no band gap in conductors (metal) due to overlapping of the VB and CB, so that a fraction of electrons can easily move through the material (e.g. copper). The semiconductors have properties between conductor and insulator due to accessible energy gap ($E_g < 3$) between VB and CB and they enable conduction of charges under certain conditions. Generally, the band-like charge transport mechanism is often applicable for highly crystalline inorganic semiconductors such as Si and Ge, in which constituent atoms are held together by strong covalent bonds with energy as high as 76 kcal/mole and hence they have high mobility of the order of $10^3 \text{ cm}^2 \text{ V}^{-1} \text{ s}^{-1}$. However, the mechanism is not very common for organic or polymeric semiconductors where constituent molecular components are held together by weak van der Waals forces with energy smaller than 10 kcal/mole which limits the charge carrier mobility in the range of $1\text{-}10 \text{ cm}^2 \text{ V}^{-1} \text{ s}^{-1}$. The charge transport in organic or polymeric semiconductors are studied by many theoretical models and experiments, but still an explicit model is lacking.²⁷ Conjugated polymers are entirely different compared to other conventional polymeric materials and possess alternating single-double bonds in their structure. Conjugation along linear carbon skeleton is the basic requirement, which makes them capable of conducting electricity when suitably doped. These alternate single and double bonds of conducting polymers are formed by overlapping two sp^2 hybridized orbitals of adjacent carbon atoms to form a σ bond between them and leaving un-hybridized p_z orbital having one unpaired electron (π electron). The overlapping of identical un-hybridized p_z orbital on adjacent carbon atoms give rise to additional π -bonding (HOMO) and π^* -anti-bonding (LUMO) orbitals which leads to electron delocalization along the backbone of the polymer. The HOMO and LUMO can be considered as analogous to the valence and conduction band in case of inorganic semiconductor. The energy gap between the HOMO and the LUMO in conventional polymer is very high and they behave like typical insulator (Figure 1.3). On the other hand, delocalization of π -electrons in conjugated polymer leads to narrow band gap and thereby they exhibit possibility of charge conduction. However, without doping, most of the conjugated polymer behaves as insulators because they do not have intrinsic charge carriers. Doping of conjugated polymer involves simply a partial oxidation (removal of

electron from HOMO) or reduction (addition of electron in LUMO) of polymer which creates charged species along backbone. The doping can be achieved efficiently by various chemical or electrochemical redox methods.²⁸ Chemical doping is carried out by exposing the polymer with oxidizing agents such as iodine vapors or reducing agents (e.g. alkali metal vapors). Electrochemical doping is achieved by immersing the polymer coated working electrode and reference electrode into electrolytic solution and a potential difference is applied between them. Consequently, the charges are induced into polymer back bone by either electron addition (reduction) or removal (oxidation) and the electrical neutrality of polymer is maintained by passing appropriate counter ion from electrolyte. Photo-doping is another method where polymer is excited with photon energy equal to or higher than energy gap of polymer leading to promotion of electron between HOMO-LUMO orbital, thereby generating a pair of electron and hole called as “exciton” (basic principle of organic photovoltaics). Charge injection and extraction at interface of metal /polymer is another method of redox doping (basic principle of OLEDs and OFET).²⁹ The removal of π -electron from neutral backbone of polymer upon chemical oxidation leads to creation of one unpaired electron (free radical) with spin $\frac{1}{2}$ and one spinless positive charge (cation) which is shown in **Figure 1.4** by taking the particular example of polypyrrole. The radical and cation are coupled to each other by local bond rearrangement to form polaron which forms a localized electronic state between energy gap of HOMO and LUMO with the lower energy states being occupied by a single unpaired electron.³⁰ Further oxidation of polymer can be achieved by either removal of electron from polaron to create new spinless defect known as the bipolaron or remaining as neutral chain to create two polarons.³¹ The former case is energetically more favorable because the formation of a bipolaron produces a larger decrease in ionization energy compared to the formation of two polarons. It is now almost accepted that charge transport in conducting polymers occurs by the movement of charge carrier through localized defect states namely polarons, bipolarons.^{30a-32} Most of the pure crystalline organic semiconductor follows band- like charge transport mechanism. However, the knowledge about transport mechanism in disordered polymeric semiconductor is still premature. Nevertheless there is theoretical explanation for charge transport mechanism in conducting polymers, which are dominated by thermally activated hopping (or tunneling processes) of charge carriers across barriers created by the isolated states or domains. These include

models such as intersoliton hopping,³³ interchain hopping of bipolarons,³⁴ variable range hopping in three, two and one dimensions.³⁵

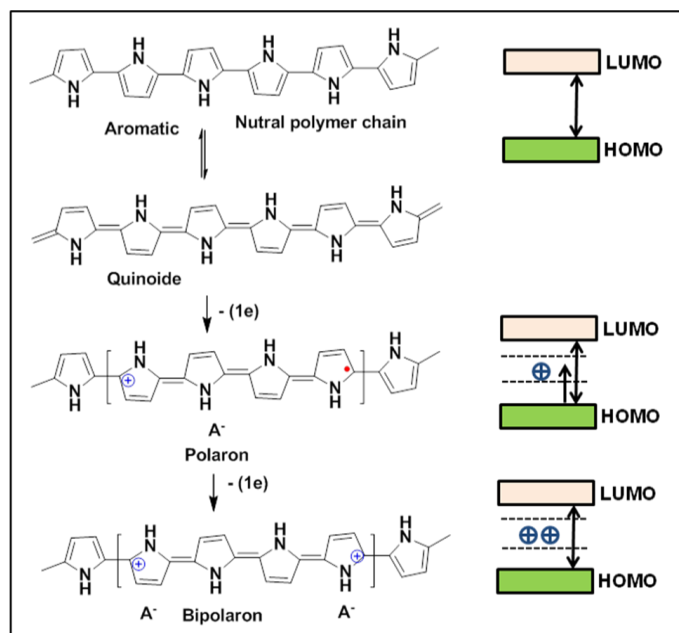


Figure 1.4 Chemical structure of polypyrrole in its neutral, aromatic and quinoid form and in oxidized polaron-bipolaron forms.

1.2 Organic Semiconductor Devices

The organic semiconductors are used mainly in three devices i) Organic light emitting diode (OLED) ii) Organic photovoltaic cell (OPV) iii) Organic field effect transistor (OFET).

1.2.1 Organic Light Emitting Diode (OLED)

Among various applications of organic semiconductors, technology based on LED using organic or polymeric semiconductor is growing very fast; in fact it has already become commercially viable. Many electronic displays such as television, mobile phone, digital camera etc. available today in the market have organic semiconductor as their active component. Because of their high mechanical flexibility, lightweight, low voltage, fast switching and low cost compared to inorganic semiconductors, they have a very bright future for further growth in this field. The basic principle of OLED involves the emission of light upon application of current (electric field) to the organic semiconductor and this phenomenon is called as electroluminescence (EL). As shown in **Figure 1.5** OLED devices can be fabricated by placing organic semiconductor in between two electrodes through which electrons (from cathode) and

holes (from anode) are injected inside the material upon application of the potential. Injected electrons and holes are transported through the organic layer which subsequently recombines to give electronically excited singlet and triplet state of molecule, which is often called as exciton.³⁶ The electronically excited state of molecules relaxes to the ground state by emitting light of certain photon energy and the color of the emission depends upon the energy gap (HOMO-LUMO) of the emissive material.³⁷

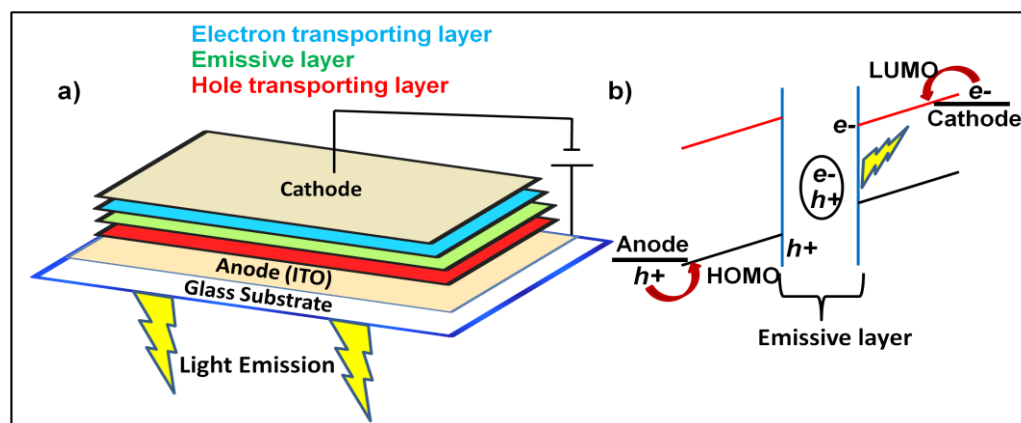


Figure 1.5 OLED a) Device configuration and b) Operation principle.

The performance of OLED device in terms of luminous power efficiency or external power efficiency (Φ_{ext}) strongly depends upon the types of electrodes used in fabrication. Usually, the high work function of anode and low work function of cathode will facilitate the hole and electron injection respectively. ITO (indium tin oxide) is more commonly preferred as anode due to its relatively high work function of 4.5-5.1 eV, which matches with the HOMO of mostly available organic molecules, additionally it is optically transparent for emitting light.³⁸ The low work function metal such as Ca, Al or alloy of Mg:Ag are used as cathode for better electron injection which minimizes the energy barrier between Fermi-level of metal and LUMO of organic material. The use of additional electron and hole transport layer in OLED device is found to be useful as compared to single layer device which maintains the charge (electron and hole) balance by enhancing the charge injection through electrode. Electroluminescence in inorganic material is not surprising and has been known for many years; light emitting devices using inorganic phosphors have been commercialized in the early 1960s. However, the double layer OLED based on small organic molecule with significant development was reported by Tang *et al.* in

1987.³⁹ Subsequently the group from Cambridge University reported the first polymeric OLED based on solution processable poly (phenylenevinylene). These two discoveries created a flurry of activities in both the fundamental science and industrial technology; afterwards many conjugated polymeric systems have been explored for their use in OLEDs.³⁶

1.2.2 Organic Photovoltaics (OPV or solar cell)

The basic principle of organic photovoltaic device is exactly opposite to that of OLED which involves conversion of solar energy radiation in to electrical energy by using small organic molecule or conjugated polymer. The major breakthrough in organic photovoltaics was created by Tang *et al.* who reported first hetero junction organic solar cell with power conversion efficiency 1 % in 1986 at Kodak.¹⁷ Further development in this field over three decades produced improved efficiency of 8.3 % reported by Konarka (in 2010) which recently reached up to 10.7 % reported by Mitsubishi Chemical.⁴⁰ The very recent report from academic development showed efficiency of 10.5 % for tandem solar cell.⁴¹ In this endeavour, the efficiency of organic solar cell remains lower and negligible compared to efficiency based on inorganic crystalline silicon which has reached up to 25 %. However, the unique physical properties of organic solar cell like light-weight, easy processing, flexibility, higher optical absorption extinction coefficient, large area and low cost make it promising for future development in this field.

The basic solar cell device architecture is made up of photo-active layer of organic or polymeric semiconductor sandwiched between two electrodes (**Figure1.6 a**). In the actual fabrication, hole blocking layer of PEDOT: PSS is spin coated on ITO (Anode) coated glass slide, on top of which the active layer of semiconductor (donor/acceptor blend) is deposited followed by vacuum deposition of buffer layer LiF and counter electrode Al (cathode). The shining of light on the surface of active material (organic semiconductor) through transparent electrode (ITO) leads to generation of electric current via five major steps i.e. i) light absorption ii) exciton formation iii) diffusion of exciton to donor-acceptor interface iv) charge separation v) charge transport and collection. Upon light absorption by active layer, the transition of electron from the HOMO to the LUMO occurs which leads to creation of hole in the HOMO and excited electron in the LUMO.⁴² These holes and electrons are still held together by columbic attraction and are called as excitons.

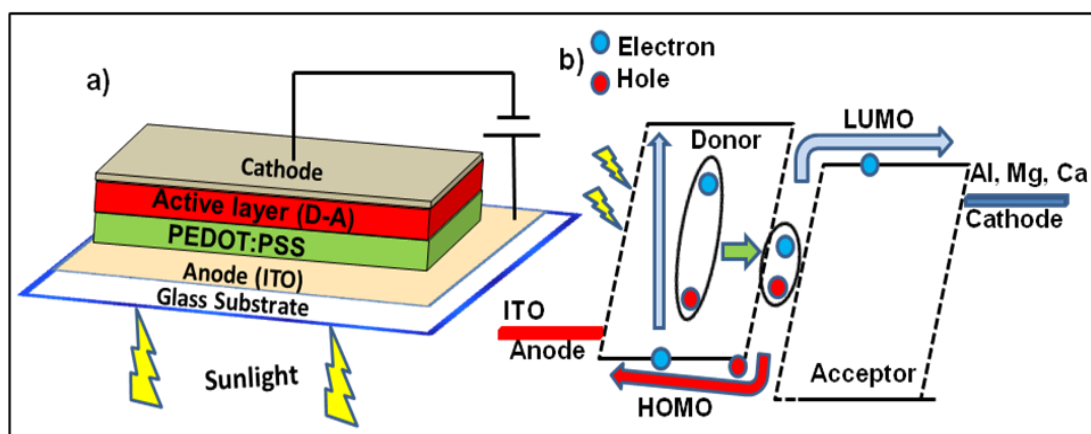


Figure 1.6 OPV a) Device configuration and b) Operation principle.

The next very important step is dissociation of exciton; if it does not separate eventually into its components electron and hole, it ultimately recombines by emitting photon or non-radioactive recombination. Since the effective charge separation occurs only at interface of donor/acceptor in bulk heterojunction solar cell (BHJ), the exciton must have to diffuse through the material to reach the interface.^{5a} Generally, the life time of exciton is very short with diffusion length limited to 5-20 nm after which they will recombine and fail to generate free charges, so that this consideration is very important during design of active layer of solar cell.⁴³ Once the charges are separated into electrons and hole, they have to transport through material towards the respective electrode and finally charge collection leads to electric current. The individual transport of holes and electrons through donor and acceptor layer respectively reduces the possibilities of charge recombination and increases the photocurrent. Furthermore, the sufficient charge carrier mobility of material plays a very vital role in charge transport. For effective application of conjugated polymers in solar cells a minimum mobility of $10^{-4} \text{ cm}^2/\text{Vs}$ is expected.⁴² The charge extraction is driven by internal electric field in cell caused by different work function of electrode. The distance d travelled by charge carrier within the material is the product of mobility μ , charge carrier life time τ and internal electric field F and is given by the equation⁴²

$$d = \mu \times \tau \times F$$

The typical characteristics of current –voltage of organic photovoltaic device in dark and under illumination is as shown in **Figure 1.7**. In dark there is no current flow in circuit and I - V curves passes through the origin. When the cell is illuminated, the I - V curves are shifted down in the forth quadrant of the graph from which lot of valuable parameters can be extracted such as open circuit voltage, short circuit current and power conversion efficiency (PCE).

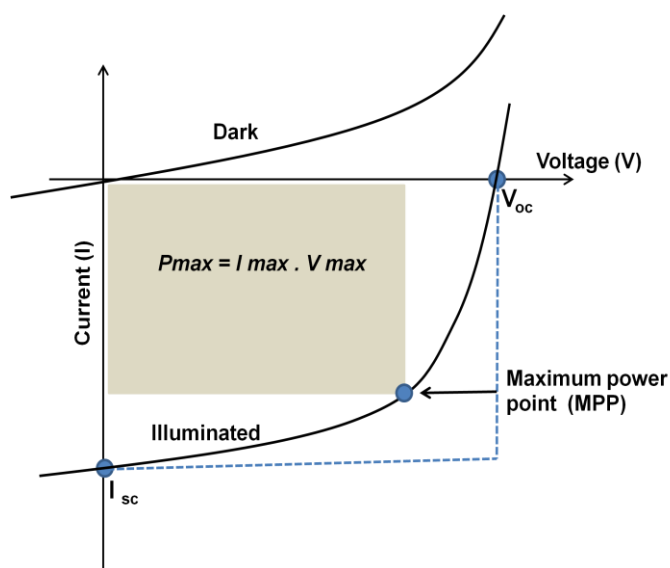


Figure 1.7 Typical graph of current versus voltage (I - V curves) for photovoltaic device under dark and illumination.

1.2.3 Organic Field Effect Transistors (OFETs)

The field effect transistor (FET) is a three terminal unipolar device in which current is controlled by an electric field. FET belongs to the most important class of electronic device which is used to amplify and switch the electronic signals and thereby it serves as a key component of integrated circuit. Beyond the various technological applications, FET is also successfully utilized to measure charge carrier mobility of organic semiconductors and the device is therefore called as OFET (organic field effect transistor). A typical OFET consists of organic or polymeric semiconductor layer, dielectric (insulating) layer and the three electrodes (source, drain and gate) fabricated on the substrate. As per user requirement OFET device can be fabricated in four possible ways by changing the position of the electrodes with respect to the semiconducting layer which is shown in **Figure 1.8**. Despite the different device configuration of OFET, the basic working principles involved in all the geometries are similar.⁴⁴ The channel of length (L) and width (W) is formed between source and

drain electrode within the semiconducting layer which is already separated from gate electrode by insulating dielectric. If the potential is applied to gate (between gate and source V_G) the induced charges are accumulated in the channel at semiconductor /dielectric interface and it serves as the other plate of capacitor. At the same time if bias is applied between source and drain (V_D), the charges formed in conducting channel will transport from source to drain which leads to current flow (I_{DS}).

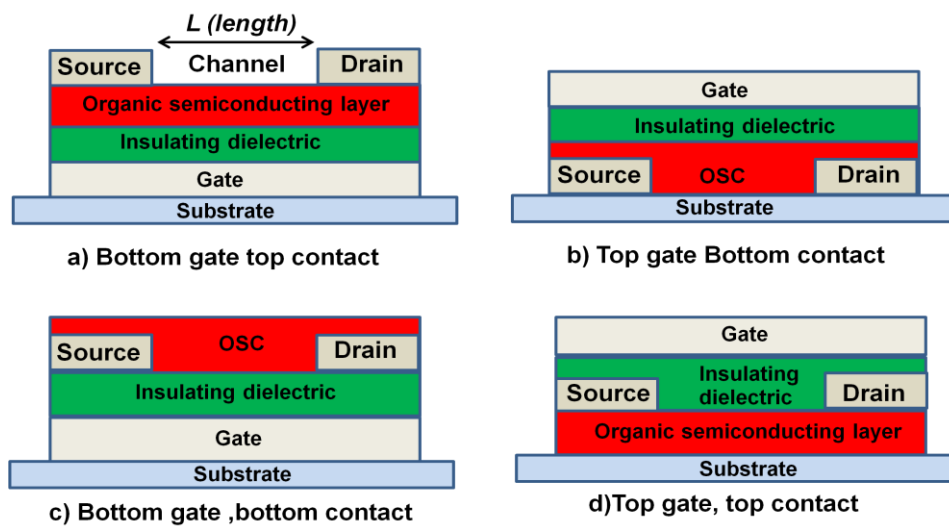


Figure 1.8 Schematic of different device configuration of OFET a) bottom gate, top contact b) top gate, bottom contact c) bottom gate, bottom contact d) top gate, top contact.

If negative voltage is applied to the gate, positive holes are accumulated in the conducting channel and holes are transported across source and drain under V_D which is classified as p-channel OFET. Whereas a positive gate voltage creates negative electrons in the conducting channel and OFET works in the n-channel mode. Thus, the formation of positive or negative charges is dependent upon the feasibility of the conducting material. In most of the case initial gate voltage is not sufficient to allow flow of the current across the source/drain due to defective semiconductor/dielectric interface. Because the induced charges can be trapped at interface or affected by other factors such as morphology or environmental condition (oxygen or water). Hence only when gate voltage is larger than certain value ($V_G >$) the charges will accumulate in channel and current flow occurs between source/drain under (V_D) this minimum gate voltage which is termed as ‘threshold voltage’ (V_T).

Characteristics of OFET device

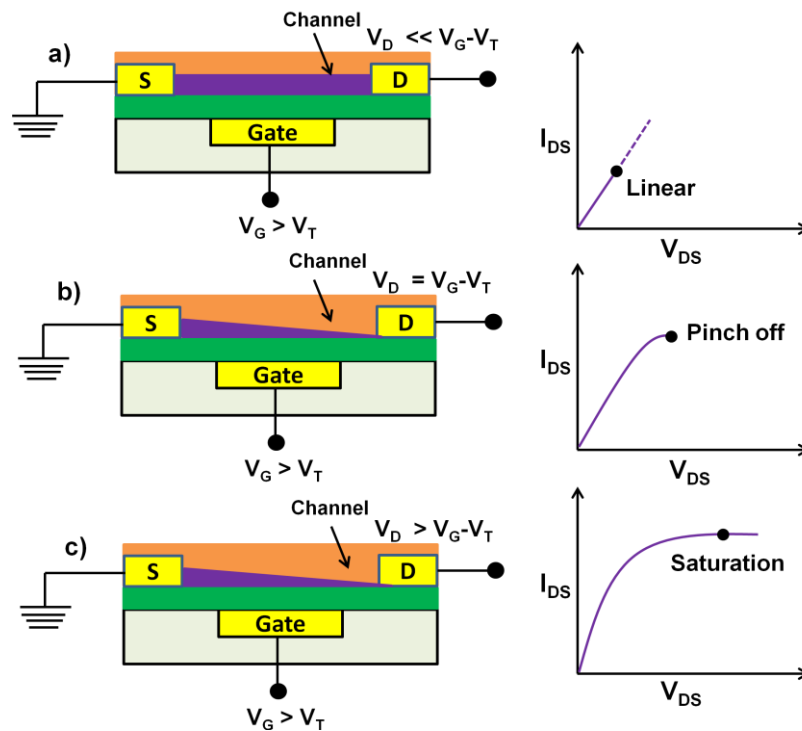


Figure 1.9 Schematic of operating regime of OFET at different source to drain voltage (V_D) a) linear b) pinch off c) saturation.

Under applied gate voltage $V_G > V_T$, if there is no bias applied between source and drain (V_D) the accumulated charge carriers are uniformly distributed within the conducting channel. As the source and drain is biased with smaller voltage $V_D \ll (V_G - V_T)$ the charge concentration will be distributed as linear gradient in the channel and the current will increase linearly with applied gate voltage. This is called as the linear region or ohmic mode which is shown in **Figure 1.9**. As drain voltage is increased further up to $V_D = V_G - V_T$ a depletion region is formed near to drain and ‘pinched off’ point occurs beyond which there is no increase in current as a function of increased drain voltage. Further increase in source and gate voltage with high electric field ($V_D > V_G - V_T$) leads to the space charge limited current flow through narrow depletion layer, where current is independent (V_G), and is called as saturation regime. All the above explained conditions at different (V_D) are schematically shown in the **Figure 1.9** (a) linear regime (b) pinch off point (c) saturation regime. The charge carrier mobility of semiconducting material can be calculated in the linear as well as saturation regime by plotting graph of drain current (I_{DS}) and square root of drain current ($\sqrt{I_{DS}}$) respectively versus gate voltage (V_G) at constant drain voltage (V_D)

which is called as transfer characteristics. The transfer curve for transistor both as semilog plot and linear plot is shown in **Figure 1.10** (a) linear and b) saturated regime. The mobility measurement in linear regime ($V_D \ll (V_G - V_T)$) can be calculated by using equation 2.⁴⁴

$$I_{ds, \text{ linear}} = \frac{W}{L} \mu C_i (V_g - V_t) V_{ds} \quad (1)$$

$$\mu_{\text{linear}} = \frac{\partial I_{ds}}{\partial V_g} \times \frac{L}{W C_i V_{ds}} \quad (2)$$

where, L and W are length and width of the channel, C_i capacitance of dielectric material, V_t threshold voltage. The mobility in saturation regime can be calculated by using slope of ($\sqrt{I_{DS}}$ versus V_G) linear plot by using equation 4.⁴⁴

$$I_{ds, \text{ sat}} = \frac{W}{2L} \mu C_i (V_g - V_t)^2 \quad (3)$$

$$\mu_{\text{sat}} = \frac{\partial I_{ds}}{\partial V_g} \times \frac{L}{W C_i (V_g - V_t)} \quad (4)$$

Threshold voltage (V_t) can be calculated by extrapolating the graph of ($\sqrt{I_{DS}}$ versus V_G) on V_G which is shown in **Figure 1.10** (c). Another important parameter $I_{\text{on}}/I_{\text{off}}$ ratio could be obtained by transfer curve which is the ratio of the current at saturation for a given applied gate voltage to that of the value of current when no gate voltage is applied (leakage current). Generally, three important parameters are needed to characterize the performance of OFET namely charge carrier mobility, threshold voltage (V_T) and $I_{\text{on}}/I_{\text{off}}$ ratio. High charge carrier mobility values ranging between of $0.1\text{-}1 \text{ cm}^2\text{V}^{-1} \text{ s}^{-1}$ are considered to be good for organic semiconductors whereas lower threshold voltage < 10 is expected for low operating voltage. The high values of $I_{\text{on}}/I_{\text{off}}$ ratio helps in good switching behavior of OFET; ideally this value should be more than 10^6 .⁴⁵ However, practically most of the OFET gives lower performance parameter because of numerous reasons out of which some are inherent poor mobility of material, contact resistance at semiconductor/material interface, morphology of semiconductor, proper selection of dielectric material, work function of source/drain electrodes etc. Material with high order of crystallinity, lamellar ordering and less grain boundary formed on thin film is highly desirable for better charge carrier mobility. The proper selection of electrode is also necessary, for instance the gold electrode having work function $\sim 5.2 \text{ eV}$ is good for injecting holes inside HOMO of

p-type material and Al with work function ~ 4.8 eV is helpful for electron injection inside the LUMO of n-type material.⁴⁶ Furthermore, the contact of these electrodes with semiconducting material should be ohmic with less contact resistance. The silicon dioxide insulator treated with HMDS or OTS SAM (self assemble monolayer) layer having dielectric constant approximately $\epsilon = 4$ is typically used in OFET, but other hydroxyl-free polymeric dielectric is also found to be effective.⁴⁶⁻⁴⁷

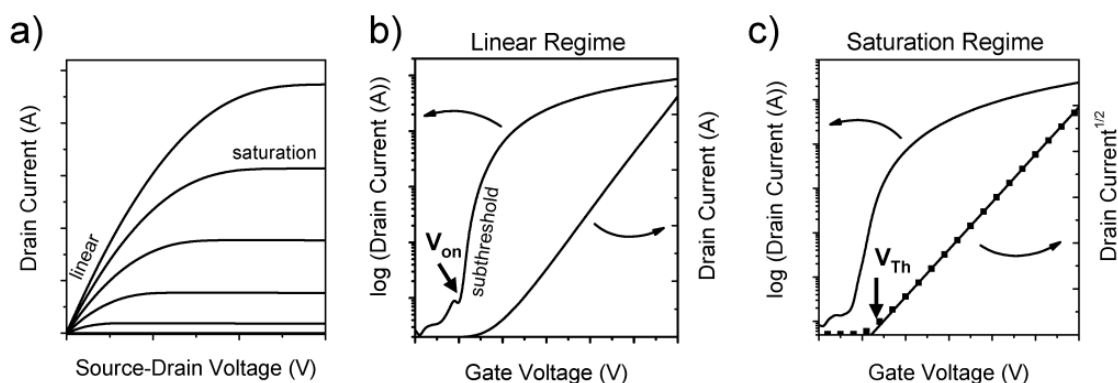


Figure 1.10 Current-voltage characteristics of an OFET (a) output characteristics (b) transfer characteristics in the linear regime ($V_D \ll V_G - V_T$) (c) transfer characteristics in the saturation regime ($V_D > V_G - V_T$). (Adapted from Ref⁴⁴)

1.3 Types of Organic Semiconductor

Organic semiconductors may be categorized in to several groups based on their chemical structure. However, they all possess one similar feature; the π -conjugated backbone which is mainly responsible for exhibition of semiconducting properties. Small molecular semiconductors are always attractive because of their easy synthesis which can be carried out in few synthetic steps with extremely high levels of purity. They exhibit definite molecular weight without variation from batch to batch. Furthermore, they have the ability to pack in more precise and well defined molecular motifs. The structure engineering in small molecule could offer the facile control of charge transport properties by modification of various molecular parameters. Since they have exact melting point, the microcrystalline thin -film of small molecule can be deposited on substrate by vacuum evaporation or organic vapor phase evaporation techniques. The rate of evaporation controls the morphology of the thin film; usually a lower evaporation rate leads to larger grains with few grain boundaries. The higher crystalline nature of small molecule could facilitate the ordered band-like charge

transport and consequently they exhibit high charge carrier mobility. Another important class of organic semiconductor is the conjugated polymers which offer numerous advantages over small molecule. The major difference from small molecule is that conjugated polymers are solution processable which simplifies the fabrication process by the use of cost effective techniques like inkjet printing, screen printing, spin coating etc. Moreover, because of high solution viscosity they can be processed on large area with high mechanical flexibility. The π -conjugated oligomers which have exact repeating units in the backbone are also used extensively as efficient semiconducting material and exhibits properties in between that of small molecules and polymers. Although in some instance conjugated dendrimers are also used as semiconducting material, aforementioned three categories (small molecule, polymer and oligomer) are majorly explored in literature as organic semiconductors. The comparison of small molecule versus polymer in terms of their charge carrier mobility is shown in **Figure 1.11** by taking the particular example of n-type organic semiconductors. In this scenario, the vacuum deposited small molecules exhibited higher charge carrier mobility than polymers. Based on electronic properties and nature of charge transport, the organic semiconductors are further divided in to three major types namely p-type (electron rich), n-type (electron deficient) and ambipolar (both hole and electron).

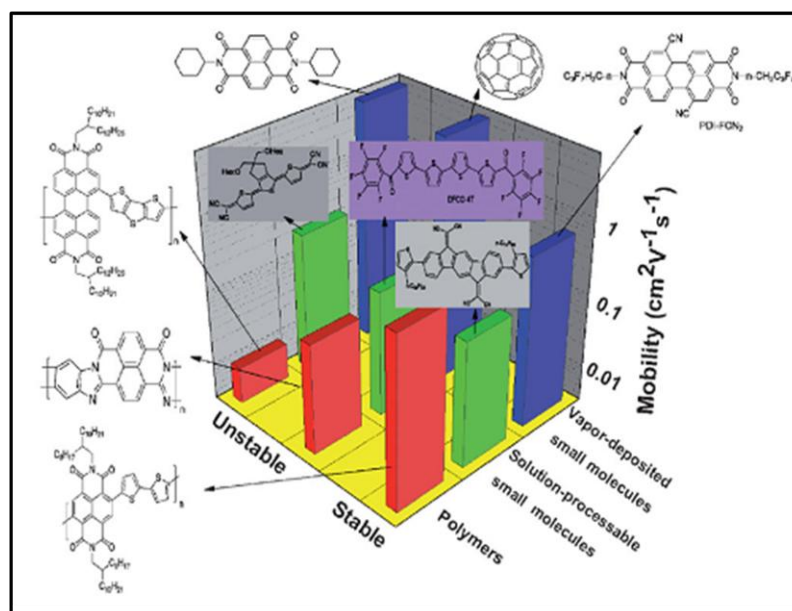


Figure 1.11 Typical n-type small molecules and polymeric semiconductors with highest reported mobility values. (Adapted from Ref⁴⁶)

1.3.1 p-Type Organic Semiconductor

Organic p-type semiconductor are also known as hole transporting material, since they are electron rich in nature and prefers to donate the electron and creates hole which are then transported through a material under applied electric field. Therefore materials having low ionization potential along with low electron affinity exhibits p-type character, for example, poly (3-hexylthiophene). The charge transport in p-type material usually occurs by injecting or removing the holes from highest occupied molecular orbital (HOMO). In order to achieve better hole injection, the HOMO energy level of material should be in the range of 4.8 to 5.2 eV to make proper alignment with the work function of the electrode such as gold (5.2 eV). In the past few decades many research groups have done extensive research on the design and synthesis of air stable p-type materials and now a huge collection of materials based on small molecules and polymers are available with high hole mobility. **Chart 1.2** shows the chemical structures of some of the common p-type organic semiconductors that have been used in the OTFTs. For instance, thin-film of pentacene (**1**) grown from vapor phase exhibited the maximum hole mobility up to $2.4 \text{ cm}^2 \text{ V}^{-1} \text{ s}^{-1}$ for OTFT and has approached the fundamental limit that is comparable to the mobility exhibited by amorphous silicon thin-film transistors.⁴⁸ The mobility as high as $1.8 \text{ cm}^2 \text{ V}^{-1} \text{ s}^{-1}$ was obtained for TIPS – functionalized pentacene (**2**) prepared via solution processed method.⁴⁹ In polymeric semiconductor, the hexyl substituted poly(thiophene) (**3**) with high degree of regioregularity (91%) packed in to a lamellar fashion with edge-on orientation exhibited the mobility of 0.5 to $0.1 \text{ cm}^2 \text{ V}^{-1} \text{ s}^{-1}$.⁵⁰ Recently, the poly(thiophene) derivative such as poly (2,5 bis(3-alkylthiophen-2yl)thieno [3,2-b] thiophene) PBTTT (**4**) was synthesized, which packed in large crystalline domain upon crystallization from the liquid crystalline phase and eventually exhibited high mobility up to 0.2 to $0.6 \text{ cm}^2 \text{ V}^{-1} \text{ s}^{-1}$.⁵¹ The copolymerization of bithiophene with dioctyl fluorene gave liquid crystalline polymer poly-9,9'dioctyl-fluorene-co-bithiophene F8T2 (**5**) which exhibited hole mobility of $0.02 \text{ cm}^2 \text{ V}^{-1} \text{ s}^{-1}$.⁵² Alkyl substituted as well as unsubstituted derivatives of oligomeric thiophene (**6**) are also found to be very promising for solution processability and exhibited hole mobility as high as $0.10 \text{ cm}^2 \text{ V}^{-1} \text{ s}^{-1}$.⁵³ Anthradithiophene (**7**) is another fused heterocyclic oligomer which exhibited hole mobility of $0.02 \text{ cm}^2 \text{ V}^{-1} \text{ s}^{-1}$ when solution cast, whereas vacuum evaporated thin films gave mobilities as high as $0.15 \text{ cm}^2 \text{ V}^{-1} \text{ s}^{-1}$.⁵⁴ Apart from these

several other thophene oligomers,⁵⁵ metalphthalocynine (**8**),⁵⁶ squareene, BODIPY, diketopyrrolopyroles (DPP) (**9**), hexabenzocoronene, and triphenylene derivavtive are also used as hole transporting material in OTFTs.⁵⁷

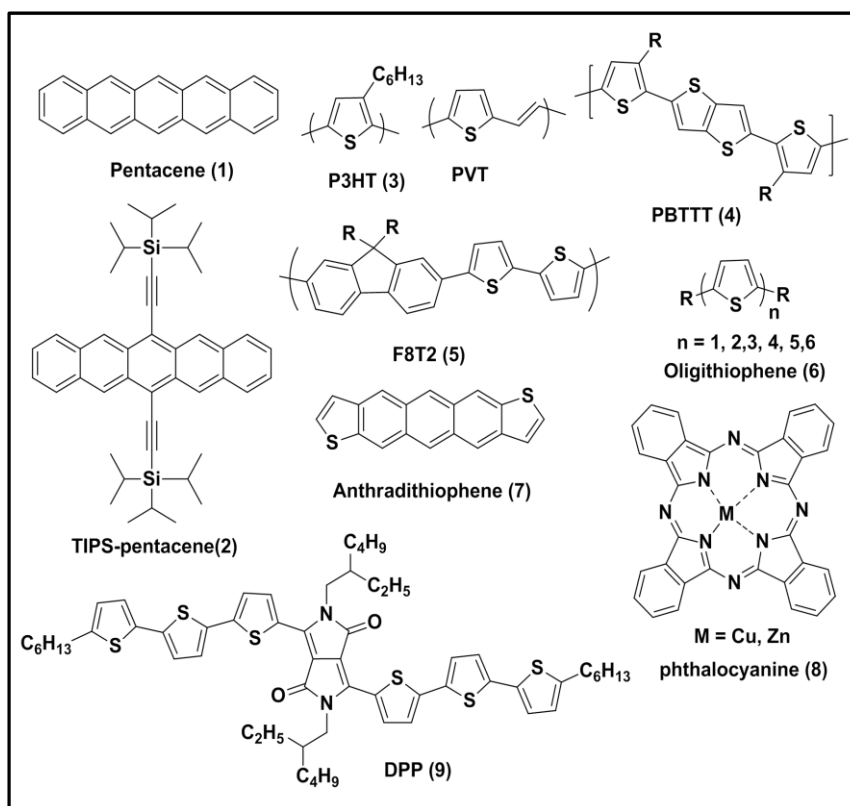


Chart 1.2 Molecular structures of the *p*-channel organic semiconductors.

1.3.2 n-Type Organic Semiconductor

Organic n-type semiconductors are also known as electron transporting material, since they are electron deficient in nature and prefer to accept the electron. N-type semiconductors are equally desired as counterpart in p-n junction devices but unfortunately their development has lagged behind that of p-type materials. One possible reason for scarcity of n-type organic semiconductor is their ambient charge carrier instability. The negative charge carriers (anions) formed at positive gate potential in OFET is often trapped by reactive species like water and oxygen that diffuses in to the semiconducting layer. However, the problem of air stability in n-type semiconductor was overcome up to certain extent by gaining deeper insights in to the design principles of semiconductor.^{44,46} For Instance, denser packing motifs and hydrophobic perfluoroalkyl side chains on n-type semiconducting core could act as kinetic barrier for diffusion of water or oxygen. Another most important and effective

strategy to increase the air stability of n-type organic semiconductor is by adjusting their redox potential by substituting with more electron withdrawing groups such as cyanide. A comprehensive electrochemical study was done by de Leeuw *et al.* on the stability of n-type semiconductor which suggested that the lowering of LUMO energy level ($> 4\text{eV}$) indeed helps to increase the thermodynamic stability of n-type semiconductor against H_2O .⁵⁸ Furthermore, the lower level of LUMO also helps in proper alignment with the electrode for better charge injection. **Chart 1.3** shows the chemical structures of some of the common n-type organic semiconductors that have been used in the OTFTs.

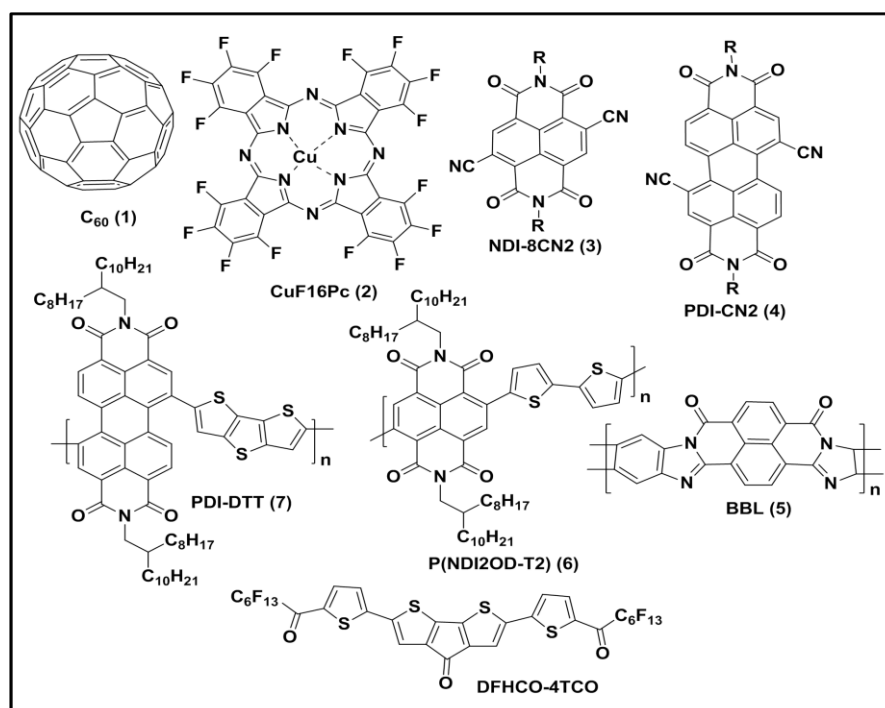


Chart 1.3 Molecular structures of the n-channel organic semiconductors.

Fullerene (C_{60}) and its derivative makes a very important class of n-type organic semiconductor in which C_{60} (1) exhibits maximum electron mobility up to $5\text{ cm}^2\text{ V}^{-1}\text{ s}^{-1}$ and $I_{\text{on}}/I_{\text{off}}$ ratio 10^6 - 10^8 in OFETs for thin film fabricated by physical vapor deposition.⁵⁹ The next promising non-fullerene derivatives are naphthalene and perylene diimide which have very high electron affinity and widely explored as n-type material. Among the various small molecular based n-type organic semiconductors, very few of them showed air-stability which includes perfluorinated copper phthalocyanine (CuF_{16}Pc) (2) which exhibited electron mobility up to $\sim 0.01\text{ cm}^2\text{ V}^{-1}\text{ s}^{-1}$.⁶⁰ *N, N'*- fluorocarbon substituted naphthalene diimides (NDI-F, NDI-XF)

showed promising electron mobility $> 0.1 \text{ cm}^2\text{V}^{-1}\text{s}^{-1}$.^{53d,61} Cyano substituted naphthalene diimides (NDI-8CN2) (**3**) and perylenediimides (PDI-CN2) (**4**) also exhibited excellent performance in OFET which showed electron mobilities up to $0.15 \text{ cm}^2 \text{ V}^{-1}\text{s}^{-1}$.⁶² Development of polymeric n-type semiconductors have further lagged behind that of small molecules. Nevertheless Jenekhe *et al.* reported ladder derivative of poly (benzobisimidazobenzophenanthroline) (BBL) (**5**) which exhibited highest reported electron mobility as high as $0.1 \text{ cm}^2 \text{ V}^{-1}\text{s}^{-1}$ reported until then.⁶³ Very recently A. Fachetti *et al.* reported very high electron mobility up to $\sim 0.85 \text{ cm}^2\text{V}^{-1}\text{s}^{-1}$ in core substituted naphthalenediimide copolymer P(NDI2OD-T2)(**6**).⁶⁴ The copolymer based on perylenediimide was also equally explored which showed mobility up to $\sim 0.01 \text{ cm}^2\text{V}^{-1}\text{s}^{-1}$ in PDI-DTT (**7**) reported by Marder *et al.*⁶⁵

1.3.3 Ambipolar Organic Semiconductor

Although not a separate class, an ambipolar organic semiconductor is one in which both the electron and hole transport could be possible depending upon the applied voltage. Unlike, unipolar OFET (p-type or n-type), fabrication of complementary inverters requires both n-channel and p-channel organic semiconductor. One way to fabricate the complementary circuit is to combine two discrete p-channel and n-channel semiconductor by separate deposition of both the layer by sequential patterning.⁶⁶ However, this approach increases processing steps, device complexity and manufacture cost and also it is very difficult to control several parameters. Hence ambipolar materials are highly desired in complementary-like inverter and OFETs which can provide both n- and p-channel performance without advanced patterning technique. **Chart 1.4** shows the chemical structures of few ambipolar polymers that have been used in the OTFTs and complementary inverters. Some of the reports based on ambipolar polymer exhibited very high electron and hole mobilities in OFET for positive and negative gate voltage respectively. For instance, core-substituted naphthalenediimide containing copolymer PNDI-T(Bz)T showed ambipolar charge transport after carefully altering thiophene units in the polymer backbone with balanced electron and hole mobility of $0.05 \text{ cm}^2\text{V}^{-1}\text{s}^{-1}$ and $0.03 \text{ cm}^2\text{V}^{-1}\text{s}^{-1}$ respectively.⁶⁷ F8BT is another polymer which has exhibited efficient and stable ambipolar transport with balanced hole and electron mobilities of about $8 \times 10^{-4} \text{ cm}^2 \text{ V}^{-1}\text{s}^{-1}$ in bottom-contact/top-gate OFET.⁶⁸ Most of the organic semiconductors which usually shows the p-channel behavior by using gold as standard electrode could also

exhibit n- channel behavior by using low work function metal such as aluminium or calcium and suitable trap-free dielectrics. Thus the hole injection from gold and electron injection from aluminum or calcium leads to ambipolar behavior in similar material even for wide band gap polymer. This was demonstrated for pentacene transistor which showed hole and electron mobility in the range of $0.1 \text{ cm}^2\text{V}^{-1}\text{s}^{-1}$.⁶⁹

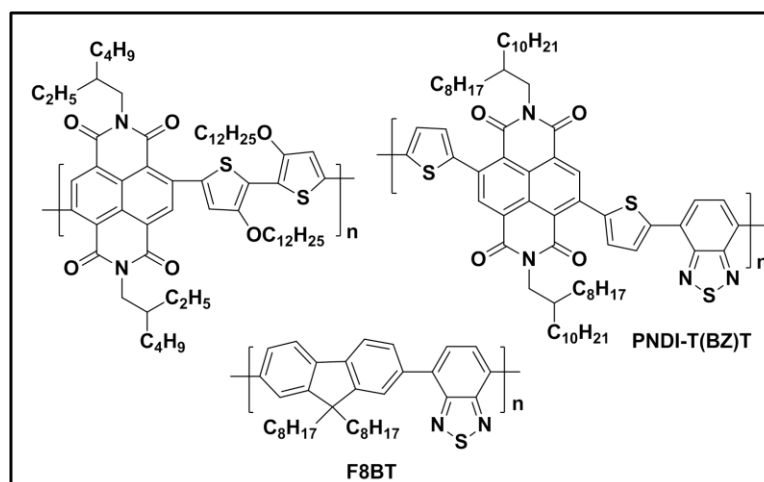


Chart 1.4 Molecular structures of the ambipolar organic semiconductors.

1.4 Basic Tools Used in the Characterization of Organic Semiconductor

Some of the general and widely explored instrumental techniques which are used to characterize organic semiconductors in terms of their basic properties such as charge carrier mobility, molecular packing, thin-film microstructure, band gap and energy levels (LUMO and HOMO) are mentioned in this section with short overview.

1.4.1 Techniques to Measure Charge Carrier Mobility (μ)

Among the various parameters which decide the high efficiency of optoelectronic devices, one common characteristic is the intrinsic charge carrier mobility and hence the performance of organic semiconductors is often judged by their high carrier mobility. For instance, in OLED the emissive layer with similar hole and electron mobilities prevents the formation of space charges and increases the external quantum efficiency of device. In OFET the source and drain current is directly proportional to charge carrier mobility and in solar cell the high charge carrier mobility (minimum $\sim 10^{-4} \text{ cm}^2\text{V}^{-1}\text{s}^{-1}$) of material ensures the better charge extraction at electrode and reduce the recombination of generated charges. In this context, it is very important to know charge carrier mobility as well as nature of charge transport (hole or electron) in organic semiconductor. In absence of any external potential, the charge transport is

purely by diffusion. But when the external potential is applied with amplitude F , a drift of charges are induced in the semiconducting material and charge carrier mobility (μ) can be calculated using the equation.^{27,70}

$$\mu = v/F$$

where, v is the charge velocity. Charge carrier mobility of organic semiconductor can be measured by using instrumental techniques such as OFET, Time of flight (TOF), space-charge limited current (SCLC), and pulse -radiolysis time resolved microwave conductivity (PR-TRMC). Among these the OFET has been already discussed in section 1.2.3 and a brief discussion on the remaining techniques are included in this section

I) Time-of-Flight (TOF)

The measurement of charge carrier mobility using TOF technique is more useful and reliable in the case where the material is more ordered with negligible defects, traps and less diffusive behavior.²⁷ In this technique the organic material is sandwiched between two electrodes and free mobile charges i.e. electrons or holes are created near one of the electrode by using short pulse of laser. The photogenerated charge carrier is then collected at another electrode by applying the electric field. Either electrons or holes are collected at electrode that depends upon the polarity of electric field. The photogenerated current is recorded as a function of time and the mobility of charges is calculated using the equation

$$\mu = \frac{v}{F} = \frac{d}{Ft} = \frac{d^2}{Vt}$$

where d is the distance between two electrodes, t is average transient time and V is the applied voltage. Since the charge carriers are photogenerated, the electrode does not have an impact on the mobility. Initially all charge carriers have almost similar velocities and for highly ordered material they are expected to reach the electrodes simultaneously without disturbance. Consequently the estimation of transient time becomes easier when photocurrent reaches half of its plateau value. On the other hand, in disordered material it is very difficult to estimate transient time of charge carriers. Although the TOF technique is more reliable and accurate for mobility measurement, it is practically difficult to utilize this technique for every new material

since it requires several micron thick films and specialized equipment. Also it is not possible to reproduce the morphology of thin film used in device in micron thick films required for TOF measurement; as a result simple techniques such as SCLC became more popular.⁷¹

II) Space-Charge Limited Current-Voltage Characteristics (SCLC)

This technique involves very simple diode configuration of anode/organic material/cathode in which the charges are injected inside the material by applying the voltage and the current obtained is measured.²⁷ The injected charges are uncompensated in undoped organic semiconductor which forms net charges, known as a space charge. Two important parameters, that has to be taken care of in order to get reliable and meaningful mobility data from SCLC measurement are i) the contact at semiconducting material/electrode interface should be ohmic which ensures that current is bulk limited and not charge injection limited and ii) the choice of electrodes should be in such a way that only electron or hole is injected at lower voltage.⁷¹ When voltage V is applied, the current density produced can be obtained by Child's law (Mott-Gurney equation)

$$J = \frac{9}{8} \epsilon \epsilon_0 \mu \frac{V^2}{L^3}$$

where, J is the current density, ϵ the dielectric constant, ϵ_0 relative vacuum permittivity, μ the mobility, L the thickness of sample. In the above equation the current density is proportional to square of the applied voltage which is characteristic of space-charge limited current (SCLC). The above assumption is true in case of ideal trap-free organic semiconductor; however in practice organic semiconductor is never trap-free, consequently less current is obtained initially at low applied voltage. In order to fill those traps, it is necessary to further increase the applied voltage and achieve maximum trap-free current to make the child's law applicable.⁷² The obtained current-voltage curves (Figure 1.12) then exhibit an initial linear (ohmic) region where charge transport is injection limited ($I \propto V$) followed by shallow trapping region where current increases with V^2 . This trap filling regime is followed by a sudden increase in current; finally the maximum limit current is reached which is the trap free SCLC region where current density shows V^2 dependence ($I \propto V^2$).

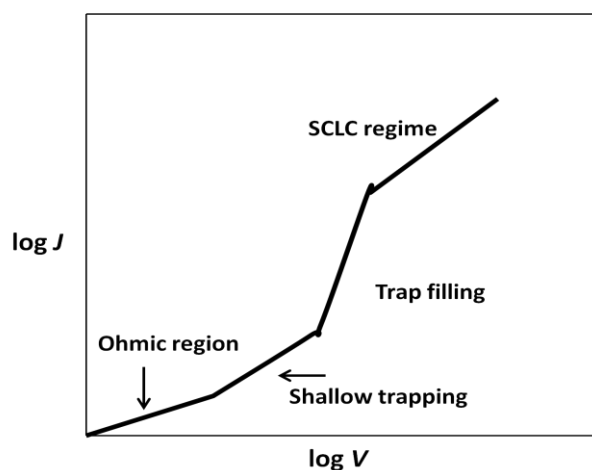


Figure 1.12 Current - voltage plot showing different operating regions in SCLC.

III) Pulse-Radiolysis Time-Resolved Microwave Conductivity (PR-TRMC)

This technique is not used in regular practice, since mobility measurement is done on very local spatial domain (for example along single polymer chain) and usually the defects in the organic semiconductor are not accounted. Hence the technique is considered to provide intrinsic mobility of material in bulk, which is the upper limit in comparison to macroscopic scale measurement such as TOF and SCLC. In this method, low density charge carriers (electron-hole pair) are generated within the bulk of the material by exciting with a pulse of very high energy electrons (m eV range).⁷³ The change in electrical conductivity $\Delta \sigma$ induced by pulse is then measured via change in microwave power reflected by the material and is therefore frequency dependent. The change in conductivity can be expressed by the equation.²⁷

$$\Delta \sigma = e (\mu_h + \mu_e) N_{e-h}$$

where, μ is the charge carrier mobility and N_{e-h} is the density of generated electron-hole pairs. The frequency of microwave radiation determines the size of local domain under study; smaller the frequency higher the region or vice versa.

1.4.2 X-ray Diffraction and Microscopic Techniques

It is widely accepted that a strong correlation exists between the thin-film morphology and performance of organic semiconductor in optoelectronic devices such as OFETs and solar cell.⁷⁴ Indeed, it is very important to analyze the molecular packing, crystalline nature and thin-film morphology of organic semiconductors which is a prerequisite to rationally improving the device performance. A number of techniques

are available for such kind of characterizations including wide angle X-ray diffraction (WXR), grazing incident angle X-ray diffraction (GIXRD) and various forms of electron microscopies.^{74b,c} Among these the WXR technique can be used to estimate the crystalline nature and molecular packing on thin-films, which gives extensive information about the organization of the molecular core. Although wide angle XRD gives information about the overall crystalline order, chain-to-chain spacing and π - π stacking distance of polymer chains, it is very difficult to extract information regarding mixed phases present in thin film such as edge on or face on packing. These preferred orientations (edge on or face on) in polymeric semiconductor are crucial to govern charge transport in OFETs. These preferred orientations can be well analyzed using grazing- incident X-ray diffraction (GIXRD) technique which allows recording of diffraction pattern in out-of-plane and in plane direction of thin-film surface.⁷⁵ Other effective tool to analyze the thin-film morphology of organic semiconductor are the transmission electron microscopy (TEM) and atomic force microscopy (AFM) which gives the visual representation of crystalline order on thin film. Particularly, the morphology obtained from AFM at microscopic length scale (nanometer size) can be well correlated with device performance.

1.4.3 UV-visible Absorption and Fluorescence Spectroscopy

UV-visible absorption spectroscopy is a very important tool which has been extensively used in the literature to study the photophysics of organic semiconductor. Using this technique lot of valuable information can be extracted such as band gap energy, aggregation (J-type or H-type) etc. It is necessary to have knowledge about the band gap of semiconductor before using in optoelectronic devices. Since it gives general idea about the photon energy required for electronic transition from valence band (HOMO) to conduction band (LUMO). The optical band gap energy of organic semiconductor can be estimated using low energy absorption edge of thin-film by using the following equation

$$E = h c/\lambda = 1240/\lambda_{\text{onset}} \text{ eV}$$

where, h = Planks constant (6.626×10^{-34} Js), c = speed of light (3.0×10^8 m/s) λ_{onset} = low energy absorption edge of thin-film and $1\text{eV} = 1.6 \times 10^{-19}$ J (conversion factor). Fluorescence spectroscopy is another most important technique which can be utilized

to characterize the excited state dynamics of organic semiconductor. The technique is utilized to measure the emission of radiation of molecule from their electronically excited state. Any electronically excited species will come back to its ground state by either radiative or non-radiative processes, the molecule which come back from its singlet excited state by radiative mechanism will emit the photon and the process is known as fluorescence. Also, many other important parameters can be estimated such as quantum yield, excited energy and electron transfer in donor-acceptor system etc. The photoinduced energy and electron transfer process usually occurs at very short time scale and it become difficult to trace more information using steady state fluorescence. This type of short time scale measurement can be carried out using time-resolved fluorescence spectroscopy (life-time).

1.4.4 Cyclic Voltammetry

This technique has become very popular, since it can be effectively used to find out different electrochemical processes involved in the molecular and macromolecular chemistry. Its application ranges from study of simple redox behavior of system to characterization of multi-electron transfer processes.⁷⁶ This method has been extensively used to estimate the relative energy levels (HOMO and LUMO) of organic semiconductor which is a prerequisite to carry out any optoelectronic characterization. The basic instrumentation technique involves the reduction or oxidation of analyte (organic semiconductor) under applied voltage which gives a cyclic voltammogram (Figure 1.16 section 1.5.2). The reduction or oxidation is equivalent to addition of electron to LUMO or removal of electron from HOMO, respectively. The onset of reduction and oxidation potential can be used to determine the LUMO and HOMO energy levels of organic semiconductor with respect to a reference standard like ferrocene by using the following equation.

$$E_{LUMO} \text{ (eV)} = - [E^{\text{red}} - E_{1/2} (Fc/Fc^+) - 4.8\text{eV}]$$

$$E_{HOMO} \text{ (eV)} = - [E^{\text{oxd}} - E_{1/2} (Fc/Fc^+) - 4.8\text{eV}]$$

where $E_{1/2} (Fc / Fc^+)$ is the onset potential of reference standard ferrocene and 4.8 eV is the known energy level of ferrocene below the vacuum level.

1.5 Naphthalene and Perylenediimide based Semiconducting Materials

Naphthalene 1,4,5,8-tetracarboxylic diimide (NDI) and perylene 3,4,9,10-tetracarboxylic diimide (PDI) belongs to a very important class of n-type organic semiconductor because of their outstanding optical, electrochemical and semiconducting properties.^{44,46,77} These are the members of the perylenediimide family which are constructed by a naphthalene unit fused at peri-position with two six membered dicarboxylic imide rings at either termini of the naphthalene unit. The structure of NDI is composed of a single naphthalene ring whereas its higher analogue PDI is composed of two naphthalene units as shown in **Figure 1.13**.

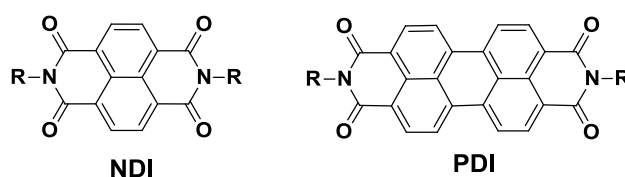


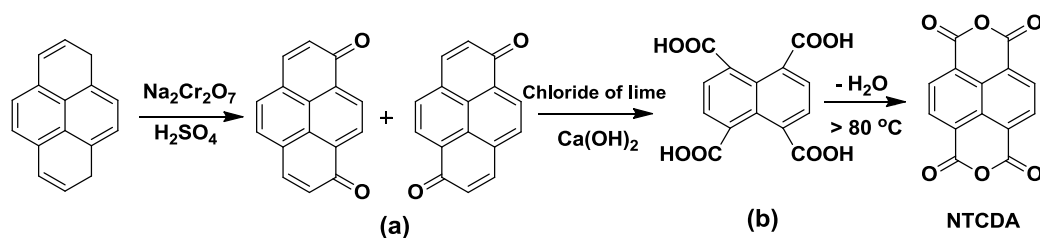
Figure 1.13 Chemical structures of naphthalene (NDI) and perylenediimide (PDI).

The higher π -conjugation in PDI leads to a reduction of the energy gap (HOMO-LUMO) and consequently PDI exhibits absorption spectra at relatively longer wavelength compared to NDI. Initially, PDI and NDI derivatives were extensively used as industrial dyes and pigments due to their high thermal and photochemical stability, chemical inertness, high tinctorial strength and intrinsic insolubility.⁷⁸ However, recently they have been explored for the application in organic electronics as electron acceptor materials (n-type) for OFETs,⁴⁶ OLEDs⁷⁹ and organic solar cell,⁸⁰ they are also used to investigate the photoinduced energy and electron transfer processes.⁸¹ The promising n-type performance of NDI and PDI derivatives originates from their high electron affinity, large molar absorption coefficient, high fluorescence quantum yield, excellent self-assembling properties via π - π stacking interaction and opportunity of structure modification. Furthermore, it is possible to induce predefined molecular electronic properties in NDI and PDI by doing structural variations with different substitution at either imide nitrogen atom or the aromatic core. By taking these advantages into consideration many researchers have contributed towards the design and synthesis of a library of molecules and polymers based on NDI and PDI. Although both the NDI and PDI derivatives are equally potential materials, NDI derivatives have received more attention in recent years due to their high electron

mobility and air stable operation in OFET.^{53d,64,82} Moreover, increasing reports of high power conversion efficiency of NDI polymers as n-type material in all polymer solar cells have highlighted them as alternate materials to existing n-type materials such as fullerene and its derivatives.^{80a,83} The synthesis of NDI derivatives are quite straight forward which involves less synthetic efforts along with better solubility and processability as compared to PDI.^{77c} The great interest in NDI based organic semiconductor is due to their robust nature, easily tunable LUMO energy level, reversible redox electrochemical properties and excellent charge transport nature. Most of the small molecular NDI based materials are highly crystalline in nature and hence their vacuum deposited thin films exhibit very high electron mobility in OFETs.^{82a} However, NDI derivatives absorbs poorly in the visible part of solar spectrum < 400 nm compared to PDI. Nevertheless, there are reports of donor-acceptor polymers comprising NDI as acceptor that exhibited absorption in the visible part of spectra and further extended up to near IR region as well in some of the copolymers.⁸⁴ Therefore they are highly sought after for BHJ all-polymer solar cells. The NDIs are considered to be ideal components to build various supramolecular π -functional materials e.g catenanes, rotaxanes, helical nanotubes and barrels etc. The use of NDI derivatives also extends to biological and medical applications.^{77c}

1.5.1 Synthesis

Naphthalene 1,4,5,8-tetracarboxylic dianhydride (NTCDA) is the most common precursor used in the synthesis of all kinds of naphthalenediimide derivatives and it is commercially available also.



Scheme 1.1 Synthesis of NTCDA.

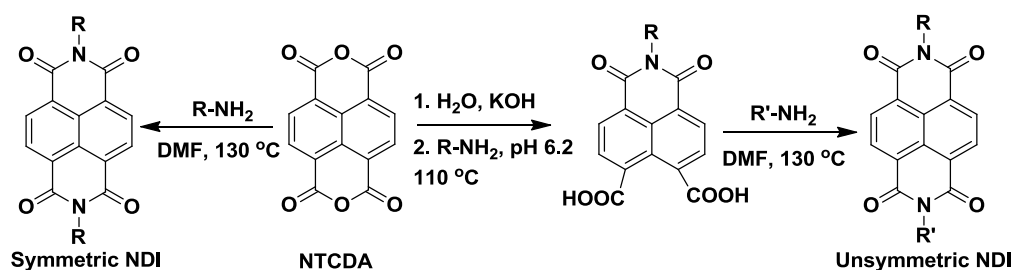
Three synthetic steps are involved in the large scale preparation of NTCDA (Scheme 1.1) which begins with the oxidation of pyrene using dichromate and sulfuric acid to form a mixture of 3,8 and 3,10 pyrenequinone (a) followed by further oxidation to naphthalene tetracarboxylic acid (b). Naphthalene tetracarboxylic acid loses water

above 80 °C to give NTCDA.⁸⁵ NTCDA can be used as the basic building block for the synthesis of π - functional small molecules as well as polymers. The literature reported synthetic methodology which has been used for the synthesis of NDI based materials are discussed in this section.

I) Small Molecule

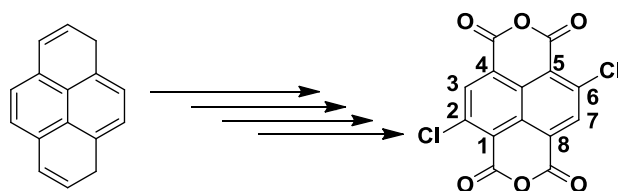
The functionalization of NTCDA can be achieved by either imidization of dianhydride ring with suitable primary amine or substitution at aromatic (bay or core) region. The imidization of NTCDA at both the dianhydride ring with similar substituents leads to symmetrical NDI derivatives. The synthesis of symmetrical NDI is a very simple one-step procedure (Scheme 1.2) in which NTCDA is condensed with two equivalents of required primary amine in high boiling solvent (at > 130 °C), usually DMF or DMAc. This is a conventional and efficient procedure which has been adopted for the synthesis of all kinds of *N,N'*-dialkyl or *N, N'*- diaryl NDI derivatives in very high yield.^{77c} This method of imidization was found to be successful and consistent with most of the primary alkyl, oligo(ethyleneoxy) and aromatic amines and hence a variety of functional groups could be introduced at imide nitrogen atom. The use of zinc acetate along with high boiling solvent like quinoline, molten imidazole and NMP was also found to be effective when aromatic, cycloaliphatic and fluoroalkyl amine were used, perhaps due to lower reactivity of these amines.^{82a,86} The role of zinc acetate catalyst is not yet clear; it might act as dehydrating agent as well as aid by increasing the solubility of the rigid core by complexation with the anhydride group. When heat sensitive or low boiling amines are used, the addition of K₂CO₃ was found to be effective to drive the reaction at lower temperature < 60 °C but for longer time. Recently, the NDI derivative has been synthesized by microwave assisted conditions where reaction drives to completion quantitatively within 5 min.⁸⁷ The synthesis of unsymmetrical NDI derivatives having two different substituents at imide nitrogen (*N, N'*- disubstituted NDI) is relatively challenging and could be achieved by two ways. The first method involves the condensation of 1:1 mixture of two different amines with NTCDA to get a statistical mixture of products which can be separated by column chromatography.⁸⁸ Another convenient approach to synthesize unsymmetrical NDI includes the complete hydrolysis of NTCDA suspension (in water 20mM) with potassium hydroxide (Scheme 1.2) followed by reacidification with phosphoric acid (H₃PO₄) at pH 6.4

which leads to diacid naphthalene tetracarboxylic acid monoanhydride. The addition of one equivalent of the first amine to this ring opened intermediate produces monoimide derivative which can be isolated in good yield. Finally the monoimide is condensed with one equivalent of the second required amine in DMF to give unsymmetrical NDI.⁸⁹



Scheme 1.2 General synthetic steps used for preparation of symmetric and unsymmetric NDIs.

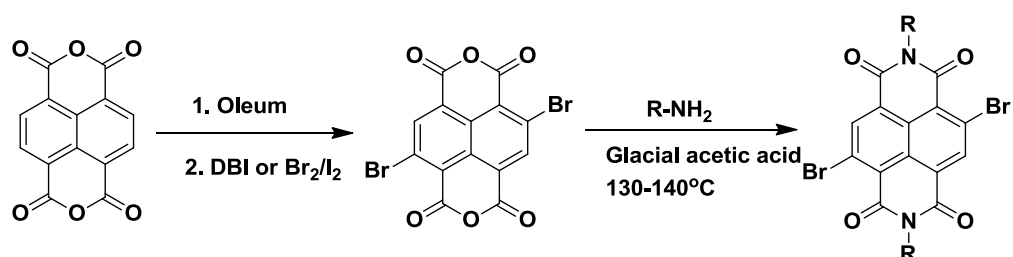
The substitution on the aromatic core of NDI at 2, 3, 6 and 7 positions leads to core or bay substituted NDI derivative which exhibits tunable optical and electrochemical properties such as narrow band gap and low reduction potential. In contrast, imide substitution does not produce any significant changes to the chromophoric properties. The core functionalized NDI based small molecules or polymers are often synthesized using 2,6-dichloro or dibromo NTCDA.^{46,77c} The synthesis of 2,6-dichloro substituted NTCDA was first reported by Vollmann which was carried out in four steps (Scheme 1.3) from pyrene by chlorination, HCl elimination and subsequent oxidation.⁹⁰ However, the subsequent reports following this procedure were unable to reproduce the results in a satisfying manner.⁹¹ A modified procedure was developed by Frank Würthner and coworkers in which they used fuming nitric acid instead of concentrated nitric acid and adjusted the reaction temperature in particular time interval.⁹¹



Scheme 1.3 Synthesis of core substituted 2, 6-dichloro NTCDA.

The synthesis of 2, 6-dichloro -substituted NTCDA requires very harsh reaction conditions such as use of harmful chlorine gas along with lengthy synthetic steps.

Therefore, the 2, 6-dibromo-substituted NTCDA was found to be very promising alternative since it could be easily synthesized by direct electrophilic substitution of NTCDA with brominating reagent (Scheme 1.4). Initial reports showed that the bromination of NTCDA could be carried out in concentrated sulfuric acid but it was very difficult to reproduce the results.⁹² The use of 20 % oleum along with dibromoisocyanuric acid (DBI) as brominating reagent was found to be successful.⁹¹ This approach yielded mixture of compounds consisting mainly of 2, 6- dibromo NTCDA and small amount of 2-monobromo and 2, 3, 6-tribromo compounds. None of these isomers was soluble in common organic solvent; consequently separation of 2, 6-dibromo isomer in pure form became very difficult. However, further imidization of crude mixture with long or branched alkyl amine in glacial acetic acid at 130 °C (Scheme 1.4) produced soluble derivatives which could be easily separated in to regioisomerically pure 2, 6-dibromo NDI derivative by column chromatography.⁹³



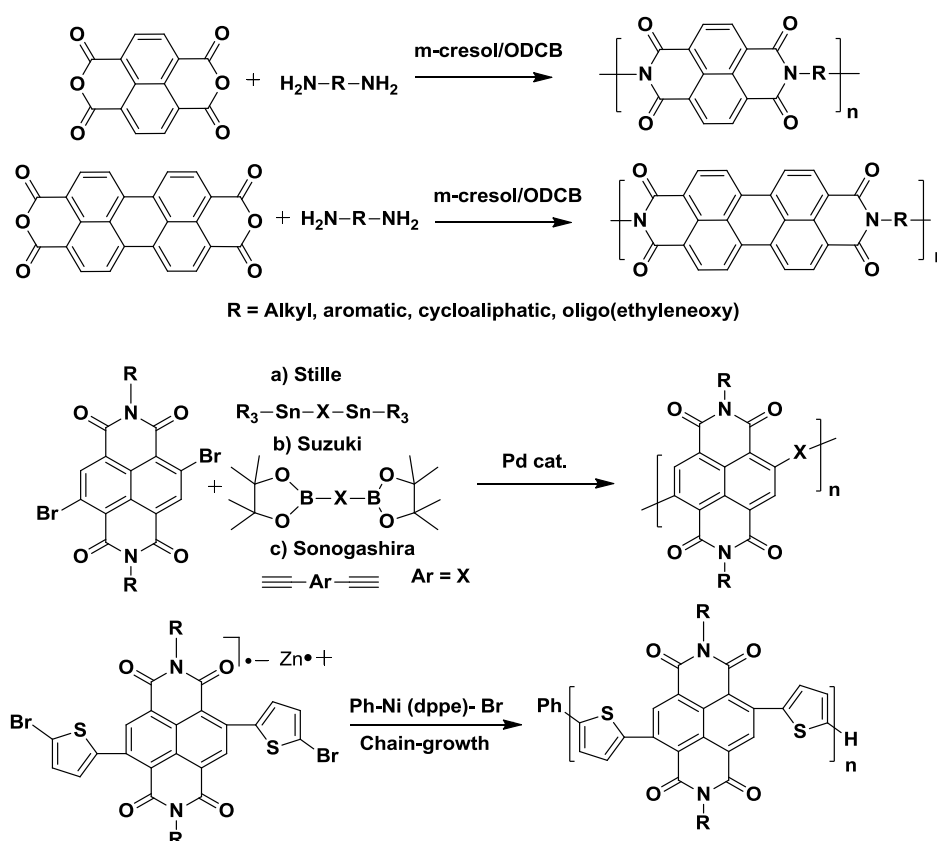
Scheme 1.4 General synthetic steps used for synthesis of core substituted NDIs.

Due to protonation of amino groups in highly protic solvent such as glacial acetic acid, primary amines become less reactive and prefer the imide formation rather than substitution at bromine or chlorine.⁹¹ The bromination of NTCDA can be also carried out efficiently using elemental bromine as brominating reagent which could avoid the use of expensive dibromoisocyanuric acid (DBI) catalyst.⁹⁴ All the core positions (2, 3, 6 and 7) of NTCDA could be brominated using excess of bromine (5.2 equivalents) by increasing the reaction time up to 4 weeks at 140 °C.⁹⁵

II) Polymer

The unique physical and optical properties of NDI and PDI containing conjugated polymers make them promising candidate for application in optoelectronic devices. Similar to the methods of synthesizing small molecules, the NDI and PDI based polymers could also be synthesized by either polyimidization or polymerization at core position via condensation polymerization (step-growth). Since NTCDA and

PTCDA have two symmetrical six membered anhydride rings, it could act as monomer towards bifunctional alkyl or aromatic amines. The one pot polycondensation of NTCDA or PTCDA with appropriate alkyl or aromatic diamine (**Scheme 1.5**) has been carried out in polar aprotic solvents such as NMP, chlorobenzene, orthodichlorobenzene and m-cresol etc. at temperature $>180\text{ }^{\circ}\text{C}$ in presence of quinoline or isoquinoline.⁹⁶ The polycondensation often occurred in two steps; first step involved the formation of high molecular weight poly (amic acid) at lower temperature ($\sim 130\text{ }^{\circ}\text{C}$) followed by ring closure to form poly(imide) at high temperature ($>180\text{ }^{\circ}\text{C}$).



Scheme 1.5 Synthesis of imide and core substituted NDI/PDI polymer.

Due to the rigid nature of the aromatic core most of the NDI and PDI containing poly (imides) are insoluble in common organic solvents and could be partially solubilized in high polar solvents like DMSO, DMF, NMP etc. after heating, which limited their use in optoelectronic devices. Core-substituted NDI based donor-acceptor polymers are a recently developed class of materials which is highly promising due to their soluble nature and low band gap along with outstanding optoelectronic properties.^{77b} The polymerization at core position of NDI has been mostly achieved using palladium

catalyzed C-C cross coupling reactions such as Stille,⁹⁷ Suzuki,^{67,98} Sonogashira,⁹⁹ Heck¹⁰⁰ etc. using 2,6-dibromo NDI as monomer (Scheme 1.5). The Stille and Suzuki polymerizations were reported as most efficient methods due to high molecular weight of polymer, high polymerization yield and ease of monomer synthesis. The mechanism of Stille polymerization involves oxidative addition of bromide containing monomer to palladium followed by transmetalation with another monomer; finally the reductive elimination yields one repeat unit and regenerated palladium catalyst. The Suzuki polymerization required the use of base such as potassium or sodium carbonate to activate the diboronic acid containing monomer. Core-substituted NDI could also be polymerized using chain-growth condition to achieve relatively narrow polydispersity index. Activated zinc and brominated thiophene-NDI form anion-radical complex (Scheme 1.5) which subsequently undergo Ni-catalyzed chain growth polymerization.¹⁰¹

1.5.2 Optical and Electrochemical Properties

NDIs and PDIs are structurally planar, rigid, neutral, chemically robust, redox-active compounds which usually showed high melting point. Since, they are composed of π -conjugated backbone, they exhibit strong optical properties like absorption and emission. For instance, the UV-visible absorption spectra of *N, N'*-dialkyl substituted NDIs showed three characteristic vibronically resolved peaks below 400 nm in chloroform and DCM (**Figure 1.14**).

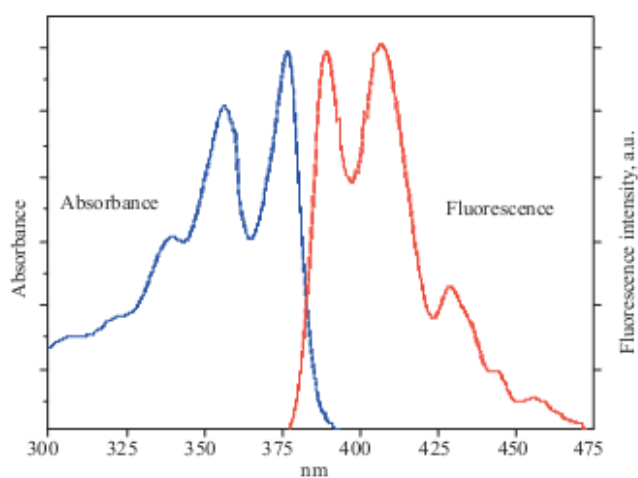


Figure 1.14 Combined absorption and emission spectra of *N, N'*-bis-*n*-butyl NDI in acetonitrile. (Adapted from Ref¹⁰²)

These fine resolved peaks corresponded to the 0–0, 0–1 and 0–2 vibronic transitions of a S_0 – S_1 transition with the intensity of the 0–0 transition being the maximum.¹⁰³ Most of the NDIs exhibited weak emission spectra with ~ 7 nm Stokes shift which was the mirror image of the absorption spectrum.^{102,104} Furthermore, the low quantum yield of NDIs (approximately 0.002) in aromatic solvents such as benzene, toluene, p-xylene suggested the formation of ground state aggregates which exhibited excimer-like emission.¹⁰³⁻¹⁰⁵ Similarly, PDIs also showed three characteristic vibronically resolved peaks in the range of 450-550 nm. Unlike NDI, the fluorescence quantum yield of PDI was nearly unity in most of the cases and the singlet excited state lifetime was approximately 4 ns.⁷⁸ The chemical modification at imide nitrogen of both NDI and PDI atom does not produce a large effect on the optical and semiconducting properties due to the orbital node present at imide nitrogen atom in the HOMO and LUMO. However, it could be used to affect the aggregation and solubility properties significantly.¹⁰⁶ In contrast, core substitution at NDI has a huge impact on the electronic and optical properties. For instance, the polymerization of NDI at 2, 6 positions with suitable donor allow to achieve higher degree of backbone coplanarity.^{106b} Additionally, along with π - π^* transition they also exhibit strong D-A charge transfer band (ICT) at lower absorption wavelength with reduced HOMO-LUMO band gap.^{84b,93} Most of the NDI derivatives exhibited solubility in less polar solvent (chloroform, DCM, toluene etc.) and polar aprotic solvent (e.g. DMF, DMSO, acetonitrile etc.). The strong π - π interaction between aromatic cores of NDI allowed them to stack in solid state as well as solution which are advantageous for various supramolecular applications.^{77c} However, it can also prove to be a major hurdle for solubility, particularly when substituted at imide position with aromatic core. Hence, solubility and aggregation properties of NDIs essentially depends upon the nature of substituents at imide nitrogen. The nature of aggregation or supramolecular assemblies in solution exhibit distinct changes in the absorption and emission bands compared to monomeric species.^{88,107} The nature of aggregation or stacks in different solvent media can be divided into two major types ‘*J*-type’ and ‘*H*-type’ depending upon spectral shift observed in absorption spectrum. Usually, *J*-type aggregates leads to a shift in the absorption spectrum to relatively longer wavelength (red or bathochromic shift) compared to monomer band, whereas *H*-type aggregation often shifts the absorption spectrum towards shorter wavelength (blue or hypsochromic shift). This phenomenon can be well explained by molecular exciton coupling theory

i.e. coupling between transition moments of the constituent molecules developed by Kasha *et al.*¹⁰⁸ The difference in the spectral properties of the two types of aggregates is caused by distinct arrangements of molecules in stacks. Molecules can stack in parallel fashion (face-to-face or plane-to-plane stacking) to form sandwich type arrangement (*H*-dimer) or head-to-tail arrangement (end-to-end stacking) to form a *J*-dimer (**Figure 1.15**). Actually, this difference in the stacking is due to the different slip angle between stacked molecules. The angle between long axes of one of the parallel molecules in stack with respect to the line of center of column within stack is called as ‘slippage angle’.

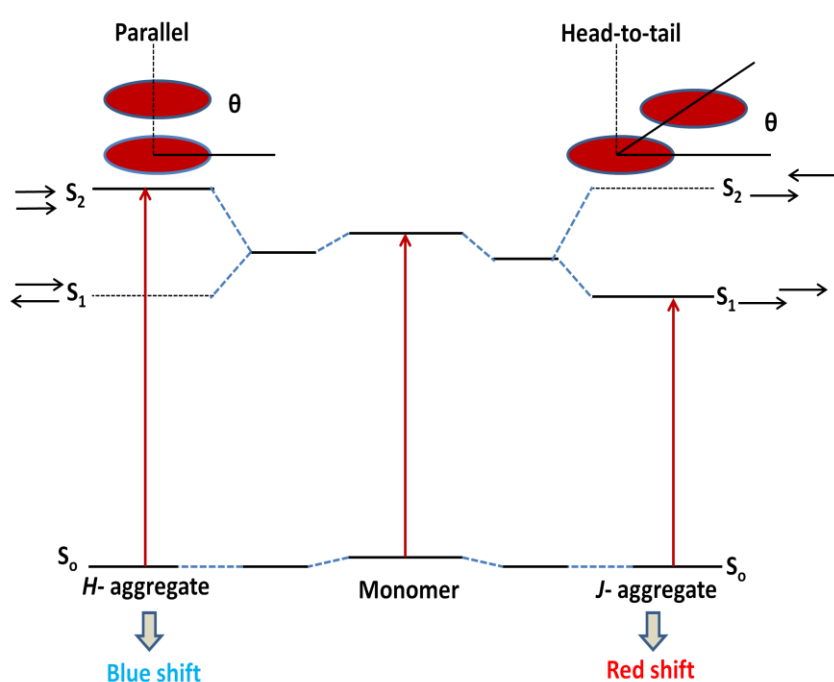


Figure 1.15 Schematic representation of relation between stacking (*J*-type or *H*-type) and spectral shift based on exciton theory.

According to exciton theory, each molecule in stack is considered as point dipole and the interaction between transition dipole in excited state of aggregate leads to splitting of energy levels; one with higher energy level and the other with lower energy level than monomer energy level (**Figure 1.15**). For *J*-aggregates with large molecular slippage, only lower energy excited state transition is allowed. As a result, they show red shifted absorption band with high fluorescence quantum yield.^{88,109} On the other hand, only higher energy transition is allowed for *H*-aggregates (small molecular slippage) which results in blue shifted absorption band.^{88,110} The *H*-type aggregates

exhibit strong quenching in fluorescence due to rapid energy relaxation to lower energy excited state. The NDI and PDI derivatives also exhibit interesting electrochemical properties; they show two reversible reduction peaks in cyclic voltammetry at relatively lower reduction potential due to high electron affinity which suggests the possibility of n-type doping.^{104,111} The corresponding peaks (**Figure 1.16**) are assigned to stepwise reduction of NDI or PDI due to formation of radical anion and dianion, so overall it is two electron reductions.^{91,96a,111} The simple *N, N'*-dialkyl derivative of NDI exhibits two reduction peaks at approximately (E_{red}^1) -1.10 V and (E_{red}^2) -1.5 V versus Fc/Fc+ in DCM or chloroform, when Ag/AgNO₃ was used as reference electrode.⁹¹ The LUMO values estimated from reduction potential of most of the NDIs are in the range of 3.6-3.9 eV which has been further lowered up to ~ 0.3 eV after substitution with electron withdrawing group at core position.^{94a,112}

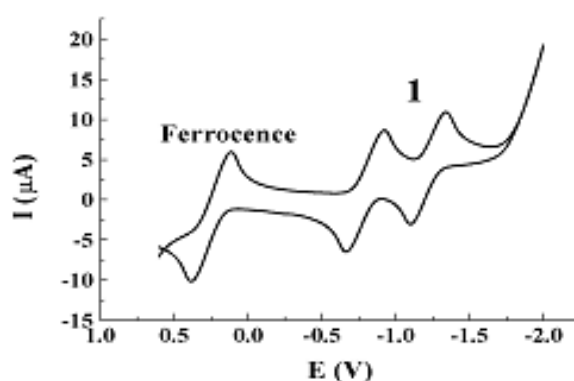


Figure 1.16 Cyclic voltammogram of *N, N'*-disubstituted NDI (in CHCl₃/TBAPF₆) at scan rate 100 mV/s. (Adapted from Ref¹⁰⁴)

1.5.3 Small Molecule based Semiconductors

The potential of naphthalenediimide (NDI) and perylenediimide (PDI) as an n-type molecular semiconductor was recognized more than a decade ago. Early investigation in 1996 by Horowitz *et al.* reported the evidences of electron conductivity for OFET fabricated from *N, N'*-diphenyl PDI **2b** (**Chart 1.5**).¹¹³ At the same time, H. E. Katz and A. Dodabalapur demonstrated the electron mobility of more than 10⁻³ cm² V⁻¹ s⁻¹ for OFET fabricated using simplest *N, N'*-dihydrogen substituted NDI **1a**.¹¹⁴ Subsequent development in this area suggested that, the performance and air stability of NDI and PDI based OFETs could be greatly improved by changing the various *N,*

N' - substituents. For example, Katz *et al.* demonstrated the electron mobility of $0.16 \text{ cm}^2 \text{ V}^{-1} \text{ s}^{-1}$ for N,N' - dioctyl NDI **1b** in vacuum which was 10^3 times more than N, N' - dihydrogen substituted NDI **1a**.^{53d} However, the OFET device made by using **1b** was not stable at ambient condition. A remarkable improvement in the ambient stability of OFET device was found by varying N, N' -substituent on NDI with fluoroalkyl chains **1c** without sacrificing the electron mobility of $0.05\text{-}0.1 \text{ cm}^2 \text{ V}^{-1} \text{ s}^{-1}$.^{53d} It was believed that the hydrophobic fluorinated side chains on imide nitrogen offered better packing of NDI core and prevented the diffusion of water or oxygen inside the active layer.^{46,62a,77b}

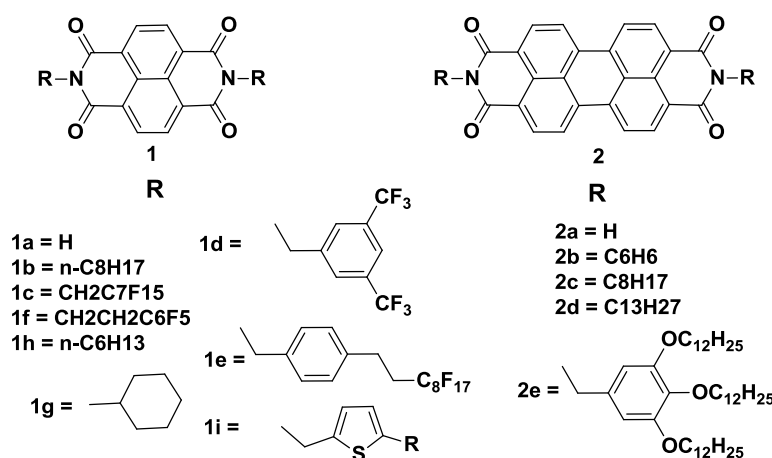


Chart 1.5 Chemical structure of some NDI and PDI based small molecule semiconductors.

See *et al.* reported two N, N' - diphenyl substituted NDI derivatives bearing perfluoroalkyl chain on phenyl ring, one with short CF_3 group **1d** and another with long perfluoroalkyl chain **1e**, the latter exhibited highest electron mobility of $0.57 \text{ cm}^2 \text{ V}^{-1} \text{ s}^{-1}$ without the use of dielectric substrate treatments.¹¹⁵ The fabrication of flexible transistor on transparent plastic (PET) substrate with fluorophenylethyl substituted NDI **1f** was demonstrated by Katz and coworkers which showed n- channel operation with electron mobility up to $0.23\text{-}0.57 \text{ cm}^2 \text{ V}^{-1} \text{ s}^{-1}$.^{86b} Another example which demonstrated the effect of varying N, N' - substituents on crystal packing and device performance was reported by Shukla *et al.*^{82a} It was found that cyclohexyl end groups on imide nitrogen of NDI assisted the intermolecular π - π stacking (**1g**) leading to optimum thin film morphology and high electron mobility of $6.2 \text{ cm}^2 \text{ V}^{-1} \text{ s}^{-1}$ which was one of the highest reported mobility for core unsubstituted NDI until then. On the other hand, n -hexyl substituted NDI **1h** derivative exhibited lower electron mobility

of $0.7 \text{ cm}^2 \text{ V}^{-1} \text{ s}^{-1}$ due to increased distance between two NDI cores. Beside alkyl, fluoroalkyl, alky phenyl and cycloalkyl some other groups were also substituted at imide nitrogen of NDI such as alkylthienyl **1i** but relatively lower mobility of $9.1 \times 10^{-3} \text{ cm}^2 \text{ V}^{-1} \text{ s}^{-1}$ was obtained.^{112b,86c} The OFET device fabricated using unsymmetrically substituted NDI derivative also exhibited promising n-type behavior with electron mobility of $0.10 \text{ cm}^2 \text{ V}^{-1} \text{ s}^{-1}$ reported for NDI derivative where one side was substituted with alkyl chain and other side with benzimidazole linkage containing fluoromethyl group.¹¹⁶ The research on PDI based molecular semiconductor was also equally pursued; Malenfant *et al.* reported the electron mobility as high as $0.6 \text{ cm}^2 \text{ V}^{-1} \text{ s}^{-1}$ for OFET fabricated using simple *N, N'*-dioctyl substituted PDI **2c** with $I_{\text{on}}/I_{\text{off}}$ ratio more than 10^5 under inert condition.¹¹⁷ Further improvement in the electron mobility up to $1.7 \text{ cm}^2 \text{ V}^{-1} \text{ s}^{-1}$ for similar PDI derivative was observed by Chesterfield *et al.*¹¹⁸ Similar PDI derivative substituted with *N, N'*-ditridecyl group **2d** and OFET device annealed at more than $140 \text{ }^\circ\text{C}$ showed improved mobility up to $2.1 \text{ cm}^2 \text{ V}^{-1} \text{ s}^{-1}$.¹¹⁹ Marder's group reported high SCLC electron mobility of $1.3 \text{ cm}^2 \text{ V}^{-1} \text{ s}^{-1}$ for discotic liquid crystalline PDI **2e**.¹²⁰ However, this value of high electron mobility was not intrinsic and found to be very sensitive for particular LC morphology which further depended upon the processing conditions. Introduction of a strong electron withdrawing group at core position of NDI and PDI derivatives was found to be another successful approach for air stable n-type operation. The stability was accounted for by the increased electron affinity of NDI or PDI which prevented the oxidation of radical anion generated in conducting channel by reactive species like water or oxygen.^{46,62a,77b} The earliest report by Jones *et al.* on cyanide substituted PDI at core position (**Figure 1.17**) showed electron mobility as high as $0.6 \text{ cm}^2 \text{ V}^{-1} \text{ s}^{-1}$ and air stable n-type operation.^{62b} The high electron mobility and air stability was accounted for by the combination of functionality at imide and core position with perfluoroalkyl chain and cyanide group, respectively.¹²¹ Later, the same group also reported two core substituted NDI derivatives with mono-CN and di-CN₂ (**Figure 1.17**) substitution in which the latter exhibited higher electron mobility of $0.15 \text{ cm}^2 \text{ V}^{-1} \text{ s}^{-1}$ in vacuum compared to mono-CN NDI derivative ($4.7 \times 10^{-3} \text{ cm}^2 \text{ V}^{-1} \text{ s}^{-1}$).^{94a} Additionally, the di-CN₂ NDI showed outstanding air stability with negligible drop in electron mobility at ambient condition whereas OFET device for mono-CN NDI underwent severe degradation of *I-V* curves. Z. Bao and F. Würthner reported the two

fluorine rich PDI derivatives by substituting core position with two (PDI-F₂) and four (PDI-F₄) fluorine atoms.¹²² PDI-F₂ exhibited herringbone type edge-to-face on packing in single crystal leading to electron mobility as high as 0.34 cm² V⁻¹ s⁻¹ along with exceptionally high I_{on} /I_{off} ratio of 10⁷. On the other hand, high core twisting in PDI-F₄ due to four chlorine atoms resulted in one order decrease in electron mobility. Core expanded derivatives of NDI also showed promising n-channel behavior in OFET. Gao and coworkers demonstrated high electron mobility of 0.51 cm² V⁻¹ s⁻¹ and I_{on} /I_{off} ratio 10⁵-10⁷ for core expanded NDI derivative fused with 2-(1,3-dithiol-2-ylidene) malonitrile groups.^{112c,123} Polander *et al.* reported the bis-NDI derivative where two NDI core was connected together at core position by conjugated bridge based on fused heterocycle ring system; thin films processed from solution exhibited electron mobility up to 1.5 cm² V⁻¹ s⁻¹.¹²⁴

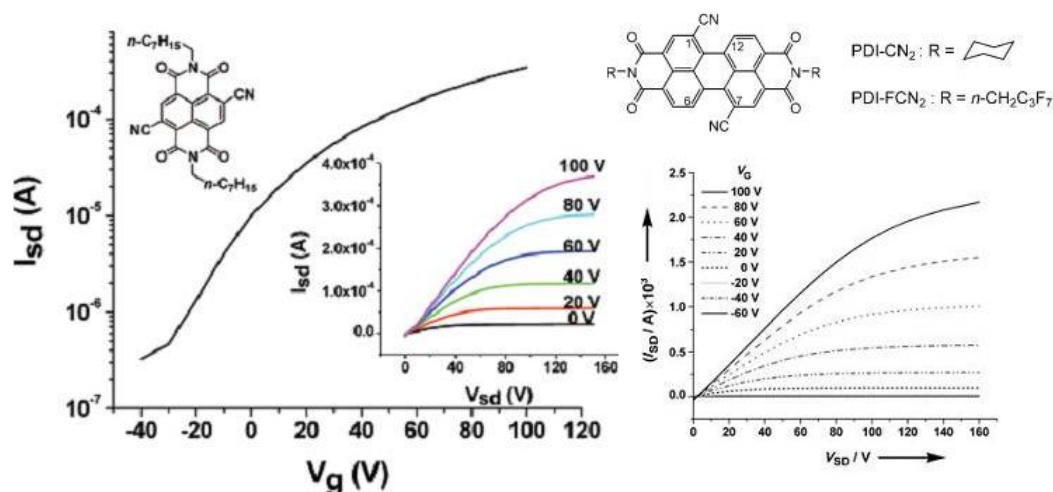


Figure 1.17 chemical structures and out -put I - V curves of NDI-CN₂ and PDI-FCN₂. (Adapted from Ref^{94a} and Ref^{62b})

1.5.4 Polymeric Semiconductors

Small molecule NDI and PDI based semiconductors have exhibited high charge carrier mobility in OFET mostly for vacuum deposited thin films. This method of thin-film deposition is found to be time consuming, expensive and needs several optimizations for getting uniform thin-film morphology.^{77a,125} Alternatively, solution techniques such as spin coating, inkjet printing and screen printing are inexpensive methods that are found to be more successful for polymers due to their high solution viscosity compared to small molecules.^{106b,126} Also, roll-to-roll fabrication over large area can be possible only using polymer which is the ultimate aim of organic

electronics.¹²⁷ The development of NDI and PDI based polymeric semiconductor has lagged behind the small molecular counterpart in the past. However, recently developed NDI and PDI based solution processable polymers exhibited electron mobility comparable to small molecules. Further development of n-channel polymeric semiconductors is still an important and active field. Babel and Jenekhe reported first n-channel TFT-active ladder poly (benzobisimidazo-benzophenanthroline) BBL (1) (Chart 1.6) in 2003 which exhibited electron mobility of $0.1 \text{ cm}^2 \text{ V}^{-1} \text{ s}^{-1}$ in OFET for spin-coated thin film after thermal annealing.⁶³ Unfortunately, the polymer was soluble only in strong acidic solution such as methane sulfonic acid (MSA) which limited their use in device.

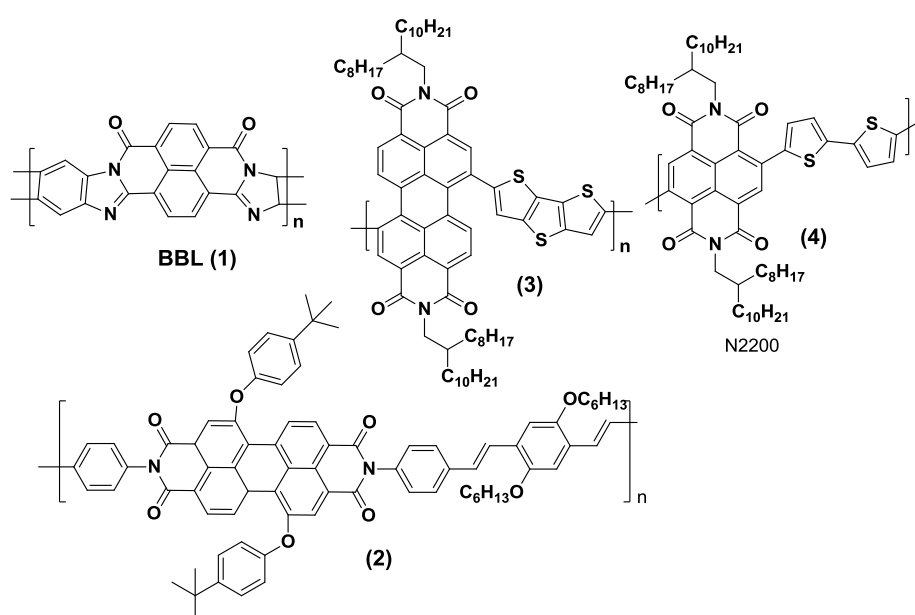


Chart 1.6 Chemical structures of some NDI and PDI based main chain polymer.

Mikroyannidis *et al.* reported the alternating copolymer of PDI bearing *tert*-butyloxy side chain at core position (2) which lead to increase in the solubility of copolymer in common organic solvents. The corresponding copolymer exhibited electron mobility of $8.5 \times 10^{-3} \text{ cm}^2 \text{ V}^{-1} \text{ s}^{-1}$ measured by SCLC method and PCE of 2.32 % in BHJ solar cell fabricated using copolymer as an acceptor (n-type).¹²⁸ As mentioned in section 1.5.1, the polymerization of rigid NDI or PDI at anhydride group with primary amine leads to insoluble poly (imides). However, the polymerization of NDI or PDI at core position by substitution of imide nitrogen atom with long or branched alkyl chain has offered considerable solubility in common organic solvents. This approach was first demonstrated by Zhan *et al.* in 2007, when they synthesized the dithienothiophene

containing core substituted PDI polymer (**3**) by Stille coupling.⁶⁵ The polymer was soluble in chloroform, THF and chlorobenzene and could be easily processed from solution, the thin-film of polymer exhibited electron mobility of $1.3 \times 10^{-2} \text{ cm}^2 \text{ V}^{-1} \text{ s}^{-1}$ in OFET. The 1:1 blend of all-polymer solar cells fabricated using this polymer as acceptor and a bi(thienylenevinylene) substituted polythiophene (PT1) as a donor exhibited power conversion efficiency around 1 % which has been further increased up to 1.48 % and 3.45 % after slight modification in polymer structure and using solvent additives, respectively.¹²⁹ Later, Facchetti's group reported the synthesis of two novel core substituted NDI and PDI copolymers with a bithiophene as an alternating co-monomer.^{97a} NDI containing copolymer with bithiophene comonomer (**4**) was commercialized as PolyeraActivInk (N2200), which has shown very high electron mobility up to $\sim 0.85 \text{ cm}^2 \text{ V}^{-1} \text{ s}^{-1}$ for printed OFETs. Furthermore, the bulk electron transport for N2200 was measured by both TOF and electron-only SCLC method, that gave electron mobility of $5 \times 10^{-3} \text{ cm}^2 \text{ V}^{-1} \text{ s}^{-1}$.¹³⁰ N2200/P3HT blends have shown ambipolar FET characteristics with balanced electron and hole mobilities of ($4 \times 10^{-3} \text{ cm}^2 \text{ V}^{-1} \text{ s}^{-1}$) and ($2 \times 10^{-3} \text{ cm}^2 \text{ V}^{-1} \text{ s}^{-1}$), respectively.¹³¹ The initial reports of solar cell device performance of the N2200 polymer, independently by Loi's and Sirringhaus's groups were not very promising.¹³² A maximum PCE of 0.2 % was obtained using solvents like chlorobenzene (CB), p-xylene, dichlorobenzene (DCB), or chloroform for device fabrication. Further improvement in PCE to 1.4 % was reported by D. Neher and coworker using P3HT as donor and N2200 as acceptor material using a 1:1 solvent mixture of p-xylene and chloronaphthalene (CN).¹³³ Recently, Kim's group demonstrated the highest reported PCE of 4.6 % in all-polymer solar cells using N2200 as acceptor and PTB7-Th as the donor polymer.^{83a} Kim *et al.* reported an NDI copolymer by introducing a vinyl (double bond) group between two adjacent thiophene units of N2200 which improved the electron mobility up to $1.8 \text{ cm}^2 \text{ V}^{-1} \text{ s}^{-1}$.¹³⁴ The increased mobility was accounted for by the extended π -conjugation in copolymer which lead to increase in the degree of coplanarity of polymer backbone. Although heteroaromatic groups like thiophene and thiophene based derivatives have dominated as the core-position linked comonomers, other comonomers such as selenophene, phenothiazine, fluorine, diethynylbenzene, benzthiadiazole, naphthalene, pyrene etc. have also emerged.¹⁰⁰ Most of them have shown good n-type performance in OFET as well as solar cells. C. Yang and J. H. Oh reported series of thiophene free NDI copolymers with acene and hetero acene unit

which exhibited electron mobility as high as $5 \times 10^{-2} \text{ cm}^2 \text{ V}^{-1} \text{ s}^{-1}$.^{98a} The charge transport in NDI based copolymer was found to be dependent upon the type of donor comonomer used and some of the copolymer also exhibited ambipolar nature in OFET. For example, Jenekhe *et al.* reported the ambipolar charge transport in NDI copolymer substituted with electron donating dialkoxybithiophene with high electron mobility up to $0.04 \text{ cm}^2 \text{ V}^{-1} \text{ s}^{-1}$ and hole mobility of $0.003 \text{ cm}^2 \text{ V}^{-1} \text{ s}^{-1}$.^{97c,135} The molecular packing, thin-film morphology and eventually device performance of core substituted NDI copolymers has been strongly influenced by nature of substituent on imide nitrogen atom.

1.6 Aim of the Thesis

The extensive literature survey done on naphthalene and perylene diimide based small molecules as well as polymers have suggested their potential application as organic semiconductor in optoelectronic devices. Particularly, the NDI containing building block has been used to construct the elegant supra-molecular π - functional material which was then utilized for various applications such as molecular sensor, conducting thin film, electron and energy transfer study, host-guest chemistry etc. In many designs apart from π - π stacking interaction, intermolecular hydrogen bonding were used as additional handle to form one dimensional (1D) self-assembly of NDI in solution as well as solid state with the hope that improved charge transport could occur along the self assembled inter-stacks. However, none of the reports gave clear evidences for how the self assembly by hydrogen bonding affected the charge transport properties of NDI in device like OFET. This is a very important question to address, since the use of bottom-up approach for the synthesis of NDI based semiconducting materials is on the rise. Although NDI and PDI based small molecular semiconductors are performing better than polymeric counterparts, their tedious fabrication with less practical utility invokes the use of these intriguing building blocks in polymeric architecture which offers simple fabrication techniques. Despite the rapid development in NDI and PDI based polymeric semiconductors, very few of them are able to reach satisfactory performance in OFET device. Therefore, this area is still important and active which demands new design strategies to synthesize the novel polymeric architecture with desirable physical and

semiconducting properties for organic electronics. In this context, the recently developed class of donor-acceptor copolymer looks promising due to several advantages like a) ability to tune the energy level over large range to achieve polymer with low band gap b) the nature of charge transport can be tuned from unipolar *n*-type or *p*-type to ambipolar c) control over the molecular packing and thin film morphology.

The objective of the present thesis work was to design and synthesize NDI containing small molecules via structure engineering to understand the effect of self assembly by hydrogen bonding on optical and charge transport properties in OFETs. This was followed by the utilizing these intriguing building blocks (NDI and PDI) in polymeric architecture that could find practical application in OFET devices. The major focus of this dissertation includes the detailed studies of structure-property relationship in NDI based conjugated polymers for which the synthesis of a variety of novel polymers was targeted by using donor-acceptor design strategy. The same could be achieved by polymerization of different donor co-monomers with NDI or PDI acceptor unit either at anhydride or core position. This was followed by understanding the impact of structure property on the solution processability, structural packing and nature of charge transport in the OFET. Furthermore, the substitution of imide nitrogen atom of core substituted NDI polymers with flexible side chains could be expected to enhance the solubility of polymer and hence solution processability. However, the proper selection of side chains is very important, because they could affect the molecular packing, thin film morphology and consequently device performance. These objectives were achieved by carrying out the work in four different projects. The initial work discussed in chapter two gives deeper insight in to the effect of self assembly by hydrogen bonding in naphthalenediimide (NDI) small molecules on their optical and charge transport properties. For that two types of NDI derivatives having difference in functional group namely ester or amide were designed and synthesized in such a way that amide derivative would form self assembly due to intermolecular hydrogen bonding thereby differentiating them from non hydrogen bondable ester derivative. Indeed, the amide derivatives showed evidence of self-organization which was traced by variations in their optical properties compared to ester. The tools like WXR, density functional theory (DFT), TEM and AFM were utilized to understand the effect of hydrogen bonding on

crystalline nature, molecular packing and thin-film morphology. Contrary to expectations, the NDI ester derivatives showed better n-type charge transport with relatively higher electron mobilities and I_{on}/I_{off} ratio compared to self assembled amide derivative. Thereafter the thesis deals with the synthesis of novel donor-acceptor polymeric architecture incorporating the NDI and PDI in polymer backbone. The third chapter involves the design and synthesis of novel class of n-type poly (imides) comprised of benzobisoxazole as an electron donor and NDI/ PDI as electron acceptor. Unfortunately, these polymers exhibited solubility only in strong protic acid such as methane sulfonic acid (MSA) due to extremely rigid nature of polymer. Photoinduced energy transfer and charge separation were studied in methanesulfonic acid (MSA) solution via absorption, excitation, and steady-state fluorescence studies. Thin films of polymers processed from MSA solution showed their n-type charge transport in OFET with moderate electron mobility. In the fourth chapter, core substituted NDI polymers were synthesized by substituting imide nitrogen atom of NDI with long branched alkyl chain for solubility purpose. Three novel polymers were synthesized by varying the different donor unit at core position of NDI namely oligo(phenylenevinylene) (OPV), benzobisoxazole (BBO) and benzthiadiazole (BT). The effect of varying donor strength on optical, electrochemical and semiconducting properties of polymers was investigated. Considerable change in the LUMO and the HOMO energy level of polymer was observed upon changing the donor unit which consequently altered the charge transport nature of polymer from ambipolar to n-type. The favorable energy levels in OPV containing polymer exhibited balanced ambipolar charge transport in OFET. The Fifth chapter discussed the influence of side chain modification at imide nitrogen of core substituted NDI polymer on molecular packing and consequently the charge carrier transport properties. For that, two oligo(phenylenevinylene) containing NDI polymer was synthesized by varying the side chains from hydrophilic linear oligo(ethyleneoxy) group to hydrophobic branched alkyl chain (2-octyldodecyl). The effect of side chain variation on molecular packing was characterized by thin-film XRD followed by charge carrier mobility measurement in SCLC. The overall findings are concluded in chapter six.

1.7 References

- (1) Cuevas, J. C.; Scheer, E. *Molecular electronics an introduction to theory and experiment*; World Scientific, 2010.
- (2) Aviram, A.; Ratner, M. A. *Chem. Phys. Lett.* **1974**, *29*, 277.
- (3) Shirakawa, H.; Louis, E. J.; MacDiarmid, A. G.; Chiang, C. K.; Heeger, A. J. *J. Chem. Soc., Chem. Commun.* **1977**, 578.
- (4) Burroughes, J. H.; Bradley, D. D. C.; Brown, A. R.; Marks, R. N.; Mackay, K.; Friend, R. H.; Burns, P. L.; Holmes, A. B. *Nature* **1990**, *347*, 539.
- (5) (a) Sariciftci, N. S.; Smilowitz, L.; Heeger, A. J.; Wudl, F. *Science* **1992**, 258, 1474(b) Sariciftci, N. S.; Braun, D.; Zhang, C.; Srdanov, V. I.; Heeger, A. J.; Stucky, G.; Wudl, F. *Appl. Phys. Lett.* **1993**, *62*, 585.
- (6) (a) Crone, B.; Dodabalapur, A.; Lin, Y. Y.; Filas, R. W.; Bao, Z.; LaDuca, A.; Sarpeshkar, R.; Katz, H. E.; Li, W. *Nature* **2000**, *403*, 521(b) Lu, J.; Pinto, N. J.; MacDiarmid, A. G. *J. Appl. Phys* **2002**, *92*, 6033(c) Schon, J. H.; Meng, H.; Bao, Z. *Nature* **2001**, *413*, 713.
- (7) (a) Shaheen, S. E.; Brabec, C. J.; Sariciftci, N. S.; Padinger, F.; Fromherz, T.; Hummelen, J. C. *Appl. Phys. Lett.* **2001**, *78*, 841(b) Brabec, C. J.; Sariciftci, N. S.; Hummelen, J. C. *Adv. Funct. Mater.* **2001**, *11*, 15(c) Granstrom, M.; Petritsch, K.; Arias, A. C.; Lux, A.; Andersson, M. R.; Friend, R. H. *Nature* **1998**, *395*, 257(d) Schmidt-Mende, L.; Fechtenkötter, A.; Müllen, K.; Moons, E.; Friend, R. H.; MacKenzie, J. D. *Science* **2001**, *293*, 1119(e) McFarland, E. W.; Tang, J. *Nature* **2003**, *421*, 616(f) Spanggaard, H.; Krebs, F. C. *Sol. Energy Mater. Sol. Cell* **2004**, *83*, 125(g) Brabec, C. J. *Sol. Energy Mater. Sol. Cell* **2004**, *83*, 273.
- (8) (a) Friend, R. H.; Gymer, R. W.; Holmes, A. B.; Burroughes, J. H.; Marks, R. N.; Taliani, C.; Bradley, D. D. C.; Santos, D. A. D.; Bredas, J. L.; Logdlund, M.; Salaneck, W. R. *Nature* **1999**, *397*, 121(b) Kraft, A.; Grimsdale, A. C.; Holmes, A. B. *Angew. Chem. Int. Ed.* **1998**, *37*, 402(c) Gong, X.; Moses, D.; Heeger, A. J.; Liu, S.; Jen, A. K.-Y. *Appl. Phys. Lett.* **2003**, *83*, 183.
- (9) (a) Yu, G.; Pakbaz, K.; Heeger, A. J. *Appl. Phys. Lett.* **1994**, *64*, 3422(b) Yu, G.; Srdanov, G.; Wang, J.; Wang, H.; Cao, Y.; Heeger, A. J. *Synth. Met* **2000**, *111–112*, 133(c) Yu, G.; Wang, J.; McElvain, J.; Heeger, A. J. *Adv. Mater.* **1998**, *10*, 1431(d) Peumans, P.; Yakimov, A.; Forrest, S. R. *J. Appl. Phys* **2003**, *93*, 3693.

- (10) (a) Chen, L.; McBranch, D. W.; Wang, H.-L.; Helgeson, R.; Wudl, F.; Whitten, D. G. *P. N. A. S.* **1999**, *96*, 12287(b) Gaylord, B. S.; Heeger, A. J.; Bazan, G. C. *P. N. A. S.* **2002**, *99*, 10954(c) Sadik, O. A.; Ngundi, M.; Wanekaya, A. *Microchim. Acta* **2003**, *143*, 187.
- (11) (a) Moses, D. *Appl. Phys. Lett.* **1992**, *60*, 3215(b) Brouwer, H. J.; Krasnikov, V. V.; Hilberer, A.; Wildeman, J.; Hadziioannou, G. *Appl. Phys. Lett.* **1995**, *66*, 3404.
- (12) (a) Lemmer, U. *Polymer. Adv. Tech.* **1998**, *9*, 476(b) Wegmann, G.; Schweitzer, B.; Hopmeier, M.; Oestreich, M.; Giessen, H.; F. Mahrt, R. *Phys. Chem. Chem. Phys.* **1999**, *1*, 1795(c) Reufer, M.; Riechel, S.; Lupton, J. M.; Feldmann, J.; Lemmer, U.; Schneider, D.; Benstem, T.; Dobbertin, T.; Kowalsky, W.; Gombert, A.; Forberich, K.; Wittwer, V.; Scherf, U. *Appl. Phys. Lett.* **2004**, *84*, 3262.
- (13) Heeger, A. J. *Chem. Soc. Rev.* **2010**, *39*, 2354.
- (14) Mühlbacher, D.; Scharber, M.; Morana, M.; Zhu, Z.; Waller, D.; Gaudiana, R.; Brabec, C. *Adv. Mater.* **2006**, *18*, 2884.
- (15) (a) Blouin, N.; Michaud, A.; Leclerc, M. *Adv. Mater.* **2007**, *19*, 2295(b) Blouin, N.; Michaud, A.; Gendron, D.; Wakim, S.; Blair, E.; Neagu-Plesu, R.; Belletête, M.; Durocher, G.; Tao, Y.; Leclerc, M. *J. Am. Chem. Soc.* **2007**, *130*, 732.
- (16) Tang, C. W. *Appl. Phys. Lett.* **1986**, *48*, 183.
- (17) Forrest, S. *MRS Bulletin* **2012**, *37*, 552.
- (18) Koezuka, H.; Tsumura, A.; Ando, T. *Synth. Met* **1987**, *18*, 699.
- (19) Reese, C.; Roberts, M.; Ling, M.-m.; Bao, Z. *Mater. Today* **2004**, *7*, 20.
- (20) Shimura, F. In *Handbook of Electronics and Photonic material*; Kasap, S., Capper, P., Eds.; Springer, 2007.
- (21) Murphy, A. R.; Fréchet, J. M. J. *Chem. Rev.* **2007**, *107*, 1066.
- (22) Günes, S.; Neugebauer, H.; Sariciftci, N. S. *Chem. Rev.* **2007**, *107*, 1324.
- (23) Argun, A. A.; Aubert, P.-H.; Thompson, B. C.; Schwendeman, I.; Gaupp, C. L.; Hwang, J.; Pinto, N. J.; Tanner, D. B.; MacDiarmid, A. G.; Reynolds, J. R. *Chem. Mater.* **2004**, *16*, 4401.
- (24) Rotzoll, R.; Mohapatra, S.; Olariu, V.; Wenz, R.; Grigas, M.; Dimmler, K.; Shchekin, O.; Dodabalapur, A. *Appl. Phys. Lett.* **2006**, *88*, 123502.
- (25) Li, F. M.; Nathan, A.; Wu, Y.; Ong, B. S. *Organic Thin Film Transistor Integration: A Hybrid Approach*; First Edition ed.; Wiley-VCH Verlag GmbH & Co. KGaA, 2011.
- (26) Kittel, C. *Introduction to Solid State Physics*; 8th ed.; Wiley, 2005.

- (27) Coropceanu, V.; Cornil, J.; da Silva Filho, D. A.; Olivier, Y.; Silbey, R.; Brédas, J.-L. *Chem. Rev.* **2007**, *107*, 926.
- (28) (a) Chiang, C. K.; Fincher, C. R.; Park, Y. W.; Heeger, A. J.; Shirakawa, H.; Louis, E. J.; Gau, S. C.; MacDiarmid, A. G. *Phys. Rev. Lett.* **1977**, *39*, 1098(b) Chiang, C. K.; Park, Y. W.; Heeger, A. J.; Shirakawa, H.; Louis, E. J.; MacDiarmid, A. G. *J. Chem. Phys.* **1978**, *69*, 5098(c) Nigrey, P. J.; MacDiarmid, A. G.; Heeger, A. J. *J. Chem. Soc., Chem. Commun.* **1979**, 594(d) MacInnes, D.; Druy, M. A.; Nigrey, P. J.; Nairns, D. P.; MacDiarmid, A. G.; Heeger, A. J. *J. Chem. Soc., Chem. Commun.* **1981**, 317.
- (29) Ziemelis, K. E.; Hussain, A. T.; Bradley, D. D. C.; Friend, R. H.; Rühle, J.; Wegner, G. *Phys. Rev. Lett.* **1991**, *66*, 2231.
- (30) (a) Bredas, J. L.; Themans, B.; Andre, J. M.; Chance, R. R.; Silbey, R. *Synth. Met* **1984**, *9*, 265(b) Bredas, J. L.; Street, G. B. *Acc. Chem. Res* **1985**, *18*, 309(c) Mizes, H. A.; Conwell, E. M. *Phys. Rev. Lett.* **1993**, *70*, 1505.
- (31) Scott, J. C.; Pfluger, P.; Krounbi, M. T.; Street, G. B. *Phys. Rev. B* **1983**, *28*, 2140.
- (32) (a) Bredas, J. L. *Mol. Cryst. Liq. Cryst.* **1985**, *118*, 49(b) MacDiarmid, A. G. *Synth. Met* **2001**, *125*, 11.
- (33) Kivelson, S. *Phys. Rev. B* **1982**, *25*, 3798.
- (34) Chance, R. R.; Brédas, J. L.; Silbey, R. *Phys. Rev. B* **1984**, *29*, 4491.
- (35) Mott, N. F.; Davis, E. A. *Electronic processes in non-crystalline materials*; Clarendon, Oxford, UK, 1979.
- (36) Grimdale, A. C.; Leok Chan, K.; Martin, R. E.; Jokisz, P. G.; Holmes, A. B. *Chem. Rev.* **2009**, *109*, 897.
- (37) (a) Zou, L.; Savvate'ev, V.; Booher, J.; Kim, C.-H.; Shinar, J. *Appl. Phys. Lett.* **2001**, *79*, 2282(b) Jen, A. K.-Y.; Liu, Y.; Hu, Q.-S.; Pu, L. *Appl. Phys. Lett.* **1999**, *75*, 3745(c) Suzuki, H. *Appl. Phys. Lett.* **2002**, *80*, 3256.
- (38) Scottand, J. C.; .Malliaras, G. G. In *Semiconducting Polymers*; G.Hadziioannou, Hutten, P. F. v., Eds.; Wiley,, 2000.
- (39) Tang, C. W.; VanSlyke, S. A. *Appl. Phys. Lett.* **1987**, *51*, 913.
- (40) Green, M. A.; Emery, K.; Hishikawa, Y.; Warta, W.; Dunlop, E. D. *Prog. Photovolt: Res. Appl.* **2013**, *21*, 827.
- (41) You, J.; Dou, L.; Yoshimura, K.; Kato, T.; Ohya, K.; Moriarty, T.; Emery, K.; Chen, C.-C.; Gao, J.; Li, G.; Yang, Y. *Nat. Commun.* **2013**, *4*, 1446.

- (42) Hoppe, H.; Sariciftci, N. S. In *Advances in Polymer Science : Polymer Solar Cells*; Springer-Verlag Berlin Heidelberg 2007.
- (43) (a) Halls, J. J. M.; Pichler, K.; Friend, R. H.; Moratti, S. C.; Holmes, A. B. *Appl. Phys. Lett.* **1996**, *68*, 3120(b) Haugeneder, A.; Neges, M.; Kallinger, C.; Spirkl, W.; Lemmer, U.; Feldmann, J.; Scherf, U.; Harth, E.; Gügel, A.; Müllen, K. *Phys. Rev. B* **1999**, *59*, 15346.
- (44) Zaumseil, J.; Sirringhaus, H. *Chem. Rev.* **2007**, *107*, 1296.
- (45) Katz, H. E.; Bao, Z. *J. Phys. Chem. B* **2000**, *104*, 671.
- (46) Wen, Y.; Liu, Y. *Adv. Mater.* **2010**, *22*, 1331.
- (47) Veres, J.; Ogier, S.; Lloyd, G.; de Leeuw, D. *Chem. Mater.* **2004**, *16*, 4543.
- (48) (a) Schön, J. H.; Kloc, C.; Batlogg, B. *Organic Electronics* **2000**, *1*, 57(b) Wu, W.; Liu, Y.; Zhu, D. *Chem. Soc. Rev.* **2010**, *39*, 1489(c) Kelley, T. W.; Boardman, L. D.; Dunbar, T. D.; Muires, D. V.; Pellerite, M. J.; Smith, T. P. *J. Phys. Chem. B* **2003**, *107*, 5877.
- (49) Park, S. K.; Jackson, T. N.; Anthony, J. E.; Mourey, D. A. *Appl. Phys. Lett.* **2007**, *91*, 063514.
- (50) Sirringhaus, H.; Brown, P. J.; Friend, R. H.; Nielsen, M. M.; Bechgaard, K.; Langeveld-Voss, B. M. W.; Spiering, A. J. H.; Janssen, R. A. J.; Meijer, E. W.; Herwig, P.; de Leeuw, D. M. *Nature* **1999**, *401*, 685.
- (51) McCulloch, I.; Heeney, M.; Bailey, C.; Genevicius, K.; MacDonald, I.; Shkunov, M.; Sparrowe, D.; Tierney, S.; Wagner, R.; Zhang, W.; Chabinyc, M. L.; Kline, R. J.; McGehee, M. D.; Toney, M. F. *Nat. Mater.* **2006**, *5*, 328.
- (52) Sirringhaus, H.; Wilson, R. J.; Friend, R. H.; Inbasekaran, M.; Wu, W.; Woo, E. P.; Grell, M.; Bradley, D. D. C. *Appl. Phys. Lett.* **2000**, *77*, 406.
- (53) (a) Dell'Aquila, A.; Mastroilli, P.; Nobile, C. F.; Romanazzi, G.; Suranna, G. P.; Torsi, L.; Tanese, M. C.; Acierno, D.; Amendola, E.; Morales, P. *J. Mater. Chem.* **2006**, *16*, 1183(b) Halik, M.; Klauk, H.; Zschieschang, U.; Schmid, G.; Ponomarenko, S.; Kirchmeyer, S.; Weber, W. *Adv. Mater.* **2003**, *15*, 917(c) Akimichi, H.; Waragai, K.; Hotta, S.; Kano, H.; Sakaki, H. *Appl. Phys. Lett.* **1991**, *58*, 1500(d) Katz, H. E.; Lovinger, A. J.; Johnson, J.; Kloc, C.; Siegrist, T.; Li, W.; Lin, Y. Y.; Dodabalapur, A. *Nature* **2000**, *404*, 478(e) Garnier, F.; Hajlaoui, R.; El Kassmi, A.; Horowitz, G.; Laigre, L.; Porzio, W.; Armanini, M.; Provasoli, F. *Chem. Mater.* **1998**, *10*, 3334.
- (54) Laquindanum, J. G.; Katz, H. E.; Lovinger, A. J. *J. Am. Chem. Soc.* **1998**, *120*, 664.

- (55) Dimitrakopoulos, C. D.; Afzali-Ardakani, A.; Furman, B.; Kymissis, J.; Purushothaman, S. *Synth. Met* **1997**, *89*, 193.
- (56) Peumans, P.; Forrest, S. R. *Appl. Phys. Lett.* **2001**, *79*, 126.
- (57) Lin, Y.; Li, Y.; Zhan, X. *Chem. Soc. Rev.* **2012**, *41*, 4245.
- (58) (a) de Leeuw, D. M.; Simenon, M. M. J.; Brown, A. R.; Einerhand, R. E. F. *Synth. Met* **1997**, *87*, 53(b) Anthopoulos, T. D.; Anyfantis, G. C.; Papavassiliou, G. C.; de Leeuw, D. M. *Appl. Phys. Lett.* **2007**, *90*, 122105.
- (59) Zhang, X.-H.; Domercq, B.; Kippelen, B. *Appl. Phys. Lett.* **2007**, *91*, 092114.
- (60) (a) Bao, Z.; Lovinger, A. J.; Brown, J. *J. Am. Chem. Soc* **1998**, *120*, 207(b) de Oteyza, D. G.; Barrena, E.; Ossó, J. O.; Dosch, H.; Meyer, S.; Pflaum, J. *Appl. Phys. Lett.* **2005**, *87*, 183504.
- (61) Katz, H. E.; Johnson, J.; Lovinger, A. J.; Li, W. *J. Am. Chem. Soc* **2000**, *122*, 7787.
- (62) (a) Jones, B. A.; Facchetti, A.; Wasielewski, M. R.; Marks, T. J. *J. Am. Chem. Soc* **2007**, *129*, 15259(b) Jones, B. A.; Ahrens, M. J.; Yoon, M.-H.; Facchetti, A.; Marks, T. J.; Wasielewski, M. R. *Angew. Chem. Int. Ed.* **2004**, *43*, 6363(c) Jung, T.; Yoo, B.; Wang, L.; Dodabalapur, A.; Jones, B. A.; Facchetti, A.; Wasielewski, M. R.; Marks, T. J. *Appl. Phys. Lett.* **2006**, *88*, 183102(d) Yoo, B.; Jung, T.; Basu, D.; Dodabalapur, A.; Jones, B. A.; Facchetti, A.; Wasielewski, M. R.; Marks, T. J. *Appl. Phys. Lett.* **2006**, *88*, 082104.
- (63) Babel, A.; Jenekhe, S. A. *J. Am. Chem. Soc* **2003**, *125*, 13656.
- (64) Yan, H.; Chen, Z.; Zheng, Y.; Newman, C.; Quinn, J. R.; Dotz, F.; Kastler, M.; Facchetti, A. *Nature* **2009**, *457*, 679.
- (65) Zhan, X.; Tan, Z. a.; Domercq, B.; An, Z.; Zhang, X.; Barlow, S.; Li, Y.; Zhu, D.; Kippelen, B.; Marder, S. R. *J. Am. Chem. Soc* **2007**, *129*, 7246.
- (66) Klauk, H.; Halik, M.; Zschieschang, U.; Eder, F.; Rohde, D.; Schmid, G.; Dehm, C. *IEEE Transactions on Electron Devices*, **2005**, *52*, 618.
- (67) Gu, C.; Hu, W.; Yao, J.; Fu, H. *Chem. Mater.* **2013**, *25*, 2178.
- (68) Zaumseil, J.; Donley, C. L.; Kim, J. S.; Friend, R. H.; Siringhaus, H. *Adv. Mater.* **2006**, *18*, 2708.
- (69) Paasch, G.; Lindner, T.; Rost-Bietsch, C.; Karg, S.; Riess, W.; Scheinert, S. *J. Appl. Phys* **2005**, *98*, 084505.
- (70) Shirota, Y.; Kageyama, H. *Chem. Rev.* **2007**, *107*, 953.

- (71) Wang, Z. B.; Helander, M. G.; Greiner, M. T.; Qiu, J.; Lu, Z. H. *J. Appl. Phys* **2010**, *107*, 034506.
- (72) Lampert, M.; Mark, P. *Current injection in solids*; Academic press, New York, 1970.
- (73) (a) Struijk, C. W.; Sieval, A. B.; Dakhorst, J. E. J.; van Dijk, M.; Kimkes, P.; Koehorst, R. B. M.; Donker, H.; Schaafsma, T. J.; Picken, S. J.; van de Craats, A. M.; Warman, J. M.; Zuilhof, H.; Sudhölter, E. J. R. *J. Am. Chem. Soc* **2000**, *122*, 11057(b) van de Craats, A. M.; Warman, J. M.; Schlichting, P.; Rohr, U.; Geerts, Y.; Müllen, K. *Synth. Met* **1999**, *102*, 1550.
- (74) (a) Opitz, A.; Wagner, J.; Bru; x; tting, W.; Salzmann, I.; Koch, N.; Manara, J.; Pflaum, J.; Hinderhofer, A.; Schreiber, F. *IEEE:Selected Topics in Quantum Electronics* **2010**, *16*, 1707(b) Huang, Y.; Kramer, E. J.; Heeger, A. J.; Bazan, G. C. *Chem. Rev.* **2014**, *114*, 7006(c) Rivnay, J.; Mannsfeld, S. C. B.; Miller, C. E.; Salleo, A.; Toney, M. F. *Chem. Rev.* **2012**, *112*, 5488(d) Beaujuge, P. M.; Fréchet, J. M. J. *J. Am. Chem. Soc* **2011**, *133*, 20009.
- (75) Wen, Y.; Liu, Y.; Guo, Y.; Yu, G.; Hu, W. *Chem. Rev.* **2011**, *111*, 3358.
- (76) Heinze, J. *Angew. Chem. Int. Ed. (Eng)* **1984**, *23*, 831.
- (77) (a) Würthner, F.; Stolte, M. *Chem. Commun.* **2011**, *47*, 5109(b) Zhan, X.; Facchetti, A.; Barlow, S.; Marks, T. J.; Ratner, M. A.; Wasielewski, M. R.; Marder, S. R. *Adv. Mater.* **2011**, *23*, 268(c) Bhosale, S. V.; Jani, C. H.; Langford, S. J. *Chem. Soc. Rev.* **2008**, *37*, 331(d) Zhao, Y.; Guo, Y.; Liu, Y. *Adv. Mater.* **2013**, *25*, 5372.
- (78) Würthner, F. *Chem. Commun.* **2004**, 1564.
- (79) Li, G.; Zhao, Y.; Li, J.; Cao, J.; Zhu, J.; Sun, X. W.; Zhang, Q. *J. Org. Chem* **2015**, *80*, 196.
- (80) (a) Earmme, T.; Hwang, Y.-J.; Murari, N. M.; Subramaniyan, S.; Jenekhe, S. A. *J. Am. Chem. Soc* **2013**, *135*, 14960(b) Lu, Z.; Jiang, B.; Zhang, X.; Tang, A.; Chen, L.; Zhan, C.; Yao, J. *Chem. Mater.* **2014**, *26*, 2907.
- (81) Schenning, A. P. H. J.; v. Herrikhuyzen, J.; Jonkheijm, P.; Chen, Z.; Würthner, F.; Meijer, E. W. *J. Am. Chem. Soc* **2002**, *124*, 10252.
- (82) (a) Shukla, D.; Nelson, S. F.; Freeman, D. C.; Rajeswaran, M.; Ahearn, W. G.; Meyer, D. M.; Carey, J. T. *Chem. Mater.* **2008**, *20*, 7486(b) Lee, W.-Y.; Oh, J. H.; Suraru, S.-L.; Chen, W.-C.; Würthner, F.; Bao, Z. *Adv. Funct. Mater.* **2011**, *21*, 4173(c) Chen, H. Z.; Ling, M. M.; Mo, X.; Shi, M. M.; Wang, M.; Bao, Z. *Chem.*

- Mater.* **2007**, *19*, 816(d) Dey, A.; Kalita, A.; Krishnan Iyer, P. *ACS Appl. Mater. Interface* **2014**, *6*, 12295.
- (83) (a) Kang, H.; Kim, K.-H.; Choi, J.; Lee, C.; Kim, B. J. *ACS Macro Lett.* **2014**, *3*, 1009(b) Hwang, Y.-J.; Earmme, T.; Subramaniyan, S.; Jenekhe, S. A. *Chem. Commun.* **2014**, *50*, 10801.
- (84) (a) Zhou, E.; Nakano, M.; Izawa, S.; Cong, J.; Osaka, I.; Takimiya, K.; Tajima, K. *ACS Macro Lett.* **2014**, *3*, 872(b) Steyrleuthner, R.; Schubert, M.; Howard, I.; Klaumünzer, B.; Schilling, K.; Chen, Z.; Saalfrank, P.; Laquai, F.; Facchetti, A.; Neher, D. *J. Am. Chem. Soc.* **2012**, *134*, 18303.
- (85) (a) Hans, E. F. D.; Louis, B. *Fundamental Processes of dye chemistry*; NTERSCIENCE PUBLISHERS LTD., LONDON 1949 (b) Röhrscheid, F. In *Carboxylic Acids, Aromatic Ullmann's Encyclopedia of Industrial Chemistry*; Wiley-VCH Verlag GmbH & Co. KGaA, 2000.
- (86) (a) Kakinuma, T.; Kojima, H.; Ashizawa, M.; Matsumoto, H.; Mori, T. *J. Mater. Chem. C* **2013**, *1*, 5395(b) Jung, B. J.; Sun, J.; Lee, T.; Sarjeant, A.; Katz, H. E. *Chem. Mater.* **2009**, *21*, 94(c) Gawrys, P.; Boudinet, D.; Kornet, A.; Djurado, D.; Pouget, S.; Verilhac, J.-M.; Zagorska, M.; Pron, A. *J. Mater. Chem* **2010**, *20*, 1913(d) Langha, H. *Heterocycles* **1995**, *40*, 477.
- (87) Pengo, P.; Pantoş, G. D.; Otto, S.; Sanders, J. K. M. *J. Org. Chem* **2006**, *71*, 7063.
- (88) Kumar, M.; George, S. J. *Chem. Eur. J.* **2011**, *17*, 11102.
- (89) (a) Horne, W. S.; Ashkenasy, N.; Ghadiri, M. R. *Chem. Eur. J.* **2005**, *11*, 1137(b) Buncel, E.; Mailloux, N. L.; Brown, R. S.; Kazmaier, P. M.; Dust, J. *Tetrahedron Lett.* **2001**, *42*, 3559.
- (90) Vollmann, H.; Becker, H.; Corell, M.; Streeck, H. *Liebigs Ann. Chem.* **1937**, *531*, 1.
- (91) Thalacker, C.; Röger, C.; Würthner, F. *J. Org. Chem* **2006**, *71*, 8098.
- (92) (a) Solomatin, G. G.; Filippov, M. P.; Shigalevskii, V. A. *J. Org. Chem. USSR (Engl. Transl.)* **1981**, *17*, 771(b) Jacquignon, P.; Buu-Hoi, N. P.; Mangane, M. *Bull. Soc. Chim. Fr* **1964**, 2517
- (93) Guo, X.; Watson, M. D. *Org. Lett.* **2008**, *10*, 5333.
- (94) (a) Jones, B. A.; Facchetti, A.; Marks, T. J.; Wasielewski, M. R. *Chem. Mater.* **2007**, *19*, 2703(b) Popere, B. C.; Della Pelle, A. M.; Thayumanavan, S. *Macromolecules* **2011**, *44*, 4767.

- (95) Gao, X.; Qiu, W.; Yang, X.; Liu, Y.; Wang, Y.; Zhang, H.; Qi, T.; Liu, Y.; Lu, K.; Du, C.; Shuai, Z.; Yu, G.; Zhu, D. *Org. Lett.* **2007**, *9*, 3917.
- (96) (a) Kung, Y.-C.; Hsiao, S.-H. *J. Mater. Chem* **2011**, *21*, 1746(b) Wang, Z. Y.; Qi, Y.; Gao, J. P.; Sacripante, G. G.; Sundararajan, P. R.; Duff, J. D. *Macromolecules* **1998**, *31*, 2075(c) Hai-jun, N.; Jing-shan, M.; Mi-lin, Z.; Jun, L.; Pei-hui, L.; Xu-duo, B.; Wen, W. *Trans. Nonferrous Met. Soc. China* **2009**, *19*, 587(d) Mistri, E. A.; Mohanty, A. K.; Banerjee, S.; Komber, H.; Voit, B. *Journal of Membrane Science* **2013**, *441*, 168(e) Ghassemi, H.; Hay, A. S. *Macromolecules* **1994**, *27*, 3116.
- (97) (a) Chen, Z.; Zheng, Y.; Yan, H.; Facchetti, A. *J. Am. Chem. Soc* **2009**, *131*, 8(b) Durban, M. M.; Kazarinoff, P. D.; Luscombe, C. K. *Macromolecules* **2010**, *43*, 6348(c) Guo, X.; Kim, F. S.; Seger, M. J.; Jenekhe, S. A.; Watson, M. D. *Chem. Mater.* **2012**, *24*, 1434(d) Zhao, Z.; Zhang, F.; Zhang, X.; Yang, X.; Li, H.; Gao, X.; Di, C.-a.; Zhu, D. *Macromolecules* **2013**, *46*, 7705.
- (98) (a) Kim, Y.; Hong, J.; Oh, J. H.; Yang, C. *Chem. Mater.* **2013**, *25*, 3251(b) Zhou, W.; Wen, Y.; Ma, L.; Liu, Y.; Zhan, X. *Macromolecules* **2012**, *45*, 4115(c) Zhou, E.; Cong, J.; Zhao, M.; Zhang, L.; Hashimoto, K.; Tajima, K. *Chem. Commun.* **2012**, *48*, 5283(d) Vasimalla, S.; Senanayak, S. P.; Sharma, M.; Narayan, K. S.; Iyer, P. K. *Chem. Mater.* **2014**, *26*, 4030.
- (99) Sajoto, T.; Tiwari, S. P.; Li, H.; Risko, C.; Barlow, S.; Zhang, Q.; Cho, J.-Y.; Brédas, J.-L.; Kippelen, B.; Marder, S. R. *Polymer* **2012**, *53*, 1072.
- (100) Sommer, M. *J. Mater. Chem. C* **2014**, *2*, 3088.
- (101) Senkovskyy, V.; Tkachov, R.; Komber, H.; Sommer, M.; Heuken, M.; Voit, B.; Huck, W. T. S.; Kataev, V.; Petr, A.; Kiriy, A. *J. Am. Chem. Soc* **2011**, *133*, 19966.
- (102) P., Y.; SerapA.; K., B.; D, Y.; I., S. *Turk. J. Chem*, *28*, 415 { 424.
- (103) Barros, T. C.; Brochsztain, S.; Toscano, V. G.; Filho, P. B.; Politi, M. J. *J. Photochem. Photobiol. A* **1997**, *111*, 97.
- (104) Ozser, M. E.; Uzun, D.; Elci, I.; Icil, H.; Demuth, M. *Photochem. Photobiol. Sci.* **2003**, *2*, 218.
- (105) Flamigni, L.; Wyrostek, D.; Voloshchuk, R.; Gryko, D. T. *Phys. Chem. Chem. Phys.* **2010**, *12*, 474.
- (106) (a) Huang, C.; Barlow, S.; Marder, S. R. *J. Org. Chem* **2011**, *76*, 2386(b) Guo, X.; Facchetti, A.; Marks, T. J. *Chem. Rev.* **2014**, *114*, 8943.
- (107) Molla, M. R.; Das, A.; Ghosh, S. *Chem. Commun.* **2011**, *47*, 8934.

- (108) Kasha, M.; Rawls, H. R.; EL-BAYOUMI Hraf El-Bayoumi, M. *Pure Appl. Chem.* **1965**, *11*, 371.
- (109) (a) Molla, M. R.; Gehrig, D.; Roy, L.; Kamm, V.; Paul, A.; Laquai, F.; Ghosh, S. *Chem. Eur. J.* **2014**, *20*, 760(b) Shao, H.; Seifert, J.; Romano, N. C.; Gao, M.; Helmus, J. J.; Jaroniec, C. P.; Modarelli, D. A.; Parquette, J. R. *Angew. Chem. Int. Ed.* **2010**, *49*, 7688(c) Tu, S.; Kim, S. H.; Joseph, J.; Modarelli, D. A.; Parquette, J. R. *J. Am. Chem. Soc.* **2011**, *133*, 19125.
- (110) (a) Basak, S.; Nandi, N.; Baral, A.; Banerjee, A. *Chem. Commun.* **2015**, *51*, 780(b) Ghosh, S.; Li, X.-Q.; Stepanenko, V.; Würthner, F. *Chem. Eur. J.* **2008**, *14*, 11343.
- (111) Lee, S. K.; Zu, Y.; Herrmann, A.; Geerts, Y.; Müllen, K.; Bard, A. J. *J. Am. Chem. Soc.* **1999**, *121*, 3513.
- (112) (a) Ortiz, R. P.; Herrera, H.; Blanco, R.; Huang, H.; Facchetti, A.; Marks, T. J.; Zheng, Y.; Segura, J. L. *J. Am. Chem. Soc.* **2010**, *132*, 8440(b) Gawrys, P.; Djurado, D.; Rimarčík, J.; Kornet, A.; Boudinet, D.; Verilhac, J.-M.; Lukeš, V.; Wielgus, I.; Zagorska, M.; Pron, A. *J. Phys. Chem. B* **2010**, *114*, 1803(c) Hu, Y.; Gao, X.; Di, C.-a.; Yang, X.; Zhang, F.; Liu, Y.; Li, H.; Zhu, D. *Chem. Mater.* **2011**, *23*, 1204.
- (113) Horowitz, G.; Kouki, F.; Spearman, P.; Fichou, D.; Nogues, C.; Pan, X.; Garnier, F. *Adv. Mater.* **1996**, *8*, 242.
- (114) Laquindanum, J. G.; Katz, H. E.; Dodabalapur, A.; Lovinger, A. J. *J. Am. Chem. Soc.* **1996**, *118*, 11331.
- (115) See, K. C.; Landis, C.; Sarjeant, A.; Katz, H. E. *Chem. Mater.* **2008**, *20*, 3609.
- (116) Deng, P.; Yan, Y.; Wang, S.-D.; Zhang, Q. *Chem. Commun.* **2012**, *48*, 2591.
- (117) Malenfant, P. R. L.; Dimitrakopoulos, C. D.; Gelorme, J. D.; Kosbar, L. L.; Graham, T. O.; Curioni, A.; Andreoni, W. *Appl. Phys. Lett.* **2002**, *80*, 2517.
- (118) Chesterfield, R. J.; McKeen, J. C.; Newman, C. R.; Ewbank, P. C.; da Silva Filho, D. A.; Brédas, J.-L.; Miller, L. L.; Mann, K. R.; Frisbie, C. D. *J. Phys. Chem. B* **2004**, *108*, 19281.
- (119) Tatemichi, S.; Ichikawa, M.; Koyama, T.; Taniguchi, Y. *Appl. Phys. Lett.* **2006**, *89*, 112108.
- (120) An, Z.; Yu, J.; Jones, S. C.; Barlow, S.; Yoo, S.; Domercq, B.; Prins, P.; Siebbeles, L. D. A.; Kippelen, B.; Marder, S. R. *Adv. Mater.* **2005**, *17*, 2580.
- (121) Piliago, C.; Jarzab, D.; Gigli, G.; Chen, Z.; Facchetti, A.; Loi, M. A. *Adv. Mater.* **2009**, *21*, 1573.

- (122) Schmidt, R.; Ling, M. M.; Oh, J. H.; Winkler, M.; Könemann, M.; Bao, Z.; Würthner, F. *Adv. Mater.* **2007**, *19*, 3692.
- (123) (a) Gao, X.; Di, C.-a.; Hu, Y.; Yang, X.; Fan, H.; Zhang, F.; Liu, Y.; Li, H.; Zhu, D. *J. Am. Chem. Soc.* **2010**, *132*, 3697(b) Tan, L.; Guo, Y.; Zhang, G.; Yang, Y.; Zhang, D.; Yu, G.; Xu, W.; Liu, Y. *J. Mater. Chem* **2011**, *21*, 18042.
- (124) Polander, L. E.; Tiwari, S. P.; Pandey, L.; Seifried, B. M.; Zhang, Q.; Barlow, S.; Risko, C.; Brédas, J.-L.; Kippelen, B.; Marder, S. R. *Chem. Mater.* **2011**, *23*, 3408.
- (125) Jones, B. A.; Facchetti, A.; Wasielewski, M. R.; Marks, T. J. *Adv. Funct. Mater.* **2008**, *18*, 1329.
- (126) Krebs, F. C. *Sol. Energy Mater. Sol. Cell* **2009**, *93*, 394.
- (127) (a) Søndergaard, R.; Hösel, M.; Angmo, D.; Larsen-Olsen, T. T.; Krebs, F. C. *Mater. Today* **2012**, *15*, 36(b) Krebs, F. C. *Sol. Energy Mater. Sol. Cell* **2009**, *93*, 1636.
- (128) Mikroyannidis, J. A.; Stylianakis, M. M.; Sharma, G. D.; Balraju, P.; Roy, M. S. *J. Phys. Chem. C* **2009**, *113*, 7904.
- (129) (a) Tan, Z. a.; Zhou, E.; Zhan, X.; Wang, X.; Li, Y.; Barlow, S.; Marder, S. R. *Appl. Phys. Lett.* **2008**, *93*, 073309(b) Cheng, P.; Ye, L.; Zhao, X.; Hou, J.; Li, Y.; Zhan, X. *Energy Environ. Sci.* **2014**, *7*, 1351.
- (130) Steyrleuthner, R.; Schubert, M.; Jaiser, F.; Blakesley, J. C.; Chen, Z.; Facchetti, A.; Neher, D. *Adv. Mater.* **2010**, *22*, 2799.
- (131) Szendrei, K.; Jarzab, D.; Chen, Z.; Facchetti, A.; Loi, M. A. *J. Mater. Chem* **2010**, *20*, 1317.
- (132) (a) Fabiano, S.; Chen, Z.; Vahedi, S.; Facchetti, A.; Pignataro, B.; Loi, M. A. *J. Mater. Chem* **2011**, *21*, 5891(b) Moore, J. R.; Albert-Seifried, S.; Rao, A.; Massip, S.; Watts, B.; Morgan, D. J.; Friend, R. H.; McNeill, C. R.; Siringhaus, H. *Adv. Energy. Mater.* **2011**, *1*, 230.
- (133) Schubert, M.; Dolfen, D.; Frisch, J.; Roland, S.; Steyrleuthner, R.; Stiller, B.; Chen, Z.; Scherf, U.; Koch, N.; Facchetti, A.; Neher, D. *Adv. Energy. Mater.* **2012**, *2*, 369.
- (134) Kim, R.; Amegadze, P. S. K.; Kang, I.; Yun, H.-J.; Noh, Y.-Y.; Kwon, S.-K.; Kim, Y.-H. *Adv. Funct. Mater.* **2013**, *23*, 5719.
- (135) Kim, F. S.; Guo, X.; Watson, M. D.; Jenekhe, S. A. *Adv. Mater.* **2010**, *22*, 478.

Chapter 2

Structure Engineering of Naphthalenediimide Small Molecules: Effect of Self-assembly on Charge Transport Properties

This chapter has been adapted from following publication

Nagesh B. Kolhe, R. N. Devi, S. P. Senanayak, B. Jancy, K. S.Narayan and S. K. Asha* *J. Mater. Chem.* **2012**, 22, 15235-15246.

2.1. Introduction

In recent years, naphthalenediimides (NDIs) have attracted much attention due to their electron deficient nature and tendency to form self-organization via aromatic π - π stacking. They were extensively utilized for the construction of supramolecular π -functional materials which exhibited very interesting electronic and spectroscopic properties that find diverse applications in biological and electronic field.¹ Particularly, they showed high electron mobilities and efficiency in optoelectronic devices such as OFETs and solar cells respectively and became popular n-type semiconducting material.² Most of the NDI based small molecular architectures exhibited tendency to form well defined molecular motifs along with high crystalline nature which helped to improve the charge carrier mobility in OFET device.^{2h,i,3} However, a fundamental requirement in the development of new materials with improved properties is the challenging task of achieving a rigorous understanding of the relationship between molecular structure and charge transport properties. Efficient charge transport has been associated with better packing leading to strong electronic coupling between neighboring molecules.⁴ However, attaining high charge carrier mobilities is not just a question of simple design principles. It is known that for the same organic molecule, the observed charge carrier mobilities vary depending on the mode of processing – vacuum deposited, spin coated or single crystal.⁵ Defects are observed even using controlled growth deposition techniques of crystalline thin-films in the form of different degree of crystallinity, morphology at the dielectric interface, grain boundaries, twinning and grain connectivity.⁶ All these strongly affect the electrical transport property of the resultant film as multiple length scales are involved in the electrical transport in such systems. The charge motion in these films have a hopping like transport at the dielectric –semiconductor interface which has higher density of defect states and band like transport is dominant in the ordered bulk of the crystalline thin films.⁷ Thus, bottom-up approaches designed at enabling microscopic control over crystal engineering has been the focus of increasing attention in this area of research, where the success is often gauged by the enhancement of the microscopic mobility. However crystal engineering is still a matter of trial and error and a simple structural variation has been shown to have a huge impact on the way a molecule organizes in the solid state. A face-to-face arrangement of molecule may enhance the π - π overlap, however charge transport seems to be further enhanced with slipped

crystal packs since 2-D structure is preserved.⁸ The rational design of molecules with improved optoelectronic properties should take into account their geometrical as well as electrical structures. For instance, pentacene crystal has a herringbone structure with an angle of 52° between molecular planes whereas perfluoropentacene are packed nearly perpendicular along the same direction.⁹ Perfluoropentacene has exhibited electron transport with mobilities $\sim 0.22 \text{ cm}^2 \text{ V}^{-1}\text{s}^{-1}$ in FET devices whereas pentacene exhibits FET hole mobilities in the range of $0.5 - 1 \text{ cm}^2 \text{ V}^{-1}\text{s}^{-1}$. In these examples, both band gap engineering of the HOMO-LUMO gap and crystal engineering of face-to-face π stacking play a role in the nature as well as efficiency and stability of charge transport. Among the n type materials other than C_{60} derivatives both naphthalene and perylene diimides (NDI/PDI) have been studied quite extensively.¹⁰ In small molecules based on naphthalene diimide (NDI) or perylene diimide (PDI) also, the effect of small structural variations on the molecular packing and thin film morphology has been intensely looked into. For instance Shukla *et al.* described the effect of a simple structural variation like that of a cyclohexyl end group on the overall crystalline packing and charge carrier mobility³ (**Figure 2.1**).

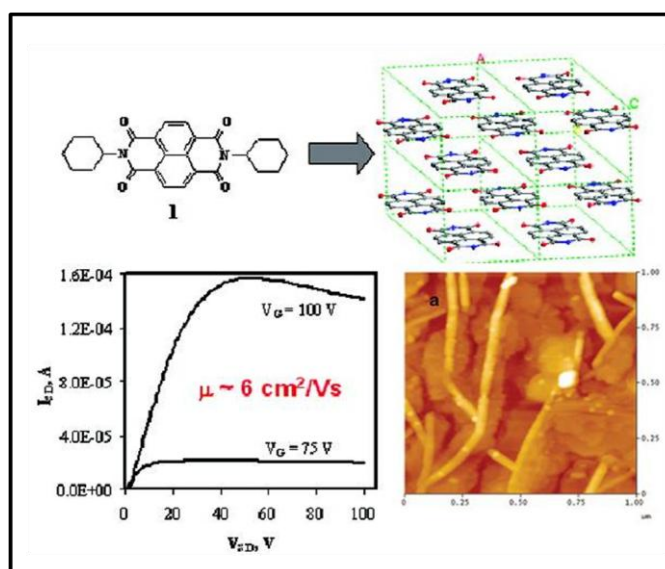


Figure 2.1 Molecular structure, crystal packing, thin film morphology (AFM) and output I - V curves of N,N' -dicyclohexyl NDI. (Adapted from Ref³)

They demonstrated a dramatic improvement in FET mobility of $\sim 6 \text{ cm}^2 \text{ V}^{-1}\text{s}^{-1}$ which was attributed to the propensity of the cyclohexyl terminated NDI derivatives to assemble into thin films with bulk phase crystalline packing. The possibility of using

non covalent interactions like π -stacking and hydrogen bonding to drive the molecule to pack in the favored arrangement for improved charge carrier transport is an interesting question to address. A few reports are available in literature where researchers have sought answers to the above question.¹¹ An example of crystal engineering taking help from hydrogen bonding interactions was provided by Wurthner *et al.* where they introduced eight chlorine substituents on the bay position of perylene derivative (Cl_8 -PTCDI) having free NH imide functionalities that could involve in H bonding^{11d} (**Figure 2.2**).

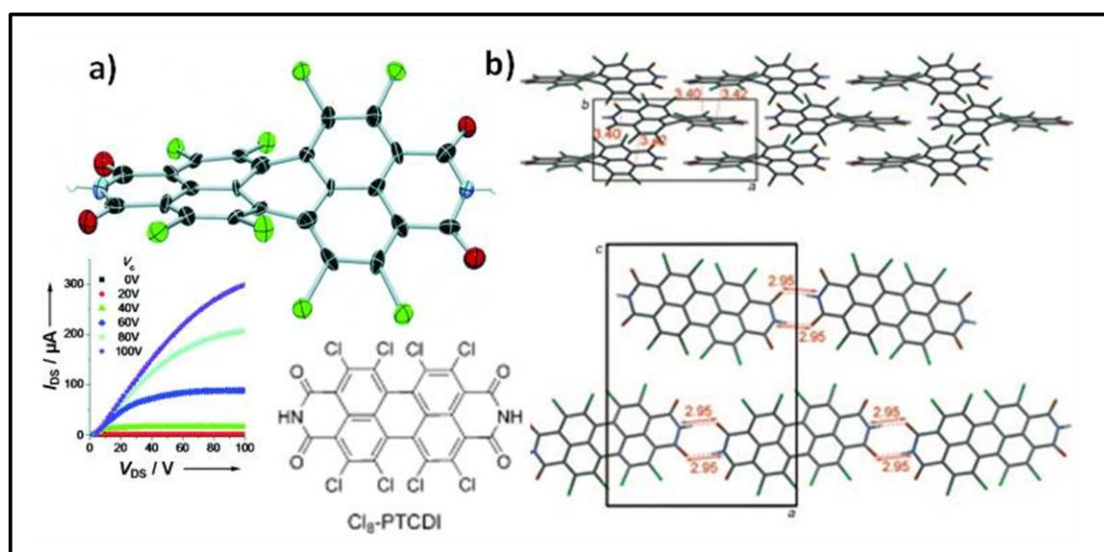


Figure 2.2 (a) molecular structure of Cl_8 -PTCDI in the single crystal and (b) packing arrangement by viewing onto a, b and a, c plane. (Adapted from Ref^{11d})

The combination of NH imide group induced H bonding and the contortion of the ring afforded by the bay substitution resulted in a two-dimensional π - π -stacked percolation path for electron transport. The molecule exhibited excellent air-stable operation with a mobility as high as $0.82 \text{ cm}^2 \text{ V}^{-1} \text{ s}^{-1}$ with $I_{\text{on}} / I_{\text{off}}$ of 10^8 . In this example, the supramolecular ordering aided crystallization in the preferred direction. However, supramolecular organization can alter or compete with free crystallization to restrict the charge transport in all directions. Thus, the question of supramolecular ordering versus crystallinity – which is better at inducing higher charge carrier mobility, is of fundamental importance.

This chapter aims to address the question of effect of three-dimensional crystalline organization versus directional self-assembly on electron transport

mobility in naphthalenediimide (NDI) derivatives. Two series of molecules based on NDI were chosen for this study having identical structure except for a replacement of ester group with amide (**Figure 2.3**).

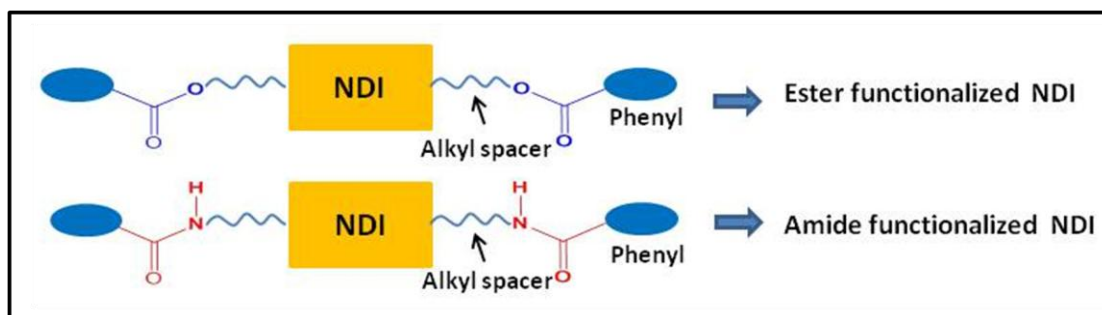


Figure 2.3 Design of naphthalenediimide based ester and amide molecules.

The NDI derivatives with ester linkage did not have the additional non-covalent interaction in the form of hydrogen bonding to direct the molecular organization, whereas the amide molecules had a directional hydrogen bonding of the amide linkage as a constraint to restrict their freedom of organization. The effect of this minor structural alteration on the self organizing properties in solution was probed using UV-Vis absorption and fluorescence emission studies. The solid state organization was studied using wide angle X-ray diffraction (WXR), differential scanning calorimetry (DSC) and polarized light microscopy (PLM). Hydrogen bonding in the amide molecules was traced using variable temperature FT-IR studies in the solid state. The charge transport characteristics of these NDI derivatives were compared in an organic field effect transistor (OFET) in bottom gate top contact geometry. A better understanding of the structure-device performance relationship in the NDI/PDI class of compounds is essential to be able to design better molecules as well as to extract the best device performance from them.

2.2. Experimental Section

2.2.1 Materials

1,4,5,8-Naphthalenetetracarboxylicdianhydride (NTCDA), 1,6-diaminohexane, 6-aminohexanol, *N,N* dimethylacetamide (DMAc), 3,4,5-trihydroxy benzoic acid and benzoyl chloride were purchased from Sigma Aldrich and used without further purification. Zinc acetate, imidazole, thionyl chloride and pyridine were purchased locally and purified using standard procedures.

2.2.2 Instrumentations Details

^1H NMR spectra were recorded using 200-MHz Bruker NMR spectrophotometer in CDCl_3 containing small amounts of TMS as internal standard. The purity of the compounds was determined by elemental analysis, as well as MALDI-TOF. Elemental analysis was done using Thermofinnigan flash EA 1112 series, CHNS analyser. The matrix used for MALDI was 2,5 dihydroxy benzoic acid dissolved in CHCl_3 which was spotted on MALDI target and allowed to dry before introducing into the mass spectrometer. The purity of the oligomers was further analyzed by SEC (size exclusion chromatography) in chloroform using polystyrene standards for the calibration. The flow rate of CHCl_3 was maintained as 1 $\mu\text{L}/\text{min}$ throughout the experiments, and the sample solutions at concentrations 2-3 mg/mL were filtered and injected for recording the chromatograms at 30 $^\circ\text{C}$. FTIR spectra were recorded using Bruker α -T spectrophotometer in the range of 4000 to 400 cm^{-1} . UV-Vis spectra were recorded using Perkin Elmer Lambda 35 UV-Vis spectrometer. The emission studies were performed by SPEX Fluorolog F112X spectrofluorimeter. The fluorescence quantum yields of the naphthalene derivatives were determined in chloroform using quinine sulfate in 0.5 M sulfuric acid ($\phi = 0.546$) as the standard by exciting at 360 nm. The optical density at λ_{382} was maintained at 0.1 ± 0.05 to avoid re-absorption artifacts. For recording solid state photo physical properties, thin films were spin coated (1000 rpm/60sec) from chloroform as well as *o*-DCB (orthodichlorobenzene) solution on a quartz plate. Thermogravimetric analysis (TGA) was performed using a PerkinElmer STA 6000 thermogravimetric analyser. Samples were run from 40 to 800 $^\circ\text{C}$ with a heating rate of 10 $^\circ\text{C}/\text{min}$ under nitrogen. Differential scanning calorimeter (DSC) measurements were performed on TA Q10 differential scanning calorimeter at a heating rate of 10 $^\circ\text{C}/\text{min}$ under nitrogen

atmosphere. Typically, 2-3 mg of samples was placed in an aluminum pan, sealed properly and scanned from - 50 to 300 °C. The phase behaviors of the molecules were analyzed using LIECA DM2500P polarized optical microscope equipped with Linkam TMS 94 heating and cooling stage connected to a Linkam TMS 600 temperature programmer. The X-ray diffraction data were recorded by using a Philips analytical diffractometer using Cu K α emission, and the spectra were recorded in the range of (2θ) 3–50° and analyzed using X'pert software. Powder X-ray diffraction of all the samples was carried out in a PANalytical X'pert Pro dual goniometer diffractometer. An X'celerator solid-state detector was employed in wide-angle experiments. The radiation used was Cu K α (1.54 Å) with a Ni filter and the data collection was carried out using a flat holder in Bragg-Brentano geometry. Care was taken to avoid sample displacement effects. Variable temperature in situ XRD experiments were carried out in an Anton-Paar XRK900 reactor. AFM images were taken by a MultimodeTM Scanning Probe Microscope equipped with Nanoscope IVTM controller from Veeco Instrument Inc., Santa Barbara in the tapping mode using a SiN probe, with maximum scan size 10 μ m x10 μ m and with vertical range of 2.5 μ m. For the AFM studies, sample were prepared by spin coating 1x10⁻³ M solution in o-DCB on glass slide and allowing to dry before subjecting to of AFM analysis. FEI-TecnaiTM-F30 electron microscope operating at 100 KV was used for HR-TEM sample observation which was equipped with Gatan digital camera for recording micrographs. Electrochemical behavior of NDI ester and amide derivatives were studied using BAS-Epsilon potentiostat.

2.2.3 Device Fabrication (OFET)

Bottom-gate top contact structures were fabricated for field effect transistor studies as per standard procedures. Hydroxyl free divinyltetramethylsiloxanebis-benzocyclobutene (BCB) polymer dielectric was spin coated at 1000 rpm for 1 min and annealed at 290 °C under glove box (N₂) atmosphere. The dielectric thin film thus formed had a capacitance per unit area (C₀) ~ 2-4 nF/cm² measured using Keithley 4200 semiconductor parameter analyzer for a film of thickness 0.5-0.6 μ m. The surface of the dielectric was coated (1500 rpm for 30 s) with a thin monolayer of Hexamethyldisilazane (HMDS) and annealed at 110 °C for 2 h This was followed by spin coating of the solution prepared from 1, 2 -Dichlorobenzene solution with

concentration 25 mg/ml at 300-400 rpm for 1 minute to obtain films with thickness ~100 nm. The average and the highest mobility magnitude of each system are mentioned in the table and is based on measurements on a number of devices (~ 10 - 15 devices of each molecule).

2.2.4 Synthesis

Synthesis of ester functionalized naphthalenediimides.

N,N'-bis[6-hydroxyhexyl]naphthalene-1,4,5,8-tetracarboxyldiimide (Naphth6diol):

1, 4, 5, 8-naphthalene tetracarboxylic dianhydride (NTCDA) (1.00 g, 3.73 mmol), 6-aminohexanol (0.96 g, 8.2 mmol) and catalytic amount of zinc acetate in DMAc (20 mL) were heated to 90 °C for three hours under nitrogen atmosphere. The reaction temperature was increased to 130 °C and stirred for 15 h under nitrogen atmosphere. The excess of solvent was distilled off and the slurry was washed several times with hexane and precipitated into acetone. The precipitate was filtered and dried in a vacuum oven (0.1 mm of Hg) for 12 hours. Yield: 1.546 g (88 %); ¹H NMR (200 MHz, CDCl₃, TFA) δ ppm: 8.87 (s, 4H, naphthalene), 4.44 (t, 4H, CH₂ OH), 4.30 (t, 4H, imideCH₂), 1.60-1.84 (16H, CH₂) FT-IR (KBr, cm⁻¹): 3545, 3515, 2930, 2863, 1690, 1658, 1592, 1433, 1402, 1390, 1345, 1262, 1090, 978, 856, 809, 748, 636, 495.

Methyl-3, 4, 5-tridodecyloxybenzoate (a): Methyl-3, 4, 5-trihydroxybenzoate (Methyl gallate) (5 g, 27.17 mmole) and activated K₂CO₃ (37.54 g) were taken in dry DMF and stirred. 1-bromododecane (23.68 g, 95.10 mmol) was added and the reaction mixture was heated to 90 °C with stirring for 36 h. The reaction mixture was cooled to room temperature, poured into water and extracted with DCM. The organic layer was washed with 5 % NaOH and brine, dried over sodium sulphate, and concentrated on rotary evaporator. The crude product was purified by column chromatography on silica gel eluting with petroleum ether: ethyl acetate 95:5 to get white solid. Yield: 11.5g (62 %) ¹H NMR (200 MHz), CDCl₃) δ ppm: 7.26 (d, 2H, aromatic), 4.01 (t, 2H OCH₂), 3.89 (s, 3H, COOCH₃), 1.78-1.26 (m, 60 H), 0.88 (t, 9H).

3, 4, 5-tridodecyloxybenzoic acid (b): Methyl-3, 4, 5-tridodecyloxybenzoate (5 g, 7.2 mmole) and KOH (0.43g, 10.8 mmol) in ethanol (40 mL) and water (20 mL) was refluxed for 12 h The reaction mixture was diluted with water and acidified with dilute hydrochloric acid, extracted with ethyl acetate. The organic layer was washed with brine and dried over sodium sulphate and solvent removed under vacuum. Yield

4.4 g (88 %) ^1H NMR (200 MHz, CDCl_3) δ ppm: 7.26 (d, 2H, aromatic), 4.01 (t, 2H OCH_2), 1.78-1.26 (m, 60 H), 0.88 (t, 9H).

3,4, 5-tridodecyloxybenzoyl chloride (c): 3, 4, 5-tridodecyloxybenzoic acid (1.5 g) was dissolved in minimum amount of thionyl chloride (5 mL) and refluxed at 90 °C for 6 h. The excess solvent was distilled off, and resultant product was vacuum dried to remove thionyl chloride Yield 1.3 g (87 %). The conversion of acid to acid chloride was monitored by FT-IR spectrum which showed complete conversion of $-\text{COOH}$ (1685 cm^{-1}) to $-\text{COCl}$ (1753 cm^{-1}).

***N,N'*-Bis[6-hexylbenzester]naphthalene-1,4,5,8-tetracarboxyldiimide (NDI-E):** (0.5 g, 1.07 mmol) of *N,N'*-bis[6-hydroxyhexyl]naphthalene-1,4,5,8-tetracarboxyldiimide (Naphth6diol) in 10 mL dry pyridine was heated to 90 °C under nitrogen atmosphere to obtain a homogeneous solution. To this solution benzoyl chloride (0.33 g, 2.36 mmol) was added drop wise over a period of 15 min. The reaction was continued for 12 h and then the excess solvent was removed by distillation under reduced pressure and the slurry was poured into acetone. The obtained precipitate was filtered and dried in vacuum oven for 12 h (0.1 mm of Hg). The crude compound was purified by column chromatography using chloroform/methanol (98:2 v/v). Yield : 0.59 g (82 %); ^1H NMR (200 MHz, CDCl_3) δ ppm: 8.73 (s, 4H, Ar naphthalene), 8.02 (d, 4H, Ar benzoyl), 7.54 (m, 2H Ar benzoyl), 7.40, (m, 4H Ar benzoyl), 4.34 (t, 4H, ester CH_2), 4.22 (t, 4H, imide CH_2), 1.80- 1.54 (16H, CH_2). ^{13}C NMR (400 MHz, CDCl_3) δ ppm: 166.56, 162.75, 132.75, 130.88, 129.44, 128.24, 126.49, 64.86, 40.70, 28.53, 27.80, 26.64, 25.73. FTIR (KBr, cm^{-1}): 2939, 2851, 1725, 1660, 1586, 1453, 1371, 1340, 1272, 1245, 1106, 772, 707; Anal. Calcd. for $\text{C}_{40}\text{H}_{38}\text{N}_2\text{O}_8$: C, 71.20; H, 5.68; N, 4.15. Found C, 70.76; H, 5.23; N, 4.15. MALDI-TOF MS (MW = 674); m/z = 697.33 [$\text{M} + \text{Na}$] $^+$, 713.28 [$\text{M} + \text{K}$] $^+$.

***N,N'*-Bis[6-hexyl-3,4,5-tridodecyloxybenzester]naphthalene-1,4,5,8-tetracarboxyldiimide (NDI-E3):** NDI-E3 was synthesized using the same procedure as that given for NDI-E but with (0.5 g, 1.07 mmol) of *N,N'*-bis[6-hydroxyhexyl]naphthalene-1,4,5,8-tetracarboxyldiimide (Naphth6diol) and (1.85 g, 2.67 mmol) 3,4,5-tridodecyloxy benzoyl chloride (c). The crude compound was purified by column chromatography using chloroform/methanol (99:1 v/v). Yield: 1.3 g (68 %). ^1H NMR (300 MHz, CDCl_3) δ ppm: 8.73 (s, 4H, Ar naphthalene), 7.22 (s, 4H, Ar benzoyl), 4.28 (t, 4H, ester CH_2), 4.20 (t, 4H imide CH_2), 3.99 (t, 12H OCH_2), 1.8-1.24 (m, 136H, CH_2),

0.86 (t, 18H, CH_3). ^{13}C NMR (200 MHz, CDCl_3) δ ppm: 166.46, 162.79, 152.75, 142.26, 130.91, 126.57, 124.91, 107.90, 73.45, 69.13, 64.93, 40.73, 31.90, 30.30, 29.62, 29.34, 28.61, 27.91, 26.69, 26.03, 25.70, 22.67, 14.10. FTIR (KBr, cm^{-1}): 2920, 2850, 1717, 1699, 1667, 1581, 1500, 1468, 1430, 1344, 1348, 1245, 1218, 1122, 993 and 770. Anal. Calcd. for $\text{C}_{112}\text{H}_{182}\text{N}_2\text{O}_{14}$: C, 75.55; H, 10.30; N, 1.57. Found C, 75.51; H, 10.85; N, 1.67. MALDI-TOF MS (MW =1780.65); m/z =1888.82 $[\text{M}+\text{Ag}]^+$.

Synthesis of amide functionalized naphthalenediimides.

Mono protection of 1, 6-diaminohexane (d): Phthalic anhydride (1.48 g, 0.02 mol) was added to the solution of acetic acid containing 1, 6- aminohexane (1.16 g, 0.02 mol) and heated at 110 °C for 3-4 h. The acetic acid was evaporated by distillation which was followed by addition of 80 mL deionized water to the resultant solution. The di-substituted derivative i.e. diphthalimido- N, N' -hexane was precipitated out from aqueous solution which was filtered off. The water soluble mono protected compound was recovered after evaporation of aqueous phase. Yield: 2.2 g (90 %). ^1H NMR (200 MHz, CDCl_3) δ ppm: 7.79-7.71 (m, 4H, Ar), 5.54 (broad, 2H, NH_2), 3.65 (t, 2H, CH_2), 2.82 (t, 2H, CH_2), 1.65 (m, 4H), 1.37 (m, 4H, CH_2).

***N*-phthalimido *N'*-benzamide hexane (e):** The mono protected amine (d) (1.2 g, 4.87 mmole) was dissolved in 40 mL acetonitrile. Then, 2.01g of K_2CO_3 was added to the solution followed by drop wise addition of benzoyl chloride (1.02 g, 7.30 mmol) at 0 °C over 15 min. The reaction mixture was stirred at room temperature for overnight. The resultant solution was poured into a mixture of 100 mL of water and 80 mL of chloroform. The compound was extracted with chloroform, dried over sodium sulphate and concentrated on rotary evaporator. The crude product was purified by column chromatography on silica gel eluting with petroleum ether: ethyl acetate 70:30. Yield : 1.0 g (60 %). ^1H NMR (200 MHz, CDCl_3) δ ppm: 7.74-7.35 (m, 9H, Ar amide and imide), 6.21 (broad, 1H, NHCO) 3.62 (t, 2H, CH_2 imide), 3.39 (t, 2H, CH_2 amide), 1.36-1.67 (m, 8H, CH_2).

***N*-phthalimido *N'*-3,4,5-tridodecyloxy benzamide hexane (f):** The mono protected amine (d) (1.8 g, 7.31 mmole) and triethyl amine (0.8 g, 7.31 mmol) was dissolved in 30 mL dry THF. 3,4,5- tridodecyloxy benzoyl chloride (c) (6.08 g, 8.78 mmol) was dissolved in 30 mL of THF in another round bottom flask which was subsequently added drop wise to the reaction mixture at 0 °C over half hour. The reaction mixture

was stirred at room temperature for overnight and extracted with chloroform (100 mL x 3), dried over sodium sulphate and concentrated on rotary evaporator. The crude product was purified by column chromatography on silica gel eluting with petroleum ether: ethyl acetate 70:30. Yield : 3.63 g (55 %). ^1H NMR (200 MHz, CDCl_3) δ ppm: 7.72-7.80 (m, 4H, Ar imide), 6.97 (s, 2H, Ar amide) 6.20 (1H, NHCO) 3.99 (t, 6H, OCH_2), 3.69 (t, 2H, CH_2 imide), 3.41 (t, 2H, CH_2 amide), 1.74-1.24 (m, 68H, CH_2), 0.86 (t, 9H, CH_3).

***N* - (6-aminohexyl) benzamide (g)**: The mixture of *N*-phthalimido *N'*-benzamide hexane (e) (0.6 g, 1.71 mmol) and hydrazine hydrate (0.71 mL) was dissolved in 20 mL of ethanol. The solution was stirred at room temperature for 48 h. The reaction mixture was filtered and evaporated followed by addition of 50 mL acetonitrile. The resultant solution was stirred for 30 min. after which it was filtered and evaporated to get the desired compound. Yield: 0.150 g (40 %). ^1H NMR (200 MHz, CDCl_3) δ ppm: 7.76-7.43 (m, 5H, Ar), 6.24 (broad, 1H, NHCO) 3.45 (t, 2H, CH_2 amide), 2.66 (t, 2H, CH_2), 1.38-1.67 (m, 8H, CH_2).

***N*-(6-aminohexyl) 3,4,5-tridodecyloxy benzamide (h)**: The mixture of *N*-phthalimido *N'*-3,4,5-tris(dodecyloxy) benzamide hexane (f) (2.8 g, 3.1 mmol) and hydrazine hydrate (2.5 mL) was dissolved in 100 mL of ethanol. The solution was stirred at room temperature for 48 h. The reaction mixture was filtered and evaporated followed by addition of 120 mL chloroform. The resultant solution was stirred for 30 min. after which it was filtered and evaporated to get the desired compound. Yield: 1.2 g (49 %). ^1H NMR (200 MHz, CDCl_3) δ ppm: 6.93 (s, 2H, Ar amide) 6.09 (1H, NHCO) 3.98 (t, 6H, OCH_2), 3.42 (t, 2H, CH_2 amide), 2.68 (t, 2H, CH_2), 1.85-1.25 (m, 68H, CH_2), 0.86 (t, 9H, CH_3)

***N,N'*-Bis[6-hexylbenamide]naphthalene-1,4,5,8-tetracarboxyldiimide (NDI-A)**: (0.5 g, 1.86 mmol) NTCDA, (0.9 g 4.10 mmol) *N* -(6-aminohexyl) benzamide (g), zinc acetate (50 mg) and 20 g of imidazole were taken in a 100 mL two neck round bottom flask and heated up to 130 °C under nitrogen atmosphere for 18 h The reaction mixture was cooled to 90 °C and treated with 150 mL of 2N hydrochloric acid. The crude product was filtered, washed with plenty of distilled water followed by washing with hot methanol and then dried in vacuum oven for 12 h (0.1 mm of Hg). The crude compound was purified by column chromatography using chloroform/methanol (98:2 v/v) Yield: 0.89 g (71 %); ^1H NMR (200 MHz, CDCl_3 + TFA) δ ppm: 8.78 (s, 4H, Ar naphthalene), 7.71-7.44 (m, 10H, Ar benzoyl), 4.22 (t, 4H, CH_2), 3.50 (t, 4H, amide)

CH₂), 1.80- 1.54 (16H, **CH₂**). ¹³C NMR (200 MHz, CDCl₃ + TFA) δ ppm:163.2, 159.9, 130.8, 130.2, 128.8, 128.1, 69.7, 47.4, 40.6, 31.3, 29.6, 29.5, 29.2. FTIR (KBr, cm⁻¹): 3299 (NH), 2938, 2852, 1697 (amide CO), 1652, 1586, 1453, 1371, 1340, 1272, 1245, 1106, 772, 707; Anal. Calcd. for C₄₀H₄₀N₄O₆: C, 71.41; H, 5.99; N, 8.33. Found C, 70.97; H, 5.64; N, 8.77. MALDI-TOF MS (MW = 672.29); m/z = 695.36 [M +Na]⁺, 711.32 [M +K]⁺.

***N,N'*-Bis[6-hexyl-3,4,5-tridodecyloxybenzester]naphthalene1,4,5,8-**

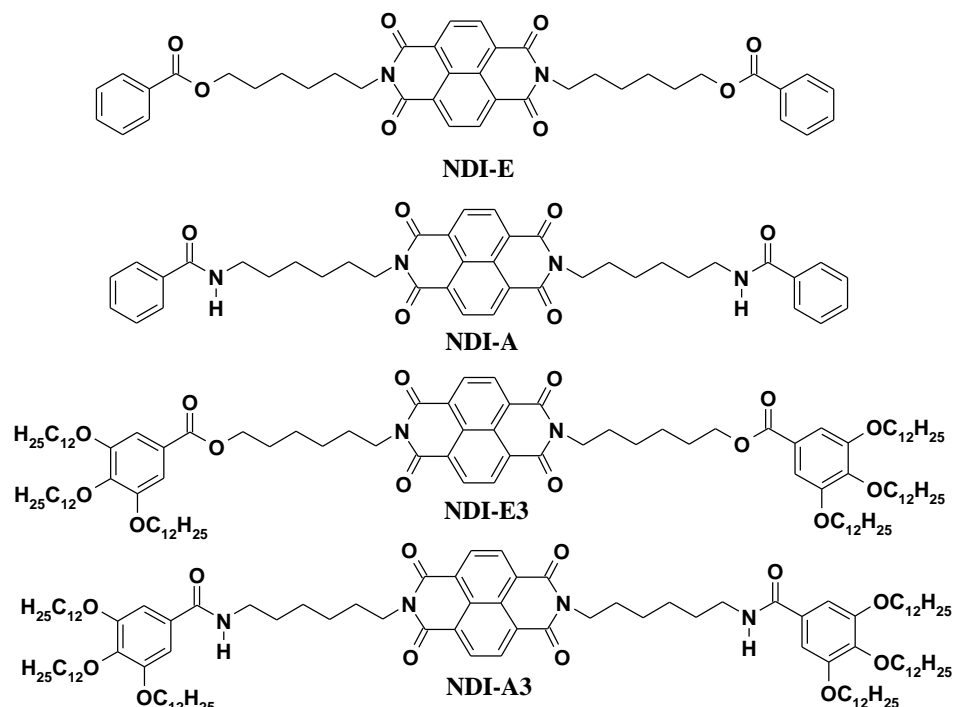
tetracaroxylidimide (NDI-A3): NDI-A3 was synthesized using the same procedure as that given for NDI-A but with (80 mg, 0.268 mmol) of NTCDA and (455 mg, 0.589 mmol) N-(6-aminohexyl) 3,4,5-tris(dodecyloxy) benzamide (**h**). Purified by column chromatography using chloroform/methanol (99:1 v/v) Yield: 0.38 g (77 %). ¹H NMR (200 MHz, CDCl₃) δ ppm: 8.67 (s, 4H, Ar naphthalene), 6.89 (s, 4H, Ar benzoyl), 6.07 (broad NH amide), 4.14, (t, 4H, imide CH₂), 3.93 (t, 12H OCH₂), 4.38 (t, 4H amide CH₂), 1.8-1.24 (m, 136H, CH₂), 0.86 (t, 18H, CH₃). ¹³C NMR (200 MHz, CDCl₃) δ ppm: 166.75, 162.21, 152.41, 140.38, 130.34, 129.11, 125.94, 105,72.83, 68.71, 39.99, 31.28, 29.65, 29.04, 28.72, 27.19, 25.83, 25.43, 22.04, 13.47. FTIR (KBr, cm⁻¹):3272 (amide NH) 2920, 2850, 1701(amide CO), 1699, 1667, 1581, 1500, 1468, 1430, 1344, 1348, 1245, 1218, 1122, 993 and 770. Anal. Calcd. for C₁₁₂H₁₈₄N₄O₁₂: C, 75.63; H, 10.43; N, 3.15. Found C, 75.82; H, 10.89; N, 3.14. MALDI-TOF MS (MW =1778.39); m/z =1886.27 [M+Ag]⁺.

2.3 Results and Discussion

2.3.1 Synthesis and Characterization

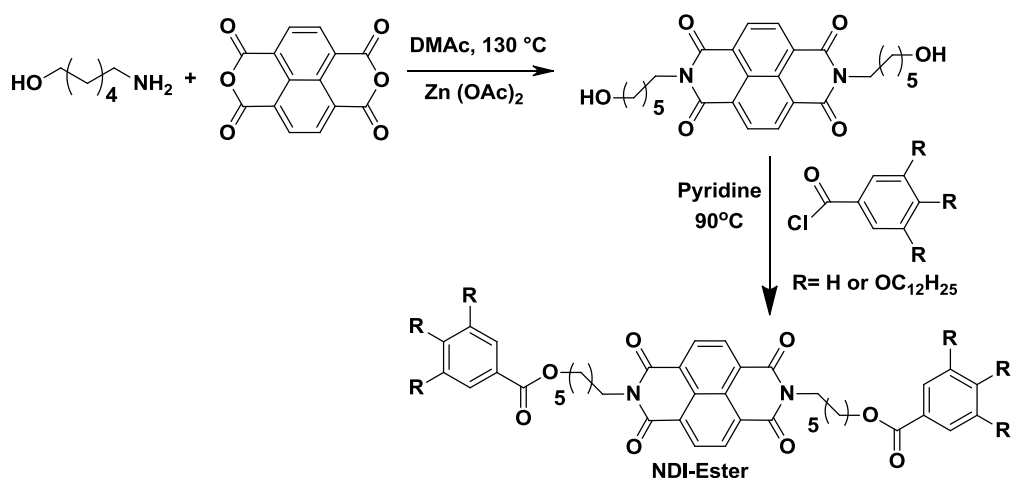
Four derivatives of naphthalenediimides (NDIs) were synthesized by varying the type of linkage (ester or amide) and the flexible alkyl chain attached to the phenyl ring - two without any terminal alkyl chain, and two with 3,4,5- tridodecyloxy substitution. The structures of all four NDIs are shown in **Scheme 2.1**. The NDI ester derivatives

were named **NDI-E** (phenyl substitution) and **NDI-E3** (3,4,5-tridodecyloxy phenyl substitution). Similarly the NDI amide derivatives were named **NDI-A** and **NDI-A3** respectively for the phenyl and 3, 4, 5- tridodecyloxy phenyl substitution.



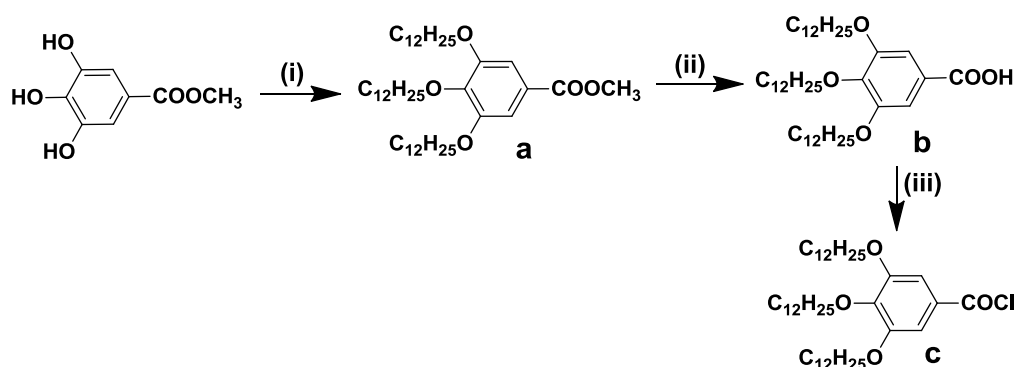
Scheme 2.1 Structures of all NDI-ester and NDI-amide molecules.

The synthesis of the ester functionalized NDI is outlined in **Scheme 2.2 a)** and detailed synthetic procedures are given in experimental section 2.2.4. The synthesis of ester molecule was very straightforward for which a core to periphery approach was adopted.



Scheme 2.2 a) Synthesis of ester functionalized naphthalenediimides.

The first step was the synthesis of hydroxyl functionalized NDI derivative (Naphth6diol) by a reaction between 1, 4, 5, 8-naphthalene tetracarboxylic dianhydride (NTCDA) and two equivalents of 6-aminohexanol in DMAc at 130 °C using $Zn(OAc)_2$ as catalyst. It was further coupled with the corresponding acid chloride such as benzoyl chloride or 3, 4, 5- tridodecyloxy substituted benzoyl chloride in dry pyridine to obtain the ester functionalized molecules. The 3,4,5- tridodecyloxy substituted benzoyl chloride (**Scheme 2.2 b**) required for synthesis of NDI-E3 was obtained from 3,4,5- trihydroxymethyl benzoate by etherification with dodecyl bromide using K_2CO_3 in DMF followed by hydrolysis of ester (**a**) to acid (**b**) which was subsequently converted to acid chloride (**c**) using thionyl chloride.

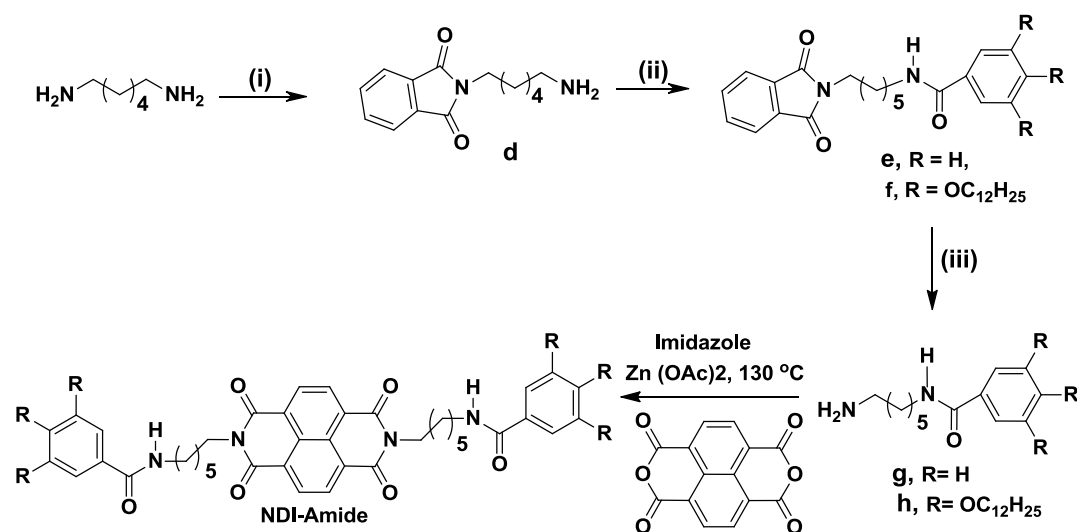


Reaction conditions : (i) DMF, K_2CO_3 , dodecylbromide, 90 °C (ii) KOH, ethanol, 85 °C (iii) $SOCl_2$ 90 °C

Scheme 2.2 b) Synthesis of 3,4,5- tridodecyloxy substituted benzoyl chloride.

The synthesis of the amide functionalized NDI is outlined in **Scheme 2.3** and detailed synthetic procedures are given in experimental section 2.2.4. A periphery to core approach was adopted for the synthesis of amide molecules in which the required acid chloride was first monocoupled with 1, 6 diaminohexane to obtain the amine terminated benzamide derivative (**g** or **h**); two equivalents of which was coupled with NTCDA in imidazole and $Zn(OAc)_2$ to obtain the final amide functionalized molecules. All molecules were purified by using column chromatography with chloroform and methanol as mobile phase. The synthesis of mono-coupled benzamide derivative (**g** or **h**) was achieved using 1, 6 diaminohexane which was first mono-protected with one equivalent of phthalic anhydride in acetic acid (**d**). The mono-protected amine (**d**) was then coupled with required acid chloride (benzoyl chloride or 3, 4, 5- tridodecyloxy benzyl chloride **c**) to induce the amide functionality in molecule (**e** or **f**). This was followed by the selective deprotection of phthalimide group using

hydrazine hydrate as proton source in ethanol to get the final amine terminated benzamide.



Scheme 2.3 Synthesis of amide functionalized naphthalenediimides.

All NDI derivatives were soluble in common organic solvents like tetrahydrofuran (THF), chloroform (CHCl₃) and toluene. The compounds were fully characterized by ¹H, ¹³C NMR spectroscopy, FT-IR, size exclusion chromatography, MALDI-TOF mass spectroscopy and elemental analysis. The labeled ¹H NMR spectra of all NDI-molecules are given in **Figure 2.4 a) and b)**. All NDI derivatives (ester and amide) showed singlet (**a**) at around 8.73-8.67 ppm which corresponded to the aromatic protons of NDI core. The phenyl group attached to hexyl spacer by ester linkage in NDI-E and amide linkage in NDI-A exhibited multiplet in the range of 8.02-7.40 ppm and 7.71-7.44 ppm (**c + d + e**) respectively. On the other hand, the aromatic protons of alkyl substituted phenyl group in NDI-E3 and NDI-A3 appeared as a singlet at 7.22 ppm and 6.89 ppm respectively (**c**). The peaks corresponding to methylene -CH₂ group attached to imide nitrogen and ester of NDI-E and NDI-E3 was slightly overlapped (**b** and **b'**) and appeared at 4.34-4.22 and 4.28-4.20 ppm respectively. Whereas, imide and amide -CH₂ protons of amide derivatives showed two distinct triplet (**b** and **b'**) at 4.22 and 3.50 ppm for NDI-A and at 4.28 and 3.93 ppm for NDI-A3. Additionally, the -NH amide proton of NDI-A3 appeared at 6.07 ppm (**e**). NDI-

E3 and NDI-A3 exhibited additional peaks in alkyl group region at 1.8-0.86 ppm which differentiated them from un-substituted NDI (NDI-E and NDI-A).

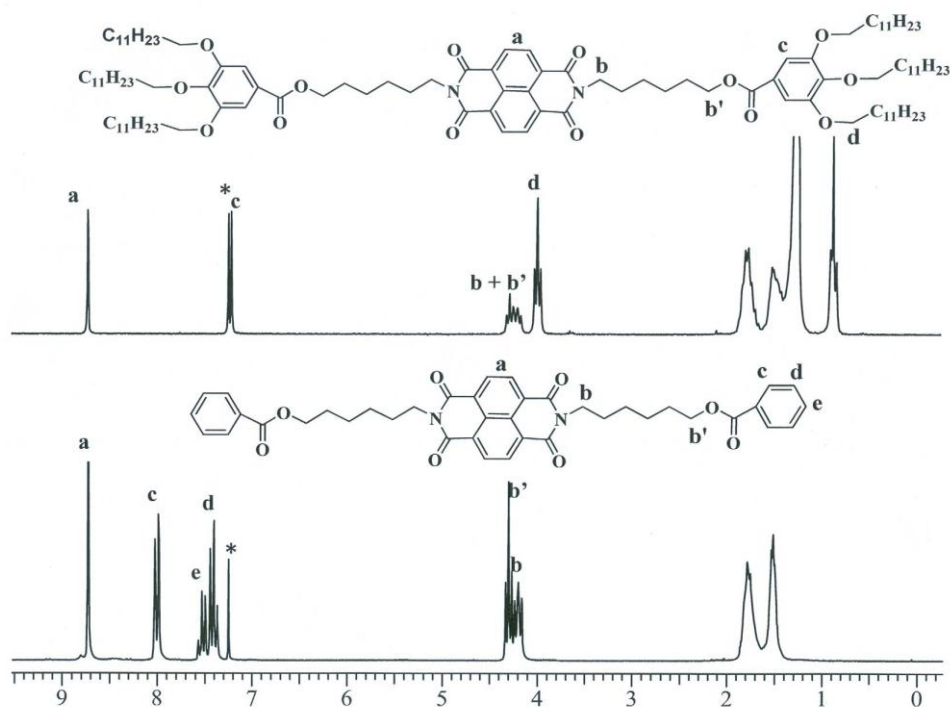


Figure 2.4 a) ¹H NMR spectra of ester NDI-E3 (top), NDI-E (bottom).

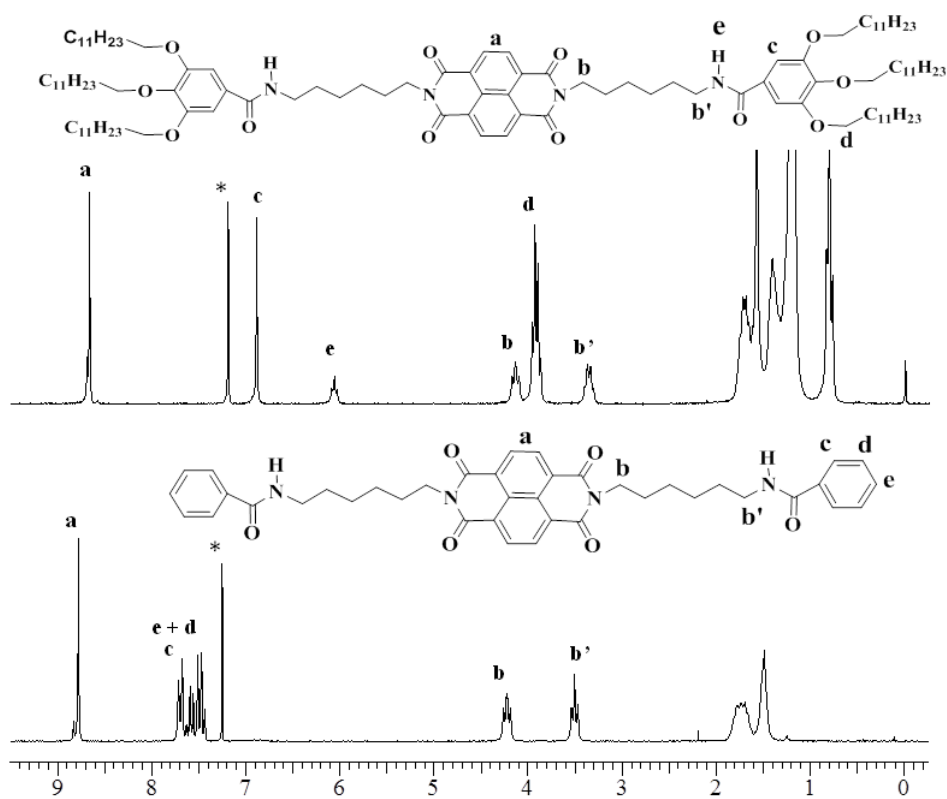


Figure 2.4 b) ¹H NMR spectra of ester NDI-A3 (top), NDI-A (bottom).

The size exclusion chromatography (SEC) analysis showed single peak for all the molecules confirming the purity. As expected, the elution time of the molecules increased with decrease in molecular weights. The amide and the ester molecule of each series differed in mass by 2 units which was well reflected in the SEC plots. Elemental analysis of the compounds was carried out to confirm the purity and the observed CHN values were matching with the calculated values which are given in section 2.2.4 (experimental procedure). The samples were subsequently subjected to MALDI-TOF analysis recorded using 2,5-dihydroxybenzoic acid and titanium dioxide as the matrix and molecular ion peaks were obtained for cationic species such as $[M+Na^+]$, $[M+K^+]$, and $[M+Ag^+]$. The MALDI spectra of the ester and amide series are given **Figure 2.5 a) and b)**. Thus, the NMR, SEC, MALDI-TOF spectra and elemental analysis of the molecules confirmed the structure and high purity of the molecules.

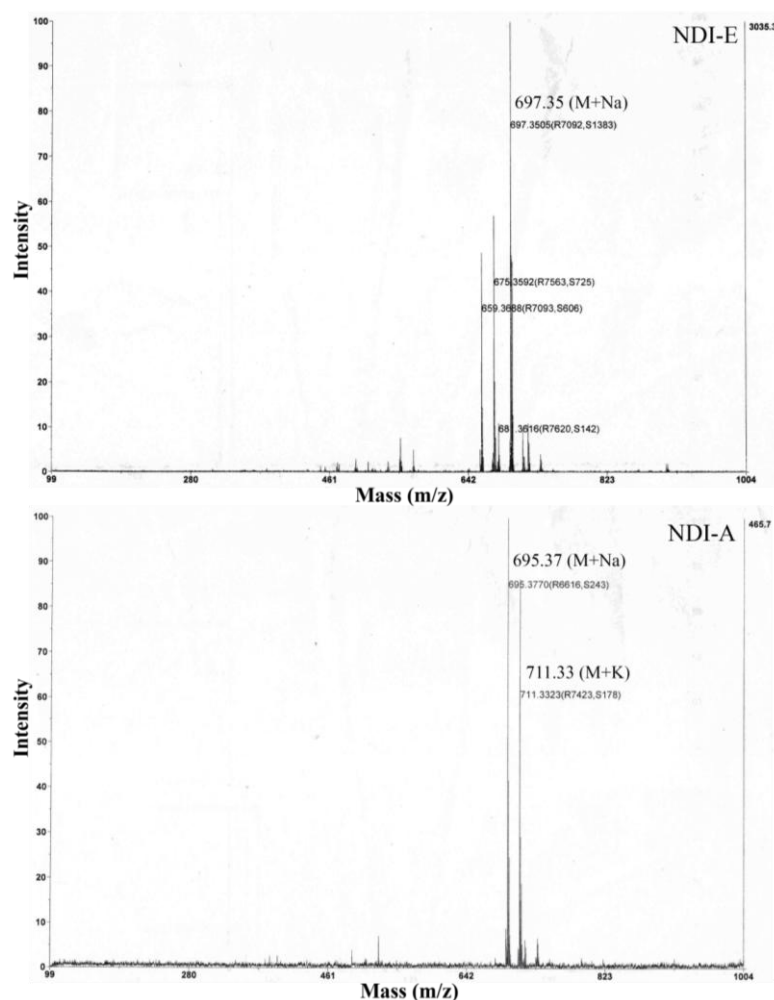


Figure 2.5 a) MALDI-TOF mass spectra of NDI-E and NDI-A.

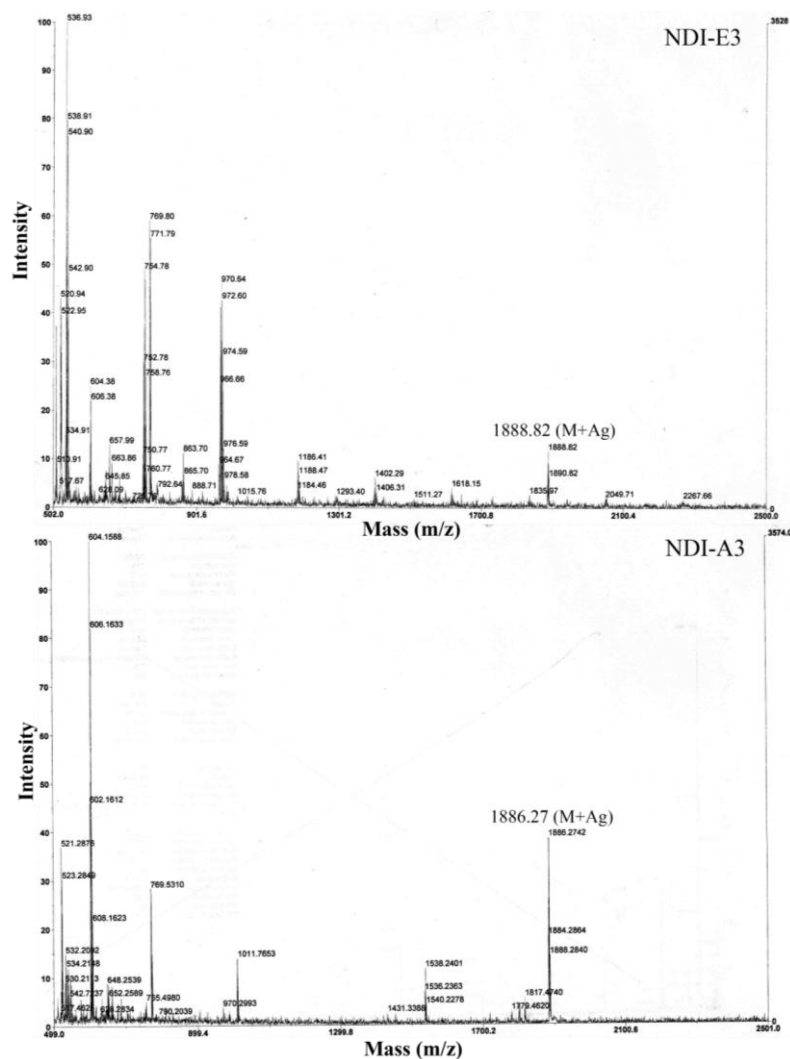


Figure 2.5 b) MALDI-TOF mass spectra of NDI-E3 and NDI-A3.

2.3.2 Optical and Electrochemical Properties

The photophysical properties of the naphthalenediimide derivatives were investigated by UV-Vis absorption and fluorescence emission spectroscopy and electrochemical properties were studied using cyclic voltammetry (CV). The variation in the optical properties of the naphthalenediimide ester versus amide derivatives was used as a tool to study their different molecular organization in chloroform. Chloroform being a good solvent for rigid π -systems like naphthalenediimides; all four NDI molecules were molecularly dissolved in it. The absorption spectrum of all naphthalenediimides in chloroform (Figure 2.6) showed three characteristic peaks at 380 nm, 360 nm and 342 nm corresponding to the 0-0, 0-1 and 0-2 vibronic transitions of a S_0 - S_1 transition with the intensity of the 0-0 transition being the maximum.¹²

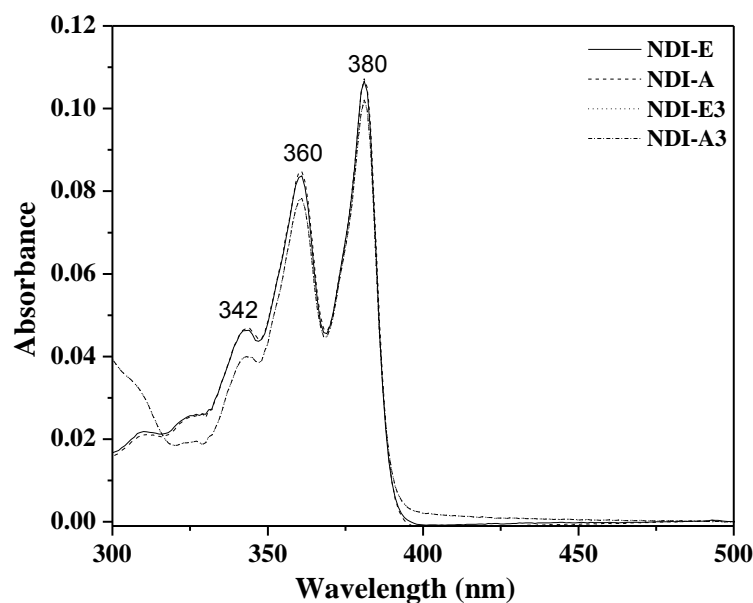


Figure 2.6 UV-Vis absorption spectra of 0.1 OD solutions of naphthalene diimides in chloroform.

No differentiation of ester versus amide linkage among the molecules was observed in absorption spectra in chloroform as solvent. On the other hand, the aliphatic non-polar solvent such as methylcyclohexane (MCH) favors both π - π stacking and hydrogen bonding thus it was very interesting to study the self-organization of ester versus amide molecule in MCH.¹³ NDI-E3 and NDI-A3 with long hydrophobic alkyl chains on phenyl group exhibited sufficient solubility in MCH whereas the NDI-E and NDI-A showed less solubility in MCH. The variable temperature UV-Vis absorption spectra were recorded in MCH (5×10^{-5} M) for NDI-E3 and NDI-A3 which is shown in **Figure 2.7**. NDI-E3 showed three characteristic peaks at 376 nm, 356 nm and 338 nm for π - π^* monomeric transition at all temperatures which resembled with the absorption spectra in chloroform. On the other hand, the absorption spectra of NDI-A3 (amide) at ambient temperature and below that exhibited significant hypochromic shifts for all vibrational bands along with red shifting (bathochromic shift) as suggested by appearance of absorption band beyond 400 nm. This drastic change in spectral pattern of NDI-A3 in MCH compared to NDI-E3 suggested the formation of *J*-type aggregates at ambient temperature due to self-assembly by intermolecular hydrogen bonding in NDI-A3.¹³⁻¹⁴ Furthermore, the thermal stability of aggregates was confirmed by recording the absorption spectra at higher temperatures and it was observed that the aggregates were quite stable up to 50 °C. The absorption spectrum

recorded at 70 °C resembled that of NDI-E3, which indicated the reversible conversion of self-assembled structure in to monomeric species.

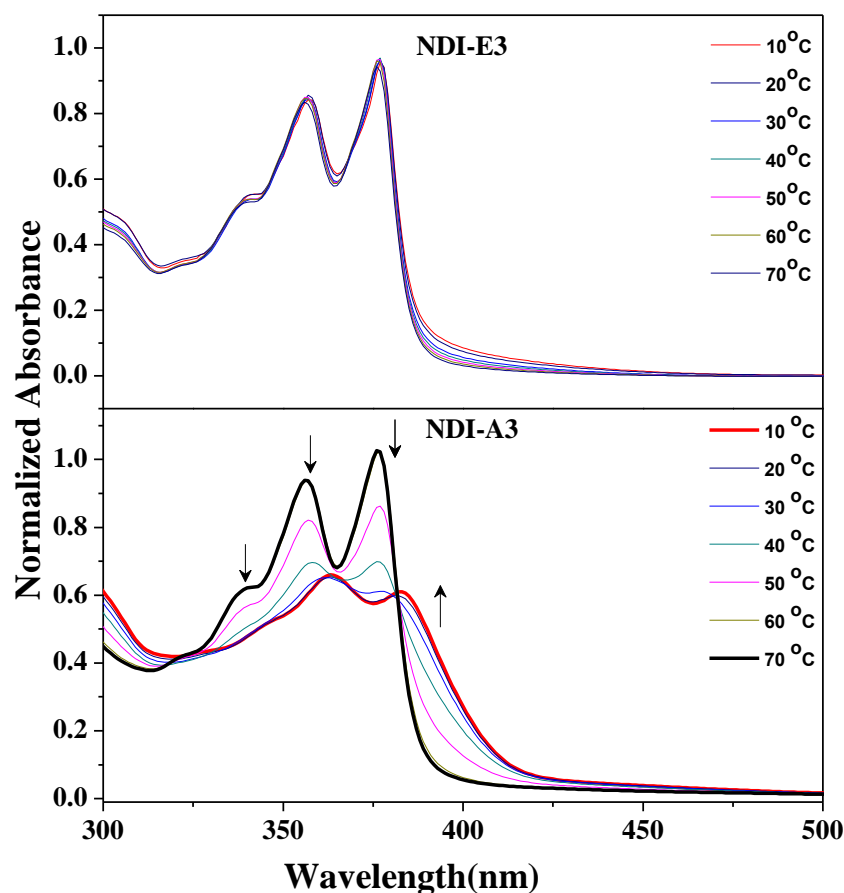


Figure 2.7 Variable temperature UV-Vis absorption spectra of solution (5×10^{-5} M) of NDI-E3 and NDI-A3 in methylcyclohexane (MCH).

From variable-temperature absorption data the propensity for aggregation can be quantified by calculating the degree of aggregation (α) using equation.¹⁵

$$\alpha_{\text{agg}}(T) \approx \frac{A(T) - A_{\text{mon}}}{A_{\text{agg}} - A_{\text{mon}}}$$

where, $\alpha_{\text{agg}}(T)$ is mole fraction of aggregate at temperature T , $A(T)$ absorption at temperature T and A_{mon} and A_{agg} are the absorbance for molecularly dissolved species and fully aggregated species, respectively. The $\alpha_{\text{agg}}(T)$ as function of temperature could be fit well to isodesmic sigmoidal curve which is shown in **Figure 2.8**. From this graph the value of $\alpha_{50}(T)$ (temperature at which $\alpha_{\text{agg}} = 0.5$) could be estimated. The value of $\alpha_{50}(T)$ for NDI-A3 in 5×10^{-5} M solution of MCH was found to be ~ 45 °C.

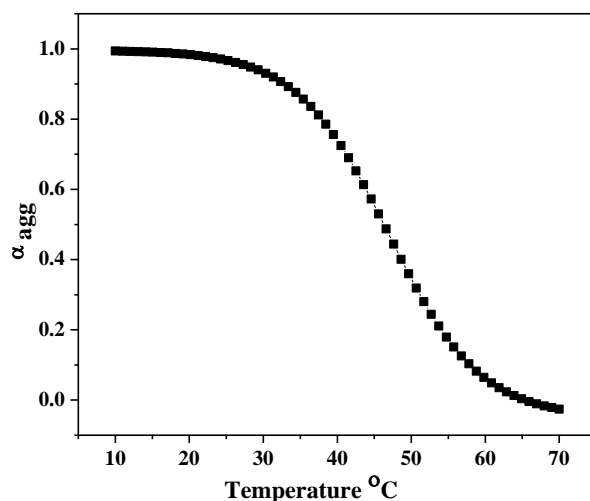


Figure 2.8 Plot of α_{agg} in MCH (5×10^{-5} M) as a function of temperature for NDI-A3

Figure 2.9 shows the fluorescence emission spectrum of all naphthalenediimide molecules recorded for 0.1 OD solutions in chloroform and excitation wavelength of 360 nm. The emission spectra was the mirror image of the absorption spectrum with the emission maximum centered at 408 nm and other peaks at 387 nm, 432 nm etc.^{12,16}

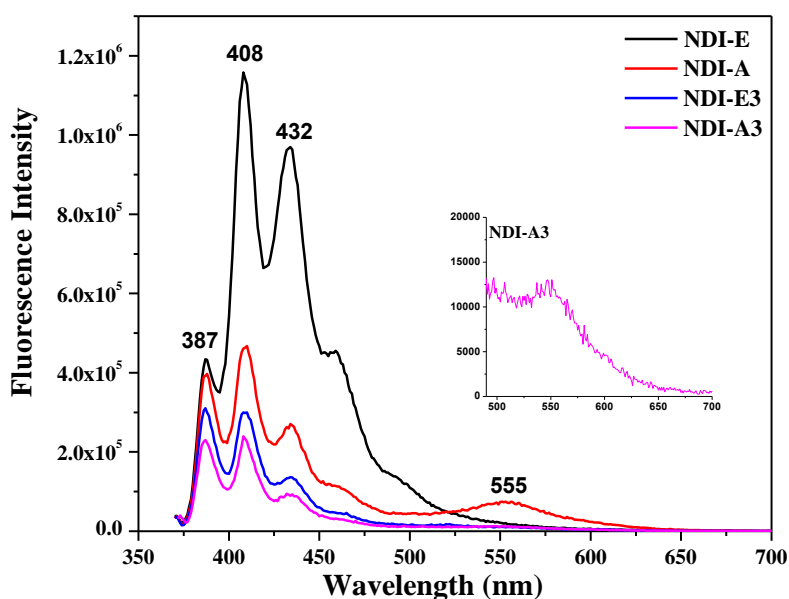


Figure 2.9 Emission spectra of 0.1 OD solutions of naphthalenediimides in chloroform ($\lambda_{ex} = 360$ nm).

The quantum yields were calculated using quinine sulfate as the standard and the values are given in **Table 2.1**. Except for NDI-E, the intensity of emission was very much quenched for the other three molecules which were also reflected in the

quantum yield values. Quenching of fluorescence was observed due to the presence of the 3, 4, 5-trialkoxy substitution in NDI-E3 and NDI-A3.¹⁷ The amide molecules NDI-A and NDI-A3 (inset) additionally exhibited broad aggregated red shifted emission peak at ~ 550 nm which reflected their strong tendency to form aggregates in chloroform. This red shifted aggregate emission at ~ 550 nm was clearly absent in the two ester molecules thereby differentiating them from the amide series of molecules in terms of their self-organization behavior. The device fabrication (discussed later) of the molecules were carried out using orthodichlorobenzene (*o*-DCB) as solvent. Therefore, the self-organization characteristics of the ester and amide molecules were studied in *o*-DCB also. Red-shifted aggregate emission around ~550 nm was observed for NDI-A in *o*-DCB also. The emission of the trialkoxy substituted derivatives NDI-A3 and NDI-E3 was quenched similar to the observation in CHCl₃. The influence on self-organization induced by hydrogen bonding of the amides was more apparent in the solid state emission than in solution.

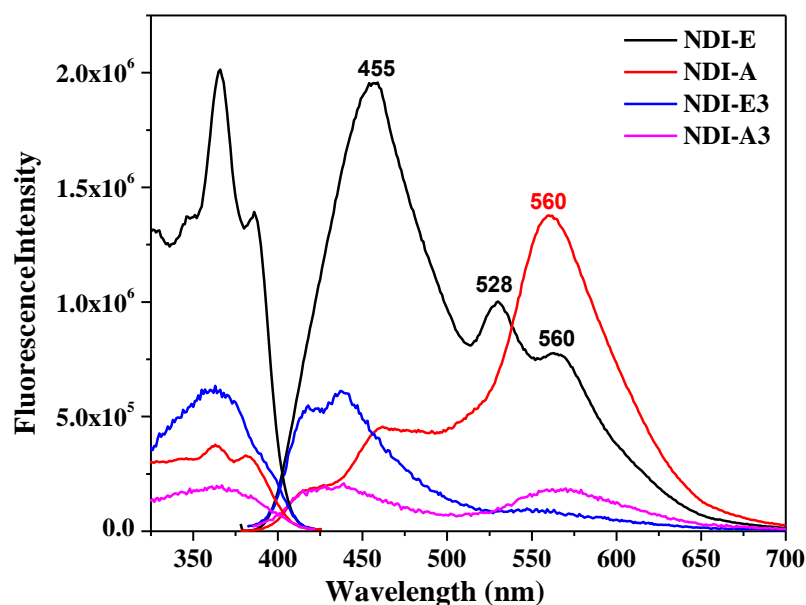


Figure 2.10 Thin-film emission ($\lambda_{\text{ex}}=360$ nm) and excitation ($\lambda_{\text{em}}=455$ nm) spectra of naphthalenediimides spin coated from chloroform solution.

Solid films were obtained by spin coating the solution of corresponding molecule in chloroform and the emission and excitation spectra are given in **Figure 2.10**. The emission spectrum of NDI-E showed monomeric emission peak at 455 nm and aggregate emission peaks were observed at ~ 528 nm and ~ 560 nm (similar observation was seen with film drop cast from *o*-DCB also). The excitation spectra

collected at 530 nm, 570 nm and at the monomer emission of 455 nm were all identical to the absorption spectra indicating that the emitting and absorbing species were identical. NDI-A showed mostly red shifted aggregate emission at ~ 565 nm with only minor contribution from monomer emission in the 400-500 nm region. A similar observation was reported for carboxyl functionalized unsymmetrical NDI derivative, where broad, featureless red shifted emission with large stock shift occurred at 545 nm which was attributed to emission from pre-assembled hydrogen bond mediated J-aggregates.^{13b,18} As observed in solution, in solid state also strong quenching of fluorescence was observed for NDI-E3 and NDI-A3 (the data has been scaled by a factor of 10 for sake of comparison). The aggregate emission at ~ 565 was also observed for NDI-A3, but with less intensity.

The electrochemical properties of the NDI derivatives were analyzed by cyclic voltammetry using three electrode system in dichloromethane (DCM) solvent and tetrabutylammonium hexafluorophosphate ($n\text{-Bu}_4\text{NPF}_6$ 0.1M/ DCM) used as supporting electrolyte. A representative cyclic voltammogram for NDI-E3 and NDI-A3 was shown in **Figure 2.11** and the electrochemical data are given in **Table 2.1**.

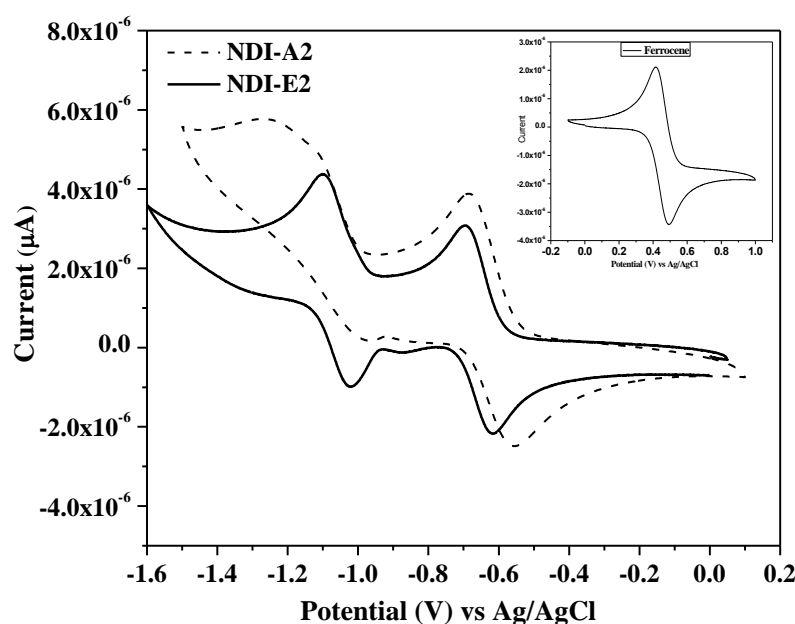


Figure 2.11 Cyclic voltammograms of NDI-E3 and NDI-A3 in CH_2Cl_2 . Inset is the cyclic voltammogram of reference standard ferrocene.

Two reversible reduction peaks corresponding to formation of radical anion and dianions were observed. The reduction potential peak values were similar for all the four molecules demonstrating that they had similar molecular electronic structure and

the electronic properties were insensitive to the nature of the imide substitution. The LUMO energy levels of the NDI derivatives were estimated based on the average onset value of the first and second reduction peak and reference energy level of ferrocene (4.8 V below the vacuum level) according to $E_{\text{LUMO}} (\text{eV}) = -e \times (E^{\text{red}}_{\text{onset}} + 4.8)$ below the vacuum level.¹⁹ The HOMO levels were calculated based on the optical band gap obtained from the solid state absorption onset measurements. The facile reduction along with ease of solution processability, makes these NDI derivatives promising candidates for use as n-type material in organic field effect transistors.

Table 2.1 Optical and electrochemical data of naphthalenediimides.

Molecule	$\phi_{\text{FL}}^{\text{a}}$	Eg (Optical) ^b	E _{pc} (V) average	LUMO (eV)	HOMO (eV)
NDI-E	0.016	3.0	-0.79	-3.66	-6.66
NDI-A	0.007	2.9	-0.76	-3.69	-6.67
NDI-E3	0.003	3.0	-0.77	-3.68	-6.70
NDI-A3	0.002	3.0	-0.76	-3.69	-6.69

(a) The fluorescence quantum yields were obtained upon excitation at 360 nm and were measured using quinine sulphate as standard, (b) calculated from the absorption edge in the solid state. E_{pc} average: average of first and second reduction peak; ($E_{1/2\text{onset}} \text{FC} = 0.35\text{V}$)

2.3.3 Bulk Organization

The NDI derivatives were examined for mesogenic characteristics using DSC, PLM and variable temperature WXR. The four NDI derivatives of the ester as well as amide series were found to be thermally stable till 400 °C which was confirmed by thermogravimetric analysis (TGA) and their 10 % wt loss temperature is given in **Table 2.2**. The thermal phase transition temperature observed from DSC along with the enthalpy of transition is also given in **Table 2.2**. The amide molecules had higher melting temperatures compared to the ester molecules due to the increased rigidity afforded by the hydrogen bonding interaction. The ester and amide molecules without any terminal alkyl substitution i.e. NDI-E and NDI-A showed only a melting transition in their DSC thermogram (**Figure 2.12**). Upon introduction of the three

flexible dodecyloxy units at the terminal phenyl group, multiple transitions appeared in the DSC thermogram in addition to a drastic reduction in the melting transitions for the NDI-E3 and NDI-A3 molecules. **Figure 2.12** shows the second heating and first cooling cycles in the DSC thermograms of NDI derivative.

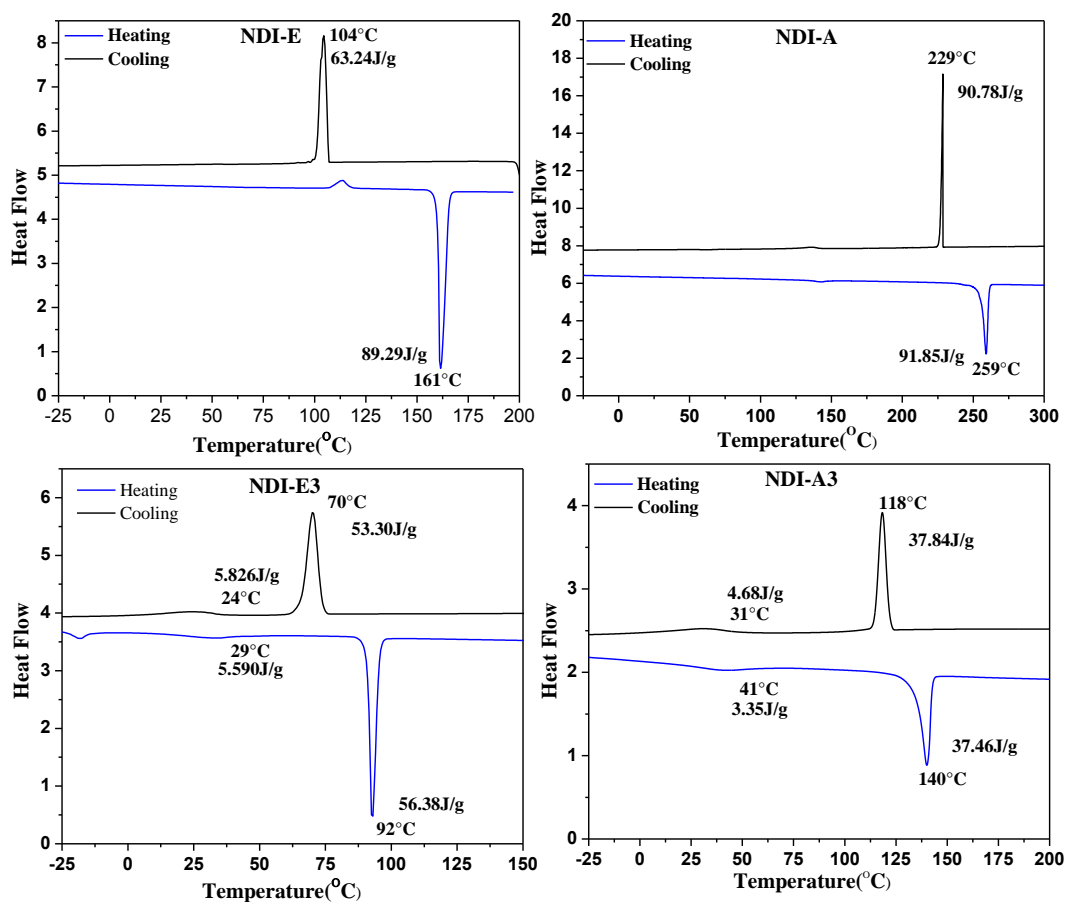


Figure 2.12 DSC heating and cooling curves for NDI-E and NDI-A (top) and NDI-E3 and NDI-A3 (bottom).

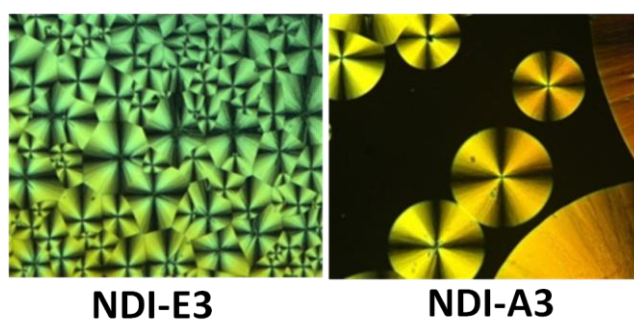


Figure 2.13 PLM images for NDI-E3 and NDI-A3 at 65 °C and 132 °C respectively.

The PLM (polarized light microscope) images showing spherulitic crystalline phase collected at 65 °C and 132 °C respectively for the two samples NDI-E3 and NDI-A3 are also given in **Figure 2.13**.

Table 2.2 Thermal characterization for naphthalenediimides.

Molecule	Temperature (°C)	Enthalpy/ Jg ⁻¹	Phase	10 wt% loss (°C)
NDI-E	161 (104)	89.29 (63.24)	Cr	382
NDI-A	259 (229)	91.85 (90.78)	Cr	431
NDI-E3	-23, 29, 92 (-32, 24, 70)	3.90, 5.82, 56.38 (2.87, 5.59, 3.30)	Spherulitic crystal	389
NDI-A3	41, 140 (31, 118)	3.35, 37.46 (4.68, 37.84)	Spherulitic crystal	400

Cr = Crystalline, I = Isotropic, Bracket indicate values during cooling

To understand the nature of the observed phases, variable temperature WXR D measurements were collected for both NDI-E3 and NDI-A3. **Figure 2.14** (top) shows the WXR D data collected between $2\theta = 3$ to 35° at various temperature intervals while cooling from the isotropic melt at 110 °C for NDI-E3. The small angle region from $2\theta = 2$ to 5° was scanned in a separate experiment and the inset in figure shows the small angle data at $2\theta = 1.91^\circ$ for the sample at room temperature (25 °C). The room temperature WXR D pattern was indexed via rigorous iteration method (DICVOL²⁰) to a monoclinic cell of dimensions $a = 47.386$ (27) Å; $b = 3.307$ (2) Å; $c = 24.799$ (15) Å; and $\beta = 104.13$ (8)°. The Bragg reflection at $2\theta = 1.91^\circ$ corresponding to d -spacing of 46.06 Å was indexed as (100) and hence assigned as the molecular length peak and a peak at $2\theta = 26.94^\circ$ (3.306 Å) was indexed as the (010). The molecular length obtained from Chem draw 3D energy minimized structure was 54.06 Å. The shorter length observed by XRD indicated considerable interdigitation of the terminal alkyl chains. In the isotropic phase at 110 °C, no peaks were observed (**Figure 2.14**) at 65 °C sharp peaks were observed both in the small angle and wide angle region indicating crystalline phase. **Figure 2.14** (bottom) shows the variable temperature WXR D pattern for NDI-A3 taken from the isotropic melt at 150 °C to room temperature (25 °C). This could also be indexed to a monoclinic cell, $a = 48.040$ (36) Å, $b = 3.831$ (3) Å, $c = 24.846$ (18) Å and $\beta = 104.09$ (9) °. The

clearly distinguishing feature between the XRD patterns of NDI-E3 and NDI-A3 was the reduced crystallinity in the latter. NDI-A3 had very few sharp peaks in the entire 2θ range of 3 to 35° . Another very important difference compared to NDI-E3 was that in the amide the peak around $2\theta = 23.37^\circ$ (3.80 \AA) was very sharp and intense and matched with the unit cell length along b axis (010) which could be assigned to the π - π -stacking of NDI-core.^{2i,18,21} Moreover, annealing increased the intensity of this peak much more than for the ester. Thus, the important observations made by analyzing the PWXRD pattern of both NDI-E3 and NDI-A3 were (a) NDI-E3 was more crystalline compared to NDI-A3 and (b) the π stacking along the b axis was much shorter for NDI-E3 at 3.307 \AA compared to 3.831 \AA for NDI-A3.

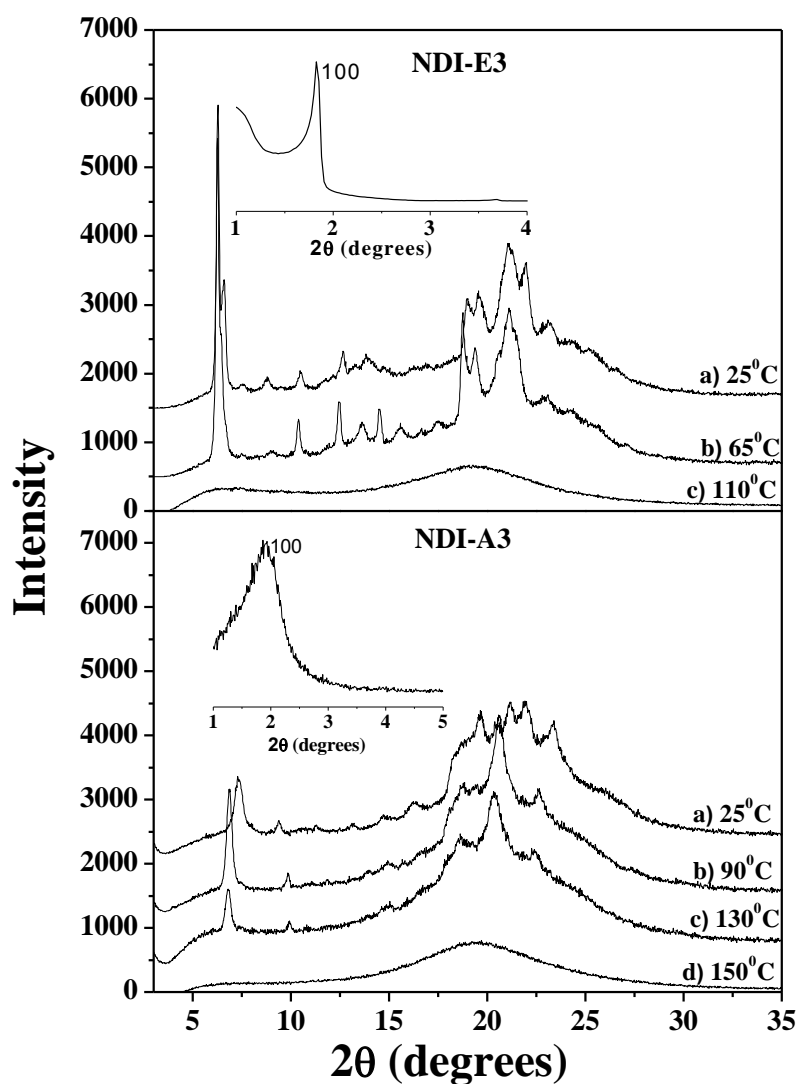


Figure 2.14 Variable temperatures X- ray diffraction pattern of (top) NDI-E3 and (bottom) NDI-A3. Inset shows the peak at low angle ($2\theta = 0.5$ to 5°).

The powder XRD pattern of NDI-E and NDI-A showed that they were more crystalline compared to NDI-E3 and NDI-A3. **Figure 2.15** shows the powder X-ray diffraction pattern of NDI-E and NDI-A. NDI-A was indexed to a monoclinic cell with cell parameters $a = 45.10$ (4) Å; $b = 7.708$ (11) Å; $c = 9.200$ (7) Å and $\beta = 99.48$ (5)°. NDI-A had a more layer -ordered structure compared to NDI-E with the peaks indexed as (200), (400), (600) and (800) along with other higher order (hkl) planes. A careful observation of systematic absences in (h00) and (0k0) planes indicated a plausible non-standard space group of $P2_1/a$. NDI-E was indexed to a monoclinic cell with parameters $a = 26.592$ (21) Å, $b = 4.687$ (2) Å, $c = 19.973$ (9) Å and $\beta = 94.56$ (3)°. The length of ~ 26 Å along the ‘a’ axis of the cell was equal to the observed d spacing at 26.20 Å ($2\theta = 3.36^\circ$) in XRD corresponding to the (100) reflection. No other peaks were observed in the low angle region $< 2\theta = 3^\circ$. Systematic absence evaluation pointed to a definite lack of screw axis when compared to NDI-A and space group was tentatively assigned as $P2/m$ since no extinction conditions could be observed.

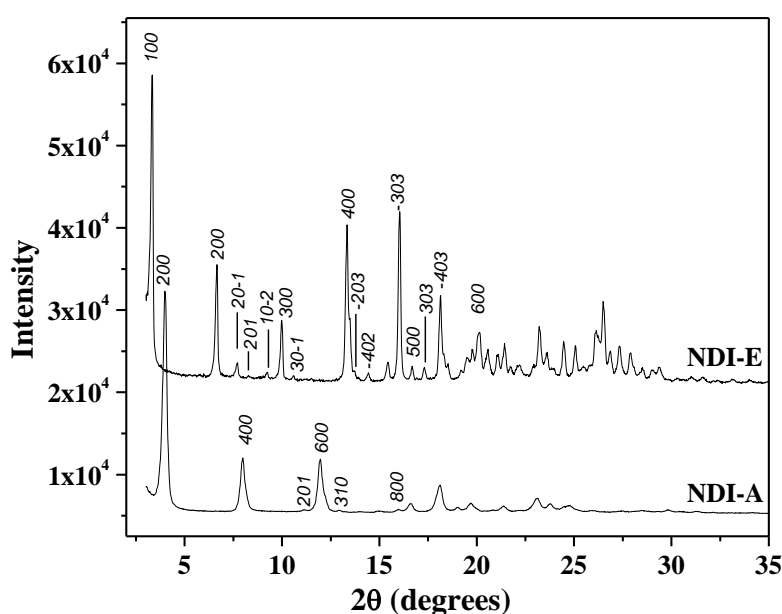


Figure 2.15 Powder WXR D data for NDI-E (top) and NDI-A (bottom).

A simple model building exercise based on molecular length comparison to the unit cell length led to some interesting observations. In the case of NDI-E, the “b” axis length of ~ 4.68 Å restricted any other orientation than a parallel face to face arrangement for the naphthalene rings occupying the corners of the unit cell. However, this distance is longer than the π - π interstack distance in the range 3.3 to 3.5

Å reported for similar systems.^{2i,21} On the other hand, fluorescence studies in the solid state showed an absence of quenching of fluorescence for NDI-E (**Figure 2.10**) indicating the absence of face-to-face π stacking interaction in these molecules. To account for these observations from WXR D as well as solid state emission, an arrangement with the end phenyl rings of two naphthalene molecules interdigitated with each other and the naphthalene rings occupying the unit cell corners was arrived at leading to an a axis length of 26.592 Å which matches with the indexed unit cell. In comparison to this structure, NDI-A exhibited an elongated a axis; however, the molecular interactions can be summarized to be more or less similar since the screw axis effects a face centering in this system reducing the distance between two naphthalene centers to ~ 23 Å (this distance also matched with observed d_{200} spacing of 22.13 Å at $2\theta = 3.99^\circ$ in XRD).

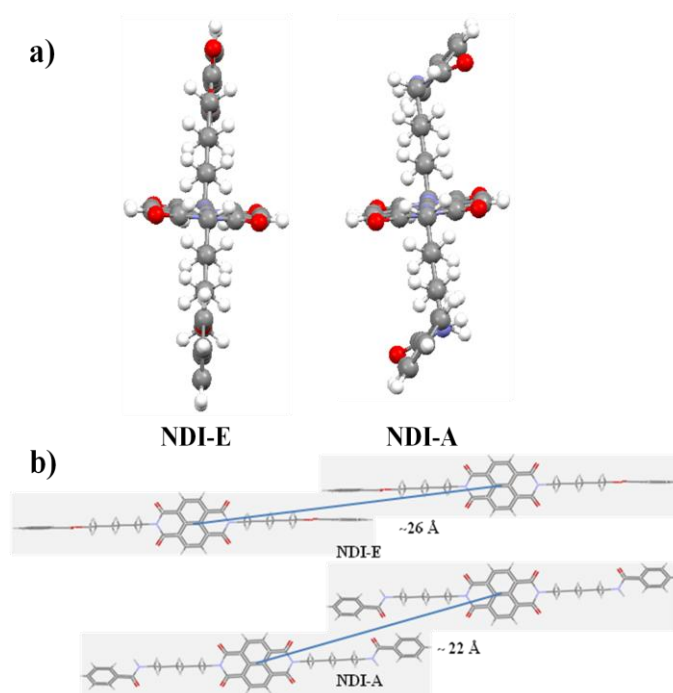


Figure 2.16 (a) DFT energy optimized structures of NDI-E and NDI-A (b) Schematic representation of molecular packing in NDI-E and NDI-A.

Density Functional Theory (DFT) was used to obtain energy minimized structures for both NDI-E and NDI-A by using the turbomole suite of programs.²² Geometry optimizations were performed using the B-P 86 functional.²³ **Figure 2.16 a)** compares the energy minimized structure of NDI-E and NDI-A with the molecules oriented along the NDI aromatic core. The NDI core was out of plane with respect to the hexyl

and phenyl planes; however unlike NDI-E the amide and phenyl rings of NDI-A were not totally perpendicular but it was twisted and had a dihedral angle of $\sim 26^\circ$. This twisting which occurred to accommodate the restraining hydrogen bonding also resulted in interdigitation to a larger extent in NDI-A. This was reflected in the shorter d -spacing value of 22.13 \AA for NDI-A compared to 26.20 \AA for NDI-E, which is shown schematically in **Figure 2.16 b**). To demonstrate the existence of hydrogen bonding in the solid state, variable temperature FT-IR studies were carried out. FT-IR spectra of both NDI-E and NDI-A were recorded in the powder form (pellet made from KBr ground with sample). **Figure 2.17** shows the expanded -NH stretching region ($4000\text{--}3300 \text{ cm}^{-1}$) and the carbonyl stretching frequency in the range $1700\text{--}1600 \text{ cm}^{-1}$ at two different temperatures (at 30°C and at 250°C) for NDI-A and at 30°C for NDI-E.

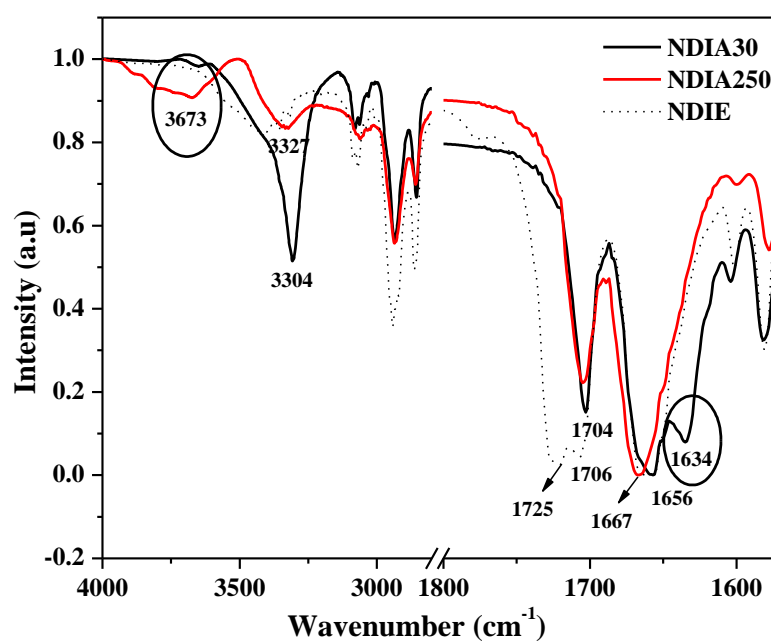


Figure 2.17 Expanded FT-IR spectra of NDI-E at 30°C and NDI-A at 30°C and 250°C showing the disappearance of the hydrogen bonded carbonyl stretch $\sim 1634 \text{ cm}^{-1}$.

The carbonyl group of naphthalenediimide has a stretching frequency at 1700 and 1660 cm^{-1} whereas the carbonyl group of amide has the amide I stretching frequency in the range $1650\text{--}1690 \text{ cm}^{-1}$. At 30°C , NDI-A showed -NH stretching vibration at 3304 cm^{-1} and three peaks were observed at 1704 , 1656 and 1634 cm^{-1} in the carbonyl stretching region. The NDI-E molecule which clearly did not have an amide I stretch also had a peak at 1659 cm^{-1} due to the carbonyl of the naphthalene core. However

clearly differentiating the two (ester vs. amide) was the peak at 1634 cm^{-1} in the NDI-A (circled peak) which was assigned as the hydrogen bonded carbonyl stretch. At $250\text{ }^{\circ}\text{C}$ the peak at 1634 cm^{-1} vanished completely and the peak at 1656 cm^{-1} also shifted to higher frequency 1667 cm^{-1} . In the -NH stretching region also, the hydrogen bonded -NH stretch at 3304 cm^{-1} reduced in intensity and shifted to 3327 cm^{-1} and a new broad peak corresponding to free -NH stretch appeared at 3673 cm^{-1} (circled peak). This shift was clearly reversible with the hydrogen bonded carbonyl and amide peaks shifting to their original values upon cooling.

2.3.4 Device Characteristics (OFET)

Bottom-gate top contact structures were fabricated for field effect transistor studies. The fabrication procedure adopted was as described in the experimental section. Except NDI-A, all the other molecules were spin coated from a solution of concentration 25 mg/ml to obtain films of $\sim 80\text{-}100\text{ nm}$ thickness. In the case of NDI-A spin coating could not be done due to poor solubility in *o*-DCB and the films could only be drop cast from *o*-DCB. This method resulted in thicker ($\sim 0.4\text{ }\mu\text{m}$) and more uniform film. The molecules NDI-E3 and NDI-A3 were heated above their melting transition temperature $100\text{ }^{\circ}\text{C}$ and $150\text{ }^{\circ}\text{C}$ respectively and then cooled to room temperature to retain them in the spherulitic crystalline phase. In the case of NDI-E and NDI-A where the melting transition temperature was very high, the samples were annealed at $150\text{ }^{\circ}\text{C}$ and $200\text{ }^{\circ}\text{C}$ respectively and then cooled to room temperature to get the optimum device performance. **Figure 2.18 a) and b)** shows the typical OFET output and transconductance characteristics of naphthalenediimides and values of electron mobility with on/off ratio are reported in **Table 2.3**. The devices showed typical n-type characteristics with a clear transition from linear to saturation behavior. The performance parameters were extracted in the saturation regime from the transconductance characteristics curves by using the following equation

$$I_{ds} = (\mu_{FET} WC/2L) (V_g - V_{th})^2$$

where I_{ds} is the drain current, W and L are, respectively, the channel width and length, C is the capacitance per unit area of the gate insulator layer, and V_{gs} and V_T are the gate voltage and the threshold voltage, respectively. The μ_{FET} values of the NDI molecules were in the order $5.7 \times 10^{-3}\text{ cm}^2\text{ V}^{-1}\text{ s}^{-1}$ (for NDI-A3) to $2 \times 10^{-2}\text{ cm}^2\text{ V}^{-1}\text{ s}^{-1}$

(for NDI-E) with the NDI-E exhibiting the most sizable performance parameters. The amide molecules exhibited relatively lower mobilities. The lower on/off ratio observed in NDI-A could be attributed to higher off currents from the residual bulk conductance of the thicker films.

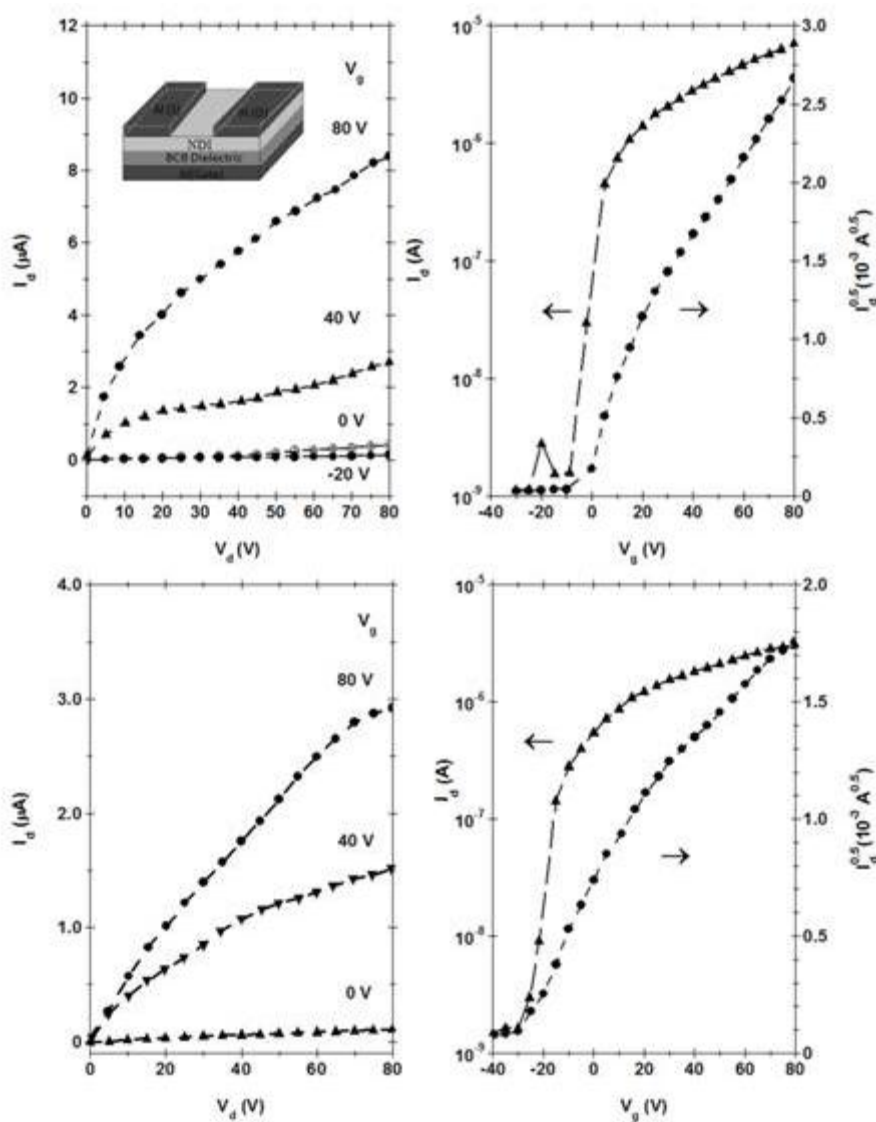


Figure 2.18 a) Typical output and transconductance curve for NDI-E (top) and NDI-A (bottom) from the transistor with $W \sim 2$ mm and $L \sim 60$ - 100 μm respectively and BCB as the dielectric with $C_0 \sim 4\text{nF}/\text{cm}^2$. Inset shows the schematic of the device.

Table 2.3 also compares the mobility values of NDI-E3 and NDI-A3 films which were not heated to isotropic phase and then cooled but only subjected to annealing at temperatures lower than their melting transitions. The mobility values were found to be one order of magnitude lower for these low temperature annealed samples which were not in the spherulitic crystalline phase. The interdigitation of the terminal alkyl

chains in NDI-E3 and NDI-A3 resulted in a stacked columnar organization with co-facial alignment along the column,²⁴ as indicated by the XRD data. The quenching of fluorescence in the solid state also indicated a co-facial alignment in these 3,4,5-tridodecyloxy terminated NDI derivatives.

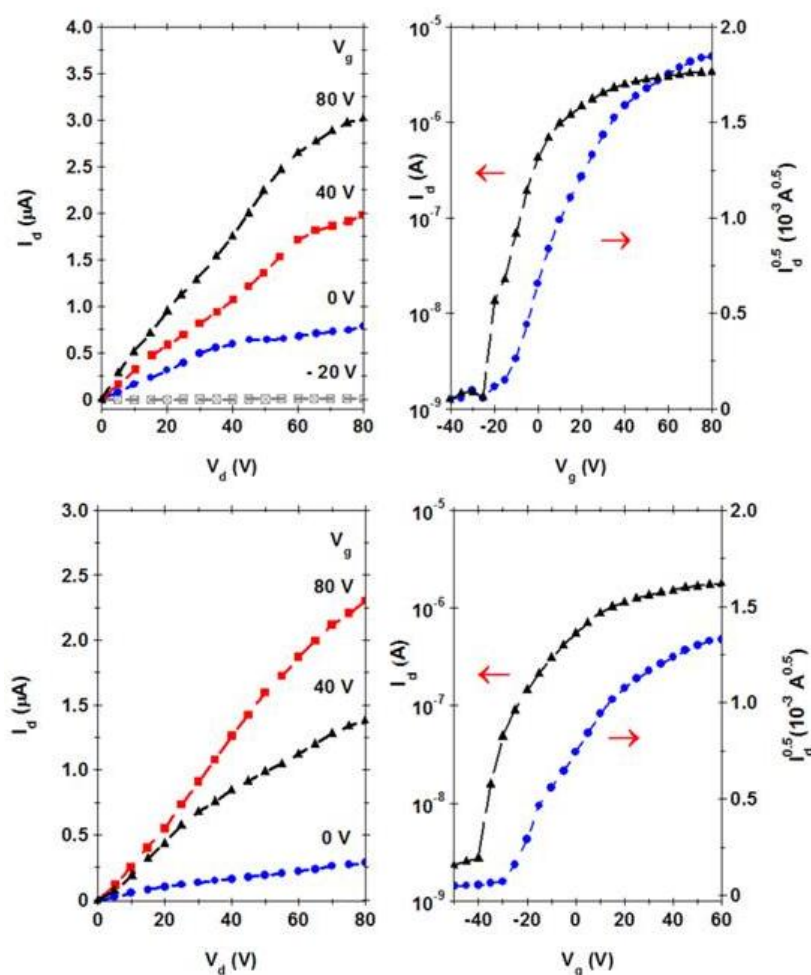


Figure 2.18 b) Typical output and transconductance curve for NDI-E3 (top) and NDI-A3 (bottom).

Therefore, higher mobilities were observed in the samples annealed at higher temperature compared to that annealed at low temperatures. However, the charge carrier mobility in the spherulitic phase of NDI-E3 and NDI-A3 was still one order lower compared to that obtained for their non-alkyl chain terminated analogues NDI-E and NDI-A. This could be attributed to the decreased electron density and the associated defects because of the alkyl chains in the spherulite systems.⁴ The effect of annealing on the thin film morphology of NDI-E and NDI-A were studied using tapping mode AFM images of thin films deposited on glass. **Figure 2.19** (top) shows

the tapping mode AFM images of thin films of NDI-E and NDI-A spin coated from *o*-DCB both at room temperature (25 °C) and after annealing to 150 °C and 200 °C respectively and then cooled to 25 °C.

Table 2.3 OFET Characteristics of the naphthalenediimides.

Molecule	μ_{avg} (cm^2/Vs)	μ_{max} (cm^2/Vs)	$I_{\text{on}}/I_{\text{off}}$	$V_{\text{th}}(\text{V})$	$T_{\text{Annealing}}$ (°C)
NDI-E	a) 2×10^{-2}	a) 6×10^{-2}	$> 10^4$	-5 to 15	150
	b) 4.3×10^{-4}	b) 5×10^{-4}			-
NDI-A	a) 9.5×10^{-3}	a) 1.7×10^{-2}	$> 10^2$	-20 to 20	200
	b) 2.6×10^{-4}	b) 4.5×10^{-4}			-
NDI-E3	a) 8.5×10^{-3}	a) 4×10^{-2}	$> 10^4$	-10 to 20	100
	b) 1.5×10^{-4}	b) 5.1×10^{-4}			50-60
NDI-A3	a) 5.7×10^{-3}	a) 1×10^{-2}	$> 10^3$	-15 to 30	150
	b) 1.4×10^{-4}	b) 4.1×10^{-4}			100

a) After annealing b) Before annealing

Figure 2.19 a) and b) shows the height and amplitude image of NDI-E at 25 °C respectively. After heat treatment the sample became smoother with improved grain size (**Figure 2.19** c and d - the height and amplitude image of NDI-E after annealing respectively). Similarly, the images on the right side of **Figure 2.19** corresponds to thin film of NDI-A before (a, b) and after (c, d) annealing. It was observed that annealing helped to improve the overall smooth morphology of the films. Thin film X-ray diffraction could be used as a tool to understand out of plane ordering of layered films of crystalline small molecules.^{6,25} **Figure 2.19** (bottom) shows the thin film (spin coated from *o*-DCB) WXRd data of NDI-E and NDI-A annealed at 150 °C and 200 °C respectively and then cooled to 25°C. The percentage crystallinity of thin film of NDI-E was much higher compared to powder with very high intense (100) peak. Lamellar ordering up to 6th order could be observed which was consistent with edge-on orientation on the substrate.^{10b,c} The thin film XRD was similar to the powder data (**Figure 2.15**) indicating that the crystal structure was retained in the thin film

also with the preferred orientation in the lamellar direction.³ Due to poor solubility of NDI-A, only a very thin film could be obtained by spin coating from hot *o*-DCB.

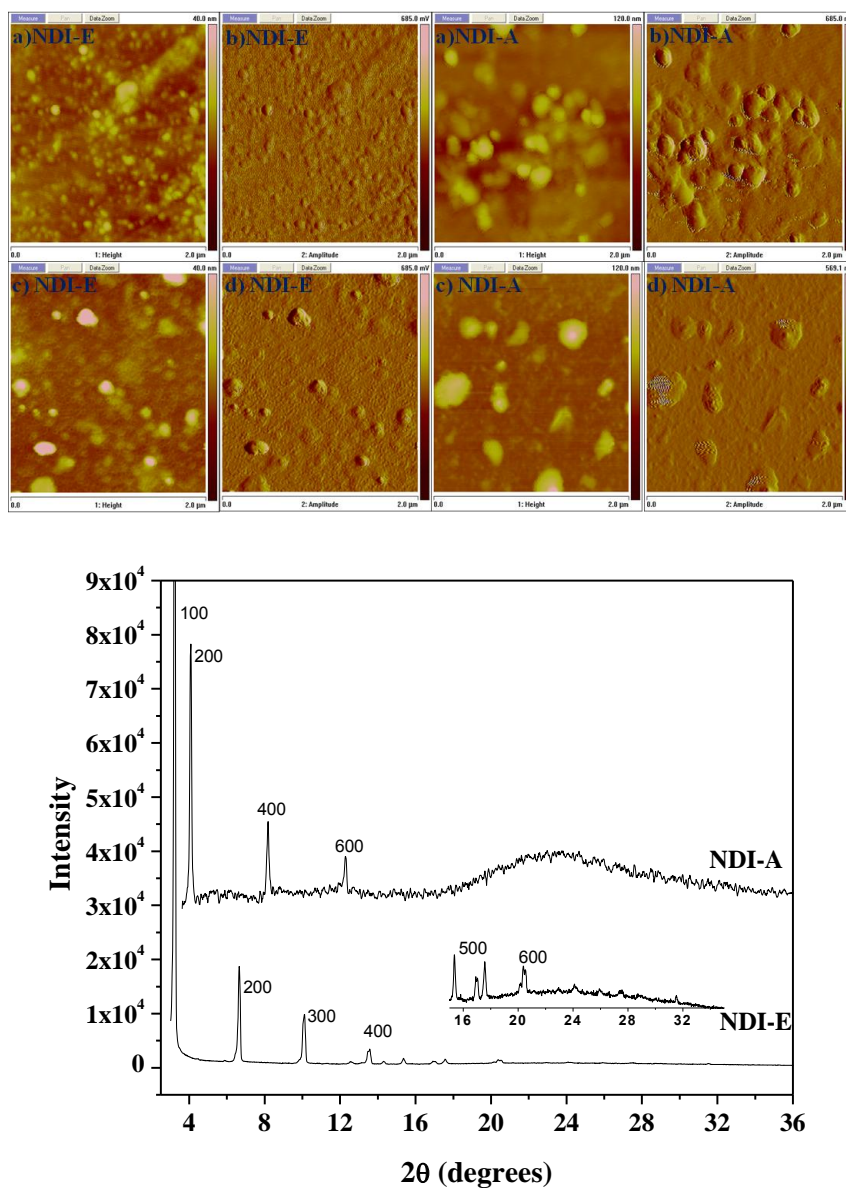


Figure 2.19 AFM images of NDI-E and NDI-A (top) taken on glass slide a) height b) amplitude before heating and c) height and d) amplitude after thermal annealing and (bottom) thin film WXR data for NDI-E and NDI-A.

Lamellar ordering up to three orders only could be observed due to the extreme low thickness of the film (the amorphous hump $\sim 2\theta = 20^\circ$ being diffraction from glass). However, the lower d_{200} value (21.62 \AA) of NDI-A compared to the molecular length of 33.91 \AA (from DFT) indicated tilted orientation on the substrate.^{2j,10e 10f} In most of bottom gate OFET configuration the preferred orientation of π -conjugated cores should be approximately perpendicular to the dielectric surface (edge –on

arrangement) for efficient charge transport from source to drain.²⁶ The tilt angle with respect to the substrate normal was given by $\cos^{-1}(21/33.91) = 50^\circ$ for NDI-A, and $\cos^{-1}(26/33.91) = 40^\circ$ for NDI-E.^{2h,27} The different dihedral twisting angle, obtained for energy minimized structure from DFT, though not important in solution, becomes an important parameter while considering the orientation on the substrate surface. In the thin film, this distortion of NDI-A from planarity resulted in lower observed crystallinity and charge carrier mobility as compared to NDI-E.⁵ Another factor favoring the improved mobility in NDI-E compared to NDI-A was the increased flexibility of the molecule as a whole due to absence of the highly restricting directional hydrogen bonding interaction which gave it more freedom to pack in a more favored bulk crystalline packing which facilitated electron transport. NDI-E had isotropic electronic charge transport owing to its flexible ordered structure. The critical role of restrictive interactions leading to reduced dimensionality on the charge carrier mobility was shown in the case of C₆₀ derivatives recently. The group of Dario M. Bassani *et al.* reported a comparative study of charge carrier mobility of C₆₀ with that of a derivatized C₆₀ capable of organizing into infinite hydrogen bonded tapes oriented along one of the crystal axis.^{11a} The charge carrier mobility of the self-assembled fullerene ribbons were found to be two- orders of magnitude lower than that of C₆₀ and this was attributed to the reduced dimensionality of the fullerene tapes as a wire-like semiconductor in contrast to C₆₀ as a bulk semiconductor. We speculate a similar reasoning of restricted dimensionality of transport for NDI-A which could explain its lower mobility compared to NDI-E. For instance, the more soluble NDI-A3 molecule formed gels in non polar solvent like methyl cyclohexane (MCH) in contrast to NDI-E3 which remained crystalline. **Figure 2.20** compares the TEM images of NDI-E3 and NDI-A3 respectively drop cast from MCH solution. It can be seen that NDI-A3 formed continuous network of highly entangled nanofibers. Although this morphology of NDI-A3 in MCH cannot be directly correlated with the thin film morphology in the OFET devices, it could be used to illustrate the reduced dimensionality of the hydrogen bonded molecules NDI-A and NDI-A3 compared with their non-hydrogen bonded ester analogues. Since the overall device performance of the ester derivatives were better compared to amides, it could be concluded that hydrogen bonding in the amides proved to be more restrictive compared to the more

crystalline ester molecules which had more freedom to realign for efficient charge transport.

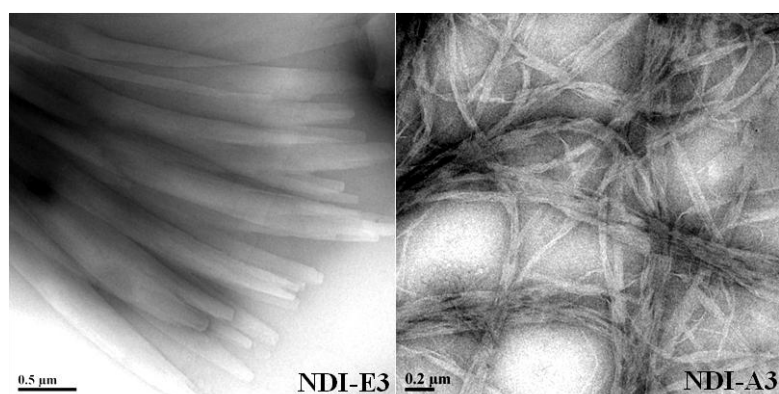


Figure 2.20 TEM (transmission electron microscope) images for NDI-E3 and NDI-A3 drop casted from 1×10^{-4} M solution of MCH.

2.3.5 Conclusions

The present work described a full account of synthesis, characterization and molecular/thin film properties of two series of naphthalene diimide (NDI) derivatives – one series had an amide group linking a terminal phenyl or 3, 4, 5-tridodecyloxy phenyl unit to a hexyl spacer substituted NDI core, while in the other series the linkage was through an ester unit. The amide linked NDI derivatives formed strong hydrogen bonded aggregates with pronounced red shifted emission both in solution and solid state. All the four NDI derivatives exhibited good n type charge transport characteristics in an OFET device in the bottom gate top contact geometry with values ranging from $2 \times 10^{-2} \text{ cm}^2 \text{ V}^{-1} \text{ s}^{-1}$ to $5.7 \times 10^{-3} \text{ cm}^2 \text{ V}^{-1} \text{ s}^{-1}$. The mobility values for the NDI ester and amide derivatives without terminal alkyl substitution were one order higher in magnitude compared to their terminal alkyl substituted counter parts. This was expected since the alkyl chains formed an insulating barrier for efficient charge transport in the NDI-E3 and NDI-A3 derivatives although they also facilitated formation of co-facially π stacked columns by interdigitation. The comparison of mobility values of the ester versus amides revealed some interesting observations. Contrary to expectations, the hydrogen bonding in the amide derivatives did not facilitate better electron mobility. The ester derivatives exhibited better device

performance compared to the amides. Analyzing the packing in these molecules based on DFT energy minimized structures and powder XRD data, especially in the case of NDI-E and NDI-A, the NDI amide derivative showed a dihedral twist of the terminal phenyl unit with respect to the naphthyl aromatic core with a consequent shortening of the molecular length packing along the a axis. This small difference in the dihedral twist angle reduced the crystallinity and resulted in a more tilted orientation of the NDI-A molecules on the substrate surface. On the whole, the present studies with NDI derivatives thus demonstrated that the restrictive directional hydrogen bonding interaction is not so favorable for efficient charge transport compared to the freedom in charge transport pathways offered by a three dimensional crystalline organization.

2.4. References

- (1) Bhosale, S. V.; Jani, C. H.; Langford, S. J. *Chem. Soc. Rev* **2008**, *37*, 331.
- (2) (a) Zhan, X.; Facchetti, A.; Barlow, S.; Marks, T. J.; Ratner, M. A.; Wasielewski, M. R.; Marder, S. R. *Adv. Mater.* **2011**, *23*, 268(b) Wurthner, F.; Stolte, M. *Chem. Commun.* **2011**, *47*, 5109(c) Wen, Y.; Liu, Y. *Adv. Mater.* **2010**, *22*, 1331(d) Zhao, Y.; Guo, Y.; Liu, Y. *Adv. Mater.* **2013**, *25*, 5372(e) Earmme, T.; Hwang, Y.-J.; Murari, N. M.; Subramaniyan, S.; Jenekhe, S. A. *J. Am. Chem. Soc.* **2013**, *135*, 14960(f) Kang, H.; Kim, K.-H.; Choi, J.; Lee, C.; Kim, B. J. *ACS Macro Lett.* **2014**, *3*, 1009(g) Babel, A.; Jenekhe, S. A. *J. Am. Chem. Soc.* **2003**, *125*, 13656(h) Jones, B. A.; Facchetti, A.; Marks, T. J.; Wasielewski, M. R. *Chem. Mater.* **2007**, *19*, 2703(i) Jung, B. J.; Sun, J.; Lee, T.; Sarjeant, A.; Katz, H. E. *Chem. Mater.* **2009**, *21*, 94(j) See, K. C.; Landis, C.; Sarjeant, A.; Katz, H. E. *Chem. Mater.* **2008**, *20*, 3609.
- (3) Shukla, D.; Nelson, S. F.; Freeman, D. C.; Rajeswaran, M.; Ahearn, W. G.; Meyer, D. M.; Carey, J. T. *Chem. Mater.* **2008**, *20*, 7486.
- (4) Vehoff, T.; Baumeier, B.; Troisi, A.; Andrienko, D. *J. Am. Chem. Soc.* **2010**, *132*, 11702.
- (5) Ortiz, R. P.; Herrera, H.; Blanco, R.; Huang, H.; Facchetti, A.; Marks, T. J.; Zheng, Y.; Segura, J. L. *J. Am. Chem. Soc.* **2010**, *132*, 8440.
- (6) Jones, B. A.; Facchetti, A.; Wasielewski, M. R.; Marks, T. J. *Adv. Funct. Mater.* **2008**, *18*, 1329.
- (7) (a) Braga, D.; Horowitz, G. *Adv. Mater.* **2009**, *21*, 1473(b) Sakanoue, T.; Sirringhaus, H. *Nat. Mater.* **2010**, *9*, 736.
- (8) Mas-Torrent, M.; Rovira, C. *Chem. Rev.* **2011**, *111*, 4833.
- (9) Tang, M. L.; Bao, Z. *Chem. Mater.* **2011**, *23*, 446.
- (10) (a) Ahmed, E.; Ren, G.; Kim, F. S.; Hollenbeck, E. C.; Jenekhe, S. A. *Chem. Mater.* **2011**, *23*, 4563(b) Chen, H. Z.; Ling, M. M.; Mo, X.; Shi, M. M.; Wang, M.; Bao, Z. *Chem. Mater.* **2007**, *19*, 816(c) Katz, H. E.; Lovinger, A. J.; Johnson, J.; Kloc, C.; Siegrist, T.; Li, W.; Lin, Y. Y.; Dodabalapur, A. *Nature* **2000**, *404*, 478(d) Tan, L.; Guo, Y.; Zhang, G.; Yang, Y.; Zhang, D.; Yu, G.; Xu, W.; Liu, Y. *J. Mater. Chem.* **2011**, *21*, 18042(e) Gawrys, P.; Boudinet, D.; Kornet, A.; Djurado, D.; Pouget, S.; Verilhac, J.-M.; Zagorska, M.; Pron, A. *J. Mater. Chem.* **2010**, *20*, 1913(f) Gawrys, P.; Djurado, D.; Rimarčík, J.; Kornet, A.; Boudinet, D.; Verilhac, J.-M.; Lukeš, V.; Wielgus, I.; Zagorska, M.; Pron, A. *J. Phys. Chem. B* **2010**, *114*, 1803(g)

- Deng, P.; Yan, Y.; Wang, S.-D.; Zhang, Q. *Chem. Commun.* **2012**, 48, 2591(h) Weitz, R. T.; Amsharov, K.; Zschieschang, U.; Villas, E. B.; Goswami, D. K.; Burghard, M.; Dosch, H.; Jansen, M.; Kern, K.; Klauk, H. *J. Am. Chem. Soc.* **2008**, 130, 4637(i)
- Zhan, X.; Tan, Z. a.; Domercq, B.; An, Z.; Zhang, X.; Barlow, S.; Li, Y.; Zhu, D.; Kippelen, B.; Marder, S. R. *J. Am. Chem. Soc.* **2007**, 129, 7246(j) Hu, Y.; Gao, X.; Di, C.-a.; Yang, X.; Zhang, F.; Liu, Y.; Li, H.; Zhu, D. *Chem. Mater.* **2011**, 23, 1204.
- (11) (a) Chu, C.-C.; Raffy, G.; Ray, D.; Guerzo, A. D.; Kauffmann, B.; Wantz, G.; Hirsch, L.; Bassani, D. M. *J. Am. Chem. Soc.* **2010**, 132, 12717(b) Yokoyama, D.; Sasabe, H.; Furukawa, Y.; Adachi, C.; Kido, J. *Adv. Funct. Mater.* **2011**, 21, 1375(c)
- Katz, H. E.; Otsuki, J.; Yamazaki, K.; Suka, A.; Takido, T.; Lovinger, A. J.; Raghavachari, K. *Chemistry Lett.* **2003**, 32, 508(d) Gsänger, M.; Oh, J. H.; Könemann, M.; Höffken, H. W.; Krause, A.-M.; Bao, Z.; Würthner, F. *Angew. Chem. Int. Ed.* **2010**, 49, 740(e) Seki, T.; Maruya, Y.; Nakayama, K.-i.; Karatsu, T.; Kitamura, A.; Yagai, S. *Chem. Commun.* **2011**, 47, 12447(f) Miyake, Y.; Hu, P.; Zhao, K.-Q.; Monobe, H.; Fujii, A.; Ozaki, M.; Shimizu, Y. *Mol. Cryst. Liq. Cryst.* **2010**, 525, 97(g) Zhang, M.-X.; Zhao, G.-J. *Chem. Sus. Chem.* **2012**, 5, 879.
- (12) Barros, T. C.; Brochsztain, S.; Toscano, V. G.; Filho, P. B.; Politi, M. J. *J. Photochem. Photobiol. A. Chemistry* **1997**, 111, 97.
- (13) (a) Molla, M. R.; Ghosh, S. *Chem. Mater.* **2011**, 23, 95(b) Molla, M. R.; Gehrig, D.; Roy, L.; Kamm, V.; Paul, A.; Laquai, F.; Ghosh, S. *Chem. Eur. J.* **2014**, 20, 760(c) Molla, M. R.; Das, A.; Ghosh, S. *Chem. Eur. J.* **2010**, 16, 10084.
- (14) Kumar, M.; George, S. J. *Chem. Eur. J.* **2011**, 17, 11102.
- (15) Bhavsar, G. A.; Asha, S. K. *Chem. Eur. J.* **2011**, 17, 12646.
- (16) Ozser, M. E.; Uzun, D.; Elci, I.; Icil, H.; Demuth, M. *Photochem. Photobio. Sci.* **2003**, 2, 218.
- (17) (a) Würthner, F.; Thalacker, C.; Diele, S.; Tschierske, C. *Chem. Eur. J.* **2001**, 7, 2245(b) Jancy, B.; Asha, S. K. *Chem. Mater.* **2008**, 20, 169.
- (18) Molla, M. R.; Ghosh, S. *Chem. Eur. J.* **2012**, 18, 1290.
- (19) Kolhe, N. B.; Asha, S. K.; Senanayak, S. P.; Narayan, K. S. *J. Phys. Chem. B* **2010**, 114, 16694.
- (20) Boultif, A.; Louer, D. *J. Appl. Cryst.* **1991**, 24, 987.
- (21) Shao, H.; Gao, M.; Kim, S. H.; Jaroniec, C. P.; Parquette, J. R. *Chem. Eur. J.* **2011**, 17, 12882.

- (22) Ahlrichs, R.; M. Bär, H. P. B.; Bauernschmitt, R.; Böcker, S.; Ehrig, M.; Eichkorn, K.; Elliott, S.; Furche, F.; Haase, F.; Häser, M.; Horn, H.; Huber, C.; Huniar, U.; Kattannek, M.; Kölmel, C.; Kollwitz, M.; May, K.; Ochsenfeld, C.; Öhm, H.; Schäfer, A.; Schneider, U.; Treutler, O.; Arnim, M. v.; Weigend, F.; Weis, P.; Weiss, H. *TURBOMOLE; (Version 5.3); Universität Karlsruhe, Karlsruhe, Germany. 2000.*
- (23) (a) Becke, A. D. *Phys. Rev. A* **1988**, *38*, 3098(b) Perdew, J. P. *Phys. Rev. B* **1986**, *33*, 8822.
- (24) (a) Wicklein, A.; Muth, M.-A.; Thelakkat, M. *J. Mater. Chem.* **2010**, *20*, 8646(b) Chen, Z.; Stepanenko, V.; Dehm, V.; Prins, P.; Siebbeles, L. D. A.; Seibt, J.; Marquetand, P.; Engel, V.; Würthner, F. *Chem. Eur. J.* **2007**, *13*, 436.
- (25) Jones, B. A.; Facchetti, A.; Wasielewski, M. R.; Marks, T. J. *J. Am. Chem. Soc.* **2007**, *129*, 15259.
- (26) (a) Horowitz, G. *J. Mater. Res.* **2004**, *19*, 1946(b) Sun, Y.; Liu, Y.; Zhu, D. *J. Mater. Chem.* **2005**, *15*, 53.
- (27) Facchetti, A.; Mushrush, M.; Yoon, M.-H.; Hutchison, G. R.; Ratner, M. A.; Marks, T. J. *J. Am. Chem. Soc.* **2004**, *126*, 13859.

Chapter 3

Synthesis of Electron Deficient Donor-Acceptor Poly(benzobisoxazole-co-imides) Containing Naphthalene or/and Perylene

This chapter has been adapted from following publication

Nagesh B. Kolhe, S. P. Senanayak, K. S. Narayan* and S. K. Asha* *J. Phys. Chem. B*, **2010**, 114, 16694–16704.

3.1. Introduction

As discussed in previous chapter, small molecular organic semiconductors exhibited improved charge carrier mobility due to well defined molecular arrangement and high crystalline nature. However, they cannot compete with polymers in terms of viscosity, mechanical flexibility, thin-film forming nature and cost effective roll to roll fabrication which are the ultimate target of large area organic (plastic) electronics.¹ Organic semiconducting materials based on π - conjugated oligomers² and polymers³ have proved to be promising for application in optoelectronic devices such as organic field effect transistor (OFETs), light emitting diode (OLEDs), and solar cells. Polybenzobisoxazoles (PBO) (**Figure 3.1**) belong to the heterocyclic rigid-rod π -conjugated polymer family which exhibits high tensile strength, high modulus and excellent thermal and environmental stability due to the high degree of intermolecular π - π interactions present in the solid state.⁴ In addition to these, they have been shown to have excellent optical and electronic properties.

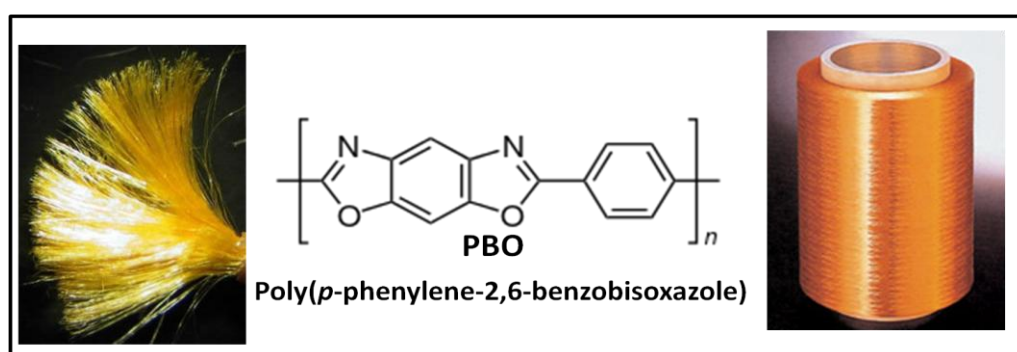


Figure 3.1 Molecular structure of PBO along with spun fibers. (Adapted from <http://www.formula1dictionary.net/zylon.html>, <http://en.wikipedia.org/wiki/Zylon>, <http://spacecollective.org/aumber/2933/Zylon>)

Pioneering work has been done on polybenzobisthiazoles (PBT) and polybenzobisoxazoles (PBO) by the group of Jenekhe *et al.*⁵ They copolymerized the rigid rod π -conjugated bisazoles with various electron rich systems like the phenylene vinylene, naphthalene, benzodithiophene, carbazole, thiophene etc and reported optoelectronic devices (OFET, OLED and solar cell) based on them (**Figure 3.2**).^{5a,c} Aromatic polyimides are also a class of high performance polymers that have gained considerable attention in microelectronics, aerospace and photoelectronics because of their excellent thermal stability, moisture resistance, mechanical strength and

electrical properties. There are examples in literature where the properties of polyimides have been improved by incorporation with ether, amide or ester functional groups.⁶ The properties that are not attainable in a single polymer can most often be realized by copolymerization of the respective monomers to obtain new polymers exhibiting good properties of both the parent homopolymers. Poly(benzoxazole-co-imide)s can be prepared by the reaction of diamines containing preformed benzoxazole moieties with dianhydrides. Combining the imide and oxazole moiety together in poly(benzoxazole-co-imide)s gives rise to a new class of rigid rod polymers having advantageous characteristics of both systems and which can fall in the niche category of *n*-type materials.⁷

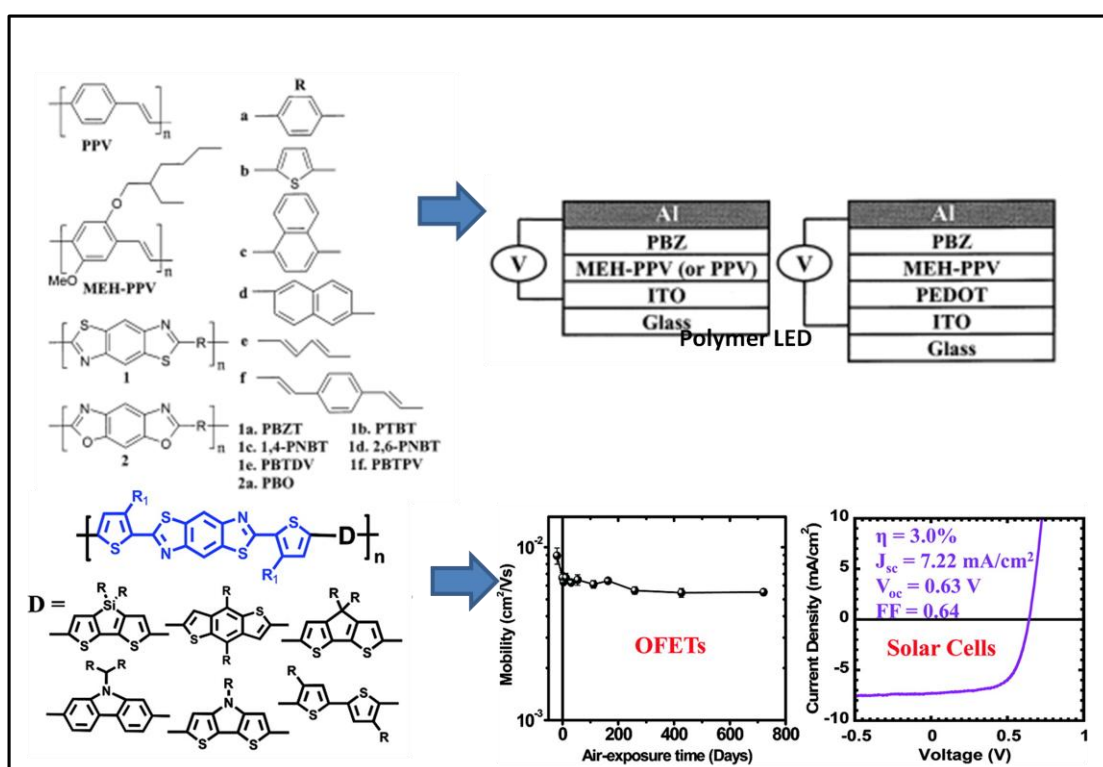


Figure 3.2 The molecular structures of some of the PBO and PBT based donor-acceptor copolymers and their application. (Adapted from Ref^{5a} and Ref⁸)

Substantial progress has been made in developing p-type conjugated polymers where mobility as high as $\sim 0.1 \text{ cm}^2 \text{V}^{-1} \text{s}^{-1}$ have been observed.⁹ Comparatively development of polymers with high electron mobility has not been so active except for a recent flurry of activity in the last couple of years.¹⁰ Exploration of new polymer semiconductors which have good air and thermal stability are important for device applications. In this context, design of new materials based on PBO and diimides of

perylene or naphthalene can provide structures with high mechanical strength and reasonable electron mobility. Processing in both these rigid aromatic systems is done through precursors which are soluble. For instance in polyimides, thermal imidization of the precursor poly(amic acid) results in films of polyimide.^{7b,c} In the PBO system also the precursor poly(o-hydroxy amide) derived from the polycondensation of diacid derivative with bis(o-amino phenol) is soluble and thermal cyclodehydration to film is possible.¹¹ But Jenekhe *et al.* have standardized a procedure for developing large area films of PBO type of polymers that can be made use for photovoltaic applications. It consists of formation of reversible Lewis acid coordination complexes by preparing isotropic solutions of the rigid rod poly(benzobisoxazole)s in nitromethane containing aluminum chloride (AlCl₃) or gallium chloride (GaCl₃).¹² This polymer-Lewis acid complex is coated on the required substrate and then washed several times with deionized water and subsequently left in deionized water overnight to ensure complete removal of the Lewis acid. Finally the polymer thin films are dried for 6 h at 80 °C in a vacuum oven. Another advantageous property of the PBO system which could be exploited in their copolymers is their ability to be spun into fibers from ordered lyotropic phases in solvents like PPA.^{4a-d} Although the liquid crystal phase is short range ordered, induced alignment of the self-organized polymer under an external force can increase the degree of orientational order over a substantially longer range in the desired direction. Perylene and naphthalenediimides are important n-type semiconducting materials which find application in photovoltaics, light emitting diodes, and field effect transistors etc because of their relative high electron affinity.¹³ Perylenediimides exhibit intense fluorescence with quantum yield reaching nearly unity. This chapter describes the synthesis, structural characterization, photophysical as well as charge transport characteristics of poly(benzoxazole-co-imides) based on perylene and naphthalenediimides in solution in methane sulfonic acid (MSA) as well as in film. Exactly alternating perylenediimide -bisoxazole and naphthalenediimide -bisoxazole copolymers as well as a random copolymer incorporating both perylene and naphthalenediimide units alternating with bisoxazole units were synthesized and characterized. The photoinduced energy transfer and charge separation was studied in MSA solution via absorption, excitation and steady state fluorescence studies. Unlike the substantial work on copolymer and blend (*p*) donor systems where energy transfer has been demonstrated,¹⁴ there are not many reports on energy transfer in (*n*) acceptor copolymer systems. The lyotropic liquid

crystalline characteristics in MSA as well as the transport characteristics in the form of thin films in Organic Field Effect Transistor (OFET) devices of these novel copolymers were also studied. We also demonstrate the degree of thermal stability in these systems where the performance increases with thermal treatment. Both the poly(benzobisoxazole)s and diimides have been shown to develop improved ordering upon subjecting to heat treatment.^{13b,15} X-ray diffraction studies have shown a structural ordering occurring upon annealing PBO fibers and energy calculations have been performed supporting this phenomenon of regularization of randomly distributed chains to more restricted chains following heat treatment.¹⁴⁻¹⁵ This ability was taken to good advantage in copolymers based on both the systems reported here. Dramatic improvement in the FET device characteristics were observed upon annealing to 150-160 °C.^{13h,16} The reasonably good n type performance and electron transport mobilities of these new poly(benzoxazole-co-imides) suggested that these are promising materials for processable high-performance applications.

3.2. Experimental Section

3.2.1 Materials

1,2,3-trichlorobenzene, Pd/C (10 %), terephthaloyl chloride, polyphosphoric acid 83 % (PPA), 4-amino benzoic acid, perylene-3,4,9,10-tetracarboxylic dianhydride (PTCDA), isoquinoline, 1,4,5,8-naphthalenetetracarboxy dianhydride (NTCDA), methane sulfonic acid were purchased from Sigma Aldrich. (PTCDA) was purified using reported procedure.^{13h} (NTCDA) was purified using sublimation and m-cresol was purchased locally and vacuum distilled twice before polymerization.

3.2.2 Instrumentations Details

¹H NMR and solid state ¹³CNMR spectra were recorded using 400-MHz Bruker NMR spectrophotometer in D₂SO₄ + D₂O containing small amounts of TMS as internal standard. Infrared spectra were recorded using a Perkin Elmer Spectrum one FT-IR spectrophotometer in the range of 4000 to 400 cm⁻¹. UV-Vis spectra were recorded using Perkin Elmer Lambda 950 UV-Vis Spectrometer. Steady state fluorescence, excitation, emission measurement were performed using Fluorolog HORIBA JOBIN YVON fluorescence spectrophotometer. The fluorescence quantum

yields of the polymer and model compounds (for perylene) were determined in MSA using Rhodamine 6G in water ($\phi = 0.95$) as the standard by exciting at 510 nm. The quantum yields for bisoxazole (quenched emission) were determined in MSA using Anthracene in cyclohexane ($\phi = 0.36$) as standard by exciting at 343 nm whereas for homopolymer (PBO) was determined in MSA using Quinine sulphate in 0.1 N H₂SO₄ ($\phi = 0.54$) as the standard by exciting at 350 nm. All the solutions were prepared having 0.1 OD at the exciting wavelength. Thermo Gravimetric analysis (TGA) was performed using a Perkin Elmer Thermo gravimetric Analyzer. Samples were run from 30 to 800 °C with a heating rate of 10 °C/min under nitrogen. The phase behaviors of the molecules were analyzed using polarized light microscope (Leitz-1350). WAXRD were recorded using Phillips x'pertpro powder X-ray diffractometer using Cu K α radiation and the spectra were recorded in the range of $2\theta = 3-50$ and at 2° per min. Electrochemical behavior of model compounds and copolymers were studied by using BAS-Epsilon potentiostat. The inherent viscosities were measured with an ubbelodhe viscometer at $30 \pm 0.1^\circ\text{C}$ in methane sulfonic acid at a concentration of 0.5 g/dL. Scanning electron microscopy (SEM) images were obtained with FEI system (Model, Quanta 200 3D Dual beam SEM with EDAX) with Tungsten filament as electron source.

3.2.3 Device Fabrication (OFET)

Bottom-contact, top-gate and top-contact, bottom-gate structures were fabricated for field effect transistor studies. Consistent, reproducible, enhanced and leakage free performance were obtained more reliably for the bottom-contact, top-gate geometry. The fabrication procedure involved initial thin film semiconductor layer spin coated in ambient from a 12 mg/ml solution in MSA of PBO and copolymers PerPBO, NapPBO and NapPerPBO at 1000 rpm for 1 min on hexamethyldisilizane (HMDS) treated glass substrates. Prior to deposition, the glass substrates were cleaned as per the standard procedure of RCA treatment. HMDS treatment of the glass substrate was done by spin coating of HMDS in liquid at 1500 rpm for 30 sec and heating the substrates at 110 °C for 2 h After the spin coating of the semiconducting layer from the MSA solution the resulting films were treated with methanol for about 30 min and then in de-ionized water for 10-12 h to remove any traces of MSA. All the devices were then dried in vacuum for 10-12 h at 70 °C to remove traces of water. After this

the semiconducting films were annealed at 150-160 °C for 30 min in glove box atmosphere. This was followed by vapor deposition of Al electrodes (10^{-6} mbar, 1 A⁰/s, 40 nm thick) on to the semiconducting film through shadow mask to obtain channels of length 60-80 μm and width of 1-2 mm. It was observed that Al formed better injecting contacts compared to Au electrodes. This is due to the fact that the LUMO level of these model polymers and monomers lie closer to the Fermi level of Al as compared to that of Au hence these polymers form a blocking contact with Au. After the electrodes deposition a dielectric bi-layer of polyvinylidene fluoride (PVDF) and Polyvinyl alcohol (PVA) were coated. The PVDF film was coated from a 60 mg/ml solution in *N, N*-Dimethylacetamide at 1000 rpm for 1 min giving a film of thickness 350 nm (Capacitance per unit area 15nF/cm²). The film was rapidly annealed at 150 °C in vacuum to facilitate the formation of a uniform β-phase. This was followed by a buffer layer of PVA coated from a 20 mg/ml solution in de-ionized water at 1000 rpm for 30 sec (Capacitance per unit area ~ 10 nF/cm²). The film was then dried in vacuum at 70 °C for 10-12 h to remove traces of water. The Al gate electrode was vapor deposited (10^{-6} mbar, 0.1 A⁰/s, 40 nm thick). The bi-layer of dielectric thus formed consisting of PVDF and PVA had effective capacitance C_0 in the range of 6-8 nF/cm² measured directly using Keithley 4200 semiconductor parameter analyzer for a film of thickness ~ 450 nm. The electrical characterization of the transistor devices were done with two identical source meters - Keithley 2400 and high impedance electrometer Keithley 6514 and cross checked with measurements from a standard Keithley 4200 semiconductor parameter analyzer. The mobility values are reported as the median values for measurement performed on a large number of devices (~ 20 -25 devices of each polymers).

3.2.4 Synthesis

Synthesis of monomers and model compounds

4, 6-dinitro 1, 2, 3-trichlorobenzene (a): To a 50 mL round-bottom flask equipped with a stirrer and condenser was added 1 g, 5.51 mmol of 1, 2, 3-trichlorobenzene and (6.2 g, 3.36 mL) 96.5 % sulphuric acid. The reaction mixture was allowed to warm to 65 °C. During this time, (1g, 0.66 mL) of 71 % concentrated nitric acid was added drop wise at such a rate as to maintain the temperature of reaction at 65 °C. Upon completion of addition, the reaction mixture was maintained at 65 °C for 5-6 h. After

completion of reaction 5-10 mL water was added drop wise to reaction mixture at such rate as to maintain the reaction temperature between 45 to 65 °C. Vigorous stirring was maintained throughout the reaction. The reaction mixture was cooled to room temperature and isolated by filtration, washed with water and air dried. Some amount of mononitrated compound was also formed during the reaction which was purified by recrystallization from methanol. Yield: 1.3 g (87 %). ¹H NMR (200 MHz, CDCl₃) δ ppm: 8.27(s, 1H). Melting point: 94-96 °C.

1,3-dihydroxy-2-chloro-4, 6-dinitrobenzene (b): To a 50 ml round-bottom flask equipped with a stirrer and condenser was added 1g, 3.69 mmol of 4, 6-dinitro 1, 2, 3-trichlorobenzene and 6.2 g of water and heated with constant agitation. When the temperature reached 35 °C, 0.88 g of sodium hydroxide (50 % solution in water) was added in one portion. Heating was continued to 75-80 °C with stirring for about 18 h. The reaction mixture was cooled to room temperature and neutralized with 2 ml of concentrated hydrochloric acid then filtered and washed with water and dried. The purity was confirmed by thin layer chromatography (TLC) which indicated single spot. This product was directly used for the next step without further purification. Yield: 0.7 g (81 %). ¹H NMR (200 MHz, CDCl₃) δ ppm: 9.05 (s 1H aromatic), 11.61 (s 2H phenolic –OH). Melting point: 168-170 °C.

Diaminodihydroxybenzene dihydrochloride (DADHB): Parr reactor equipped with a stirrer was charged with (10 g, 42.55 mmol) of 1,3-Dihydroxy-2-chloro-4, 6-dinitrobenzene, 50 mL of glacial acetic acid, 15 mL of water, 3.5 g of sodium acetate and 0.6 g of Pd/C (10 %). The sealed reactor was charged with 400 psi of hydrogen gas and temperature was brought to 40 °C. The temperature was maintained between 40 to 50 °C during the course of reaction. After a brief induction period, the uptake of hydrogen became extremely rapid and hydrogen pressure was maintained between 100-400 psi during the reaction. Upon completion of reaction, no further uptake of hydrogen was observed. The reactor was cooled to room temperature, and 34 mL of concentrated hydrochloric acid containing 0.85 g of SnCl₂.2H₂O was added to the reaction mixture. The crude product with catalyst was isolated by filtration. This material was dissolved in 20 mL of water at 85 °C for 30 min and catalyst was removed by filtration. Water (15-20 mL) was added to the filtrate along with 42 mL of hydrochloric acid and the catalyst-free material was precipitated from the brown solution. The crude compound was dried and recrystallized by following procedure.

Recrystallisation: 4 g of the crude DADHB was added in 3.5 mL of hydrochloric acid and heated until complete dissolution. 0.5 g of charcoal and 0.25 g of $\text{SnCl}_2 \cdot \text{H}_2\text{O}$ were added and refluxed for a period of 15 min. The charcoal was removed by filtration and filtrate was cooled to 0 °C. White needles of the recrystallized product were isolated by filtration. Yield: 1.8 g (20 %). ^1H NMR (200 MHz, DMSO- d_6) δ ppm: 6.98 (s, 1H, aromatic), 7.53 (s, 1H, aromatic), 9.98 (broad, NH_2), 11.12 (s, 2H, OH protons). Melting point: 252-254 °C. Anal. Calcd. for $\text{C}_6 \text{H}_{10} \text{Cl}_2 \text{N}_2 \text{O}_2$: C, 33.82; H, 4.73; N, 13.15. Found C, 32.82; H, 4.98; N, 10.53.

Synthesis of (2,6-Di(*p*-amino phenyl)benzo[1,2-*d*;5,4-*d'*]bisoxazole) (bisoxazole diamine): 50 g of Polyphosphoric acid (PPA) containing 83 % of P_2O_5 was taken in a 250 mL three necked round bottom flask equipped with an overhead stirrer. PPA was heated at 200 °C for 1 h and then the temperature was reduced to 100 °C under continuous flow of nitrogen. 2.4 g (0.011 mmol) of diaminodihydroxybenzene dihydrochloride (DADHB) was then added and the reaction mixture was stirred at the same temperature for approximately 2 h. After complete dehydrochlorination, 3.08 g (0.22 mmol) of 4-aminobenzoic acid was added and the reaction mixture heated to 120 °C for 4 h. The temperature of the reaction mixture was slowly increased to 150 °C over a period of half an hour and maintained at the same temperature for further 10 hr. The temperature was then further increased to 170 °C over a period of half an hour and continued at same temperature for 2 h. Finally the reaction mixture was cooled to 100 °C and poured in to 500 mL of distilled water. The reaction mixture was filtered off and the residue was thoroughly washed with 5 % sodium bicarbonate solution and then with distilled water. The crude compound (3.2 g) was further purified by dissolving in 60 mL DMSO and heating at 80 °C for 1 h. The compound was then cooled to room temperature and 200 mL of toluene was added and cooled to 0 °C for 2-3 h. The cooled solution was filtered off and filtrate was poured in to another previously cooled (at 0 °C) 300 mL of toluene and kept overnight at 0-5 °C. Yellow crystals formed in solution was filtered off and dried at 80 °C in vacuum. Yield: 2.35 g (61%). ^1H NMR (200 MHz, DMSO- d_6) δ ppm: 8.10 (s, 1H oxazole), 7.91 (d, 4H aromatic), 7.87 (s, 1H oxazole), 6.75 (d, 4H aromatic). ^1H NMR (400 MHz, D_2SO_4 in D_2O) δ ppm: 8.45 (s, 1H oxazole), 8.33 (d, 4H aromatic), 8.26 (1H, oxazole) 7.68 (d, 4H aromatic). FT-IR (KBr, cm^{-1}): 3316 (NH str), 1622 (C=N of oxazole), 1285 and 1055 (C-O-C str.). Anal. Calcd. for $\text{C}_{20} \text{H}_{14} \text{N}_4 \text{O}_2$: C, 70.17; H, 4.12; N, 16.37. Found C, 70.48; H, 3.47; N, 17.25.

2, 6 -diphenyl benzobisoxazole (model compound M1): A similar procedure as that described above was adopted using 1.14 g (9.38 mmol) of benzoic acid instead of 4-aminobenzoic acid along with 30 g of polyphosphoric acid (PPA) and 1 gm (4.69 mmol) of diaminodihydroxybenzene dihydrochloride (DADHB). The crude compound was recrystallised from toluene and dried at 80 °C in vacuum. Yield: 1.2 g (82 %). ¹H NMR (400 MHz, CDCl₃ + TFA) δ ppm: 8.41 (1H, oxazole), 8.26 (4H, aromatic), 8.08 (1H oxazole), 7.70-7.66 (m, 6H, aromatic). FTIR (KBr, cm⁻¹): 1622 (C=N of oxazole), 1285 and 1055 (C-O-C str.). Anal. Calcd. for C₂₀ H₁₂ N₂ O₂: C, 76.91; H, 3.87; N, 8.97. Found C, 77.17; H, 3.58; N, 8.79.

***N,N'*-diphenyl- 3,4,9,10-perylenetetracarboxylic-diimid (model compound M2):** A mixture of 0.5 g (1.27 mmole) 3,4,9,10-perylenetetracarboxylicdianhydride, 20 g of imidazole, 50 mg of zinc acetate and 0.28 mL (3.17 mmole) of aniline was stirred at 100 °C in a two-necked round bottom flask. The temperature of the reaction mixture was increased to 160 °C and maintained at the same temperature for 7 to 8 h. The reaction mixture was then cooled to room temperature and acidified with 2N hydrochloric acid. The precipitate was then filtered off and washed with plenty of water and dried under vacuum at 100 °C overnight. Yield: 0.5 g (83 %). ¹H NMR (400 MHz, CDCl₃ + TFA) δ ppm: 8.92 (8H, perylene), 7.59 (6H, aromatic), 7.32 (4H, aromatic). Anal. Calcd. for C₃₆ H₂₀ N₂ O₄: C, 79.40; H, 3.70; N, 5.14. Found C, 77.27; H, 3.00; N, 6.92.

Synthesis of polymer

Poly (p-phenylenebenzobisoxazole) PBO: A cylindrical vessel equipped with two additional side openings and fitted with mechanical stirrer and a nitrogen inlet/outlet was used as the polymerization setup. To this setup, 0.852 g, 4 mmol of DADHB, (0.812 g, 4 mmol) of terephthaloyl chloride, and 6 g of polyphosphoric acid (83 %) were added. The resulting mixture was dehydrochlorinated under continuous nitrogen flow at 65 °C for more than 16 h. Then the mixture was heated to 100 °C for another 16 h. It was then cooled to room temperature with constant stirring and 1.6 g P₂O₅ was added to generate polyphosphoric acid. The mixture was stirred for 2 h at 80 °C and then cooled to room temperature. A further 1.43 g P₂O₅ was then added to the reaction mixture to increase the P₂O₅ concentration. The mixture was heated to 160 °C for 16 h with constant stirring and then at 200 - 220 °C for an additional 4 hrs. The thick viscous polymer was precipitated into water and washed with plenty of water to

remove the polyphosphoric acid and then dried under vacuum at 100 °C for 24 hrs. (Yield: 0.9 g 96 %) FT-IR (KBr, cm^{-1}): 2926, 2858, 1620, 1574, 1462, 1264, 1103, 851.

PerPBO: A two necked 50 mL round bottom flask equipped with nitrogen inlet /outlet was charged with 20 mL of m-cresol, 1 mL isoquinoline and 0.5 g (1.46 mmol) bisoxazole diamine. After complete dissolution of monomer at 80 °C, 0.5 g (1.46 mmol) 3,4,9,10-perylenetetracarboxylic dianhydride (PTCDA) was added to the flask in one portion. The reaction was kept at 80-90 °C for 24 h. and then the temperature was slowly increased to 180 °C and maintained at same temperature for 12-14 h. The reaction mixture was further heated at 210 °C for 5-6 h. For work up, the excess m-cresol was distilled off by vacuum distillation and the resulting dark red solution was poured into acetone (300 mL). The resulting solid was washed repeatedly with aqueous sodium hydroxide (1N) solution, followed by water and methanol. After drying under vacuum at 100 °C overnight, polymer was obtained as a dark red solid (0.8 g, 80 %). ^1H NMR (400 MHz, D_2SO_4 in D_2O) δ ppm: 8.85 (8H, perylene), 8.52-8.34 (6H, aromatic and oxazole), 7.79 (4H, aromatic). ^{13}C NMR (solid state) δ ppm: 90, 106, 115, 121, 127, 132, 138, 148, 150, 161, 164. FTIR (KBr, cm^{-1}): 3090, 1699, 1668, 1608, 1592, 1504, 1435, 1402, 1340, 1252, 1171, 1054, 1021, 835. Anal. Calcd. (CHN): C, 75.32; H, 3.02; N, 7.98. Found C, 73.45; H, 3.06; N, 10.92.

NapPBO: A similar procedure as that described for the PerPBO copolymer was adopted using 0.391 g (1.46 mmol) 1,4,5,8-Naphthalenetetracarboxylic dianhydride (NTCDA) in place of perylenetetracarboxy dianhydride. The polymer was obtained as a yellow solid (0.73 g, 86 %). ^1H NMR (400 MHz, D_2SO_4 in D_2O) δ ppm: 8.74 (4H, naphthalene), 8.51-8.32 (6H, aromatic and oxazole), 7.68 (4H, aromatic). ^{13}C NMR (solid state) δ ppm: 91, 108, 115, 125, 129, 138, 147, 161. FTIR (KBr, cm^{-1}): 3093, 1712, 1673, 1607, 1581, 1505, 1432, 1411, 1342, 1249, 1188, 1055, 1022, 856. Anal. Calcd. (CHN): C, 70.71; H, 2.97; N, 9.70. Found C, 67.30; H, 2.44; N, 9.63.

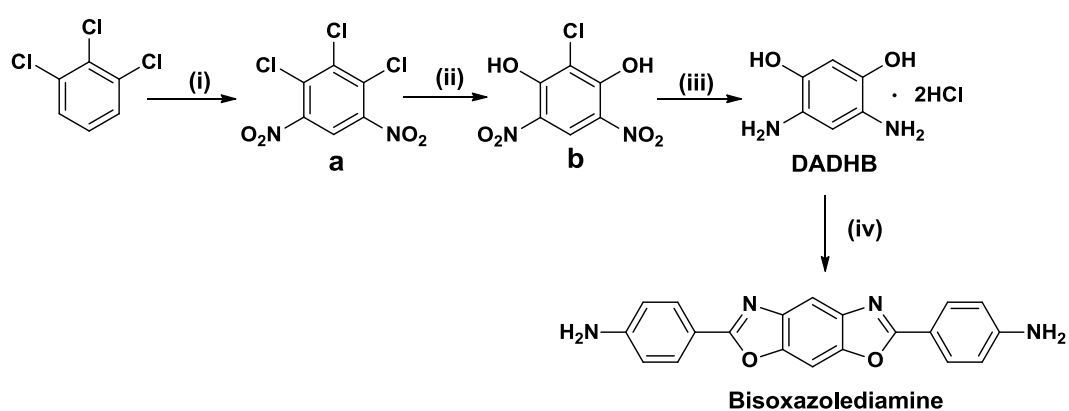
NapPerPBO: A similar procedure as that described for the PerPBO copolymer was adopted using 0.286 g (0.73 mmol) PTCDA and 0.195 g (0.73 mmol) NTCDA along with 0.5 g (1.46 mmol) of bisoxazolidiamine. The random copolymer was obtained as a dark red solid (0.85 g, 80 %). ^1H NMR (400 MHz, D_2SO_4 in D_2O) δ ppm: 8.85 (perylene), 8.76 (naphthalene) 8.50- 8.35 (6H, aromatic and oxazole), 7.72 (4H, aromatic). FTIR (KBr, cm^{-1}): 3088, 1711, 1702, 1670, 1607, 1592, 1510, 1431, 1410,

1344, 1252, 1177, 1052, 1020, 844. Anal. Calcd. (CHN): C, 73.29; H, 2.92; N, 8.77. Found C, 70.90; H, 1.43; N, 9.26.

3.3 Results and Discussion

3.3.1 Synthesis and Characterization

Diaminodihydroxybenzene dihydrochloride (DADHB) monomer required for synthesis of poly (p-phenylenebenzobisoxazole) (PBO) was synthesized in three steps (**Scheme 3.1**) using 1, 2, 3-trichlorobenzene as starting material according to literature reported procedure.^{4b}

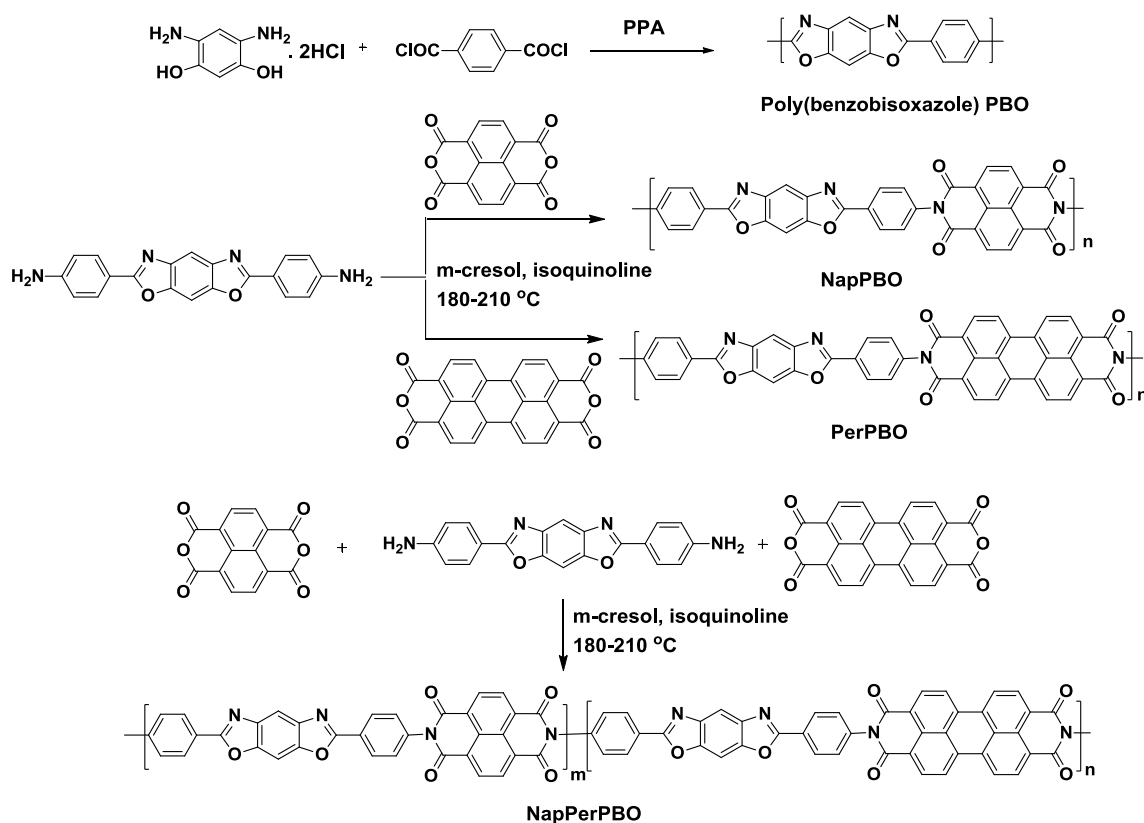


Reaction conditions: i) $\text{HNO}_3/\text{H}_2\text{SO}_4$ 65 °C ii) $\text{NaOH}/\text{H}_2\text{O}, \text{HCl}$ 80 °C iii) $\text{H}_2/\text{Pd/C}$, NaOAc , Acetic acid 400psi iv) polyphosphoric acid, 170 °C

Scheme 3.1 Synthesis of monomer DADHB and bisoxazolediamine.

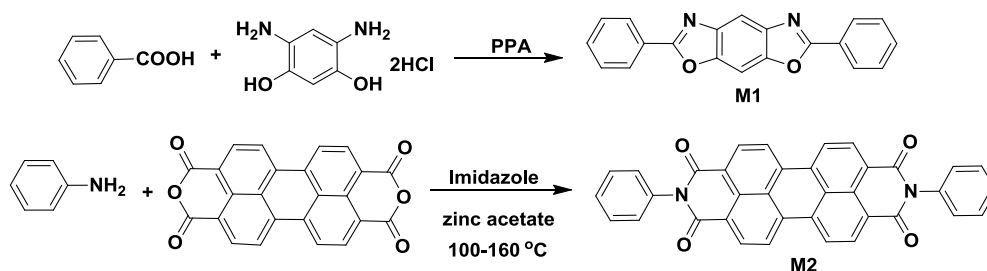
The nitration of 1, 2, 3-trichlorobenzene at 4 and 6 position was carried out using nitrating mixture (sulfuric acid and nitric acid). The presence of chlorine guaranteed that only dinitration occurred at positions 4 and 6 in the benzene ring with no possibility of trinitration. After displacement of 1, 3-dichloro groups by hydroxyl groups, the final catalytic hydrogenation step combines reduction of nitro to amine groups and hydrogenolysis of the 2-chlorine atoms and yielded the high quality monomer (DADHB). A suitable bisoxazole diamine monomer (2,6-Di(p-amino phenyl) benzo[1,2-d:5,4-d']bisoxazole) required for synthesis of poly(benzobisoxazole-co-imides) was synthesized in PPA at 170 °C using 4-aminobenzoic acid and DADHB following literature procedure (**Scheme 3.1**).¹⁷ The synthesis of poly (p-phenylenebenzobisoxazole) (PBO) and copoly(benzoxazole)

imides is given in **Scheme 3.2** and the detailed procedure is given in the experimental section (3.2.4.).



Scheme 3.2 Synthesis of homo and copolymers.

PBO homopolymer was synthesized by condensation polymerization using diaminodihydroxybenzene dihydrochloride (DADHB) and terephthaloyl chloride in polyphosphoric acid (PPA) containing 83 % P_2O_5 as reported in the literature.^{4a,c,18}



Scheme 3.3 Synthesis of model Compound M1 and M2

The poly (benzobisoxazole-co-imides) containing naphthalene or perylenediimide was synthesized by condensation of diamino-bisoxazole monomer with 1,4,5,8-naphthalenetetracarboxylic dianhydride (NTCDA) or perylene-3,4,9,10-

tetracarboxylicdianhydride (PTCDA) to form the polyimides PerPBO or NapPBO in a one- step imidization in *m*-cresol and isoquinoline at 180-210 °C in good yields. A random copolymer of bisoxazole diamine with perylene and naphthalene dianhydride NapPerPBO was also synthesized by taking 0.5 moles each of both dianhydrides and reacting with one equivalent of bisoxazole diamine.

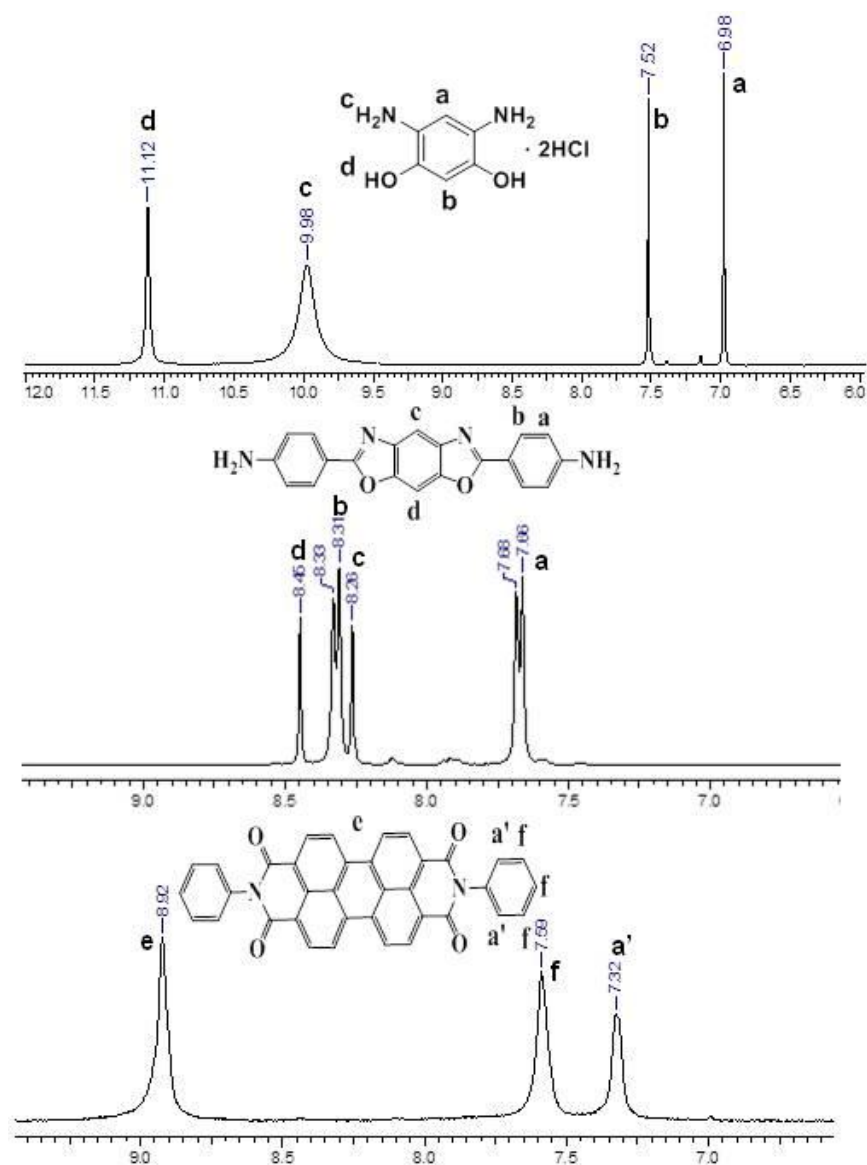


Figure 3.3 ¹H NMR spectra of monomer and model compound.

There was a recent report where a carboxyl terminated perylenediimide was condensed with DADHB in PPA as a comonomer along with terephthalic acid as the main monomer.¹⁹ This route could introduce only < 2 mol % of perylenediimide into the polymer backbone and that too in a random manner. The imidization route adopted in our procedure has the advantage of producing exactly 1:1 alternating

copolymer of perylene or naphthalene diimides with benzobisoxazole units. Model compounds which were representative of the benzobisoxazole unit (M1) and perylenediimide unit (M2) were synthesized as shown in **Scheme 3.3**. The structure of monomers and copolyimides was confirmed by ^1H NMR recorded in deuterated sulfuric acid (D_2SO_4) and DMSO-d_6 and also by solid state ^{13}C NMR and FT-IR spectroscopy. The ^1H NMR spectra of the monomer (DADHB and bisoxazole diamine) and model compound M2 was shown in **Figure 3.3** which was further used to structurally identify the peaks in the proton NMR spectra of the polymers.

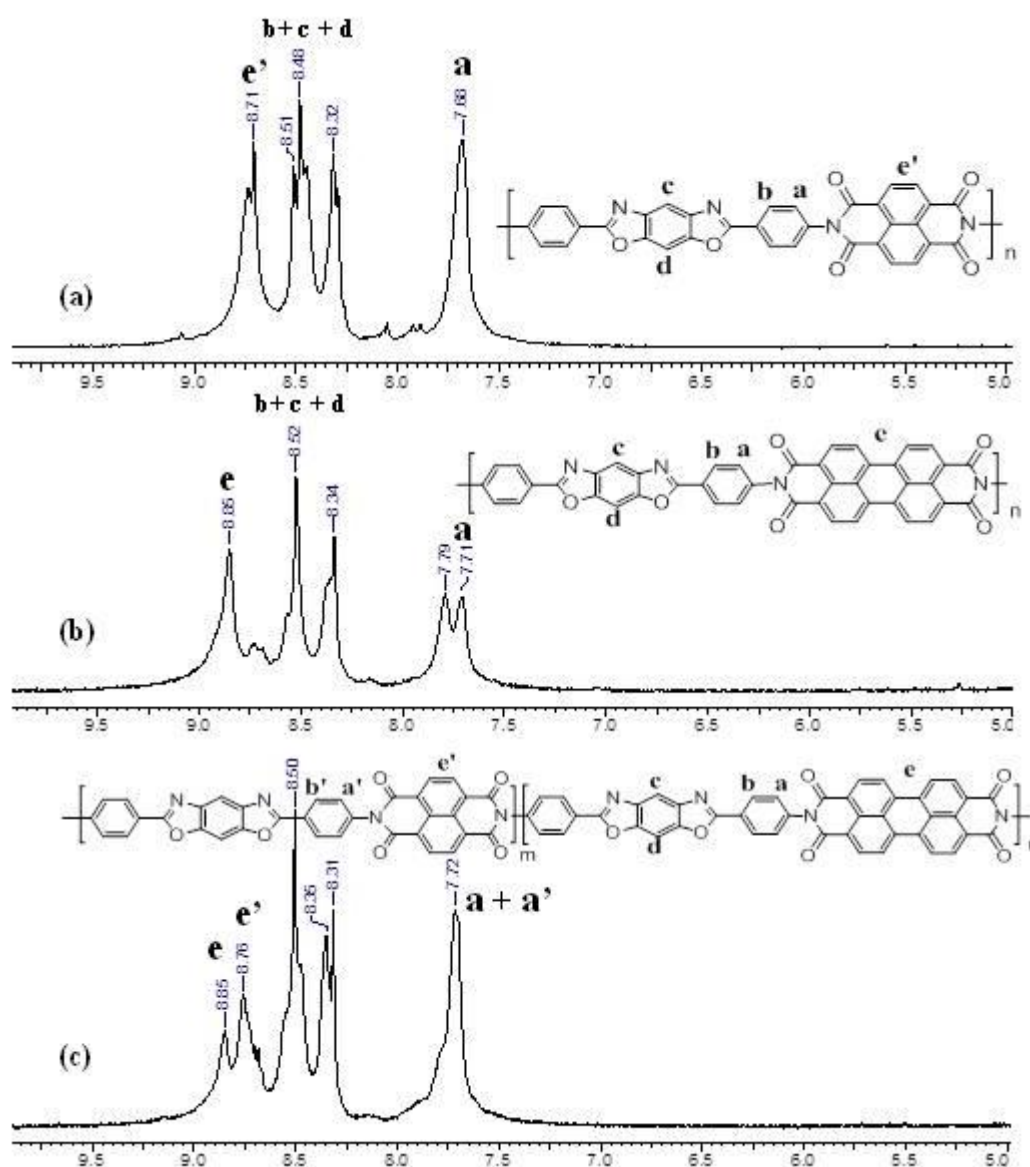


Figure 3.4 ^1H NMR spectra of (a) NapPBO (b) PerPBO and (c) NapPerPBO recorded in D_2SO_4 .

Figure 3.4 shows the labeled ^1H NMR spectra of polymers – (a) NapPBO (b) PerPBO and (c) NapPerPBO. It could be seen from the **Figure 3.4** that the intensity of the four protons of the naphthalene ring (e') was more than that due to the eight protons corresponding to that of perylene (e) indicating higher incorporation of naphthalene compared to perylene into the random chain even though they were taken in equal mole ratio in the feed. An exact calculation of the incorporation of perylene with respect to naphthalene could not be made since there was a slight overlap of the perylene protons with those of the naphthalene protons; however, approximately it was calculated to be 70:30 naphthalenediimide: perylene diimide.

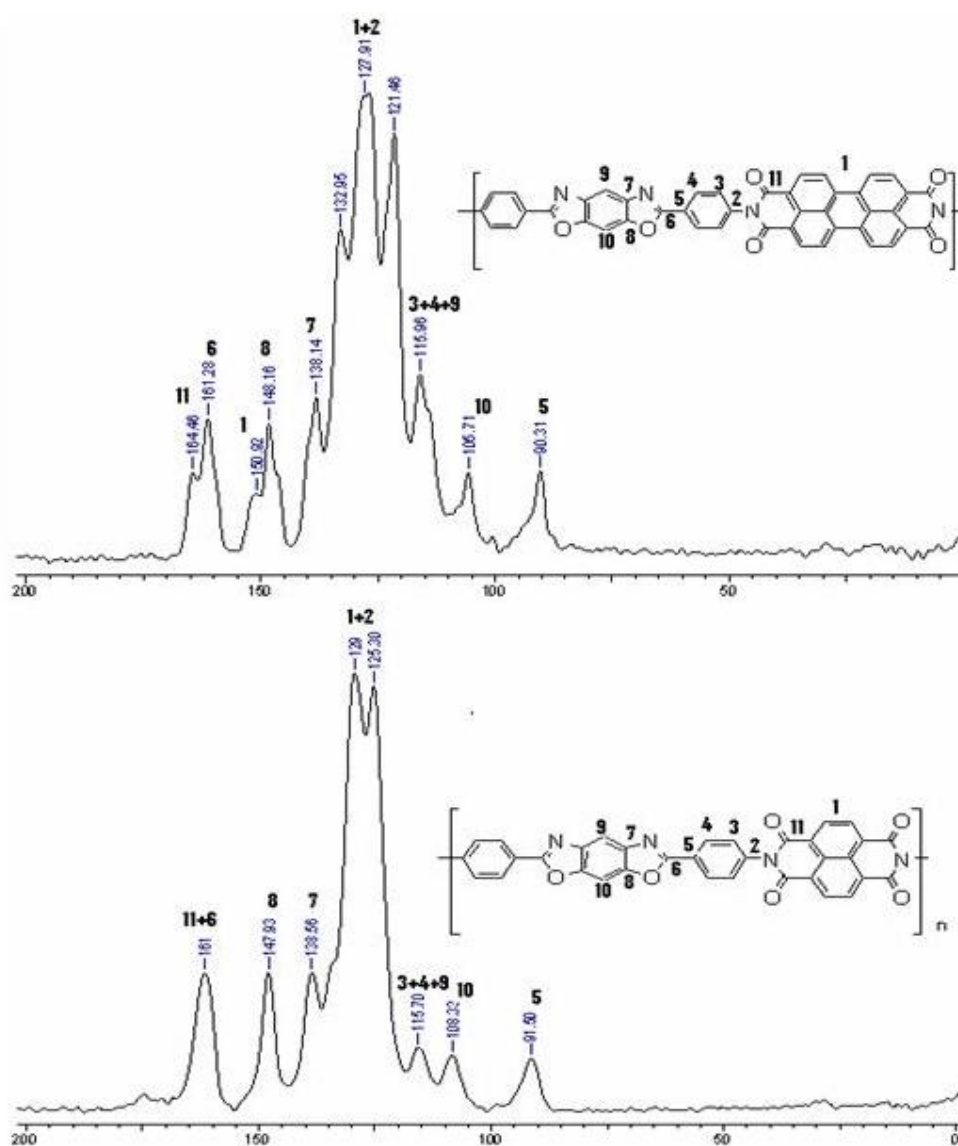


Figure 3.5 Solid state ^{13}C NMR spectra of naphthalene and perylenediimide copolymers.

Similarly, the solid state ^{13}C NMR spectra of the naphthalene and perylene PBO copolymers (**Figure 3.5**) also clearly confirmed the structure of the polymers. The peak corresponding to carbonyl region of perylene and naphthalene appeared at 164 and 161 ppm respectively. The peak corresponding to the C-O of benzoxazole ring appeared at 161 ppm.²⁰ In the PerPBO copolymer these two were clearly differentiable at 164 and 161 ppm whereas in the NapPBO polymer the carbonyl as well as C-O of oxazole ring appeared as a single peak at 161 ppm. Completion of imidization in polymers could also be confirmed by FT-IR as shown in the **Figure 3.6** by following the disappearance of the 6-membered anhydride peak at 1774 cm^{-1} and the appearance of the characteristic imide peak at 1699 cm^{-1} and 1668 cm^{-1} (indicated by arrows) in the copolymers containing perylene.^{13g} In the naphthalene copolymer, the peak was observed at 1712 cm^{-1} and 1673 cm^{-1} .

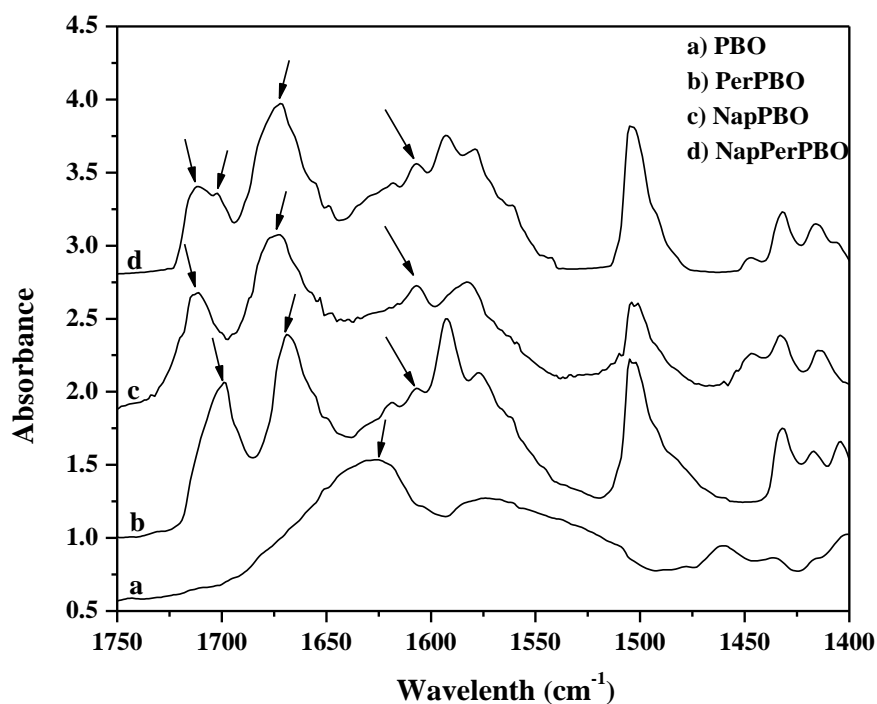


Figure 3.6 FT-IR spectrum of homopolymer a) PBO and copolymer b) PerPBO c) NapPBO d) NapPerPBO.

In the random copolyimide containing both perylene and naphthalenediimide units in the back bone, two imide stretching peaks were observed at 1712 and 1702 cm^{-1} corresponding to naphthalene and perylene imides respectively. In all the copolyimides, along with imide stretching peak an additional peak was observed at 1610 cm^{-1} corresponding to the characteristic peak of benzoxazole ring. Thus the

NMR as well as FTIR spectra could successfully be utilized to confirm the incorporation of the various units in the copolymer backbone. The insolubility of the copolymers in common organic solvents like tetrahydrofuran (THF) and chloroform (CHCl_3) made molecular weight determination by size exclusion chromatography (SEC) impossible. However, as is the practice in the case of similar rigid rod polymers reported in literature, the inherent viscosities were measured for the homo and copolymers in methane sulfonic acid (MSA) at 30 °C.^{4a} The inherent viscosity values η_{inh} in (dL/g) are given in the **Table 3.1**. The homopolymer PBO which was polymerized in PPA had very high viscosities - 5.27 dL/g and the polymer also was precipitated in the form of long fibers. However, the incorporation of the imides drastically reduced the viscosity of the copolymers resulting in polymers with low inherent viscosities and average molecular weights.²¹ The inherent viscosity values for PerPBO and random copolymer NapPerPBO was ~ 0.24 dL/g only. The NapPBO copolymer had the lowest viscosity among the copolymers. The direct comparison of the viscosity values of the homopolymer PBO with these poly (oxazoleimide)s is not justified since the conditions of polymerization were different.

Table 3.1 10 % Weight loss temperature, Inherent viscosity and yield of homo and copolymers.

Polymers	10% Wt. loss (°C) ^a	Viscosity η_{inh} (dL/g) ^b	Yield (%) ^c
PBO	666	5.27	96
PerPBO	535	0.24	80
NapPBO	432	0.15	86
NapPerPBO	496	0.23	80

a) Temperature represents 10 % weight loss in TGA measurements at heating rate of 10 °C/min under nitrogen b) Inherent viscosity measured in MSA (0.5 g/dL) at 30 ± 0.1 °C c) Final yield of the precipitated and washed sample.

PBO is known to polymerize in high molecular weights from PPA as solvent. The polyimides of perylene and naphthalenediimides reported in literature are however not very high due to the inherent low solubility of the formed polymer.²² Therefore, the

inherent viscosity of 0.2 dL/g reported here indicated reasonably high molecular weight and the perylene containing polymers were obtained as dark red powders. The **Figure 3.7** shows the TGA thermograms of the homo and copolymers and the 10 % weight loss temperatures are given in **Table 3.1**. PBO had the 10 % weight loss temperature above 660 °C, but with incorporation of the imide units, this was decreased to 535 °C for perylene and to 470 °C for naphthalene copolymer indicating that the disruption of the rigid rod structure of PBO decreased the overall thermal stability of the system. The differential scanning calorimetry (DSC) data recorded for copolymers did not show any melting transition up to a temperature 350 °C.

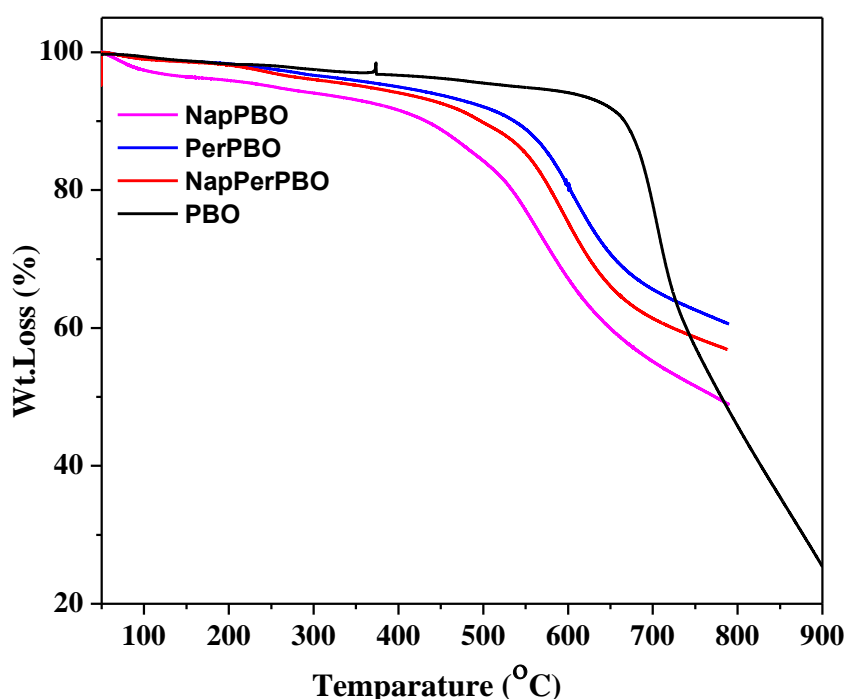


Figure 3.7 TGA thermograms of homo and copolymers.

3.3.2 Liquid Crystalline Phases

Perylene or naphthalenediimides are known to induce thermotropic liquid crystallinity in small molecules or oligomers; whereas rigid rod polymers like PBO are known to form lyotropic liquid crystalline phases in solvents like MSA, PPA etc at a critical concentration from which polymer fibers having good mechanical properties can be spun. The three copolymers however did not exhibit any thermotropic liquid crystalline characteristics in the DSC thermogram or under the polarized light microscope (PLM). The formation of lyotropic mesophases (critical concentration)

was studied by preparing different concentration of polymer solutions in methanesulfonic acid (MSA). The sample dope was sealed between glass slides, annealed at 80 °C for 15 min and allowed to stand in a desiccator for 6 h and then examined under the PLM.²³ It was found that PBO formed mesophases as confirmed by the observation of birefringence under crossed polarizers beyond a critical concentration of 5 wt % (clearing temperature 85 °C). Typical birefringent pattern as reported in literature was observed.²³⁻²⁴ For the PerPBO copolymer, the critical concentration was observed at ~ 6 wt % (clearing temperature 80 °C) and beautiful bright red birefringence typical of perylene was observed. The NapPBO copolymer's critical concentration was observed at 10 wt % (clearing temperature 80 °C) and green birefringence was observed. The NapPerPBO random copolymer showed red birefringence beyond a critical concentration of 8 wt% (clearing temperature 80 °C). **Figure 3.8** shows the PLM images of the lyotropic phases of the polymers observed under crossed polarizers.

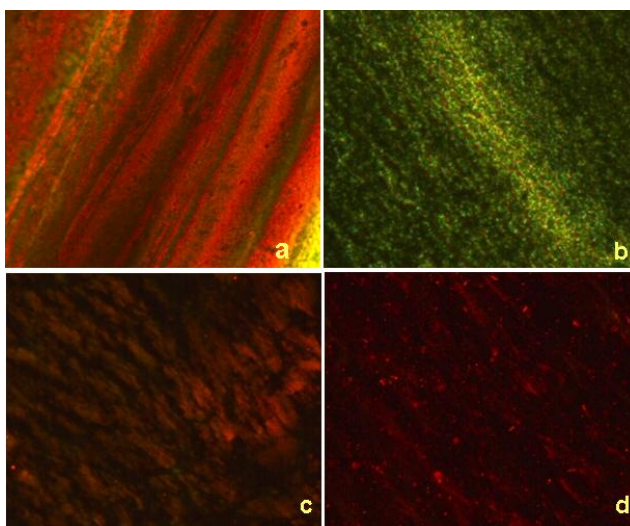


Figure 3.8 Crossed-polarized optical micrographs of a) 5 % PBO (b) 10 % NapPBO (c) 6 % PerPBO and (d) 8 % NapPerPBO in MSA.

The disruption of PBO packing by either perylene or naphthalenediimides units did not destroy the mesophase tendency of the polymers. In these imide-oxazole copolymers the diimide units at every alternative position introduced a kink in the polymer backbone; however, this deviation from backbone linearity did not deleteriously affect the propensity for liquid crystal formation. Perylene as well as naphthalenediimides are well-known for their π - π stacking interaction in solutions as

well as in solid state and this also aids in parallel chain packing leading to observation of mesophases.

3.3.3 Wide Angle X-ray Diffraction (WAXRD)

The ordered structure of the copolymers was investigated by wide angle X-ray diffraction (WAXRD) as shown in **Figure 3.9** and all the related information is listed in **Table 3.2**. PBO has a characteristic WAXRD pattern with two major diffraction peaks around $2\theta = 16.1^\circ$ ($\sim 5.50 \text{ \AA}$) and $2\theta = 26.5^\circ$ (3.35 \AA). The former corresponds to “side-to-side” distance on (200) plane (due to lateral packing of stacks - interstack) and the latter to the “face-to-face” distance on (010) plane (stacking -intrastack) between two neighbouring rod molecular chains of Poly(benzobisoxazole)s respectively.²⁵

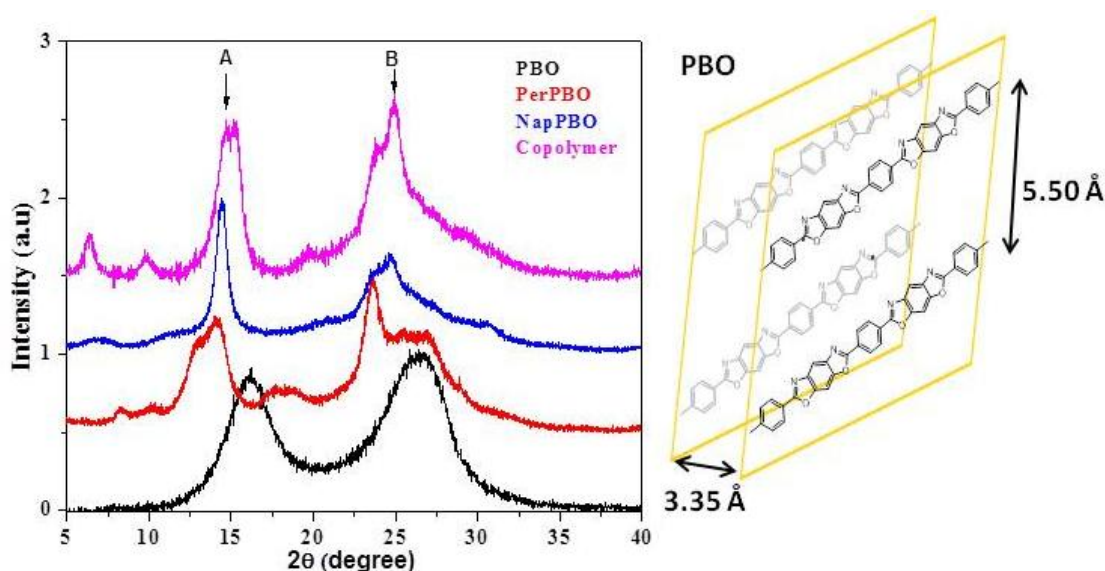


Figure 3.9 Wide angle X-ray diffraction curves for homo and copolymer and cartoon showing the packing in PBO.

The copolymers PerPBO, NapPBO as well as NapPerPBO had several peaks in the $2\theta = 3$ to 35° range. In all copolymers the periodic order corresponding to the 5.50 \AA side-to-side spacing was shifted to higher d -spacing. The introduction of perylene or naphthalenediimide units is expected to increase the side-to-side distance in the copolymers. The 3.36 \AA which corresponded to the face-to-face PBO stacking was observable, though only as a shoulder in the case of the NapPerPBO and NapPBO polymer. The PerPBO polymer had a sharp peak $\sim 3.7 \text{ \AA}$ whose sharpness indicated better ordering. This corresponded to the π - π stacking in perylene aromatic ring.

Normally the perylene π - π stacking is observed at ~ 3.5 Å.²⁶ The expansion in this π - π stacking is due to the incorporation of benzoxazole units between the perylene units. This π - π stacking peak in the NapPBO polymer was observed at 3.59 Å. In the NapPerPBO random copolymer, sharp peaks were observed at both 3.57 and 3.76 Å corresponding to the π - π stacking of both perylene and naphthalene. Thus the WAXRD also gave structural proof for the incorporation of the diimides into bisoxazole backbone.

Table 3.2 XRD results of the copolymers.

Polymer	$2\theta^\circ$		d-spacing (Å)	
	A	B	A	B
PBO	16.13	26.53	5.50	3.35
PerPBO	14.35	23.70	6.24	3.76
NapPBO	14.50	24.73	6.14	3.59
NapPerPBO	14.06	23.75	6.02	3.76
	15.20	24.09	5.81	3.57

3.3.4 Photophysical Studies

The UV-Vis absorption and emission spectra of the copolymers and the model compounds were recorded in MSA solution. **Figure 3.10** shows the UV-Vis absorption spectra of the polymers and model compounds recorded in MSA. PBO exhibited characteristic absorption peaks at 403 and 428 nm.²⁵ In the PerPBO copolymer the broad peak ~ 346 nm is attributed to bisoxazole unit, and the latter three peaks at 475, 510 and 547 nm are the characteristic absorption of perylene diimide. In the NapPBO copolymer, the absorption of naphthalene diimide was overlaid by that of the bisoxazole absorption and a broad peak at 368 nm having a shoulder at 386 nm was observed. In the NapPerPBO random copolymer of perylene and naphthalenediimide with bisoxazole also the peaks lower than 400 nm corresponded to the absorption of naphthalenediimide and bisoxazole whereas the three peaks beyond 450 nm corresponded to that of perylenediimide. **Figure 3.10 A)** shows the stackplot of the absorption spectra of the model compounds M1 and M2

along with that of the 1:1 molar blend of M1 and M2 recorded in MSA. The absorption corresponding to the perylene unit was blue shifted in the copolymers compared to the perylenediimide model compound M2. The coefficient of absorption of the bisoxazole is much higher compared to that of perylene diimide, therefore, the 1:1 molar blend of M1 and M2 had lower intensities of absorption for perylene. The absorption of the blend resembled a linear superposition of the respective model compounds. This difference in behaviour of the copolymers compared to the blend is a clear indication that in the copolymers there was a perturbation of the electronic transition in the ground state upon covalent linkage.

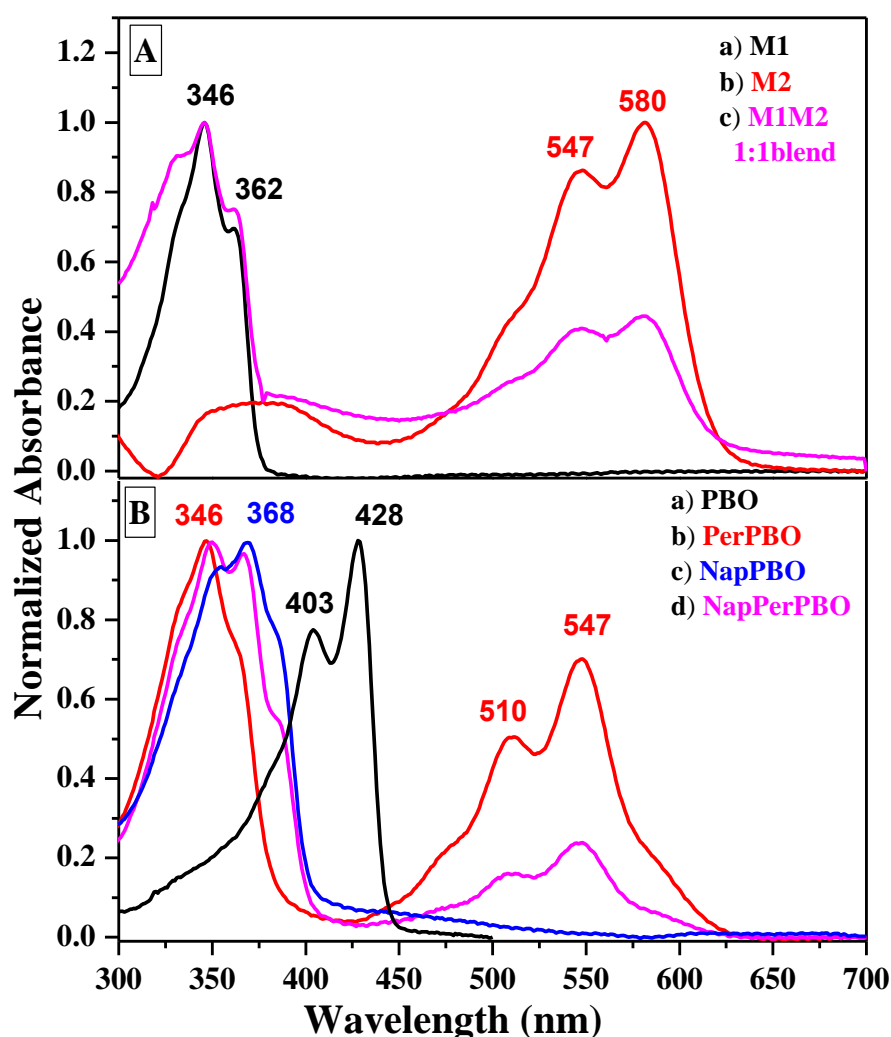


Figure 3.10 UV-Vis absorption spectra of [A] model compounds M1, M2 and a 1:1 blend of M1 and M2 and [B] the copolymers along with PBO recorded in MSA.

Comparing the absorption spectra of the PerPBO copolymer with the random copolymer NapPerPBO, the peak intensities of the perylene part was much reduced in the latter. This is due to lower incorporation of perylene as well as due to the

naphthalene diimide absorption also enhancing the optical density at 350 nm in the latter. The absorption of PBO was red shifted by ~ 70 nm compared to its own model compound M1 due to the planarity and rigidity of the benzobisoxazoles which resulted in increased conjugation upon polymerization. On the other hand, the absorption of the benzoxazole moiety in all the copolymers with perylene or naphthalenediimide was blue shifted by ~ 80 nm compared to the homopolymer PBO. The imide linkage at every alternate position in the copolymers resulted in a disruption of the extended π network of the PBO promoting strong hypsochromic shift. **Figure 3.11** shows the absorption (black) and emission (red) spectra of the model compounds M1 and M2 showing the spectral overlap of the bisoxazole emission with that of the perylene absorption. This is the primary requirement for Förster energy transfer between Donor (D) – Acceptor (A) systems.²⁷

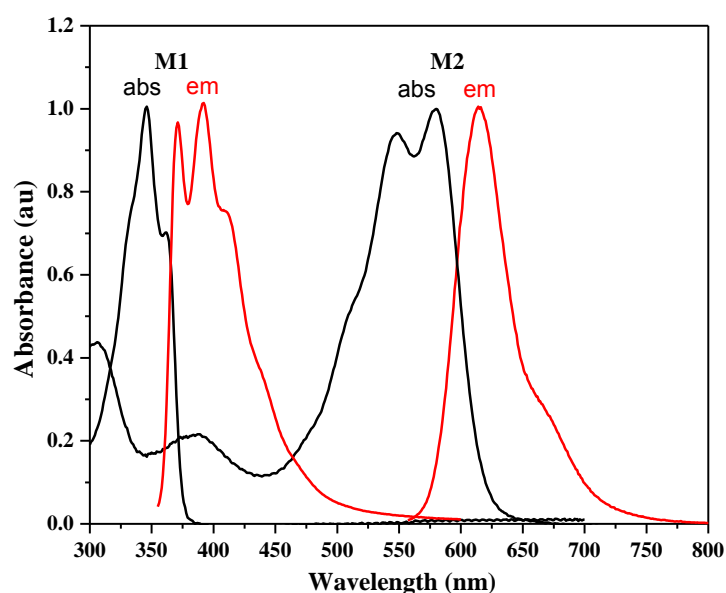


Figure 3.11 Absorption (black) and emission (red) spectra of model compounds M1 and M2 in MSA (0.1 OD solutions).

Although heterocyclic benzobisoxazole are electron deficient, compared to the highly electron withdrawing perylenediimides, the bisoxazole has very weak electron accepting properties; hence it can act as donor to perylene diimides.²⁸ Since there was no overlap between the absorption spectra of the bisoxazole and perylene units, it was possible to selectively excite either of them by choosing appropriate excitation wavelength. An effective method to study the energy/electron transfer resulting from photoexcitation between a covalently linked D-A molecule is to examine the

photoluminescence quenching observed on blending the individual components.²⁷ The emission spectra were recorded and the quantum yields determined (**Table 3.3**) for the model compounds and copolymers in MSA by exciting at both the bisoxazole absorption λ_{max} of 345 nm as well as at the perylene absorption λ_{max} of 545 nm. **Figure 3.12** top shows the emission spectra of the copolymer PerPBO along with that of M1 and a 1:1 blend of M1 and M2 upon excitation at 345 nm (all solutions having 0.1 OD at the bisoxazole absorption maxima of 347 nm).

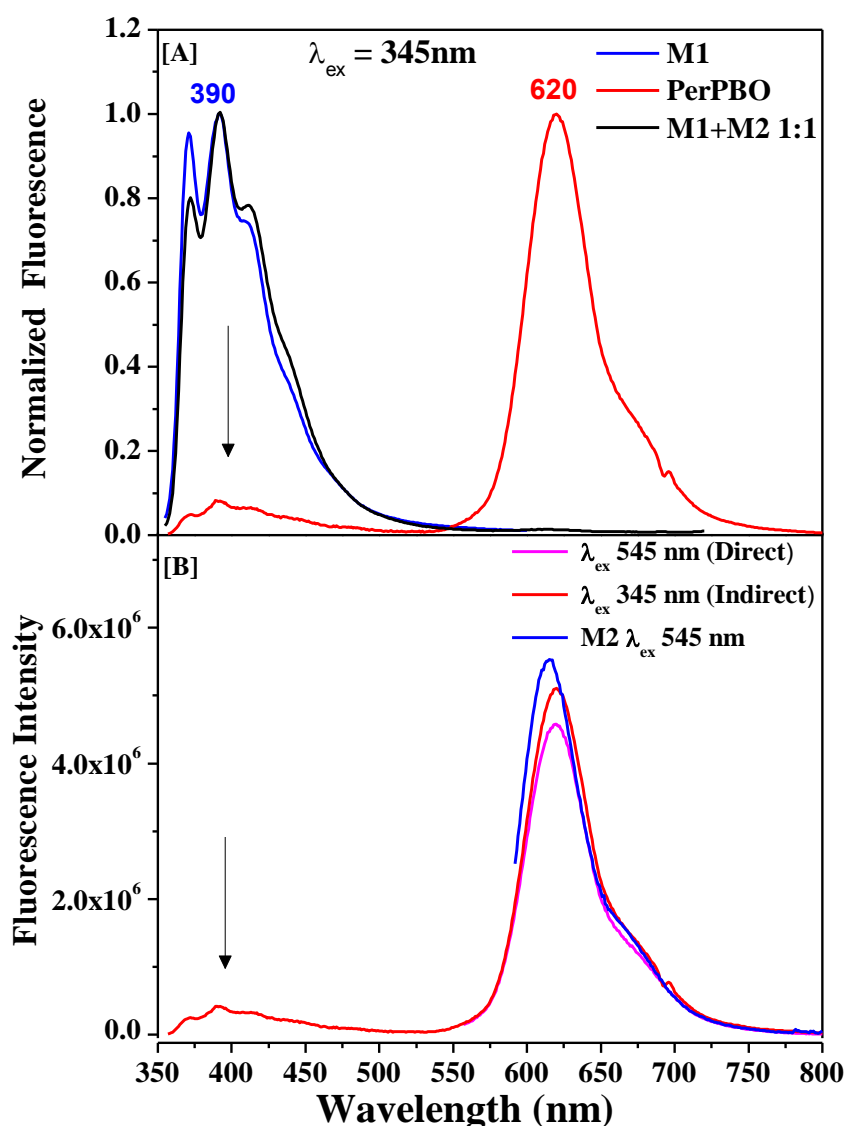


Figure 3.12 Emission spectra of M1 and a 1: 1 molar mixture of M1 and M2 along with PerPBO in MSA (0.1 OD solutions); excitation: 345 nm.

The 1:1 blend and M1 exhibited almost identical emission at λ_{max} of 390 nm. M2 did not have any appreciable emission upon excitation at 345 nm (not shown in figure).

The PerPBO copolymer, on the other hand, had almost complete quenching ($\sim 92\%$, $\phi_{\text{MSA}} = 0.008$) of the bisoxazole emission at 390 nm (indicated by arrow) but had an intense peak corresponding to perylene emission at λ_{max} of 620 nm, indicating a near complete energy transfer.

Table 3.3 Photophysical properties of the copolymer and model compounds in MSA.

Polymers	Absorption peak λ (nm)	Emission λ_{max} (nm)	Quantum yield $\phi_{\text{bisoxazole}}^c$	Quantum yield ϕ_{Per}^d
M1	345, 365	391 ^a	0.71	-
M2	510, 545, 580	615 ^b	-	0.65
PBO	403, 428	438 ^{a'}	0.25	-
PerPBO	346, 475, 510, 547	390 ^a , 620 ^{a, b}	0.008	0.51
NapPBO	349, 368, 386	390 ^a , 445 ^a	0.013	-
NapPerPBO	349, 366, 386, 475, 510, 545	390 ^a 445 ^a , 618 ^{a, b}	0.020	0.59

a) Excitation at 345 nm (a') Excitation at 403 nm b) Excitation at 545 nm c) The fluorescence quantum yields were obtained upon excitation at 343 nm and were measured using anthracene as a standard; for PBO the excitation wavelength was 402 nm and quinine sulfate was the reference. d) The fluorescence quantum yields were obtained upon excitation at 510 nm and were measured using rhodamine-6G as a standard.

The excitation spectra were recorded to examine if energy transfer took place from oxazole to perylene unit. **Figure 3.13** compares the absorption and excitation spectra for PerPBO copolymer measured by monitoring the emission of the acceptor perylenediimide at 620 nm. Besides the absorption of perylene, an absorption band corresponding to oxazole unit with maxima at 347 nm was also present in the excitation spectra. This suggested that upon photo-excitation, energy transfer channel existed between the bisoxazole to perylene units. However, the intensity of the sensitized or indirect emission from perylene was not 100 %. It was slightly quenched (7 %) when compared to the reference compound. This slight quenching of the

emission indicated that apart from energy transfer, an additional process of quenching like electron transfer from bisoxazole to perylene was also involved. The excitation spectra in **Figure 3.13** also showed that a clear difference existed between the absorption and excitation spectra in the bisoxazole absorption region of 300- 400 nm. This indicated that direct electron transfer also occurred upon excitation of the bisoxazole moiety.²⁹

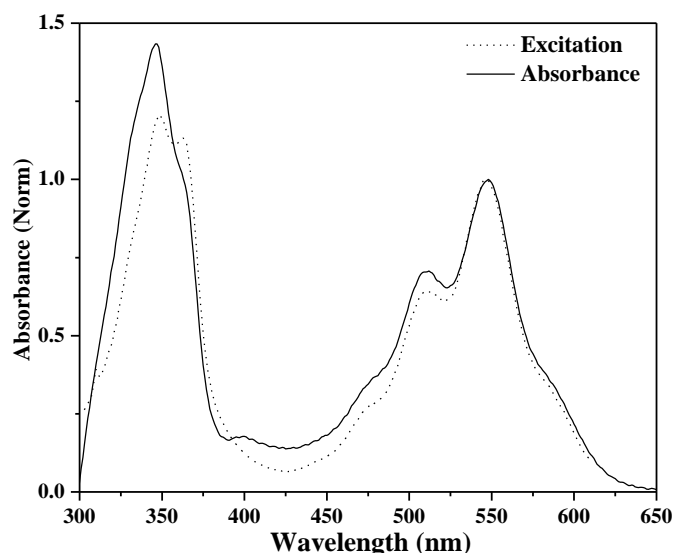


Figure 3.13 Normalized absorption (solid lines) and excitation (dotted lines) spectra of the PerPBO copolymer in MSA.

Figure 3.12 B) bottom compares the emission from M2 and copolymer PerPBO both upon direct (perylene) excitation at 545 nm as well as sensitized / indirect excitation at 345 nm. The indirect emission from PerPBO was higher in intensity compared to the emission upon direct excitation of the perylenediimide unit. This observation is very similar to that reported by J. Pan et. al where dendrons with perylene core and oxadiazole periphery exhibited strong light harvesting potential and gave intense perylene emission upon excitation of the oxazole periphery compared to direct perylene excitation.¹³ⁱ Similarly in the copolymer PerPBO, the PBO units act as a funnel channelling energy to the perylene units. If there were no other quenching pathway the emission intensity from perylenediimide upon direct excitation (545 nm) should have been the same as that of M2. However, the perylene emission from the copolymer upon direct excitation also was quenched (~18 %) and quantum yields of the perylene emission was also lower ($\phi_{MSA} = 0.51$) compared to that from M2 ($\phi_{MSA} = 0.65$). Photoexcitation of the perylene unit cannot result in energy transfer but

charge separation can still occur resulting in quenching of the perylene fluorescence. **Figure 3.14** shows the schematic representation of the possible energy and electron transfer pathways upon excitation at 345 nm or 545 nm. An important point of consideration in this energy / electron transfer processes is the fact that the PBO units are protonated in MSA which could result in enhanced delocalization and planarization of the heterocyclic and aromatic ring leading to better electronic coupling.³⁰ This would facilitate the energy/electron transfer from bisoxazole to perylene upon excitation at 345 nm corresponding to λ_{\max} of absorption of bisoxazole.

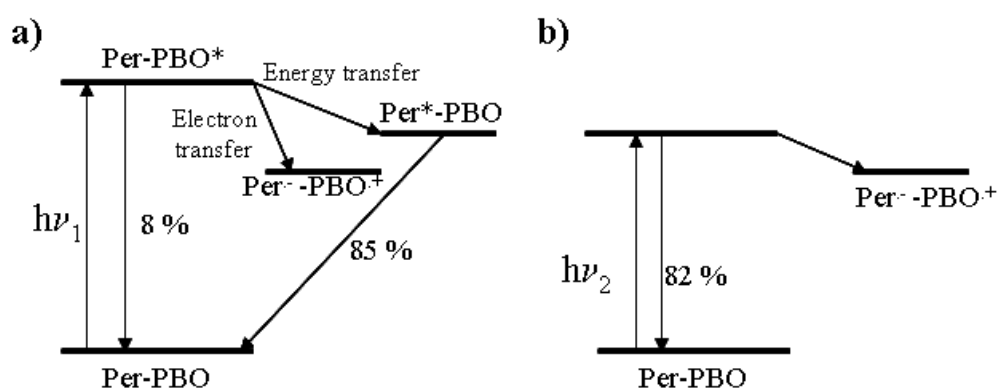


Figure 3.14 Schematic diagram of the PerPBO copolymer showing energy and electron transfer pathways upon excitation of (a) PBO λ_{ex} : 345 nm and (b) Perylene λ_{ex} : 545nm.

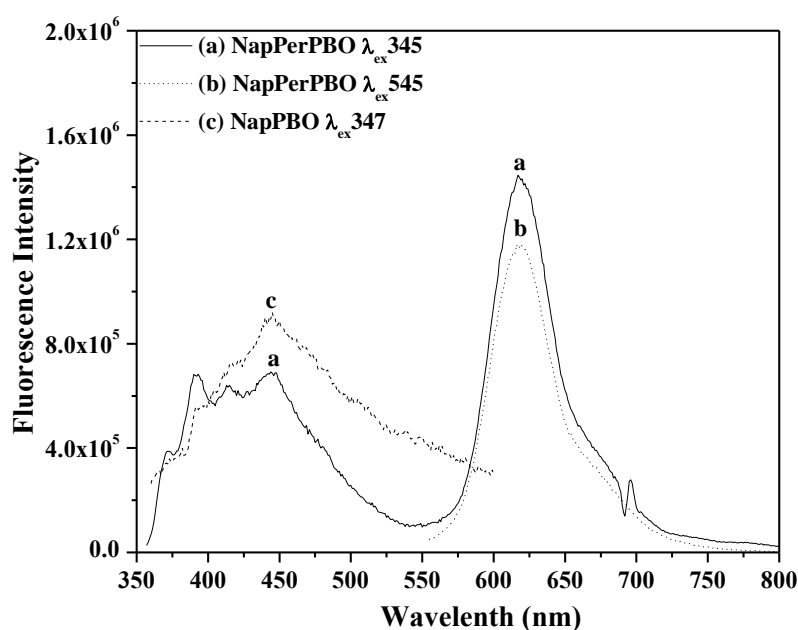


Figure 3.15 Emission spectrum of the NapPBO and NapPerPBO in MethaneSulfonic acid upon indirect (347 nm) and direct (545 nm) excitation (MSA) (0.1 OD solutions).

Figure 3.15 shows the emission from the copolymers NapPBO and NapPerPBO upon excitation at 345 nm. The polymer showed characteristic naphthalene emission at λ_{max} of 445 nm. The NapPerPBO random copolymer showed emission from naphthalene as well as from perylene units. The indirect excitation (at donor wavelength) resulted in higher intensity of perylene emission compared to direct excitation (at acceptor wavelength) as was observed in the case of PerPBO copolymer. The additional gradient in the energy levels from the PBO unit to the perylene units due to the presence of naphthalene units should benefit the energy transfer process. Photoexcitation studies were carried out in the solid state for the various copolymers. Films were prepared by spincoating from MSA solution, washing in deionized water and leaving it in deionized water for several hours followed by washing with acetone and drying in vacuum oven at 60 °C overnight. **Figure 3.16** shows the absorption (inset: PL for PerPBO copolymer) spectra of the film samples.

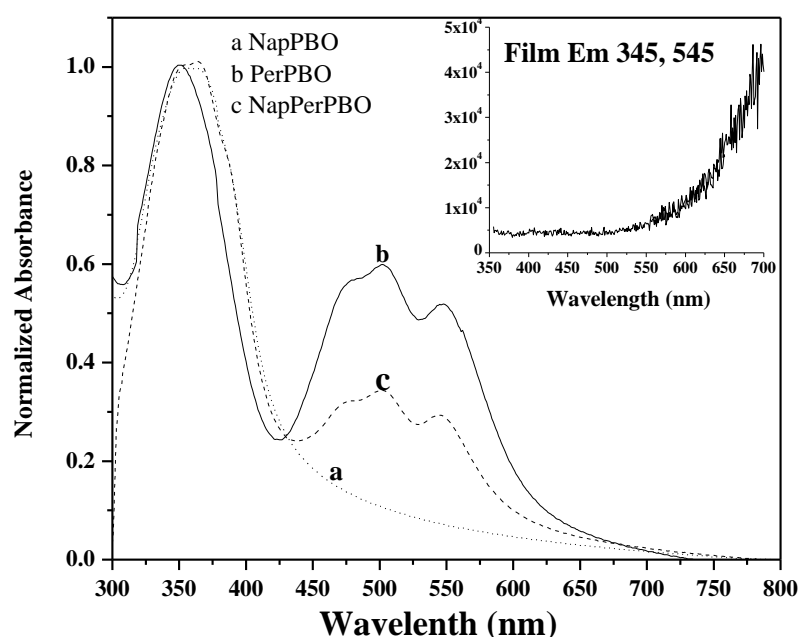


Figure 3.16 Normalized Absorption spectra of the copolymers in solid state (film), inset shows the quenched emission both upon direct (345 nm) and indirect (545 nm) excitation for PerPBO film.

The absorption showed a change in the peak intensity ratios of the 0-0, 0-1 transitions along with a red shift of the onset in perylene which is a signature of H type or face to face π - π stacking interaction of the perylene aromatic cores.³¹ The PBO homopolymer film showed a weak red shifted emission at 498 nm, (which has been attributed to excimer or aggregate formation)³² but the emission was totally quenched in the

copolymer films for both direct as well as indirect excitation.^{13g} The complete quenching of fluorescence of both chromophores demonstrated efficient chain packing taking place in the solid state.

3.3.5 Electrochemical Properties

The effect of molecular structure upon electrochemical properties was explored through the measurement of the electrochemical reduction using cyclic voltammetry (CV). The model compounds and polymers were deposited as thin films from MSA on to the platinum working electrode which was immersed in deionized water overnight, washed with acetone, dried in vacuum oven at 60 °C and then their CV recorded in 0.1 M *n*-Bu₄NPF₆ / acetonitrile solution. The CV measurement was repeated to check reproducibility and this process of film deposition was found to be perfectly reproducible for CV measurement. **Figure 3.17** shows cyclic voltammetry curves for copolymers and the values of the redox potentials along with calculated HOMO/LUMO energy levels for monomers, copolymer and model compounds were mentioned in **Table 3.4**.

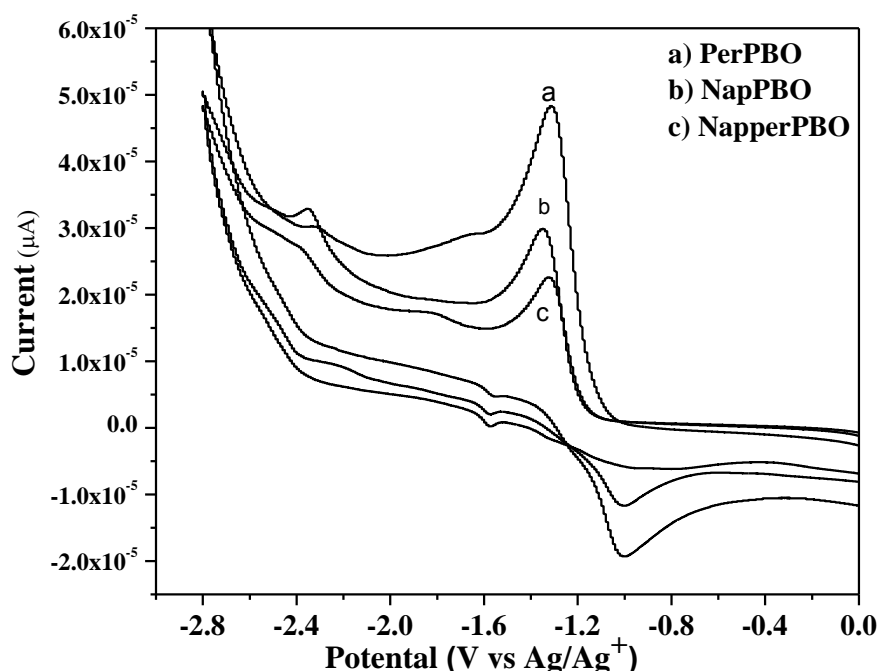


Figure 3.17 Cyclic voltammograms of reduction of a) PeryPBO b) NapPerPBO c) NapPBO in 0.1 M *n*-Bu₄NPF₆ / acetonitrile at scan rate 0.2 V/s.

The potential was measured against Ag/Ag⁺ reference electrode (Ag wire in 0.01 M AgNO₃) using internal standard Ferrocene / Ferrocenium (FC/FC⁺) redox system.

Perylenediimides generally exhibit two reversible reduction peaks in the cathodic scan corresponding to the first and second one electron stepwise reduction of the perylene core to the monoanion and dianion respectively.³³ M2 easily got reduced exhibiting two quasi-reversible reduction peaks at -1.37 V and -1.04 V respectively at a scan rate of 0.2 V/s. The cyclic voltammogram of model compound M1 could not be recorded in solution (acetonitrile) due to poor solubility; neither could it be drop casted as a thin film from chloroform dispersion. Therefore, for comparison the cyclic voltammogram was recorded for the diamine monomer (bisoxazole-diamine) which was soluble in DMF. The reduction potential of benzoxazole is known to be very high (-2.3 V) and DMF as a solvent is known to be stable up to -3 V. Bisoxazole diamine exhibited two reversible peaks at -2.3 V and -2.7 V. The homopolymer PBO exhibited a reduction peak at -2.36 V which is well matched with that reported in literature.³⁴

Table 3.4 Redox potential and HOMO/LUMO values of model compounds and copolymers.

Polymers/ model compounds	Epc ₁ /Epa ₁ (V)	Epc ₂ /Epa ₂ (V)	Bisoxazole part in copolymers Epc/Epa (V)	LUMO (eV)	HOMO (eV)	E _g (opt) (eV)
Bisoxazole- diamine	-2.30/-2.28	-2.70/-2.60	-	-2.50	-5.60	3.10
M2	-1.04/-0.84	-1.37/-1.07	-	-3.80	-5.86	2.06
PBO	-2.36/-1.97	-	-	-2.83	-5.60	2.77
PerPBO	-	-1.34/-1.08	-2.48/-2.35	-3.70	-5.76	2.06
NapPBO	-	-1.36/-1.20	-2.47/-2.35	-3.68	-6.56	2.88
NapPerPBO	-	-1.37/-1.18	-2.47/-2.35	-3.68	-5.74	2.06

a) Epc = cathodic peak potential; Epa = anodic peak potential.

b) Each measurement is calibrated with ferrocene/ferrocenium redox system Vs Ag/Ag⁺ reference electrode.

PerPBO copolymer showed a single reversible reduction peak at -1.31 V due to reduction of perylene moiety and upon increasing the potential further, another reduction peak was observed at -2.3 V corresponding to reduction of the bisoxazole group. One irreversible oxidation peak of bisoxazole also appeared during the anodic

scan at 1.5 V. NapPBO and NapPerPBO polymer also exhibited reduction peaks at -1.32 V and -1.34 V respectively and a second reduction peak for bisoxazole at same reduction potential as that observed in the case of PerPBO copolymer. It is thus evident from the CV data that the reduction potential for perylene or naphthlene containing copolymer was low compared to that of poly(benzobisoxazole). Unlike the model compound M2, the PBO copolymers with perylene or naphthalenediimide had only a single reduction peak corresponding to that of the imide. It has been reported in literature that in the homologues diimides – perylene, terrylene and quaterrylene, as the conjugation increased the spacing between the two successive 1e reduction waves decreased until the two peaks completely overlapped.³³ Similarly, in the PBO copolymers also the two reduction peaks merged into one single 2e peak, due to the extensive π overlap among the perylene and naphthalenediimide units existing in the polymer. Cyclic voltammogram of copolymer indicated that there was no marked difference of reduction potential of perylene and naphthalene unit in polymer backbone since their LUMO values were nearly same.³⁵ LUMO energy level of polymer and model compounds were estimated based on the onset of the polymer reduction peak and reference energy level of ferrocene (4.8 V below the vacuum level) according to $E_{\text{LUMO}} (\text{eV}) = -e \times (E^{\text{red onset}} + 4.8)$ below the vacuum level.^{13a} HOMO energy level were estimated from optical band gap and the LUMO energy level and are listed in **Table 3.4**. HOMO/LUMO energy level values for free model compound (M2) and in copolymer were nearly same for perylene as well as bisoxazole group as their reduction potential remained same upon polymerization. In case of PerPBO and NapPerPBO copolymer the HOMO energy level values were -5.76 eV and -5.74 eV respectively and in case of NapPBO the corresponding HOMO energy value was -6.56 eV. On the other hand, HOMO energy value for benzobisoxazole part was -5.60 V³⁴ which was above the HOMO of perylene and naphthalene. The LUMO energy level value for benzoxazole part was much higher (-2.5 eV) than either perylene or naphthalene group. Thus these energy level values gave additional support to energy and electron transfer from bisoxazole to perylene on exciting the bisoxazole.²⁷

3.3.6 Device Characteristics (OFET)

The devices fabricated from these polymers showed excellent saturation n-type transport with Al as the source/drain and gate electrode as indicated from the gate

dependant output curve and transconductance curves shown in **Figure 3.18** for PerPBO and NapPerPBO.

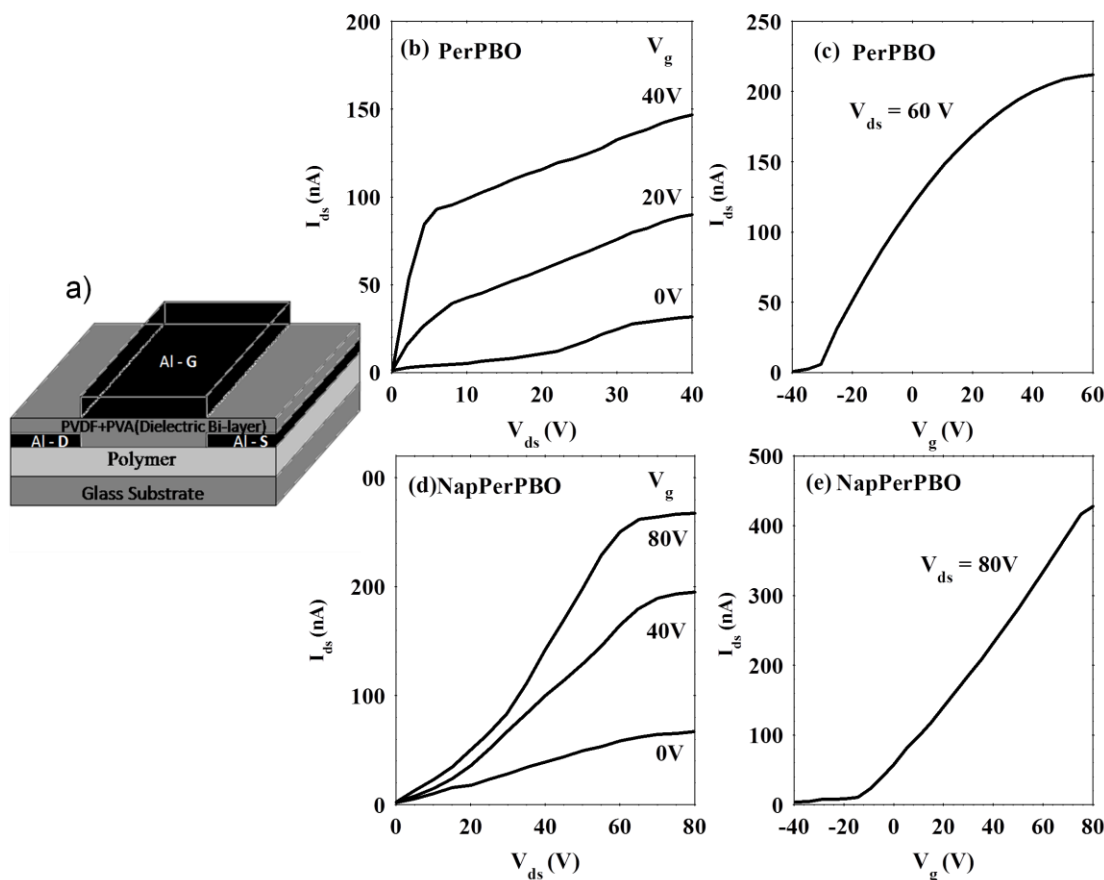


Figure 3.18 a) Schematic of a bottom contact top gate OFET, (b, c) transistor curves for PerPBO polymer, (d, e) transistor curves for NapPerPBO polymer.

The saturation region carrier mobility was calculated with the standard transconductance characteristics of the drain source current (I_{ds}) in the saturation mode: $I_{ds} = (\mu_{FET}WC_0/2L)(V_g - V_t)^2$ where μ_{FET} is the field effect electron mobility, C_0 is the effective capacitance, W the channel width, L the channel length of the transistor, V_g and V_t are the gate and threshold voltage respectively and the results are summarized in **Table 3.5**. All the FETs based on these polymer systems exhibited good current modulation with on/off ratio greater than 10^2 upon annealing (150-160 °C for 30 minutes). In contrast, the unannealed samples displayed poor mobilities. The large improvement upon annealing is illustrated by the values of μ_{FET} for PerPBO before and after annealing (**Table 3.5**).^{13b,36} **Figure 3.19** shows the SEM images of PerPBO copolymer before and after annealing at 160 °C for one hour clearly showing differences in morphology upon annealing. Annealing can provide the polymer chains

enough energy to access better conformational arrangement and sufficient time to have optimized alignment of the polymer chain within the micro domain itself and in the process decreasing the trap state density. Specifically, annealing can introduce better phase separation in the segmented copolymer which can explain the higher transport properties.^{13b}

Table 3.5 OFET characteristics of the copolymers.

Polymer	μ_e ($\text{cm}^2\text{V}^{-1}\text{s}^{-1}$)	$I_{\text{on}}/I_{\text{off}}$
PBO	$(1\pm 0.16) \times 10^{-4}$	6×10^2
PerPBO	$(0.8\pm 0.18) \times 10^{-4}$ $(6.2 \times 10^{-6})^{\text{a}}$	2×10^3
NapPBO	$(8\pm 1.04) \times 10^{-4}$	2×10^3
NapPerPBO	$(2\pm 0.31) \times 10^{-3}$	4×10^2

a) Without annealing

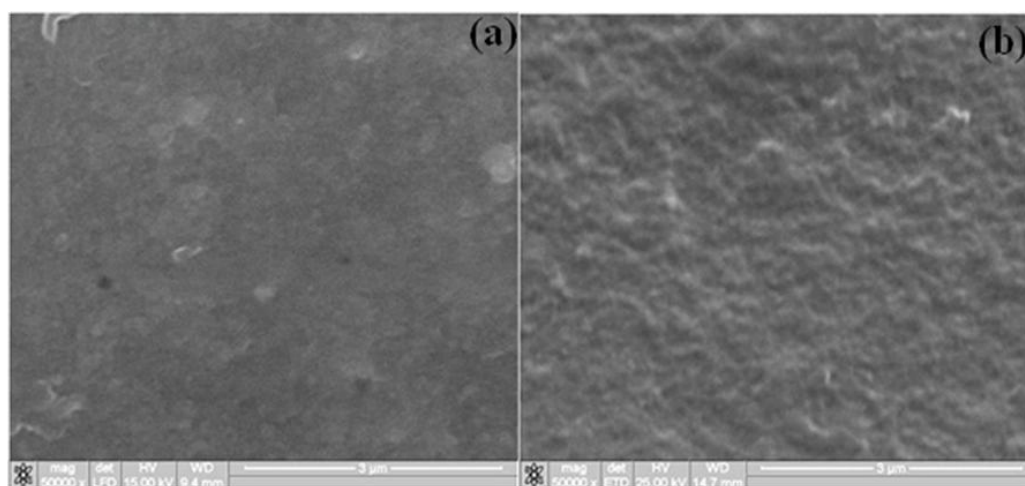


Figure 3.19 SEM image of PerPBO (a) before annealing and (b) after annealing at 160 °C for 1 h.

The observation from a large number of devices tested showed a trend where the random copolymer containing both perylene and naphthalene diimides exhibited the highest mobility of $0.2 \times 10^{-2} \text{ cm}^2 \text{ V}^{-1}\text{s}^{-1}$ with an on/off ratio of 4×10^2 . The alternating copolymer of perylenediimide with benzobisoxazole i.e. PerPBO had

mobilities similar to that of the homopolymer PBO. The copolymer of naphthalenediimide with benzobisoxazole (NapPBO) (**Figure 3.20**) showed charge carrier mobility which was an order of magnitude higher than the perylene based copolymer and followed the trend where μ_{FET} for naphthalene derivatives showed greater values than μ_{FET} of perylene derivatives.³⁷

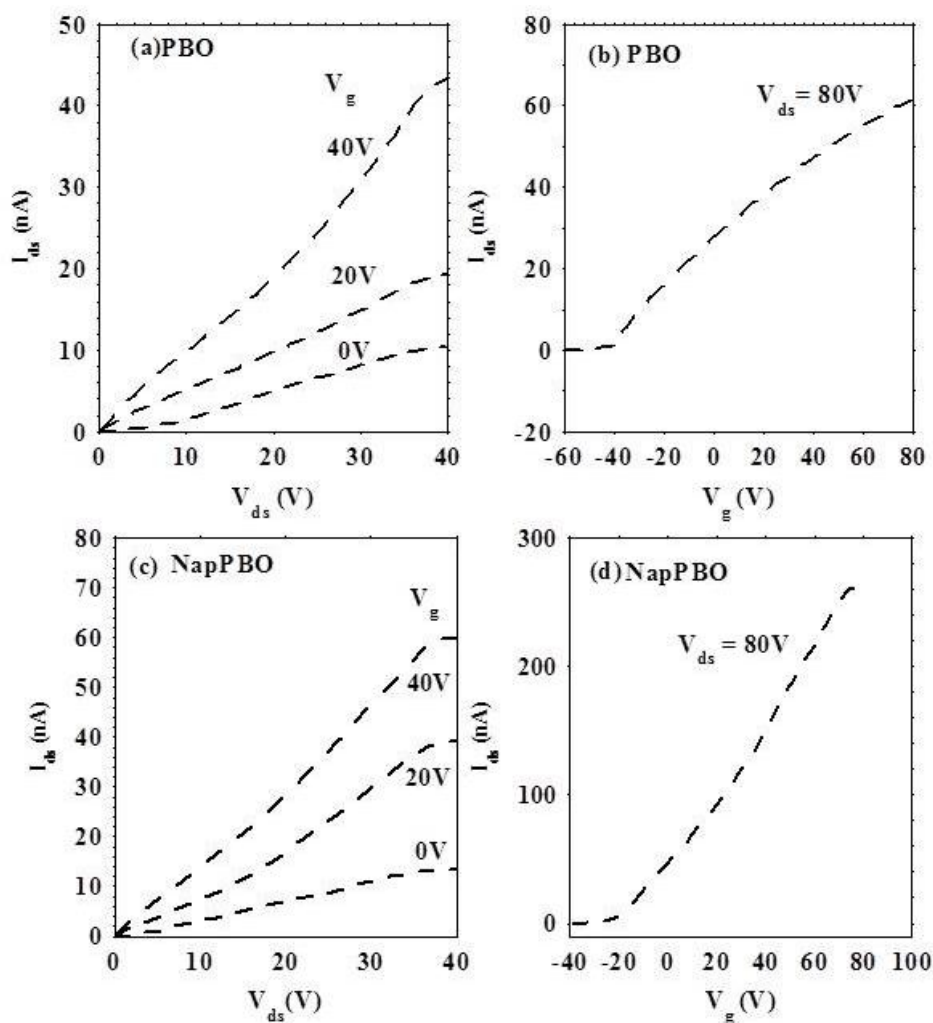
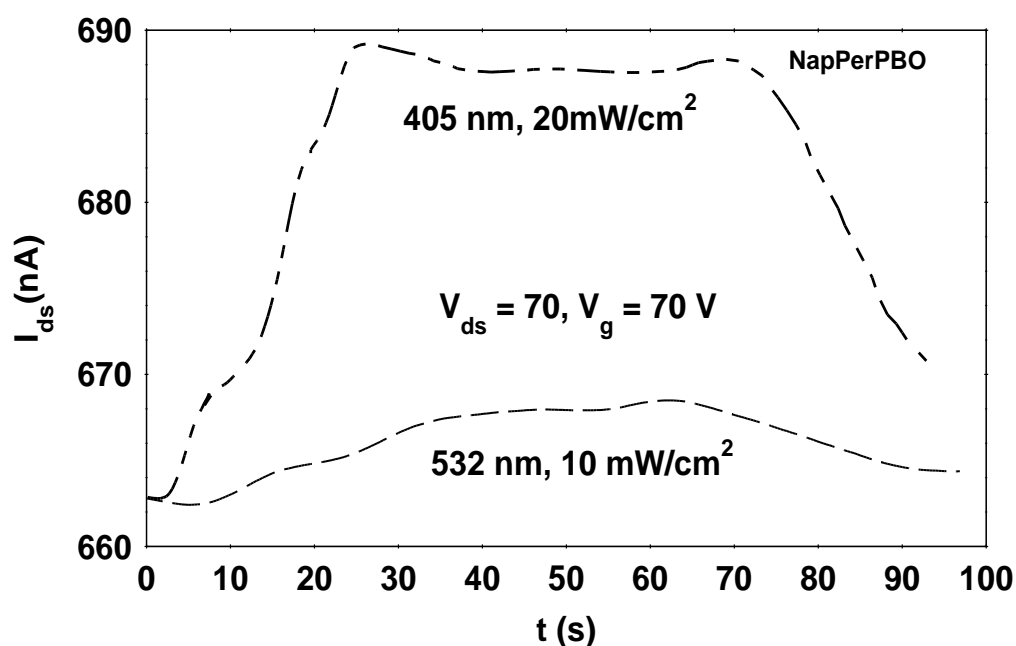


Figure 3.20 $I_{\text{ds}}-V_{\text{ds}}$ characteristic (a, c) and transconductance curves (b, d) of FET for PBO polymer (a, b) and NapPBO (c, d) at different V_{g} .

The transport in the random copolymer can be described in terms of a 1-D Anderson localization model. Introduction of impurities or defects (which are like energetic barriers) cause the scattering of the electron wave function thus affecting the wave propagation.³⁸ If the barrier is not large enough then the electron continues in its extended state. But in the case of multidimensional (for example in quasi-one dimensional-variable range hopping) transport the charge carrier primarily may hop

along a “one dimensional” chain but it can also occasionally have an intra-chain hop to avoid energetic disorder and thus the wave function can still remain delocalized. So under the assumption of one dimensional charge transport when a segment of a guest polymer is introduced in the host matrix of polymer the transport properties of this random copolymer (host + guest) thus formed is less compared to that of the corresponding parent homopolymers due to the additional scattering in electronic wave propagation. The absence of a decrease of μ_{FET} in the present case of the random copolymer indicated the equivalence of the naphthalene transport levels with respect to the perylene transport levels as also suggested by the similar LUMO levels. Additionally, the higher μ_{FET} of the random copolymer can be attributed to better lateral structural ordering as indicated from the relatively higher intensity peaks in the lower 2θ value ($5-12^\circ$) in WXR (Figure 3.9). Furthermore, it had sharp peak for π - π stacking and improved persistence length compared to NapPBO. This structural ordering can arise from an improved stacking of the NapPBO in the confined and



comparatively more rigid structure of PerPBO, thus improving the transport properties of the random copolymer.

Figure 3.21 Photo-response of NapPerPBO in the FET geometry at different wavelengths (405 nm and 532 nm).

The comparatively higher μ of the random copolymers can also be explained in terms of a Semi-classical Marcus model. The larger μ in the NapPerPBO copolymer can

arise from the better structural ordering, which is the outcome of a better stacking of the naphthalene units in the confined and more rigid structure of Per-PBO which can decrease the reorganization energy. Additionally the π - π stacking distance could be less in this system resulting in a higher value of the transfer integral. The interplay of these parameters can result in a more favourable μ for the random co-polymer than other polymers chosen. Photocurrent (I_{ph}) measurements of the FET structures (**Figure 3.21**) also provide an insight into the carrier generation and transport mechanisms and ascertain the contribution of each of the homo-polymer. The photocurrent spectra largely followed the combined absorption as indicated by the response at $\lambda = 532$ nm and $\lambda = 405$ nm for the different polymer systems. Upon photo excitation with a source at the wavelength corresponding to the absorption with the V_g and V_{ds} held constant, I_{ds} exhibited an increase. The I_{ph} magnitude in the random copolymer NapPerPBO indicated a higher contribution from the NapPBO absorption compared to PerPBO absorption region. Nevertheless, a small but discernible I_{ph} was present at $\lambda = 532$ nm corresponding to the perylene absorption. It was observed that the current induced by $\lambda = 405$ nm excitation had a stronger electric field dependence (especially at higher field) compared to the current induced by $\lambda = 532$ nm excitation (**Figure 3.22**).

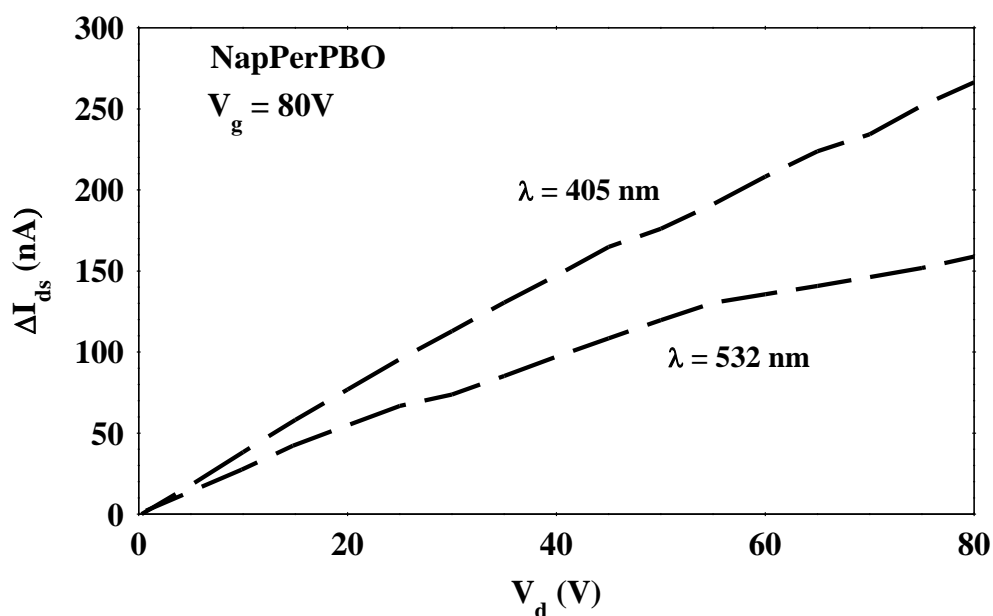


Figure 3.22 Change in I_{ds} in the NapPerPBO FET upon photoexcitation incident from the glass substrate side at different wavelength (magnitude normalized for equivalent power/area).

This behavior could be attributed to the field dependent carrier generation from the NapPBO unit or the field dependent carrier transport mechanism.³⁹ The difference in the behavior of the ΔI_{ds} (V) arising from the two types of carriers pointed to the higher field dependent carrier generation term in the NapPBO segments of the chain.

3.3.7 Conclusions

An alternating copolymer of benzobisoxazole and perylenediimide and/or naphthalene diimide was synthesized and the effect of molecular structure upon electronic and redox properties were studied. The presence of the imide linkage at every alternate position did not deleteriously affect the mesophase formation ability of these copoly(benzoxazole imide)s. All the oxazole-imide copolymer exhibited lyotropic mesophases in MSA at similar critical solution concentration as that of the homopolymer PBO. The PerPBO copolymer showed interesting funneling behavior upon indirect excitation at the bisoxazole wavelength. Almost exclusive emission from perylene units was observed at 620 nm upon selective excitation of bisoxazole (345 nm) indicating highly efficient (> 90 %) energy transfer from bisoxazole to perylene. The emission at 620 nm was higher in intensity upon indirect excitation (345 nm) compared to the direct excitation of perylene moiety at 545 nm. The quenching of perylene fluorescence upon direct excitation showed that electron transfer also played an important role. There was complete quenching of fluorescence in spin coated films both upon direct as well as indirect excitation. The copolymer solution in MSA were protonated resulting in improved planarity leading to better electronic coupling and energy transfer from bisoxazole to perylene / naphthalene diimide units. On the other hand, the geometry was different in the solid state resulting in total quenching of fluorescence of both bisoxazole and perylene units. The electrical transport characteristics of these copolymers were determined in a FET device configuration which showed their n type charge transport nature. It was observed that the random copolymer exhibited higher mobility, on-off ratio and wavelength dependent I_{ds} photo-response.

3.4. References

- (1) (a) Krebs, F. C. *Sol. Eng. Mater. Sol. Cell* **2009**, *93*, 1636(b) Søndergaard, R.; Hösel, M.; Angmo, D.; Larsen-Olsen, T. T.; Krebs, F. C. *Mater. Today* **2012**, *15*, 36.
- (2) Murphy, A. R.; Fréchet, J. M. J. *Chem. Rev.* **2007**, *107*, 1066.
- (3) (a) Facchetti, A. *Chem. Mater.* **2011**, *23*, 733(b) Grimsdale, A. C.; Leok Chan, K.; Martin, R. E.; Jokisz, P. G.; Holmes, A. B. *Chem. Rev.* **2009**, *109*, 897.
- (4) (a) Afshari, M.; Sikkema, D. J.; Lee, K.; Bogle, M. *Polym. Rev.* **2008**, *48*, 230(b) Lysenko, Z. US Patent, 1988; Vol. 4766244(c) So, Y.-H. *Prog. Polym. Sci.* **2000**, *25*, 137(d) Chae, H. G.; Kumar, S. *J. Appl. Poly. Sci.* **2006**, *100*, 791(e) Kuroki, T.; Tanaka, Y.; Hokudoh, T.; Yabuki, K. *J. Appl. Poly. Sci.* **1997**, *65*, 1031.
- (5) (a) Alam, M. M.; Jenekhe, S. A. *Chem. Mater.* **2002**, *14*, 4775(b) Babel, A.; Jenekhe, S. A. *J. Phys. Chem B* **2002**, *106*, 6129(c) Ahmed, E.; Kim, F. S.; Xin, H.; Jenekhe, S. A. *Macromolecules* **2009**, *42*, 8615.
- (6) (a) Liou, G.-S. *Macromol. Chem. Phys.* **2000**, *201*, 1141(b) Chen, X.; Sun, Q.; Huang, Y.; Cai, W. *J. Appl. Poly. Sci.* **2008**, *110*, 1891.
- (7) (a) Preston, J.; Dewinter, W. F.; Black, W. B. *J. Poly. Sci. Part A: Polym. Chem.* **1969**, *7*, 283(b) Hsu, S. L.-C.; Chang, K.-C.; Huang, Y.-P.; Tsai, S.-J. *J. Appl. Poly. Sci.* **2003**, *88*, 2388(c) Hsu, S. L.-C.; Luo, G.-W.; Chen, H.-T.; Chuang, S.-W. *J. Poly. Sci. Part A: Polym. Chem.* **2005**, *43*, 6020(d) Liou, G.-S. *J. Poly. Sci. Part A: Polym. Chem.* **1999**, *37*, 4151.
- (8) Ahmed, E.; Subramanian, S.; Kim, F. S.; Xin, H.; Jenekhe, S. A. *Macromolecules* **2011**, *44*, 7207.
- (9) (a) Sirringhaus, H.; Tessler, N.; Friend, R. H. *Synth. Met.* **1999**, *102*, 857(b) McCulloch, I.; Heeney, M.; Bailey, C.; Genevicius, K.; MacDonald, I.; Shkunov, M.; Sparrowe, D.; Tierney, S.; Wagner, R.; Zhang, W.; Chabinyc, M. L.; Kline, R. J.; McGehee, M. D.; Toney, M. F. *Nat. Mater.* **2006**, *5*, 328.
- (10) (a) Wen, Y.; Liu, Y. *Adv. Mater.* **2010**, *22*, 1331(b) Chen, Z.; Zheng, Y.; Yan, H.; Facchetti, A. *J. Am. Chem. Soc.* **2009**, *131*, 8.
- (11) Tullos, G. L.; Powers, J. M.; Jeskey, S. J.; Mathias, L. J. *Macromolecules* **1999**, *32*, 3598.
- (12) (a) Jenekhe, S. A.; Johnson, P. O. *Macromolecules* **1990**, *23*, 4419(b) Manoj, A. G.; Alagiriswamy, A. A.; Narayan, K. S. *J. Appl. Phys.* **2003**, *94*, 4088.

- (13) (a) Durban, M. M.; Kazarinoff, P. D.; Luscombe, C. K. *Macromolecules* **2010**, *43*, 6348(b) Hüttner, S.; Sommer, M.; Thelakkat, M. *Appl. Phys. Lett.* **2008**, *92*, 093302(c) Schmidt, R.; Oh, J. H.; Sun, Y.-S.; Deppisch, M.; Krause, A.-M.; Radacki, K.; Braunschweig, H.; Könemann, M.; Erk, P.; Bao, Z.; Würthner, F. *J. Am. Chem. Soc.* **2009**, *131*, 6215(d) See, K. C.; Landis, C.; Sarjeant, A.; Katz, H. E. *Chem. Mater.* **2008**, *20*, 3609(e) Gawrys, P.; Boudinet, D.; Kornet, A.; Djurado, D.; Pouget, S.; Verilhac, J.-M.; Zagorska, M.; Pron, A. *J. Mater. Chem.* **2010**, *20*, 1913(f) Chen, H. Z.; Ling, M. M.; Mo, X.; Shi, M. M.; Wang, M.; Bao, Z. *Chem. Mater.* **2007**, *19*, 816(g) Mikroyannidis, J. A.; Stylianakis, M. M.; Sharma, G. D.; Balraju, P.; Roy, M. S. *J. Phys. Chem C* **2009**, *113*, 7904(h) Wang, Z. Y.; Qi, Y.; Gao, J. P.; Sacripante, G. G.; Sundararajan, P. R.; Duff, J. D. *Macromolecules* **1998**, *31*, 2075(i) Pan, J.; Zhu, W.; Li, S.; Zeng, W.; Cao, Y.; Tian, H. *Polymer* **2005**, *46*, 7658.
- (14) Gupta, D.; Kabra, D.; Kolishetti, N.; Ramakrishnan, S.; Narayan, K. S. *Adv. Funct. Mater.* **2007**, *17*, 226.
- (15) Tashiro, K.; Hama, H.; Yoshino, J.-I.; Abe, Y.; Kitagawa, T.; Yabuki, K. *J. Poly. Sci. Part B: Polym. Phys.* **2001**, *39*, 1296.
- (16) Babel, A.; Jenekhe, S. A. *J. Am. Chem. Soc.* **2003**, *125*, 13656.
- (17) Evstafev, V. P.; Braz, G. I.; Yakubovich, A. Y. *Chem Heterocycl Compd* **1970**, *6*, 682.
- (18) Wolfe, J. F.; Arnold, F. E. *Macromolecules* **1981**, *14*, 909.
- (19) Xu, X.-H.; Liu, X.-Y.; Zhuang, Q.-X.; Han, Z.-W. *J. Appl. Poly. Sci.* **2010**, *116*, 455.
- (20) Promislow, J. H.; Preston, J.; Samulski, E. T. *Macromolecules* **1993**, *26*, 1793.
- (21) Mackinnon, S. M.; Wang, Z. Y. *J. Poly. Sci. Part A: Polym. Chem.* **2000**, *38*, 3467.
- (22) Jancy, B.; Asha, S. K. *J. Poly. Sci. Part A: Polym. Chem.* **2009**, *47*, 1224.
- (23) Yu, S. C.; Gong, X.; Chan, W. K. *Macromolecules* **1998**, *31*, 5639.
- (24) Kumar, S.; Dang, T. D.; Arnold, F. E.; Bhattacharyya, A. R.; Min, B. G.; Zhang, X.; Vaia, R. A.; Park, C.; Adams, W. W.; Hauge, R. H.; Smalley, R. E.; Ramesh, S.; Willis, P. A. *Macromolecules* **2002**, *35*, 9039.
- (25) Guo, P.; Wang, S.; Wu, P.; Han, Z. *Polymer* **2004**, *45*, 1885.
- (26) Shi, M.-M.; Chen, H.-Z.; Shi, Y.-W.; Sun, J.-Z.; Wang, M. *J. Phys. Chem B* **2004**, *108*, 5901.

- (27) Bauer, P.; Wietasch, H.; Lindner, S. M.; Thelakkat, M. *Chem. Mater.* **2007**, *19*, 88.
- (28) McNeill, C. R.; Abrusci, A.; Zaumseil, J.; Wilson, R.; McKiernan, M. J.; Burroughes, J. H.; Halls, J. J. M.; Greenham, N. C.; Friend, R. H. *Appl. Phys. Lett.* **2007**, *90*, 193506.
- (29) Neuteboom, E. E.; Meskers, S. C. J.; van Hal, P. A.; van Duren, J. K. J.; Meijer, E. W.; Janssen, R. A. J.; Dupin, H.; Pourtois, G.; Cornil, J.; Lazzaroni, R.; Brédas, J.-L.; Beljonne, D. *J. Am. Chem. Soc.* **2003**, *125*, 8625.
- (30) (a) Shen, D. Y.; Venkatesh, G. M.; Burchell, D. J.; Shu, P. H. C.; Hsu, S. L. *J. Polym. Sci. Part B: Polym. Phys.* **1982**, *20*, 509 (b) Wang, S.; Wu, P.; Han, Z. *Macromolecules* **2003**, *36*, 4567.
- (31) Jancy, B.; Asha, S. K. *Chem. Mater.* **2008**, *20*, 169.
- (32) Osaheni, J. A.; Jenekhe, S. A. *Macromolecules* **1994**, *27*, 739.
- (33) Lee, S. K.; Zu, Y.; Herrmann, A.; Geerts, Y.; Müllen, K.; Bard, A. J. *J. Am. Chem. Soc.* **1999**, *121*, 3513.
- (34) Osaheni, J. A.; Jenekhe, S. A. *Chem. Mater.* **1995**, *7*, 672.
- (35) Sandanaraj, B. S.; Demont, R.; Thayumanavan, S. *J. Am. Chem. Soc.* **2007**, *129*, 3506.
- (36) Narayan, K. S.; Alagiriswamy, A. A.; Spry, R. J. *Phys. Rev. B* **1999**, *59*, 10054.
- (37) Singh, T. B.; Erten, S.; Günes, S.; Zafer, C.; Turkmen, G.; Kuban, B.; Teoman, Y.; Sariciftci, N. S.; Icli, S. *Organic Electronics* **2006**, *7*, 480.
- (38) Kohlman, R. S.; Epstein, A. J.; 2nd ed.; Marcel Dekker, New York, 1998.
- (39) Narayan, K. S.; Kumar, N. *Appl. Phys. Lett.* **2001**, *79*, 1891.

Chapter 4

Core Substituted Naphthalenediimide Copolymers for Ambipolar OFETs: Effect of Varying Donor Strength on Optical, Electrochemical and Semiconducting Properties

This chapter has been adapted from following publication

Nagesh B. Kolhe, A. Z. Ashar, K. S. Narayan* and S. K. Asha* *Macromolecules* **2014**, 47, 2296-2305.

4.1. Introduction

The rigid π -aromatic structure of NTCDA and PTCDA leads to their intrinsic insolubility in common organic solvents and consequently most of the polyimides containing naphthalenediimide (NDI) and perylenediimides (PDI) unit were found to be insoluble in nature which limits their solution processability and hence device (OFET and solar cell) application.¹ However, the recent synthetic strategy developed in this area opens the door for new solution processable NDI and PDI based materials. For instance, The NTCDA could be functionalized at 2,6-position (core or bay position) by halogen (bromine or chlorine) followed by substitution of imide nitrogen atom with solubilizing linear or branched alkyl chains.² In this way the core positions of NDI are free to undergo copolymerization with appropriate monomer by various C-C bond forming cross coupling polymerization such as Suzuki,³ Stille⁴ etc. Also, the core-substituted NDI polymer exhibited interesting optical and electronic properties.⁵

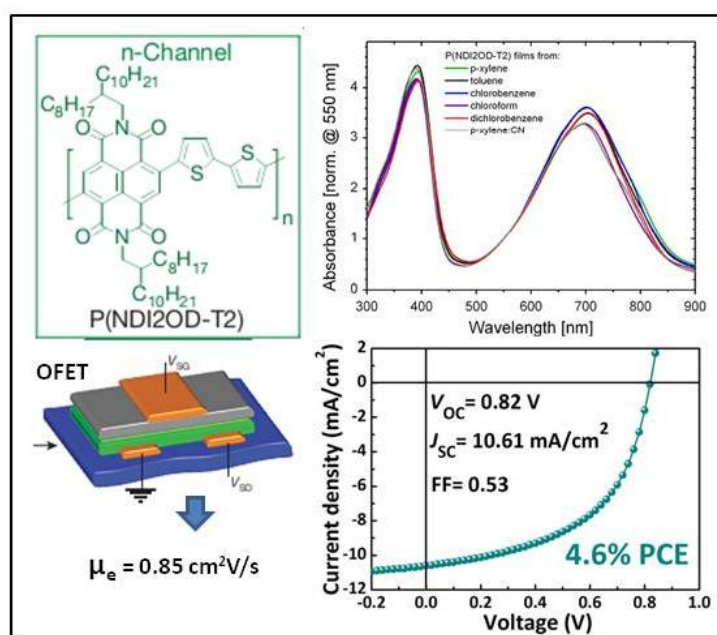


Figure 4.1 Molecular structure of core-substituted NDI polymer with UV-Vis absorption spectra, OFET electron mobility and solar cell efficiency (as n-type). (Adapted from Ref⁶)

For example, A. Fachetti *et al.* reported core-substituted NDI linked donor-acceptor (D-A) copolymers (**Figure 4.1**) which has shown very high electron mobilities up to $\sim 0.85 \text{ cm}^2 \text{ V}^{-1}\text{s}^{-1}$ in organic field effect transistors (OFETs) along with intermolecular charge transfer band (ICT) in UV-Vis absorption spectrum.^{6a,b,7} Recent reports also

suggested the high solar cell efficiency of core-substituted NDI polymer in bulk-heterojunction solar cell as n-type material.^{6c,8} Conjugated polymers and oligomers are widely classified as electron (n-type), hole (p-type) and electron-hole (ambipolar) transporting material, depending upon the nature of their charge transport.⁹ Although the majority of materials reported are p-type with high performance parameters in terms of hole mobility and air stability, the scenario for n-type and ambipolar materials are also improving steadily, due to accomplishment of rational molecular design and solution processable polymeric semiconductors.¹⁰ Unlike, unipolar OFET either p-type or n-type, fabrication of complementary inverters requires both n-channel and p-channel organic semiconductor and this approach showed low power dissipation, wide noise margins, and higher robustness. One way to fabricate the complementary circuit is to combine two discrete p-channel and n-channel semiconductor which needs separate deposition and sequential patterning of both the layer. However, this approach increases the device complexity and manufacturing cost and also it is very difficult to control several parameters. Hence ambipolar materials based on polymeric semiconductor with high and balanced electron and hole mobilities are highly desired¹¹ due to their application in complementary-like circuits¹² and in light emitting diode¹³ without advanced patterning technique. The criteria for any material to exhibit ambipolarity is that they should possess lower lying LUMO (lowest unoccupied molecular orbital) < -4.0 eV for better electron injection and higher lying HOMO (highest occupied molecular orbital) ensuring energy band gap < 1.8 eV for hole and electron injection from same type of electrode.¹⁴ The understanding obtained from recent reports¹⁵ in this regard suggests that a molecular design involving D copolymer architecture by suitable selection of donor and acceptor units allows a fine tuning of energy level (HOMO/LUMO) as well as efficient charge injection of both holes and electrons from same type of electrode. Naphthalenediimide (NDI),^{12b,15a} diketopyrrolopyrrole (DPP),^{15b} benzthiadiazole (BT)¹⁶ and isoindigo¹⁷ have been used as acceptor units in recently reported ambipolar D-A polymers with the DDP-based copolymer exhibiting high electron and hole mobility (> 1 cm² V⁻¹s⁻¹).¹⁸ Among the rylene diimide the perylene and naphthalenediimides are known as an important class of n-type material due to their high electron affinity, good absorption, thermal and photochemical stability, and π -stacking behavior which facilitates favorable solid state packing.¹⁹ Furthermore, donor-acceptor copolymers comprising naphthalenediimide (NDI) as acceptor were found to be potential

materials due to their relatively high n-type charge carrier mobility with low band gap,^{6a} air stability,²⁰ solution processability^{4a} and ambipolarity capabilities.^{12b} The optical and semiconducting properties of NDI polymers are strongly dependent on the type of donor co monomer used. For instance, co monomers based on thiophene,^{7,21} phenothiazine,^{3a} selenophene,²² fluorene^{3b}, diethynylbenzene²³ etc have been used along with core substituted NDI, where mostly n-type charge transport was observed. Core-substituted NDI polymer incorporating strong electron donating alkoxydithiophene as co monomer was reported to exhibit ambipolar charge transport with hole mobility (maximum $10^{-3} \text{ cm}^2 \text{ V}^{-1} \text{ s}^{-1}$) an order of magnitude lower than electron mobility(**Figure 4.2**).^{12b,15a}

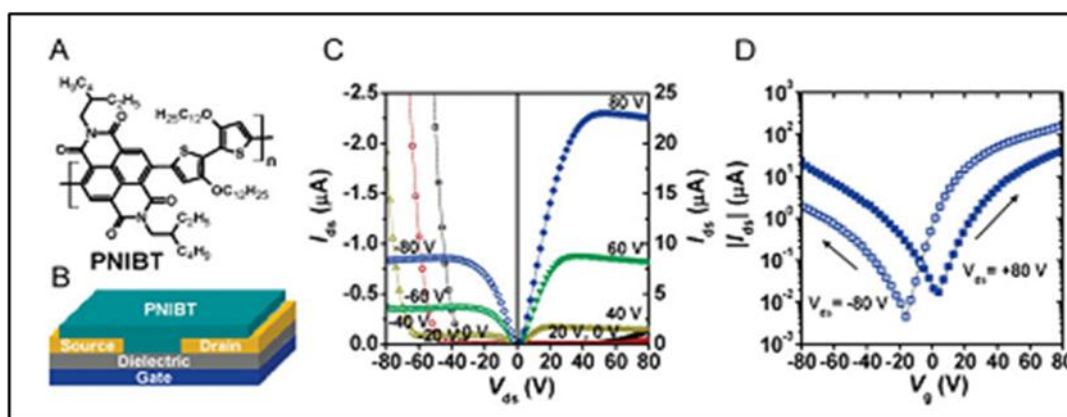


Figure 4.2 A) Chemical structure of the copolymer PNIBT, B) schematic of field-effect transistors C) output and D) transfer characteristics of the polymer field-effect transistor after annealing at 200 °C. (Adapted from Ref^{12b})

Another recent report on copolymers of benzothiadiazole with core substituted NDI which were connected through thiophene linkers indicated switching of OFET behavior from unipolar p-type with two thiophene as linker unit to ambipolar with single thiophene as linker.¹⁴ In the past decade, second generation of semiconducting polymers (named by Heeger²⁴) based on poly(p-phenylenevinylene) (PPV) derivatives were very extensively used as donor material in light emitting diodes²⁵ and bulk heterojunction solar cells²⁶ with various acceptor moieties including naphthalene diimide.²⁷ PPV has been shown to function as a strong electron donor towards perylenediimide in main chain polymers incorporating them.²⁸ Besides, the extended π -conjugation and rigid aromatic planar conformation of PPVs enable self assembly via π -stacking which can strongly alter the electronic properties of the material.²⁹

Thus, PPV is an interesting donor to study along with core substituted naphthalene diimide as an equally desired semiconducting material. Another equally interesting building unit is the poly (benzobisthiazoles) PBT and poly (benzobisoxazoles) PBO, which belong to the heterocyclic rigid-rod π -conjugated polymer family. They exhibit high tensile strength, high modulus, and excellent thermal and environmental stability due to the high degree of intermolecular π - π interactions present in the solid state.³⁰ In addition to these they have been shown to have weak electron deficient nature and therefore have been used as electron acceptor³¹ or as electron donor in combination with strongly electron deficient moiety.^{1a,32} The inherent insolubility of poly(benzobisoxazoles) in common organic solvent requires harsh processing condition from acidic solution³³ which makes their use limited. However, recently developed alternative approaches to synthesize soluble building blocks of benzobisoxazole permits the synthesis of soluble derivatives of poly (benzobisoxazole).³⁴

In this chapter we have synthesized novel core substituted naphthalenediimide (NDI) based alternating copolymers incorporating oligo(*p*-phenylene vinylene) (NDI-*alt*-OPV), benzthiadiazole ((NDI-*alt*-BT) and benzobisoxazole (NDI-*alt*-BBO) and studied their photophysical, electrochemical and semiconducting properties. A random copolymer incorporating ~30 mol % of BBO (Bisoxazole-2) along with ~70 mol % OPV co monomer (NDI-*r*-OPV/BBO) was also synthesized for device studies as the NDI-*alt*-BBO did not have sufficient solubility. An alternate copolymer of core substituted NDI with OPV has so far not been reported in literature. Although heteroaromatic moiety like benzobisazoles and benzthiadiazole are reported as mild acceptor towards strong donor, we have shown in previous chapter that it can function as donor towards strong acceptor like rylene diimide.^{1a} Consequently, benzobisoxazole and benzthiadiazole is expected to behave as a weak electron donor compared to OPV in NDI-Donor polymer. As expected, a strong intramolecular charge transfer from OPV to NDI was observed in NDI-*alt*-OPV polymer. Furthermore, the exactly alternating NDI and oligo (*p*-phenylenevinylene) linkage extended the conjugation length of polymer thereby inducing backbone planarity which also improved the thin-film crystalline nature. Due to favourable energy level LUMO (3.75 eV) and HOMO (5.44 eV), NDI-*alt*-OPV showed balanced ambipolar charge transport exhibiting average hole and electron mobility as high as 2.1×10^{-3}

$\text{cm}^2 \text{V}^{-1} \text{s}^{-1}$ and $3.09 \times 10^{-3} \text{ cm}^2 \text{V}^{-1} \text{s}^{-1}$ respectively whereas NDI-*r*-OPV/BBO showed dominant n-type charge transport with moderate electron mobility $4 \times 10^{-4} \text{ cm}^2 \text{V}^{-1} \text{s}^{-1}$.

4.2. Experimental Section

4.2.1 Materials

1,4,5,8-Naphthalenetetracarboxylic dianhydride (NTCDA), 2-octyl dodecanol, 2-ethylhexyl bromide, 2-ethylhexylamine, 1-4-hydroquinone, 4-formyl phenylboronic acid, Tetrakis(triphenyl-phosphine) palladium (0), Aliquat -336, Triethylphosphite, 2,3,1-Benzthiadiazole-4,7-bis(boronic acid pinacol ester) were purchased from Sigma Aldrich and used without further purification.

4.2.2 Instrumentations Details

^1H NMR and ^{13}C NMR spectra were recorded using 200 and 400 MHz Bruker NMR spectrophotometer in CDCl_3 containing small amounts of TMS as internal standard. Mass spectra were recorded on Voyager-De-STR MALDI-TOF (Applied Biosystems, Framingham, MA, USA) equipped with 337 nm pulsed nitrogen laser used for desorption and ionization. $1\mu\text{M}$ solution of sample was premixed with DHB (2,5 dihydroxy benzoic acid) matrix in CHCl_3 and mixed well before spotting on 96-well stainless steel MALDI plate by dried droplet method for MALDI-TOF analysis. The GPC analysis of monomers and polymers was performed on GPC model PL GPC 220 in chloroform using polystyrene standards for the calibration. The flow rate of CHCl_3 was maintained as 1 mL/min throughout the experiments, and the polymer solutions at concentrations 2-3 mg/mL were filtered and injected for recording the chromatograms at 30 °C. FTIR spectra were recorded with ATR mode using Bruker α -T spectrophotometer in the range of 4000 to 400 cm^{-1} . Absorption spectra were recorded using Perkin Elmer Lambda 35 UV-Vis spectrophotometer. The emission studies were performed by (HORIBA JOBIN YVON) SPEX Fluorolog F112X spectrofluorimeter. Thermo gravimetric analysis (TGA) was performed using a TGA Q 5000 thermogravimetric analyser. Samples were run from 40 to 900 °C with a heating rate of 10 °C/min under nitrogen. DSC (differential scanning calorimeter) measurements were performed on TA Q10 differential scanning calorimeter at a heating rate of 10 °C/min under nitrogen atmosphere. The thin film X-ray diffraction data were recorded by using a Rigaku model Dmax-2500 diffractometer using $\text{Cu K}\alpha$.

(1.54 Å) emission, and the spectra were recorded in the range of (2θ) 2–50°. AFM images were taken by a MultimodeTM Scanning Probe Microscope equipped with Nanoscope IVTM controller from Veeco Instrument Inc., Santa Barbara in the tapping mode using a Si probe. Electrochemical cyclic voltammetry behavior of NDI polymers were studied by using BAS-Epsilon potentiostat.

Sample preparation:

For the UV-Vis absorption and emission studies, thin films were prepared by dissolving polymer in *o*-DCB (orthodichlorobenzene) and spin coated (1000 rpm/60 s) on quartz plates. For the XRD analysis, thin films were prepared by drop-casting the polymer solution on glass slide. For AFM images, polymer solution was drop-casted on HMDS treated glass slide and further annealed at 150 °C.

4.2.3 Device Fabrication (OFET)

Organic field effect transistors (OFETs) were fabricated in bottom-gate/ top-contact geometry with Au (gold) source/ drain electrode. Au gate electrode was deposited using thermal evaporation ($\sim 10^{-6}$ mbar) on RCA cleaned glass substrates. Poly (methyl methacrylate) solution in propylene carbonate (100 mg/mL) was spin coated at 800 rpm for 60 s and annealed at 110 °C for 1 h in N₂ filled glove box. Dielectric surface was passivated by spin coating (1000 rpm, 60 s) with hexamethyldisilazane (HMDS) and annealed at 110 °C for 1 hour. The formed dielectric layer had a capacitance per unit area (C_i) ~ 10 nF/cm² measured using Keithley 4200 semiconductor parameter analyzer. Semiconductor layer was deposited by drop casting the filtered (0.22 μm pore size) solution of 10 mg/mL polymer in 1,2 dichlorobenzene and annealed at 150 °C for 1 h in N₂ atmosphere. Gold source and drain contacts were deposited on organic layer through shadow mask under high vacuum. The channel length (L) and width (W) were 60-100 μm and 1.5-2.5 mm, respectively. The average mobility value of each polymer is mentioned in the Table 4.4 and is based on measurements on a number of devices (~ 10 -15 devices of each polymer).

4.2.4 Synthesis

Synthesis of monomer

2,6-Dibromo-1,4,5,8-naphthalenetetracarboxylic dianhydride (NTCDA-Br₂) : 1,4,5,8 - naphthalene tetracarboxylic dianhydride (NTCDA) (5 g, 18.65 mmol) and Iodine (0.2 g) were taken in 250 mL three neck round bottom flask followed by addition of 80 mL of fuming sulfuric acid (Oleum 40-50 %) in one portion. The reaction mixture was stirred for 2 h at room temperature after which bromine (Br₂) (2 mL, 37.3 mmole) was added drop wise over half- hour. The reaction temperature was increased to 50 °C and stirred at same temperature for 48-50 h. The reaction mixture was poured in to ice cubes (drop by drop) very slowly; yellow precipitate of NDI-Br₂ (and other isomers) was obtained which was filtered and washed with plenty of water until neutralization of filtrate (checked by filter paper). The final compound was dried at 60 °C for 24 h in vacuum oven. Yield: 7.4 g (93 % by considering 2, 6 isomer). The insoluble nature of NDI-Br₂ limits purification and the structural characterization so that crude compound was directly used for next step.

2-octyl-1-dodecylbromide (a): Triphenylphosphine (7.36 g, 28.07 mmol) was dissolved in 60 mL of dichloromethane (DCM) and resultant solution was purged with argon for 15 minutes at 0 °C followed by addition of Br₂ (1.43 mL, 28.07 mmol) at room temperature. After that 2-octyl-1-dodecanol (10 mL, 28.07 mmol) was added drop wise via additional funnel over half-hour and reaction mixture was stirred at room temperature for overnight under argon. After complete evaporation of DCM, residue was mixed with hexane and filtered. The filtrate was concentrated to yield yellow oil which was purified by column chromatography using pet ether. The pure compound was isolated as colorless oil Yield: 8.26 g (80 %). ¹H NMR (200 MHz, CDCl₃) δ ppm: 3.45-3.42 (d, 2H), 4.15 (d, 4H), 1.57 (m, 1H), 1.26 (m, 32H), 0.87, (m, 6H).

N-(2-octyldodecyl)phthalimide (b): 2-octyl-1-dodecylbromide (8.26 g, 22.85 mmol) and potassium phthalimide (4.65 g, 25.13 mmol) was added in to a 25 mL dry DMF. The reaction mixture was stirred for 16 h. at 90 °C and cooled to room temperature after which it was poured into 150 mL water and extracted with (3 x 100 mL) DCM. The collected organic layers (DCM) were washed with 0.2 N KOH (150 mL), water, saturated ammonium chloride (200 mL) and dried over sodium sulfate. The organic layer was concentrated under reduced pressure to obtain crude compound as yellow

oil which was purified by column chromatography using pet ether/DCM solvent system. Yield: 7.32 g (75 %). ^1H NMR (200 MHz, CDCl_3) δ ppm: 7.71 (m, 2H), 3.57 (d, 2H) 4.15, 1.86 (m, 1H), 1.22 (m, 32H), 0.86, (m, 6H).

2-decyl-1-dodecylamine (c): The mixture of *N*-(2-octyldodecyl) phthalimide (4.2 g, 9.82 mmol) and hydrazine hydrate (80 %) 2.5 mL was stirred in 60 mL methanol at 90-95 °C for 24 h. The conversion of starting material into product (amine) was monitored by TLC; after disappearance of starting imide, the solid residue formed in reaction mixture was filtered and filtrate was evaporated under reduced pressure. The resultant residue was mixed with 100 mL DCM and washed with 10 % KOH (2 x 20 mL). The aqueous layer was extracted with DCM (3 x 50 mL), washed with brine (2 x 50 mL) and dried over sodium sulfate. The evaporation of DCM afforded yellow oil which was used for next step without purification. Yield: 2.54 g (87 %). ^1H NMR (200 MHz, CDCl_3) δ ppm: 2.60 (d, 2H), 1.46 (m, 1H) 1.25 (m, 32H), 0.86, (m, 6H).

***N, N'*-(2-ethylhexyl)-2,6-dibromo-1,4,5,8-naphthalene diimide (NDI-2-E.H-Br₂):** The mixture of brominated NTCDA i.e. NTCDA -Br₂ (6g, 14.08 mmol) was suspended in 100 mL of glacial acetic acid and stirred for short period of time to get homogeneous dispersion which was followed by addition of (10.36 mL, 63.38 mmol) of 2-ethylhexyl amine. The reaction mixture was stirred and refluxed (at 120 °C) for 3h to complete dissolution and cooled to room temperature. The reaction mixture was concentrated under reduced pressure to about 1/10th of original volume and then precipitated in to methanol to yield reddish brown powder that was filtered and dried under vacuum. The crude product was column purified by using pet ether/ethyl acetate and pet ether/DCM solvent system and purified compound was again washed with hot acetone to get yellow powder of pure compound. Yield: 1.8 g (20 %, by considering 2, 6 isomer). Melting point (243-245 °C); ^1H NMR (200 MHz, CDCl_3) δ ppm: 8.99 (s, 2H, aromatic), 4.15 (d, 4H), 1.93 (m, 2H), 1.32, (m, 16 H), 0.92 (t, 12H). ^{13}C NMR (500 MHz, CDCl_3) δ ppm: 161.23, 161.06, 139.19, 128.39, 127.77, 125.29, 124.09, 45.15, 37.76, 30.61, 28.53, 23.96, 23.07, 14.08, 10.57. FTIR (ATR, cm^{-1}): 3050, 2920, 2851, 1707, 1652, 1557, 1432, 1363, 1308, 1230, 1199, 990; MALDI-TOF MS (Calcd m/z 648.43); Found m/z = 648.03. Anal. Calcd. for $\text{C}_{30}\text{H}_{36}\text{N}_2\text{O}_4\text{Br}_2$: C, 55.57; H, 5.60; N, 4.32. Found C, 56.03; H, 5.40; N, 4.32.

***N, N'*-Bis (2-octyldodecyl)-2,6-dibromo-1,4,5,8-naphthalenediimide (NDI-2-O.D-Br₂):** Mixture of brominated NTCDA i.e. NTCDA -Br₂ (5 g, 11.73 mmole) was suspended in 100 mL of glacial acetic acid and stirred for short period of time to get

homogeneous dispersion which was followed by addition of (13.96 g, 46.94 mmol) of 2-octyldodecyl amine. The reaction mixture was stirred and refluxed (at 120 °C) to complete dissolution for 3h and cooled to room temperature. The reaction mixture was concentrated under reduced pressure to about 1/10th of original volume and then precipitated in to methanol to yield reddish brown powder that was filtered and dried under vacuum. The crude product was column purified by using pet ether/ethyl acetate solvent system and again re-crystallized from 1:1 mixture of hexane and acetone to get yellow powder of pure compound. Yield: 1.8 g (15 %, by considering 2, 6 isomer. Melting point (85-86 °C); ¹H NMR (200 MHz, CDCl₃) δ ppm: 8.98 (s, 2H, aromatic), 4.15 (d, 4H), 1.97 (m, 2H), 1.22, (m, 64 H), 0.86 (m, 12H). ¹³C NMR (500 MHz, CDCl₃) δ ppm: 161.16, 161.00, 139.14, 128.36, 127.73, 125.27, 124.06, 45.43, 36.44, 31.90, 31.87, 31.53, 30.01, 29.62, 29.58, 29.52, 29.33, 26.32 29.28, 22.67, 14.11. FTIR (ATR, cm⁻¹): 3050, 2920, 2851,1707, 1652, 1557, 1432, 1363, 1308, 1230, 1199, 990; MALDI-TOF MS (Calcd m/z 985.06); Found m/z = 985.345. Anal. Calcd. for C₅₄ H₈₄ N₂O₄ Br₂: C, 65.84; H, 8.60; N, 2.84. Found C, 66.09; H, 8.67; N, 2.27.

***N, N'*- Bis -(2-octyldodecyl)-2,6-(4-formyl) diaryl-1,4,5,8-naphthalene Diimide (NDI-2-O.D-CHO):** A mixture of aqueous 2M Na₂CO₃ (1.5 mL) and dioxane (8-10 mL) was repeatedly degassed by purging with argon gas for half an hour, into which 4-formyl-phenyl boronic acid (0.306 g, 2.04 mmol) and *N, N'*-di-(2-octyldodecyl)-2,6-dibromo-1,4,5,8-naphthalene diimide (0.7 g, 0.71 mmole) along with 2 mol% (12 mg) of Pd(PPh₃)₄ was added. The mixture was heated in an argon atmosphere for 12 h, after which it was quenched with the addition of 10 % aqueous HCl. The organic layer was extracted with DCM, washed consecutively with water and brine. The organic layer was dried over Na₂SO₄ and concentrated. The crude compound was purified by column chromatography over silica gel with Petroleum ether / Ethyl acetate (95:5 v/v) followed by petroleum ether / DCM (40:60 v/v) as eluent. Yield: 600 mg (83 %). Melting point (115-117 °C); ¹H NMR (200 MHz, CDCl₃) δ ppm: 10.13 (s, 2H, -CHO) 8.63 (s, 2H, naphthalene), 8.01 (d, 4H phenyl), 7.53 (d, 4H phenyl), 4.03 (d, 4H), 1.89 (m, 2H), 1.20, (m, 64 H), 0.83 (m, 12H). ¹³C NMR (500 MHz, CDCl₃) δ ppm: 191.68, 162.48, 162.41, 146.63, 146.43, 135.89, 135.13, 129.80, 128.72, 127.36, 125.88, 123.16, 44.88, 36.40, 31.88, 31.87, 31.46, 30.03, 29.63, 29.62, 29.58, 29.53, 29.32, 29.26, 26.28, 22.66, 22.64, 14.09. FT-IR (ATR, cm⁻¹): 2955,2921, 2850,1703, 1666, 1606,1582, 1442, 1428,1387, 1333, 1306, 1264, 1196,

929; MALDI-TOF MS (Calcd m/z 1035.48); Found m/z = 1036.604 [M+1]. Anal. Calcd. for $C_{68}H_{94}N_2O_6$: C, 78.87; H, 9.15; N, 2.71. Found C, 77.62; H, 9.53; N, 2.18

1, 4-di (2-ethylhexyloxy) benzene (d): 1, 4-hydroquinone (12 g, 109 mmol) and potassium hydroxide (30.6 g, 545 mmol) was taken in a two neck round bottom flask and dry DMSO was added in to it under nitrogen environment. The mixture was stirred for 30-45 min at room temperature. 2-ethylhexyl bromide (48.45 mL, 272 mmol) was added to the reaction mixture at room temperature and reaction mixture was further stirred for two days at room temperature. The conversion was monitored by TLC. For work up, reaction mixture was cooled and poured in crushed ice. The organic layer was extracted with chloroform, washed consecutively with water and brine. The organic layer was dried over Na_2SO_4 and solvent was evaporated by a vacuum rotary evaporator. The crude mixture was purified by silica column having pet ether as a mobile phase. Yield: 18 g (50 %). 1H NMR (200MHz), $CDCl_3$; δ : 6.82 (s, 4H), 3.77 (d, 4H), 1.70 (t, 2H), 1.45 (m, 16H), 0.89 (m, 12H).

2,5 bisbromomethyl 1,4 di-(2-ethylhexyloxy) benzene (e): 1, 4-di (2-ethylhexyloxy) benzene (5 g, 14.94 mmol) and p-formaldehyde (3.13 g, 104.5 mmol) was taken in a two neck round bottom flask, into which glacial acetic acid was added. Hydrobromic acid (HBr) (4.47 g, 56.04 mmol) was then added into the reaction mixture under nitrogen atmosphere at room temperature. The reaction mixture was heated to 80-90 $^{\circ}C$ for 24 h, cooled and poured into a beaker containing crushed ice and filtered to collect the precipitate. The precipitate was re-crystallized by dissolving in glacial acetic acid and cooled for crystallization. After 24 h crystals were formed which were filtered, collected and dried. Yield: 4.28 g (55 %). 1H NMR (200MHz), $CDCl_3$; δ : 6.84 (s, 2H), 4.51 (s, 4H), 3.85 (d, 4H), 1.74 (t, 2H), 1.57-1.32 (m, 16H), 0.93 (m, 12H).

2,5-di-2-ethylhexyloxy-1,4 xylenebis(diphosphonate) (f) : 2,5 bisbromomethyl 1,4 di-(2-ethylhexyloxy) benzene (2 g, 3.84 mmol) and triethylphosphite (5 mL) was taken in a one neck round bottom flask. The reaction mixture was kept at 130-140 $^{\circ}C$ under N_2 atmosphere and stirred for 24 h. The excess triethylphosphite and ethyl bromide was removed by vacuum distillation. A highly viscous liquid was obtained as product. Yield: 2.38 g (98 %). 1H NMR (200MHz), $CDCl_3$; δ : 6.90 (s, 2H), 3.98 (m, 8H), 3.77 (d, 4H), 3.25 (d, 4H), 1.68 (m, 2H), 1.50-1.17 (m, 18H), 0.89 (m, 12H). Anal. Calcd. for $C_{31}H_{58}O_8P_2$: C, 59.98; H, 9.42 Found C, 59.51; H, 9.74.

OPV-diboronic acid pinacol ester (OPV) : 2,5-di-2-ethylhexyloxy-1,4-xylenebis(diphosphonate) (3 g, 4.73 mmol) and 4-formyl phenyl boronic acid pinacol ester (2.19 g, 9.46 mmol) were dissolved in 20 mL dry THF under N₂ atmosphere. NaH (0.246 g 10.27 mmol) and 15 mL dry THF were taken in another 100 mL two neck round bottom flask. The mixture of diphosphonate and boronic ester was then added slowly to the round bottom flask containing NaH and THF at 0 °C and the reaction mixture was stirred for half an hour at the same temperature. Thereafter, the reaction mixture was stirred at room temperature overnight when the colour of the reaction mixture turned greenish. The reaction was quenched with 20-25 mL methanol and evaporation of the organic layer yielded a sticky greenish solid mass, which was added in 500 mL water and extracted with DCM. The organic layer was dried over Na₂SO₄ and solvent was evaporated by a vacuum rotary evaporator. The crude compound was purified by column chromatography over silica gel with petroleum ether / Ethyl acetate (95:5 v/v) as eluent. Yield: 1.6 g (35 %). Melting point (190-192 °C); ¹H NMR (200 MHz, CDCl₃) δ ppm: 7.81-7.12 (m, aromatic and vinylic 14H), 3.95 (d, 4H), 1.81 (m, 2H), 1.35, (m, 24 H), 1.24(m,16H) 0.97 (m, 12H). ¹³C NMR (400 MHz, CDCl₃) δ ppm: 151.27, 140.71, 135.12, 128.68, 126.81, 125.74, 124.46, 110.30, 83.73, 71.79, 39.76, 30.92, 29.23, 24.87, 24.22, 23.08, 14.11, 11.33. FTIR (ATR, cm⁻¹): 2959, 2925, 2858, 1603, 1494, 1462, 1416, 1396, 1355, 1321, 1261, 1198, 961; MALDI-TOF MS (Calcd m/z 790.55); Found m/z = 790.180, 791.182 [M+1]. Anal. Calcd. for C₅₀H₇₂B₂O₆: C, 75.95; H, 9.18 Found C, 74.50; H, 9.33.

Triethyl orthochloroacetate : Triethyl orthoacetate (1,1,1-triethoxy ethane) (8.1 g, 20.02 mmol) and *N*-chlorosuccinimide (7g, 19.07 mmol) was dissolved in 60 mL of carbon tetrachloride or DCM. The reaction mixture was stirred with heating at 60 °C for 4-5 h. The precipitate of succinimide was filtered off, the filtrate was evaporated. The residual liquid was vacuum distilled at (68-70 °C at 10/mm) to obtained the mixture of mono and dichloro substituted compound (major triethyl orthochloroacetate) which was used for next step without purification. ¹H NMR (200 MHz, CDCl₃) δ ppm: 1.20 (t, 9H), 3.56 (q, 6H).

2,6-bis(chloromethyl)benzo[1,2-d;5,4-d']bisoxazole (Bisoxazole-1): A dry solution of DMSO (4 mL) containing diaminodihydroxybenzene dihydrochloride (0.85 g, 4 mmol) and pyridine (0.7 mL, 8 mmol) was added via a syringe to the triethyl orthochloroacetate (3.92 g, 20 mmol) and the catalyst La(OTf)₃ (5 mol %) in a

round bottom flask. The reaction mixture was stirred at 55 °C for 1 h and then cooled. The reaction was diluted with water and the product collected by filtration. The crude compound was re-crystallized from heptanes. Yield: 0.62 g (62 %). Melting point: 161-162 °C. ¹H NMR (CDCl₃) δ ppm: 8.06 (s, 1H), 7.73 (s, 1H), 4.78 (s, 4H). ¹³C NMR δ ppm: 36.5, 94.1, 111.6, 138.9, 149.6, 162.0.

2,6-Dimethylbenzo[1,2-d;5,4-d]bisoxazole-diethylphosphonate Ester (Bisoxazole-2):

Triethylphosphite (1.04 mL, 3.5 mmol) and 2,6-bis(chloromethyl)benzo[1,2-d;5,4-d']bisoxazole³² (0.450 g, 1.75 mmol) were heated to 150 °C for 7 h. The reaction was cooled and the crude product solidified. The crude product was recrystallized from xylene, and monomer bisoxazole-2 was obtained as yellow needles. Yield: 520 mg (65 %). Melting point (110-112 °C); ¹H NMR (200 MHz, CDCl₃) δ ppm: 7.96 (s, 1H aromatic), 7.66 (s, 1H aromatic), 4.18 (q, 8H), 3.62-3.51 (d, 4H), 1.32, (t, 12H). ¹³C NMR (400 MHz, CDCl₃) δ ppm: 159.4, 159.39, 148.91, 138.87, 109.90, 93.36, 63.08, 63.01, 28.94, 27.56, 16.38, 16.33 FTIR (ATR, cm⁻¹): 2964, 2911, 1615, 1580, 1428, 1389, 1361, 1297, 1163, 1046, 940; MALDI-TOF MS (Calcd m/z 460.11); Found m/z = 461.11 [M+1], 483.09 [M+Na], 499.055 [M+K]. Anal. Calcd. for C₁₈ H₂₆ N₂O₂P₂: C, 46.96; H, 5.69; N, 6.09 Found C, 47.13; H, 5.68; N, 5.81.

Synthesis of polymer

NDI-*alt*-OPV: *N,N'*-di-(2-octyldodecyl)-2,6-dibromo-1,4,5,8-naphthalene diimide (0.5 g, 0.51 mmole), OPV-diboronic pinacol ester (0.403 g, 0.51 mmol), Pd(PPh₃)₄ (29.45 mg, 5 mol %) and Aliquat-336 (144 mg, 0.357 mmol) were taken in a 50 mL two neck round bottom flask and the reaction assembly was evacuated by applying vacuum. 2 M aqueous solution of K₂CO₃ (1.6 mL) and toluene 10-12 mL was degassed with nitrogen for 15 min and added to the reaction mixture under nitrogen atmosphere. The reaction mixture was stirred at 90-95 °C for 3 days. Phenylboronic acid (31 mg, 0.255 mmol) was added under nitrogen and stirred at same temperature for 3 h followed by addition of bromobenzene (0.1 mL). The black reaction mixture was further stirred at 90-95 °C for 10 h. The polymer solution was precipitated in 300-400 mL methanol, stirred for 2 h and filtered on buchner funnel, washed with plenty of methanol and hexane. The polymer was dried in vacuum oven overnight and subjected to a soxhlet extraction with methanol and acetone. The polymer was obtained as a black solid, Yield: 0.48 g (72 %) ¹H NMR (200 MHz, CDCl₃) δ ppm: 8.70 (s, 2H), 7.65-7.18 (m, aromatic and vinylic 14H), 3.99 (broad, 8H), 1.90 (broad, 4H), 1.22 (m), 0.85 (m). ¹³C NMR (500 MHz, CDCl₃) δ ppm: 162.94, 162.77, 151.38,

147.37, 139.35, 138.22, 135.90, 128.81, 128.25, 127.33, 126.98, 126.54, 125.56, 124.53, 122.81, 110.43, 71.80, 44.85, 39.83, 36.44, 31.89, 31.57, 30.96, 30.08, 29.63, 29.30, 26.39, 24.29, 23.14, 22.65, 14.09, 11.35. (FTIR (ATR, cm^{-1}): 2921, 2853, 1704, 1665, 1432, 1378, 1306, 1262, 1032, 962; GPC: M_n , 8200; M_w , 12600 M_n/M_w , 1.53

NDI-*alt*-BT: NDIBT was synthesized using same procedure as that given for NDI-*alt*-PPV, but with NDI-2-O.D-Br₂ (0.5 g, 0.51 mmol) and 2,3,1-Benzthiadiazole-4,7-bis(boronic acid pinacol ester) (0.197 g, 0.51 mmol) as starting monomer. NDI-*alt*-BT was obtained as brown solid 300 mg (82%) ¹H NMR (200 MHz, CDCl₃) δ ppm: 9.04 (s, 2H), 7.96 (s, 2H), 3.97 (broad, 4H), 1.85 (broad), 1.22 (m), 0.85 (m). ¹³C NMR (500 MHz, CDCl₃) δ ppm: 162.80, 162.54, 153.12, 141.90, 135.73, 134.72, 127.75, 126.46, 125.03, 44.98, 36.37, 31.90, 31.44, 30.12, 29.64, 29.34, 26.45, 22.67, 14.10. FT-IR (ATR, cm^{-1}): 2921, 2852, 1706, 1664, 1580, 1443, 1376, 1307, 1263, 1022, 855; GPC : M_n , 6840; M_w , 11100; M_n/M_w , 1.62

NDI-*alt*-BBO: *N*, *N'*-di-(2-octyldodecyl)-2,6,4-formyl diaryl-1,4:5,8-naphthalene diimide (0.517 g, 0.5 mmol) and potassium *tert*-butoxide (161 mg, 1.44 mmol) were taken in 50 mL two neck round bottom flask and the reaction assembly was evacuated by applying vacuum. 5-6 mL of dry dioxane was added under nitrogen atmosphere and the mixture was stirred for half an hour. 2,6-Dimethylbenzo[1,2-d;5,4-d]bisoxazole-diethylphosphonate ester bisoxazole-2 (0.230 g, 0.5 mmol) was dissolved in 15 mL dry dioxane and added to the reaction mixture under nitrogen atmosphere. The reaction mixture was stirred at 100 °C for 48 h. The polymer solution was cooled, precipitated in 300-400 mL methanol, stirred for 2h, filtered on buckner funnel, washed with plenty of methanol and hexane. The polymer was dried in vacuum oven overnight and subjected to soxhlet extraction with methanol and acetone. The polymer was obtained as a dark red solid, Yield: 0.45 g (76 %) ¹H NMR (200 MHz, CDCl₃+ TFA) δ ppm: 8.68 (s, 2H), 8.22-7.50 (m, 10H), 4.03 (broad, 4H), 1.86 (broad), 1.21 (m), 0.84 (m). ¹³C NMR: Not possible due to insolubility. FTIR (ATR, cm^{-1}): 2918, 2849, 1703, 1662, 1577, 1434, 1363, 1307, 1265, 1108, 964 ; GPC : Not recorded due to insufficient solubility in chloroform and THF.

NDI-*r*-OPV/BBO: Copolymer was synthesized using same procedure as that given for NDI-*alt*-BBO, but with NDI-2-O.D-CHO (0.6 g, 0.58 mmol, 1eq.) 2,5-di-2-ethylhexyloxy-1,4 xylenebis(diphosphonate) **f** (0.257 g, 0.406 mmol, 0.7 eq.) and bisoxazole-2 (80 mg 0.174 mmol, 0.3 eq.) as starting monomer. The copolymer was

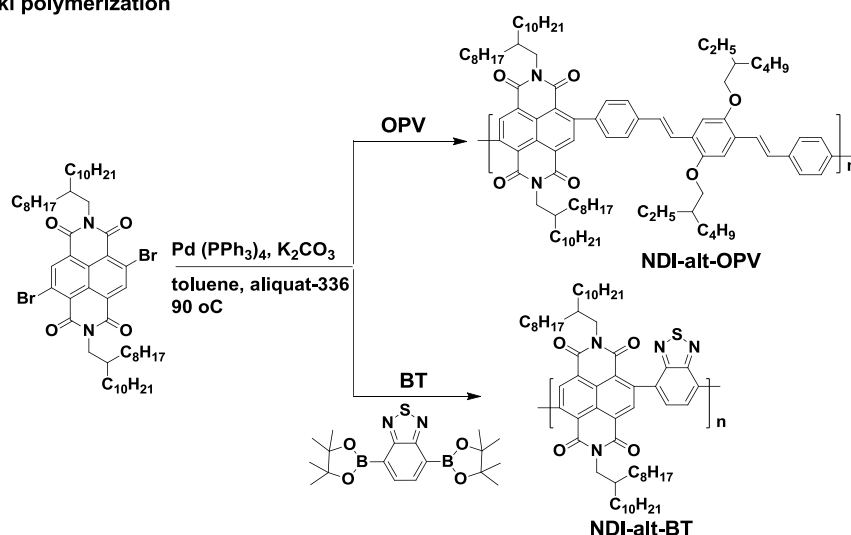
obtained as a black solid, Yield: 0.38 g (71 %) ^1H NMR (200 MHz, CDCl_3) δ ppm: 8.69 (s, 2H), 8.03-7.18 (m), 4.01 (broad), 1.90 (broad), 1.21 (m), 0.84 (m). ^{13}C NMR: Not possible due to sufficient solubility. FT-IR (ATR, cm^{-1}): 2921, 2852, 1704, 1664, 1582, 1436, 1371, 1307, 1259, 1028, 964; GPC : M_n , 5100; M_w , 8700 M_n/M_w , 1.70.

4.3 Results and Discussion

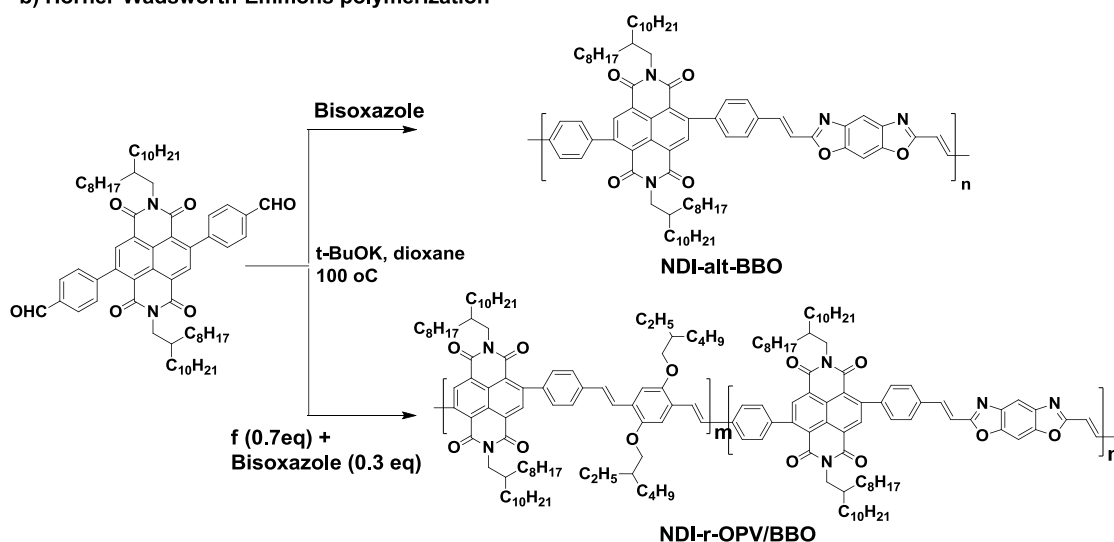
4.3.1 Synthesis and Characterization

As outlined in **Scheme 4.1** NDI-*alt*-OPV and NDI-*alt*-BT was synthesized by Suzuki coupling polymerization and NDI-*alt*-BBO and NDI-*r*-OPV/BBO were synthesized by Horner-Wadsworth-Emmons (HWE) polymerization.^{31b,35}

a) Suzuki polymerization

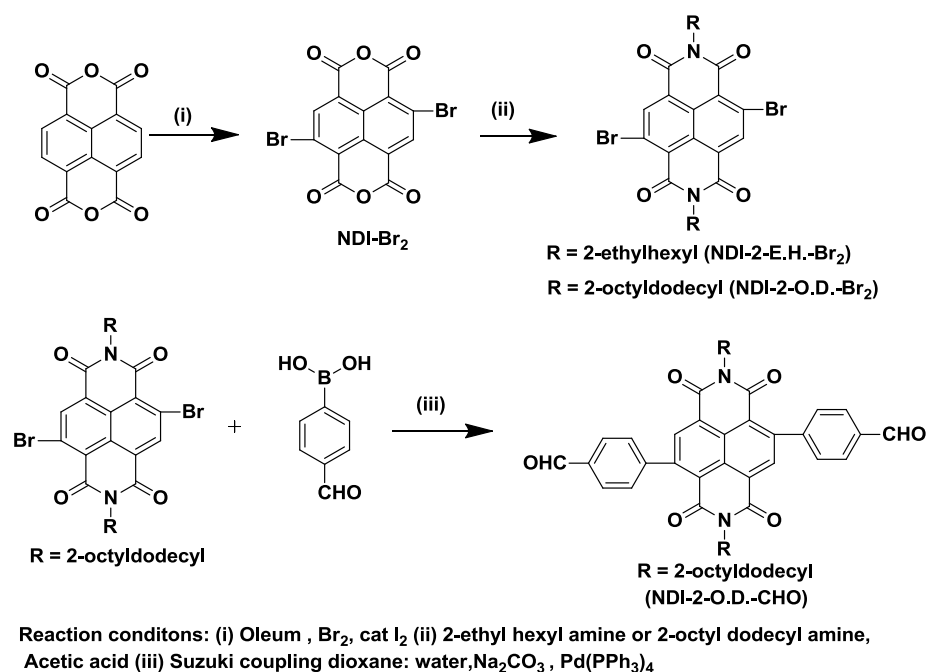


b) Horner-Wadsworth-Emmons polymerization



Scheme 4.1 Synthesis of copolymers.

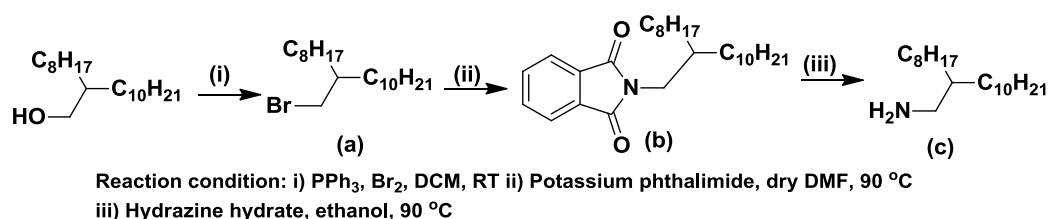
The synthetic route used for NDI based monomers are depicted in **Scheme 4.2**. The synthesis of *N,N*-bis(2-ethyl-hexyl)-2,6-dibromonaphthalene-1,4:5,8-tetracarboxylic diimide (NDI-2-E.H-Br₂) and *N,N*-bis(2-octyl-dodecyl)-2,6-dibromonaphthalene-1,4:5,8-tetracarboxylic diimide (NDI-2-O.D-Br₂) were carried out using literature reported procedure by selecting 2-ethylhexyl and 2-octyldodecyl branched side chains to ensure enough solubility to polymer.^{4a,36} The synthesis of core-substituted NDI based monomers was begun with the bromination of NTCDA at 2, 6-position (NTCDA -Br₂).



Scheme 4.2 Synthesis of core-substituted NDI based monomers.

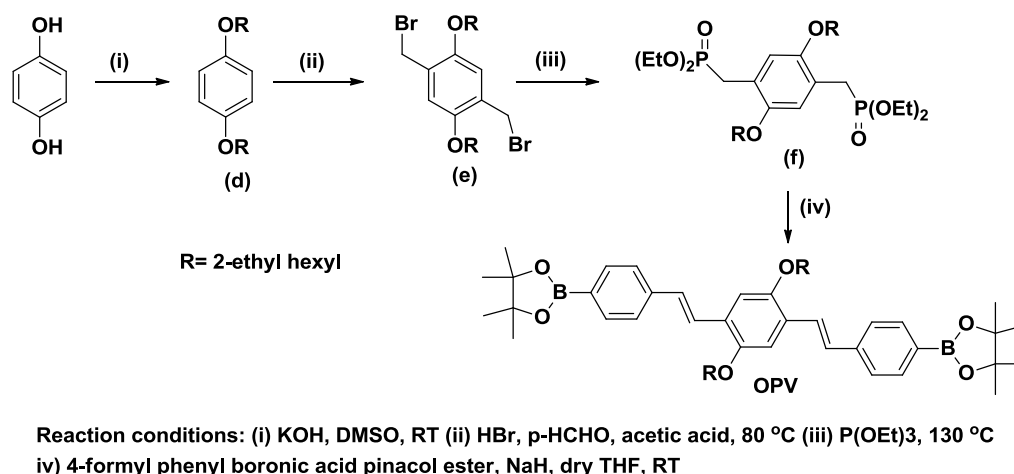
The bromination of NTCDA was carried out in fuming sulphuric acid (Oleum, 40 %) in presence of catalytic amount of iodine and elemental bromine was used as brominating reagent. This approach yielded mixture of compounds consisting mainly of 2, 6- dibromo NTCDA and small amounts of 2-monobromo and 2, 3, 6-tribromo compounds. None of these isomers was soluble in common organic solvent; consequently separation of 2, 6-dibromo isomer in pure form became very difficult. However, further imidization of crude mixture with long or branched alkyl amine such as 2-ethylhexyl amine and 2-octyl dodecylamine in glacial acetic acid at 130 °C produced soluble derivatives (NDI-2-E.H-Br₂) and (NDI-2-O.D-Br₂) respectively. This has been separated in to regioisomerically pure 2, 6-dibromo NDI derivative by column chromatography and re-crystallization. The 2-octyl-1-dodecylamine (c)

required for synthesis of NDI-2-O.D-Br₂ was obtained from 2-octyl-1-dodecolol (Scheme 4.3) in three steps; the detailed synthetic procedures are given in experimental section (4.2.4). N, N'- Bis - (2-octyldodecyl)-2, 6-(4-formyl) diaryl-1, 4:5, 8-naphthalene diimide (NDI-2-O.D-CHO) was synthesized by Suzuki coupling between NDI-2-O.D-Br₂ and 4-formyl phenyl boronic acid in 83 % yield (Scheme 4.2).^{2c}



Scheme 4.3 Synthesis of 2-octyl-1-dodecylamine.

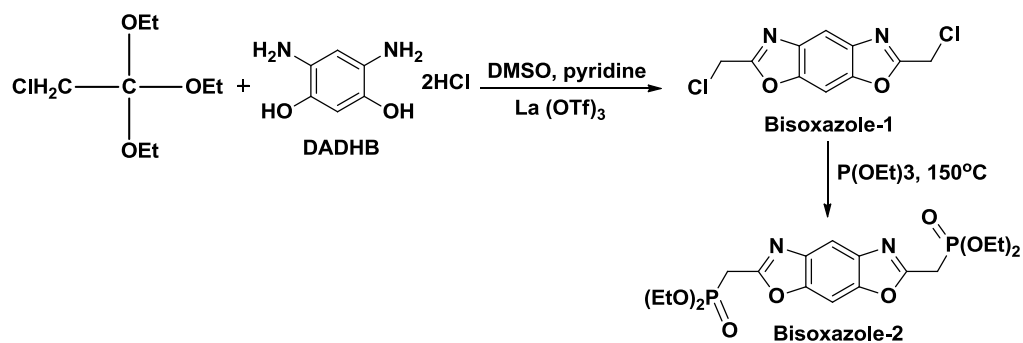
The comonomer OPV-diboronic acid pinacol ester (OPV) required for Suzuki polymerization was synthesized from 2,5-di-2-ethylhexyloxy-1,4 xylenebis(diphosphonate) (f) and 4-formylphenyl boronic acid pinacole ester by Wittig-Horner olefination (Scheme 4.4) to get exclusively the trans product. 2,5-di-2-ethylhexyloxy-1,4 xylenebis(diphosphonate) (f) was obtained from 1,4-hydroquinone in three steps; the detailed synthetic procedures are given in experimental section (4.2.4).



Scheme 4.4 Synthesis of OPV monomer.

The comonomer Dimethylbenzo[1,2-d;5,4-d]bisoxazole-diethyl phosphonate ester (Bisoxazole-2) required for Wittig polymerization was obtained from 2,6-bis(chloromethyl)benzo[1,2-d; 5,4-d']bisoxazole (Bisoxazole-1) (Scheme 4.5). The Bisoxazole-1 was synthesized by literature reported procedure³⁴ using

diaminodihydroxybenzene dihydrochloride (synthesis was given in chapter 3) and triethyl orthochochloroacetate in presence of 5 mole % $\text{La}(\text{OTf})_3$. Bisoxazole-1 was heated in triethylphosphite at $150\text{ }^\circ\text{C}$ to yield 2,6-Dimethylbenzo[1,2-d;5,4-d]bisoxazole-diethyl phosphonate ester (Bisoxazole-2), which was purified by recrystallization from heptane.



Scheme 4.5 Synthesis of Bisoxazole monomer.

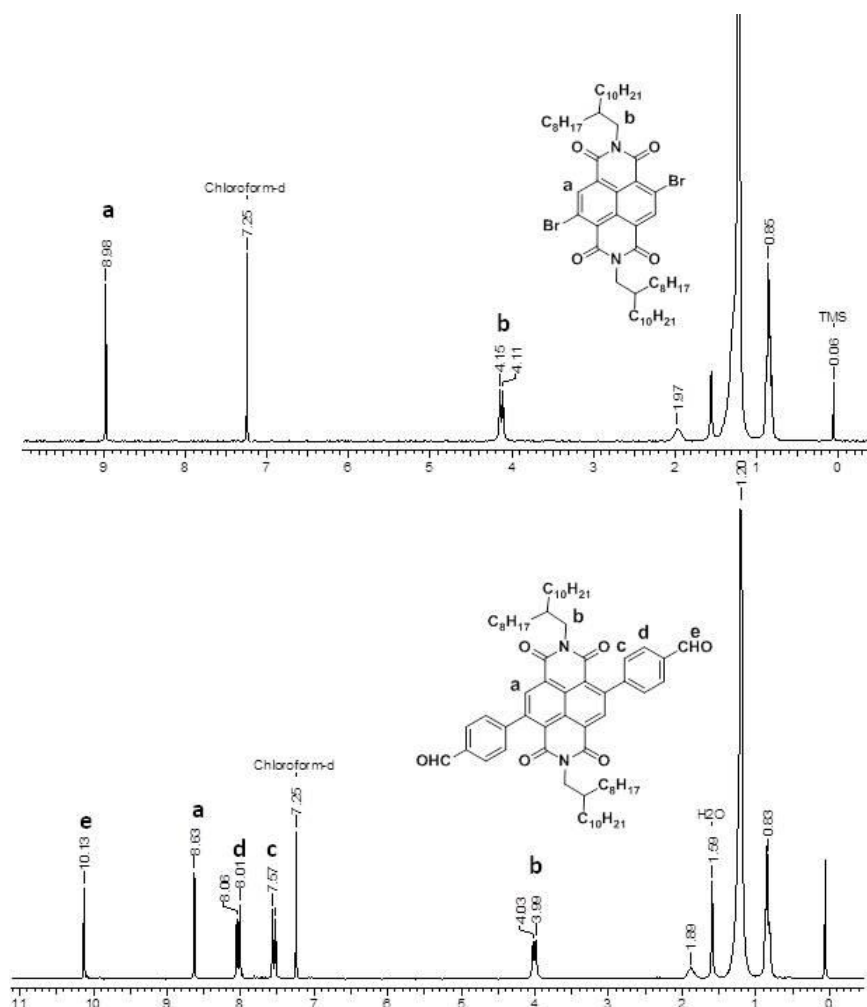


Figure 4.3 a) ^1H NMR spectra of core-substituted NDI monomers.

All the monomers were purified by column chromatography and solid compounds were further recrystallized in order to achieve maximum possible purity. NDI-*alt*-OPV and NDI-*alt*-BT was precipitated in methanol and purified by soxhlet extraction with methanol, acetone and chloroform whereas chloroform extraction was skipped for NDI-*alt*-BBO and NDI-*r*-OPV/BBO. Chloroform extracts were then concentrated under reduced pressure and re-precipitated in methanol; the polymer was then collected by filtration. The choice of oligo(phenylenevinylene) OPV, benzobisoxazole (BBO) and benzothiadiazole (BT) as the aromatic and heteroaromatic donor comonomer respectively in the polymers was based on their different electron donating ability and the extended π -conjugation which would provide a handle to fine tune the optical and semiconducting properties of the NDI polymers. Except NDI-*alt*-BBO, which had rigid aromatic units, the polymers exhibited good solubility in common organic solvents such as chloroform, THF, chlorobenzene and orthodichlorobenzene (ODCB).

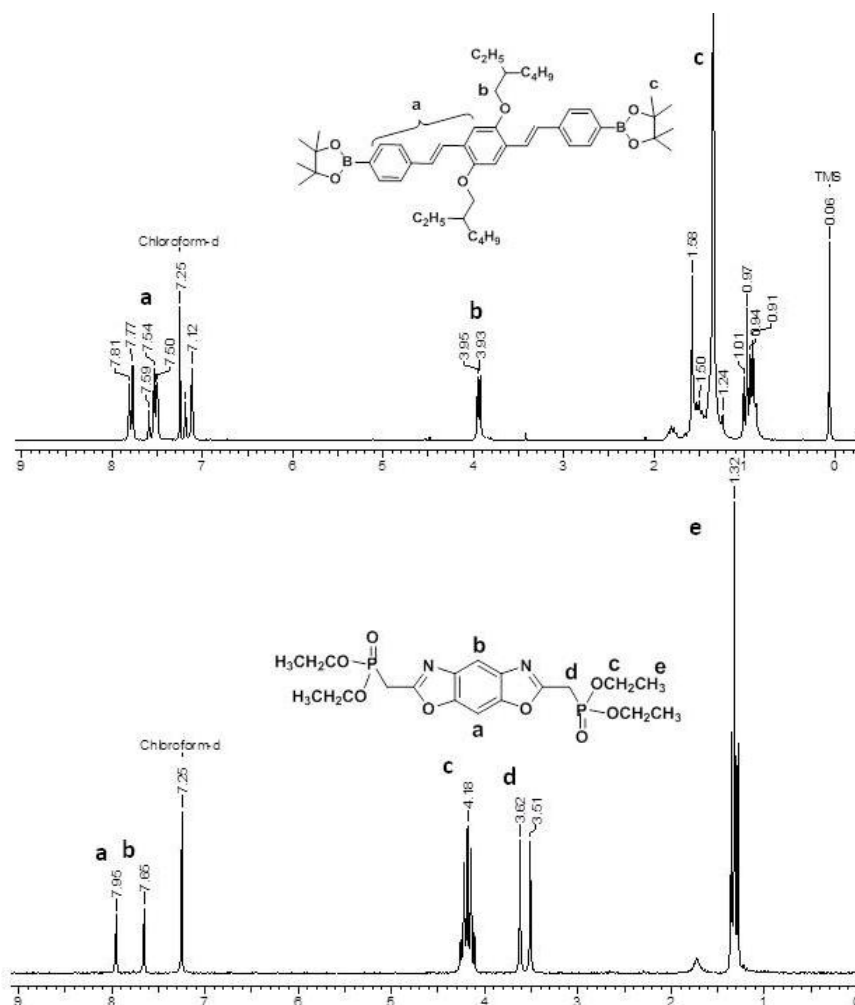


Figure 4.3 b) ^1H NMR spectra of OPV and Bisoxazole monomers.

To increase the solubility of BBO containing polymer, random copolymer incorporating different mole ratios of BBO (Bisoxazole-2) to co monomer (f) were synthesized. It was found that the maximum incorporation of 30 % (in feed) of BBO was possible to retain solubility in NDI-*r*-OPV/BBO after which the copolymer was completely insoluble. The structure of all monomers and polymers were characterized by ^1H NMR, ^{13}C NMR, and FT-IR and MADI-TOF spectra. The labeled ^1H NMR spectra of all monomers are given in **Figure 4.3 a) and b)**. Both the copolymer NDI-*alt*-OPV and NDI-*alt*-BT synthesized by Suzuki polymerization showed noticeable peak broadening in their ^1H NMR spectra (**Figure 4.4 a)** which confirmed the formation of copolymer. Furthermore, the peak corresponding to aromatic region of NDI (a) in NDI-2-O.D.-Br₂ monomer (δ 8.98 ppm) was shifted to lower chemical shift value in NDI-*alt*-OPV (δ 8.70 ppm).

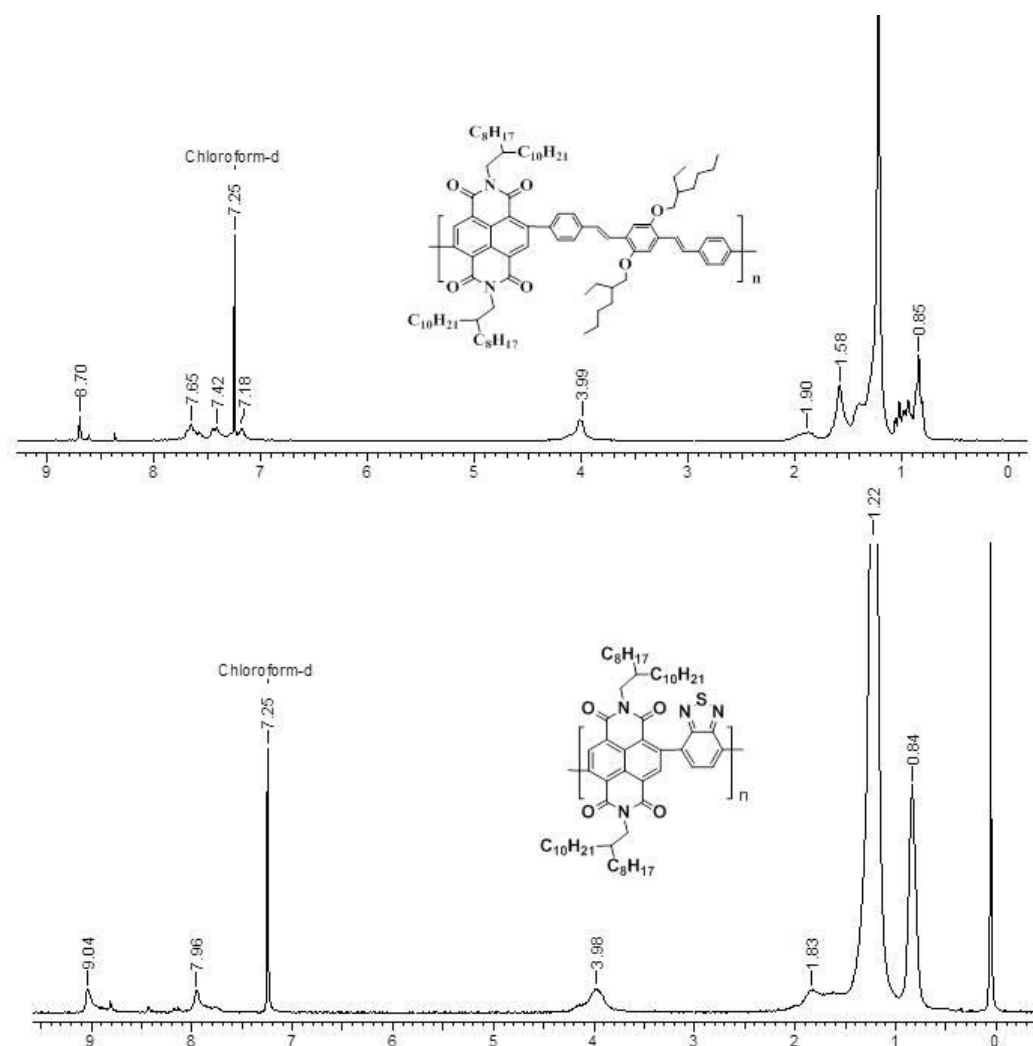


Figure 4.4 a) ^1H NMR spectra of NDI-*alt*-OPV and NDI-*alt*-BT.

While in NDI-*alt*-BT copolymer this peak has shifted to higher chemical shift value (δ 9.04 ppm) which suggested the lower electron donating nature of benzthiadiazole (BT) comonomer as compared to oligo (phenylenevinylene) (OPV). The ^1H NMR spectra of NDI-*alt*-BBO (**Figure 4.4 b**) was recorded in CDCl_3 containing few drops of trifluoroacetic acid (TFA). However, the ^1H NMR spectrum of BBO containing copolymer NDI-*r*-OPV/BBO could be recorded in CDCl_3 without addition of TFA. The spectrum showed the peaks corresponding to both the OPV and BBO unit which confirmed the random incorporation of both OPV and BBO monomer in NDI-*r*-OPV/BBO.

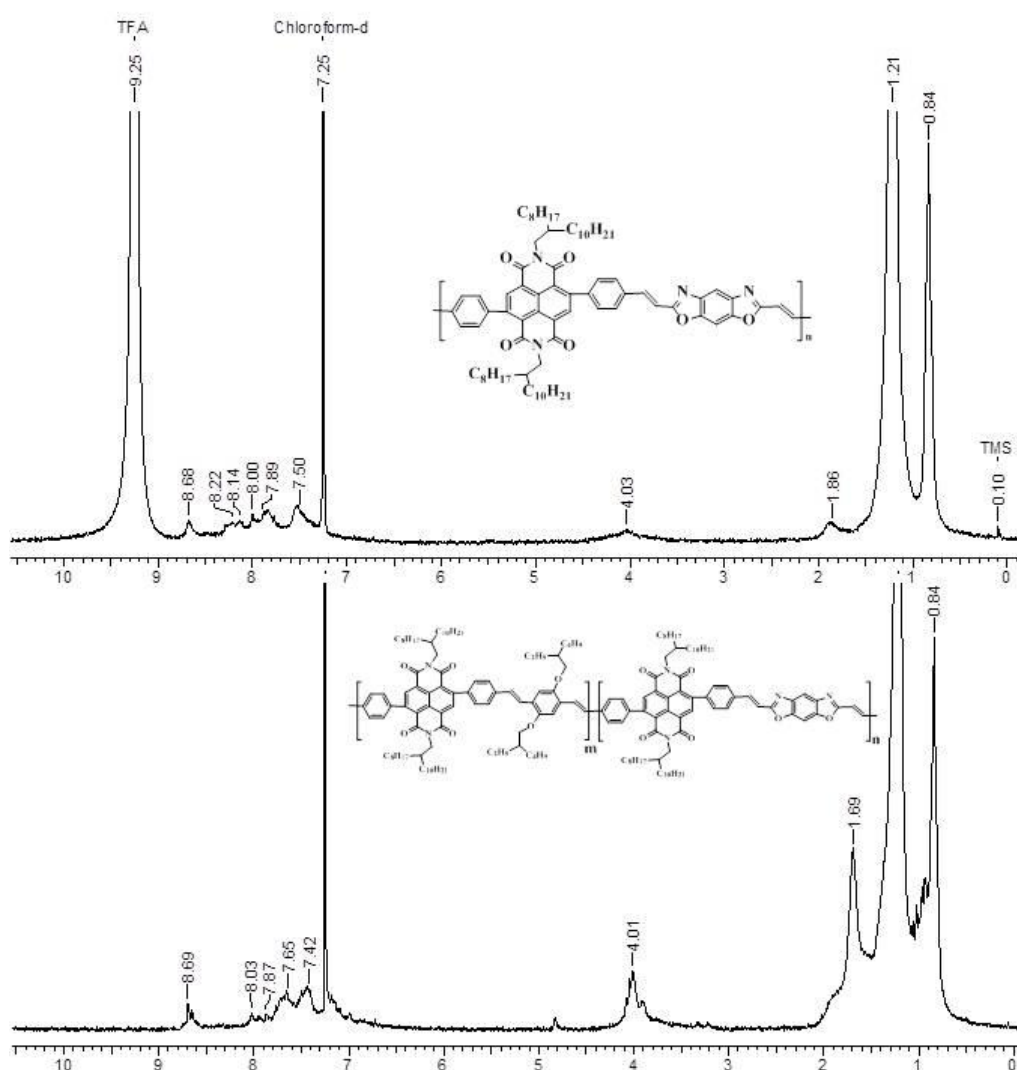


Figure 4.4 b) ^1H NMR spectra of NDI-*alt*-BBO and NDI-*r*-OPV/BBO.

Elemental analysis of the monomers was carried out to confirm the purity and the observed CHN values were matching with the calculated values which are given in section 2.2.4 (experimental procedure).

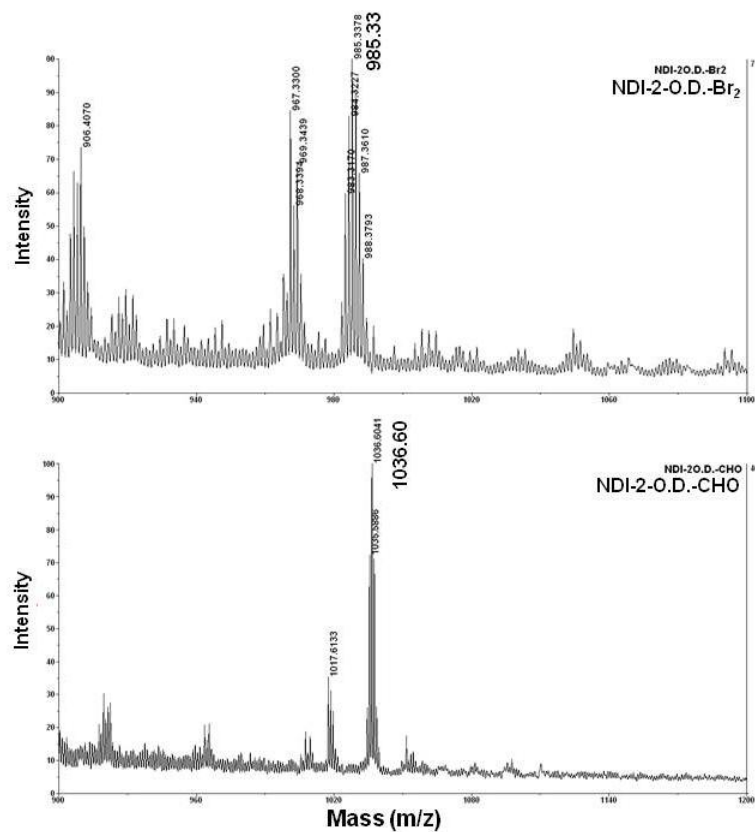


Figure 4.5 a) MALDI-TOF mass data for core-substituted NDI monomers.

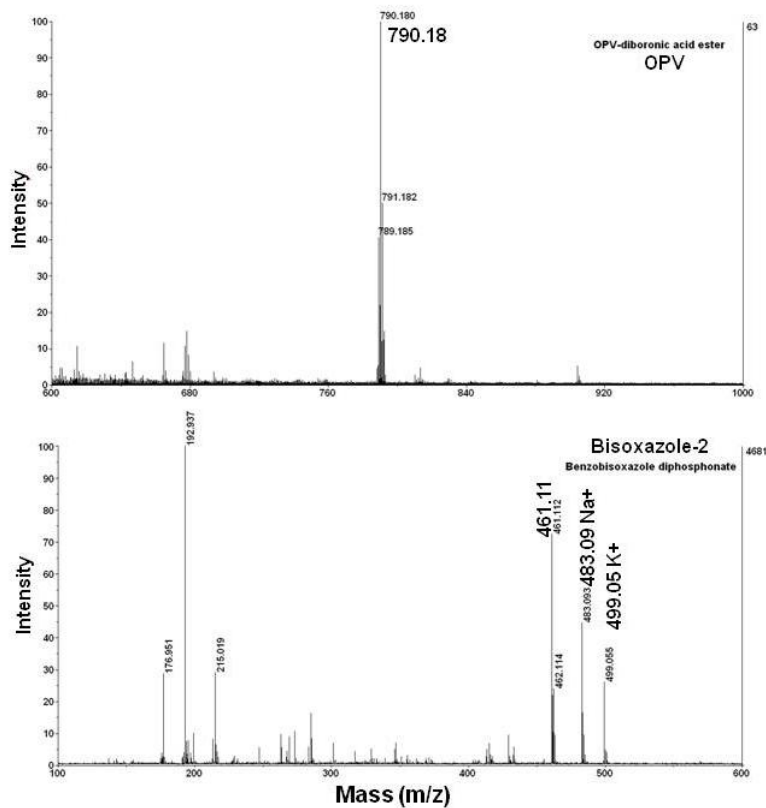


Figure 4.5 b) MALDI-TOF mass data for OPV and Bisoxazole monomers.

The samples were subsequently subjected to MALDI-TOF analysis recorded using 2,5-dihydroxybenzoic acid as the matrix and molecular ion peaks were obtained for cationic species such as $[M+1]$, $[M+Na^+]$ and $[M+K^+]$. The MALDI spectra of the monomers are given in **Figure 4.5 a)** and **b)**. Thus, the NMR, MALDI-TOF spectra and elemental analysis of the molecules confirmed the structure and high purity of the monomers. Molecular weight of polymers were determined by gel permeation chromatography (GPC), using polystyrene standards for the calibration with chloroform as eluent and GPC traces are shown in **Figure 4.6**.

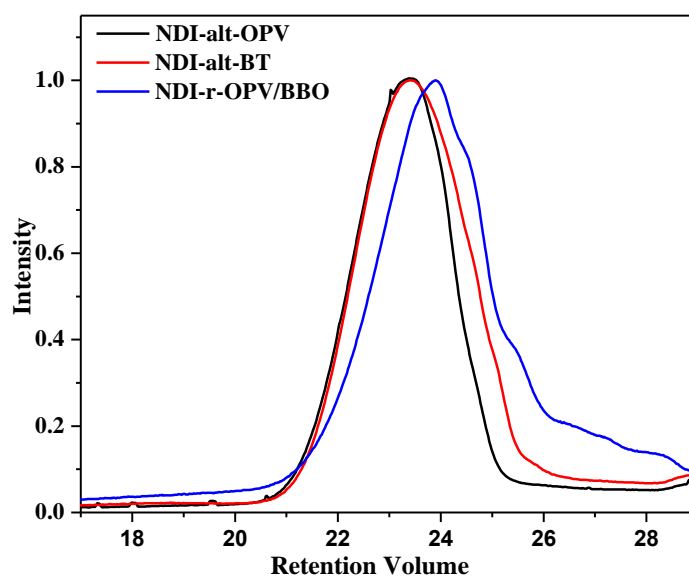


Figure 4.6 GPC traces for copolymers in chloroform using polystyrene as internal standard.

The molecular weight determination of NDI-*alt*-BBO was not possible due to insufficient solubility. All polymers exhibited moderate number-average (M_n) and weight average (M_w) molecular weight as reported for similar class of polymers.^{3a,28b}

^{31b} The lower molecular weights of these polymers are accounted for by their rigid aromatic structure, which reduced their solubility in the reaction medium. The estimated values of M_n , M_w and polydispersity index ($PDI = M_w/M_n$) for polymers are listed in **Table 4.1**. Thermal properties of polymers were determined by thermogravimetric analysis (TGA) as well as DSC measured under N_2 atmosphere. TGA curves (**Figure 4.7**) showed thermal stability up to 400 °C for all polymers. The 10 % weight loss temperature (T_d) is shown in **Table 4.1**. DSC curves recorded for NDI-*alt*-OPV (**Figure 4.8**) showed broad endothermic peak at 310 °C during heating

cycle and exothermic peak at 256 °C during second cooling cycle which indicated the crystalline nature of NDI-*alt*-OPV. On the other hand, NDI-*alt*-BT, NDI-*alt*-BBO and NDI-*r*-OPV/BBO did not show any melting transition until 350 °C (**Figure 4.8**). The observed values of glass transition temperatures (T_g) were found to be almost similar for all polymer ≈ 80 °C.

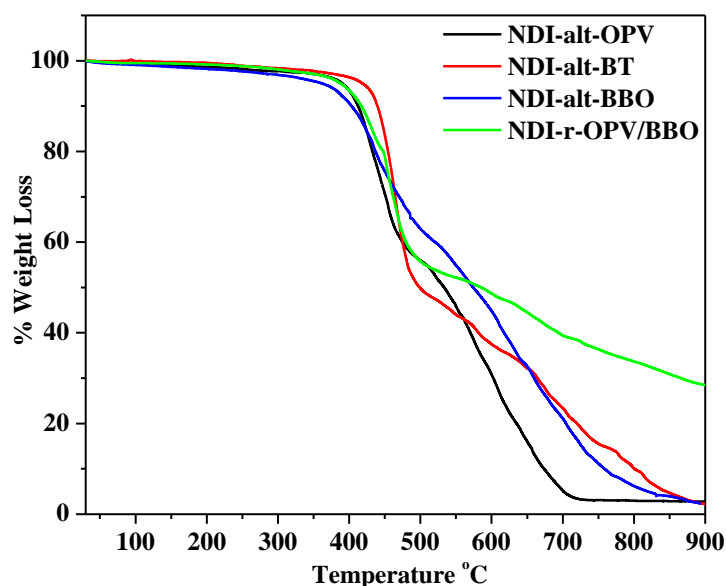


Figure 4.7 TGA curves for polymer.

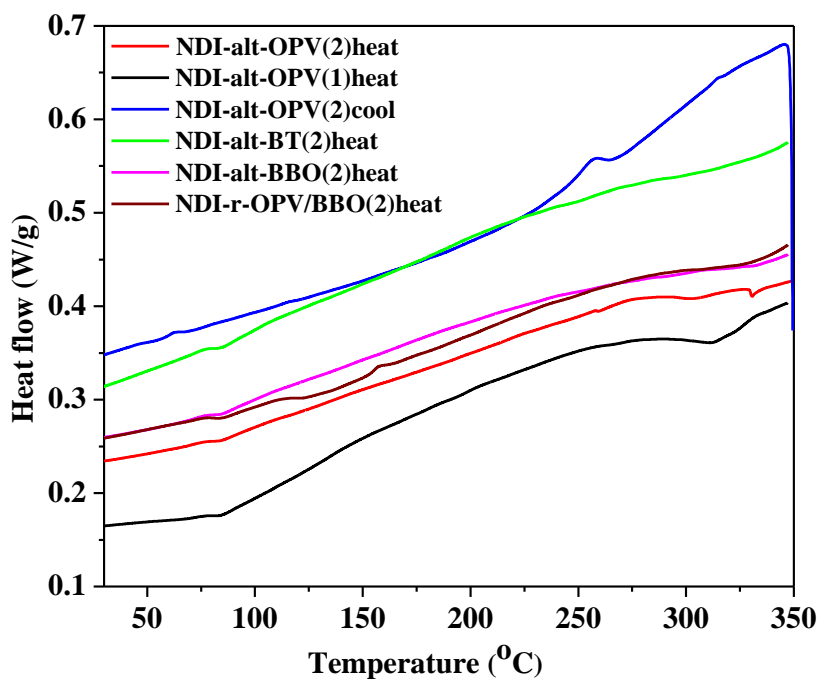


Figure 4.8 DSC curves for polymers during second heating cycle (cooling curve only for NDIPPV is shown here).

Table 4.1 Molecular weight and thermal properties of polymer.

Sr. No.	Polymer	Yield (%)	Mn ^a	Mw ^a	Mw/Mn ^a	T _d ^b (°C)
1	NDI- <i>alt</i> -OPV	72	8200	12600	1.53	412
2	NDI- <i>alt</i> -BT	82	6800	11100	1.62	403
3	NDI- <i>alt</i> -BBO	76	- ^c	- ^c	- ^c	417
4	NDI- <i>r</i> -OPV/BBO	71	5000	8600	1.72	439

^a Number- average molecular weight (Mn), weight-average molecular weight (Mw), and polydispersity index (Mw/ Mn) ^bDecomposition temperature 10 % weight loss estimated using TGA under N₂. ^c GPC was not possible due to insufficient solubility.

4.3.2 Photophysical Properties

The photophysical properties of the NDI polymers were investigated by UV-Vis absorption and fluorescence emission spectroscopy. The absorption spectra of all polymers were measured in dilute chloroform solution (except NDI-*alt*-BBO, which was measured in dichlorobenzene) as well as in thin films spin coated from ODCB as shown in **Figure 4.9** and relevant details are summarized in **Table 4.2**. Similar to previous report on core substituted NDI polymers,^{3,7,21-23} the absorption spectra of polymer solution exhibited peaks in two distinct regions – a high energy absorption band at ~ 360-380 nm, which was attributed to π - π^* transition and another low energy band at ~ 480- 550 nm assigned to intramolecular charge transfer (ICT) from different donors to NDI. Compared to other sets of polymers, the ICT absorption maxima was red shifted for NDI-*alt*-OPV (λ_{\max} 536) as a result of the increased conjugation due to the planar polymer backbone and strong electron donating ability of OPV. Furthermore, broadening of absorption band at ~ 410 nm occurred due to π - π^* transition of the OPV conjugated backbone^{28a,b} which overlapped with the NDI absorption. The lower energy absorption band (ICT) was hypsochromically shifted to λ_{\max} 480 nm for NDI-*alt*-BBO which is accounted for by the decreased electron donating character^{15a,23} of BBO unit compared to OPV. The poorer electron donating character combined with twisted polymer backbone (discussed later in DFT section)

resulted in a more blue shifted ICT absorption band (λ_{max} 450 nm) for NDI-*alt*-BT, also the spectrum at π - π^* absorption region resolved to fine vibration pattern showing less overlap between NDI and BT core due to twisted polymer backbone. The copolymer NDI-*r*-OPV/BBO which contained both the donor unit OPV and BBO showed red shifted lower energy absorption edge compared to NDI-*alt*-BBO.

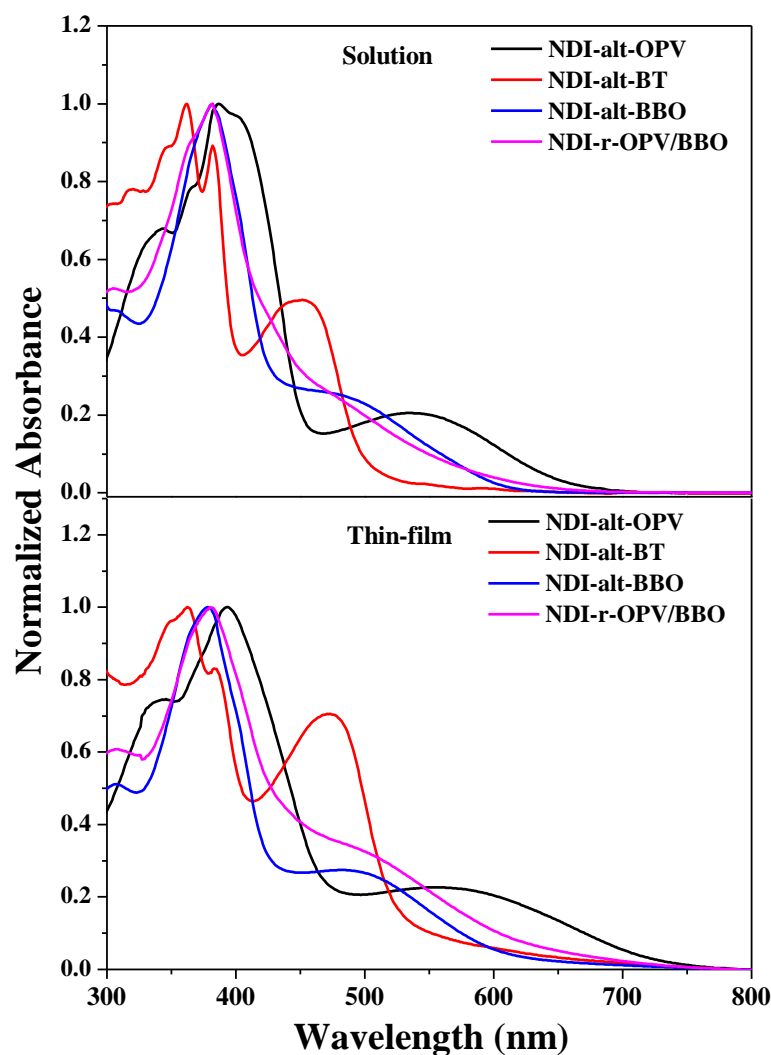


Figure 4.9 UV-Vis absorption spectra of dilute ($\sim 5 \times 10^{-6}$ M) solutions of NDI polymers in chloroform (top) and thin film (bottom).

A considerable red shifting of absorption peaks was observed in spin coated thin films compared to that recorded in solution which is anticipated due to the interchain aggregation and chain planarization in the solid state.^{6b} Noticeably, the large red shift of ICT absorption maxima (~ 28 nm) from solution to thin-film for NDI-*alt*-OPV compared to other polymers clearly indicated more ordered nature of thin film^{6b} of

NDI-*alt*-OPV which was further substantiated by XRD and AFM analysis. The optical band gaps of polymers (E_g^{opt}) calculated from lower energy absorption onset of thin film is listed in **Table 4.2**. An optical band gap of 1.69 eV was obtained for NDI-*alt*-OPV, which was the lowest among all other poly (p-phenylenevinylene) (PPV) homopolymer reported so far.³⁷

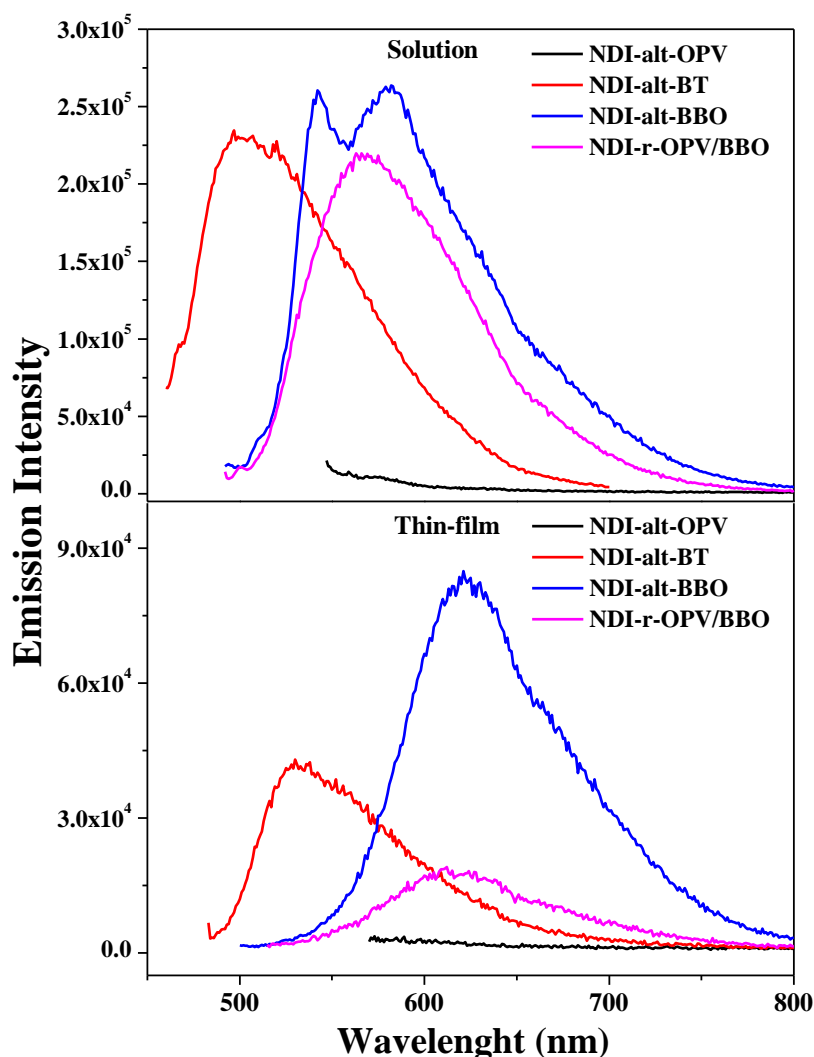


Figure 4.10 Emission spectra of dilute ($\sim 5 \times 10^{-6}$ M) solutions of NDI polymers in chloroform (top) and thin film (bottom).

Fluorescence emission spectra of polymers measured in solution and thin-films is shown in **Figure 4.10**. A complete quenching of fluorescence emission was observed both in solution and thin film of NDI-*alt*-OPV whereas NDI-*alt*-BT and NDI-*alt*-BBO showed emission band centered at 502 nm and 580 nm respectively. The fluorescence quenching in NDI-*alt*-OPV could be attributed to increased intra-molecular charge

transfer (electron) from OPV to NDI.^{38,28a,b} A random incorporation of benzobisoxazole donor unit in copolymer NDI-*r*-OPV/BBO along with OPV resulted in emission band centered at 566 nm which had less intensity compared to NDI-*alt*-BBO homopolymer. Consistent with the observation from solution and thin film absorption spectra, an overall decrease in fluorescence intensity along with red shifting of emission spectra was observed in thin films compared to that recorded in solution indicating higher extent of the interchain aggregation in solid state.³⁸

Table 4.2 Photophysical data of NDI polymers.

Polymer	Solution		Thin-film		E_g^{opt}
	$\lambda_{abs}(nm)$	$\lambda_{em}(nm)$	$\lambda_{abs}(nm)$	$\lambda_{em}(nm)$	
NDI- <i>alt</i> -OPV	386, 536	-	393, 564	-	1.69
NDI- <i>alt</i> -BT	360,450	502	362,473	531	2.38
NDI- <i>alt</i> -BBO	381, 480	580	381, 490	621	2.03
NDI- <i>r</i> -OPV/BBO	381, 480	566	381, 490	620	1.87

4.3.3 Electrochemistry

The effect of different donor moiety on the reduction potential of NDI core was examined through the measurement of the electrochemical reduction using cyclic voltammetry (CV). The polymers were deposited as thin films from chloroform solution on to the platinum working electrode and then their CV was recorded in 0.1 M *n*-Bu₄ NPF₆ / acetonitrile solution. **Figure 4.11** shows cyclic voltamograms of all polymers and values of electrochemical redox potentials are listed in **Table 4.3**. The potential was measured against Ag/Ag⁺ reference electrode (Ag wire in 0.01 M AgNO₃) using internal standard Ferrocene / Ferrocenium (FC/FC⁺) redox system. All polymers exhibited two quasi-reversible reduction peaks - the first peak due to polymer anion and second due to dianion formation which resembled that of the other reported NDI based polymers.^{3,7,21-23} NDI-*alt*-OPV showed reduction peak at -1.06/-1.42 V with moderate peak current whereas significant decrease in reduction potential with increased peak current was observed for NDI-*alt*-BT and NDI-*alt*-BBO which had reduction peak at -0.89/-1.33 V and -0.86/-1.32 V respectively. The decrease in

reduction potential of NDI-*alt*-BT and NDI-*alt*-BBO could be attributed to the electron withdrawing nature of BT and BBO respectively (heterocyclic moiety) which made NDI core more electron deficient.

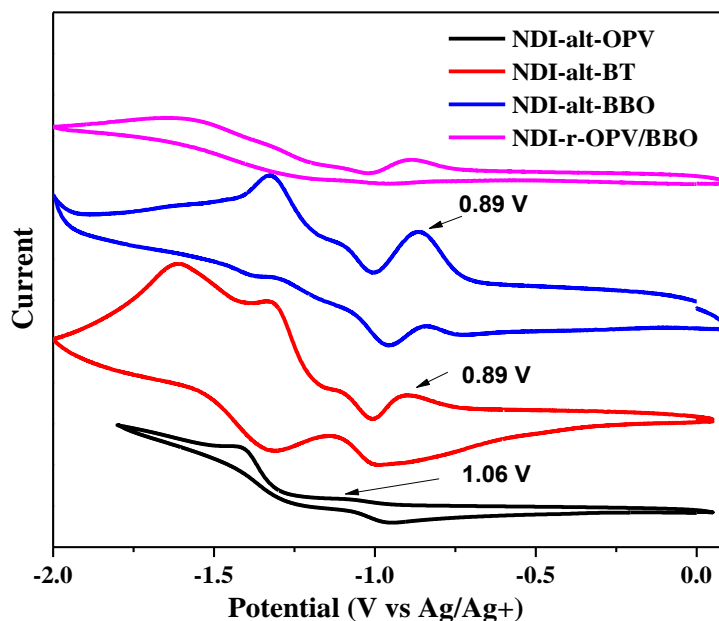


Figure 4.11 Cyclic voltammograms of NDI polymers as thin film in 0.1 M $n\text{-Bu}_4\text{NPF}_6$ acetonitrile solution.

The small incorporation of BBO moiety in the random copolymer also resulted in lower reduction potential of copolymer NDI-*r*-OPV/BBO which was observed at -0.88/-1.32 V. Furthermore, NDI-*alt*-OPV and NDI-*alt*-BBO showed oxidation peaks at 0.82/1.2 V (quasi-reversible) and 1.26 V (irreversible) respectively during anodic scan whereas no oxidation peak was observed for NDI-*alt*-BT and NDI-*r*-OPV/BBO within the solvent window. The quasi-reversible oxidation peak observed in NDI-*alt*-OPV suggested propensity of p-doping in polymer. HOMO and LUMO energy level and electrochemical band (E_g^{ele}) gaps of polymers were estimated based on the onset of oxidation and reduction peak respectively assuming absolute energy level of ferrocene to be 4.8 eV below the vacuum level and values are listed in **Table 4.3**. For NDI-*alt*-BT and NDI-*r*-OPV/BBO, the HOMO energy level was estimated from its thin film optical band gap and the LUMO energy level. The LUMO energy level of NDI-*alt*-OPV was found to be -3.75 eV due to intrinsic properties of NDI.^{7,21} The LUMO energy level of NDI-*alt*-BT, NDI-*alt*-BBO and NDI-*r*-OPV/BBO was lowered by ~ 0.23 eV compared to NDI-*alt*-OPV and was found at -3.96 eV, -3.98 eV and -3.94 eV respectively, due to lower reduction potential. The HOMO energy level

of donor –acceptor conjugated polymer mostly depends upon electron donating strength of donor moiety and conformation of polymer backbone (repeat unit).^{15a} A decrease (or lower lying) in HOMO energy levels is anticipated with decrease in the electron donating nature of the donor moiety. As expected, HOMO energy level of NDI-*alt*-OPV was found to be -5.44 eV which was further decreased in NDI-*alt*-BT, NDI-*alt*-BBO, and NDI-*r*-OPV/BBO to -6.34 eV, -6.01 eV and -5.85 eV respectively. The dramatic decrease of HOMO energy level in NDIBT was accounted for by both electron withdrawing nature of BT unit and twisted polymer backbone which is discussed in the following section in detail.

Table 3 Electrochemical data with HOMO/LUMO energy level and band gaps estimated from cyclic voltammetry and DFT. (Ag/Ag+ reference electrode was used for electrochemical measurement).

Polymers	Cyclic voltammetry					DFT (B3LYP/6-31G**) ^e		
	$E_{1/2}^{\text{red}}$ (V)	$E_{1/2}^{\text{ox}}$ (V)	LUMO (eV)	HOMO (eV)	$E_g^{\text{ele c}}$	LUMO (eV)	HOMO (eV)	E_g
NDI-<i>alt</i>-OPV	-1.06, -1.42	0.82, 1.2	-3.75	-5.44 ^a -5.52 ^b	1.77	-3.33	-5.00	1.66
NDI-<i>alt</i>-BT	-0.89, -1.33	-	-3.96	-6.34 ^a	-	-3.43	-6.29	2.85
NDI-<i>alt</i>-BBO	-0.86, -1.32	1.26	-3.98	-6.01 ^a -5.95 ^b	1.97	-3.45	-5.53	2.08
NDI-<i>r</i>-OPV/BBO	-0.88, -1.32	-	-3.94	-5.81 ^a	-	-3.38	-5.17	1.79

a) HOMO Values calculated from LUMO and E_g optical b) HOMO Values calculated from E onset of oxidation c) E_g^{ele} calculated from LUMO and HOMO ^b e) DFT results for model (dimer).

4.3.4 Computational Studies

Density functional theory (DFT) calculations were performed on oligomeric models (dimer) to gain a deeper insight into the energy levels, band gap and molecular orientation of donor and acceptor in the polymer backbone. The energy levels were calculated from optimized geometry using B3LYP functional and polarized 6-31g*

basis set. The *N*- 2-octyl dodecyl bulky substituent in NDI unit and 2-ethyl hexyloxy substituent in OPV unit were replaced with methyl groups to reduce the computational time. The surface plots for oligomeric models are shown in **Figure 4.12** and values of energy level and band gaps are listed in **Table 4.3**.

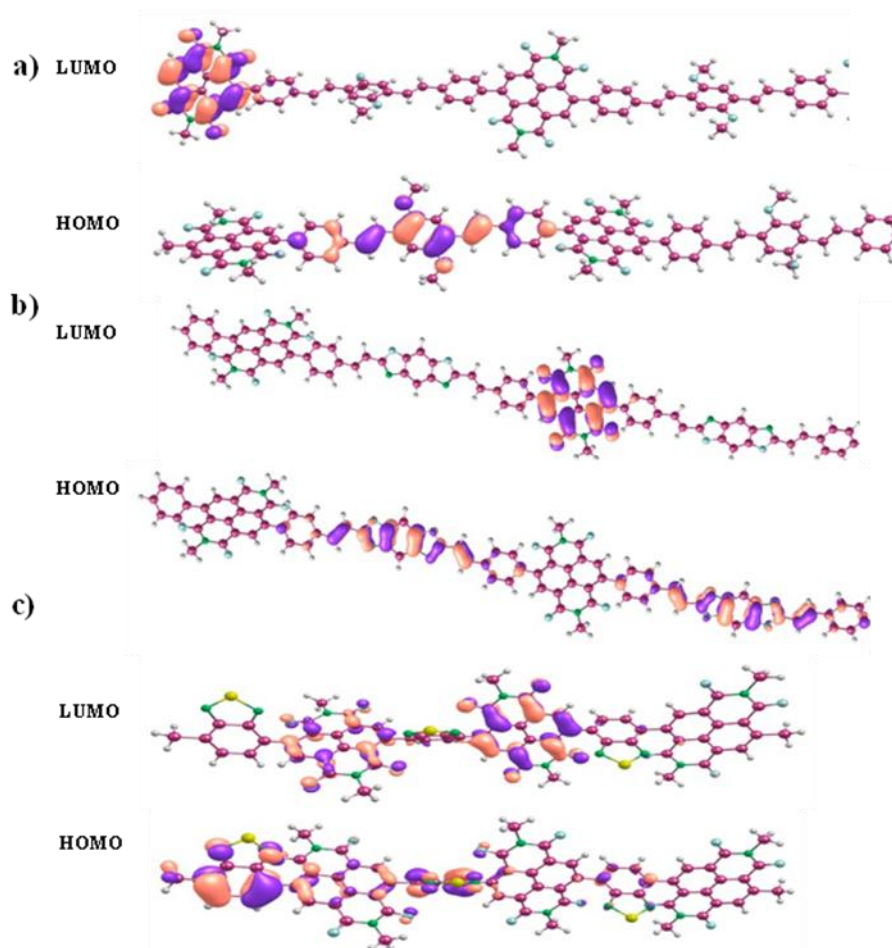


Figure 4.12 The HOMO and LUMO surface plots for oligomers (dimer models) a) NDI-*alt*-OPV b) NDI-*alt*-BBO c) NDI-*alt*-BT.

As generally observed in NDI donor -acceptor conjugated polymers,^{14,23} the LUMO wave functions are localized on NDI core and HOMO wave functions are localized on OPV, BT and benzobisoxazole moiety. Consistent with experimental result from cyclic voltammetry, a decrease in LUMO energy level was found in NDI-*alt*-BT and NDI-*alt*-BBO compared to NDI-*alt*-OPV. The HOMO energy level and consequently band gap were found to be strongly dependent upon electron donating nature of donor as well as molecular orientation of donor and acceptor in corresponding polymers.^{15a,39} **Figure 4.13** compares the minimum energy optimized structure of oligomeric models which showed more coplanar and rigid conformation for NDI-*alt*-

OPV and NDI-*alt*-BBO having dihedral angle ca. $\sim 37^\circ$ and ca. $\sim 38^\circ$ respectively between NDI core and donor unit.

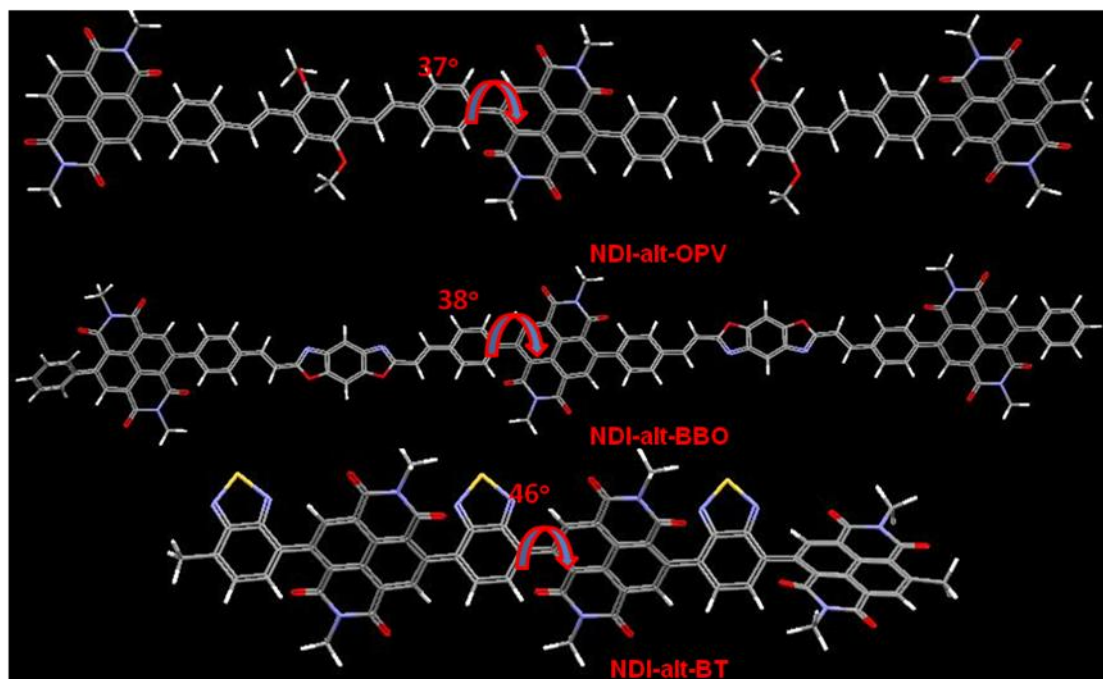


Figure 4.13 DFT optimized geometry (B3LYP/ 6-31g* Level) of dimer (NDI-*alt*-OPV and NDI-*alt*-BBO) and trimer (NDI-*alt*-BT) models with calculated dihedral angle.

The observed values of dihedral angles are almost similar with NDI Polymer which exhibited high electron mobility in OFETs due to rigid aromatic and coplanar structure. The HOMO energy level for NDI-*alt*-OPV was found to be -5.00 eV whereas HOMO level was lowered to -5.53 eV for NDI-*alt*-BBO due to decrease in electron donating strength of BBO. Since the BT unit is directly attached to NDI core the non bonded repulsive interaction between carbonyl group of NDI and sulphur of BT showed twisted conformation for NDI-*alt*-BT having dihedral angle ca. $\sim 46^\circ$ which further reduced the HOMO level to -6.29 eV. The highest value of theoretical (2.85 eV) and optical band gap (2.38 eV) was observed for NDI-*alt*-BT which also accounted for twisted polymer chain conformation. The study was also done for mixed OPV and BBO polymer (NDI with one each unit of OPV and BBO) to see the average reduction potential in NDI-*r*-OPV/BBO. As expected the HOMO (-5.17 eV) and LUMO (-3.38 eV) energy level values for NDI-*r*-OPV/BBO were lying in between that of the two homopolymers.

4.3.5 Thin Film Morphology

The solid state morphology, molecular packing and crystalline nature of NDI polymers were analyzed using X-ray diffraction (XRD) measurement and atomic force microscopy (AFM). The X-ray diffraction pattern of thermally annealed thin film of NDI-*alt*-OPV (**Figure 4.14**) showed sharp (100) peak at $2\theta = \sim 4.83^\circ$ which corresponded to a lamellar interchain *d*- spacing^{21,38} of 18.24 Å. A relatively broad peak was observed for NDI-*alt*-BBO at $2\theta = \sim 4.51^\circ$ with slightly higher *d*- spacing of 19.54 Å indicating less crystalline nature of NDI-*alt*-BBO compared to NDI-*alt*-OPV.

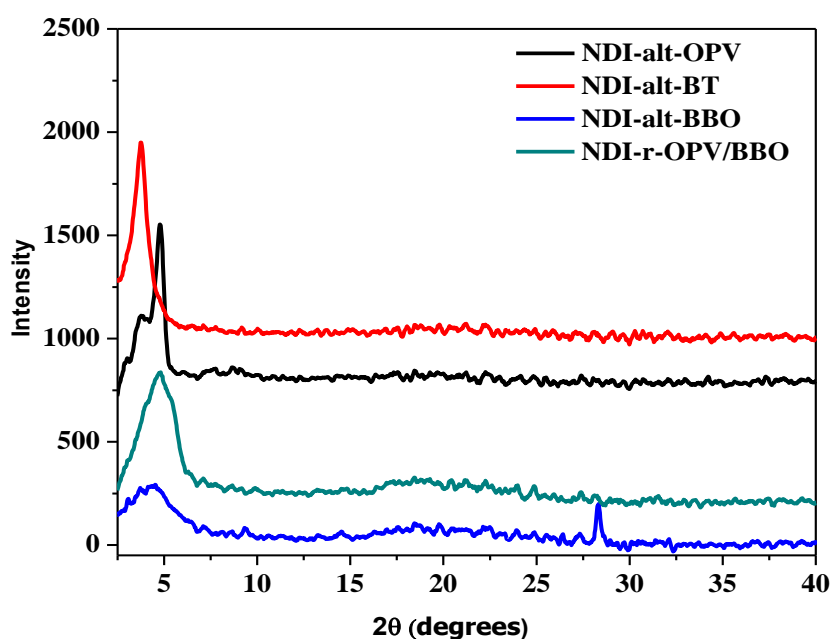


Figure 4.14 XRD patterns of NDI polymer thin film samples.

Additionally, a peak at lower *d*- spacing 3.14 Å ($2\theta = \sim 28.34^\circ$) attributed to π - π stacking of bisoxazole aromatic ring^{1a} was also observed in case of NDI-*alt*-BBO. Consistent with theoretical optimized oligomeric model (**Figure 4.13**) twisting of polymer backbone in NDI-*alt*-BT resulted in increased interchain *d*-spacing of 23.62 Å ($2\theta = \sim 3.73^\circ$) with no significant effect on crystallinity. Both the polymer NDI-*alt*-OPV and NDI-*alt*-BBO had coplanar structure and almost similar dihedral angle ca. $\sim 38^\circ$. However, NDI-*alt*-OPV had higher crystallinity as indicated by the sharp and high intense reflection in XRD. A possible reason for higher crystallinity in NDI-*alt*-OPV is the increased intermolecular side-chain interaction due to interdigitation of alkyl chain (2-ethyl hexyl) on OPV comonomer in addition to interdigitation of 2-octyldodecyl chain on the NDI core.³⁸ On the other hand; the NDI core is pushed

apart in NDI-*alt*-BBO to accommodate π - π stacking of benzobisoxazole aromatic ring. This was also reflected in the copolymer (NDI-*r*-OPV/BBO) containing higher incorporation of OPV compared to BBO as co monomer. A relatively sharp and intense peak was observed at $2\theta = \sim 4.70^\circ$ corresponding to a d -spacing value of 18.78 Å and additionally, improved crystallinity was observed for the copolymer as compared to NDI-*alt*-BBO homopolymer. This clearly indicated better interchain packing in NDI-*r*-OPV/BBO and NDI-*alt*-OPV due to side-chain interdigitation on OPV comonomer. Tapping mode AFM images were taken from HMDS treated and thermally annealed (at 150 °C) thin films of NDI-*alt*-OPV and NDI-*r*-OPV/BBO to correlate the morphological features. As seen in **Figure 4.15**, NDI-*alt*-OPV showed granular morphology with large interconnecting domains having root mean square roughness of 3.08 nm. The NDI-*r*-OPV/BBO showed large aggregates on the surface with very high roughness of 8.31 nm (RMS), probably attributable to the poor solubility of the copolymer in ODCB.

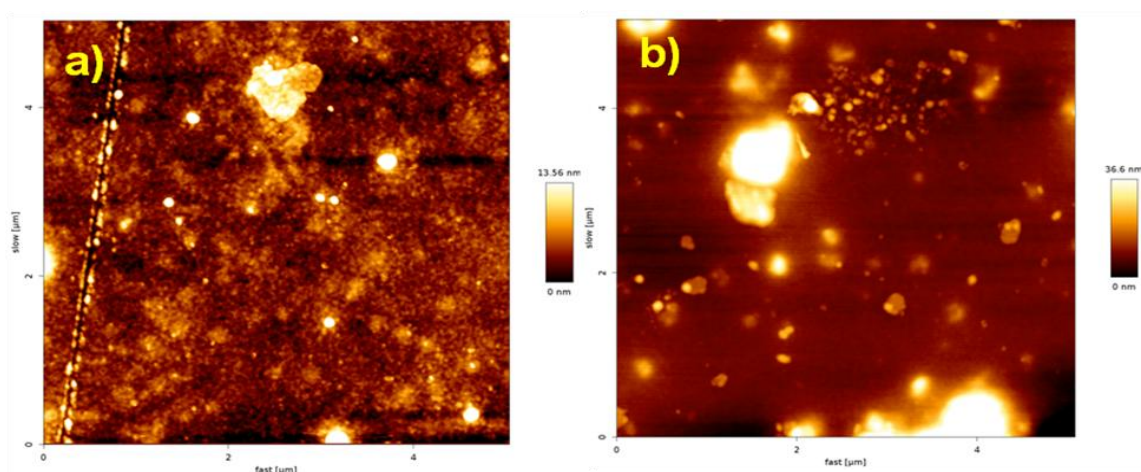


Figure 4.15 AFM images of thin films (image size 5 μ m x 5 μ m) of a) NDI-*alt*-OPV and b) NDI-*r*-OPV/BBO.

4.3.6 Device Characteristics (OFETs)

The effect of three different donors on semiconducting properties of NDI copolymers were analyzed by fabricating bottom-gate top contact field effect transistor geometry with Au (gold) as the source/drain and gate electrode. The fabrication procedure adopted was as described in the experimental section. Active layer of all polymer were drop casted from a 10 mg/mL solution of ODCB to obtain films of ~80-100 nm

thickness. All the substrates were annealed at 150 °C and then cooled to room temperature to get the optimum device performance. All the fabrication and measurements were performed in inert atmosphere inside the glove box. The performance parameters were extracted in the saturation regime from the transconductance characteristics curves by using the following equation.

$$I_{ds} = (\mu_{FET} WC/2L) (V_g - V_{th})^2$$

Where I_{ds} is the drain current, W and L are, respectively, the channel width and length, C is the capacitance per unit area of the gate insulator layer, and V_{gs} and V_T are the gate voltage and the threshold voltage, respectively.

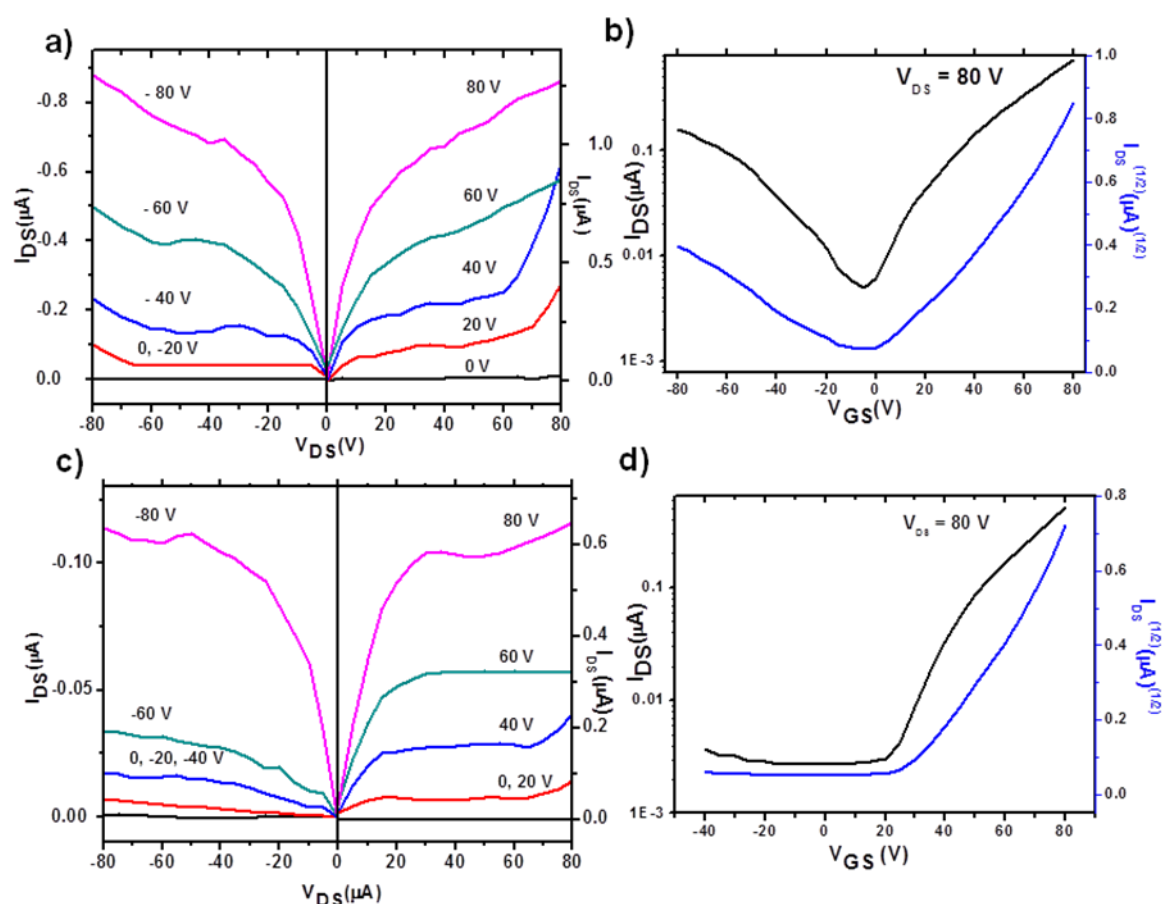


Figure 4.16 Typical output and transconductance curve for NDI-*alt*-OPV (top a, b) and NDI-*r*-OPV/BBO (bottom c, d) in bottom-gate/top contact OFETs annealed at 150 °C.

The charge transport nature of copolymers was found to depend upon electron donating ability of donor co-unit. The NDI-*alt*-OPV showed both p-type and n-type

charge transport with typical ambipolar features, whereas NDI-*r*-OPV/BBO exhibited dominant n-type charge transport with negligible p-type character and NDI-*alt*-BT exhibited only n-type charge transport. The measurement of OFET was not possible for NDI-*alt*-BBO due to insufficient solubility in ODCB. **Figure 4.16** shows the typical OFET output and transconductance characteristics of NDI-*alt*-OPV (top a, b) and NDI-*r*-OPV/BBO (bottom c, d) and values of electron and hole mobility with on/off ratio are reported in **Table 4.4**.

Table 4.4 OFET Characteristics of the NDI polymers.

Polymer	(μ_e) cm^2/Vs	(μ_h) cm^2/Vs	V_t (V)	$I_{\text{on/off}}$	μ_e/μ_h
NDI- <i>alt</i> -OPV	a) 3.09×10^{-3}	a) 2.1×10^{-3}	9	10^5	1.47
NDI- <i>r</i> -OPV/BBO	a) 4.0×10^{-4}	a) 2.1×10^{-6}	11	10^3	190
	b) 9.0×10^{-4}	-	7	10^3	-
NDI- <i>alt</i> -BT	a) 1.59×10^{-3}	-	36	10^3	-

a) Mobility measurement done with gold (Au) source/drain electrode b) Mobility measurement done with aluminium (Al) source/drain electrode

NDI-*alt*-OPV showed balanced electron ($\mu_e = 3.09 \times 10^{-3} \text{ cm}^2 \text{ V}^{-1} \text{ s}^{-1}$) and hole ($\mu_h = 2.1 \times 10^{-3} \text{ cm}^2 \text{ V}^{-1} \text{ s}^{-1}$) mobilities with lower μ_e/μ_h ratio (1.47) which is comparable with literature reported core substituted naphthalene diimide based polymers.^{15a,21,36} The oligo (phenylenevinylene) acted as a strong donor pushing the HOMO energy to a deep value of - 5.44 eV in NDI-*alt*-OPV, which was deeper compared to any other NDI-based donor-acceptor polymers (based on electron rich hetero atom-free benzene or acene donors) reported so far.²³ As a consequence, the hole injection also became as feasible as electron injection. Up to the best of our knowledge, this is the first report on NDI-*alt*-OPV polymer which showed ambipolar charge transport with similar mobility values for both electron and hole. The incorporation (30%) of weak donating benzobisoxazole comonomer along with OPV comonomer in NDI-*r*-OPV/BBO reduced the LUMO and HOMO energy levels to -3.94 eV and -5.85 eV respectively. The change of energy level in NDI-*r*-OPV/BBO resulted in transition of charge transport from balanced ambipolar to electron dominating charge transport ($\mu_e = 4.0 \times 10^{-4} \text{ cm}^2 \text{ V}^{-1} \text{ s}^{-1}$) with negligible hole mobility of ($\mu_h = 2.1 \times 10^{-6} \text{ cm}^2 \text{ V}^{-1} \text{ s}^{-1}$) and

higher ratio ($\mu_e/\mu_h = 190$). Particularly the lowering of HOMO energy level to - 5.85 eV increased the barrier to hole transport leading to lower hole mobility value for NDI-*r*-OPV/BBO. Despite the lowering of LUMO energy level to - 3.94 eV in NDI-*r*-OPV/BBO, the electron mobility value was comparatively lower (one order) than NDI-*alt*-OPV which is attributed to poor solid state morphology and thin film crystallinity compared to NDI-*alt*-OPV. These results are consistent with the thin film crystallinity and morphology observed by XRD and AFM for NDI-*alt*-OPV. Since NDI-*r*-OPV/BBO showed dominant n-type charge transport, OFET measurement was also done with aluminium as source/drain electrode (Al is better for electron injection). NDI-*r*-OPV/BBO exhibited unipolar electron charge transport with mobility value of $9 \times 10^{-4} \text{ cm}^2 \text{ V}^{-1} \text{ s}^{-1}$.

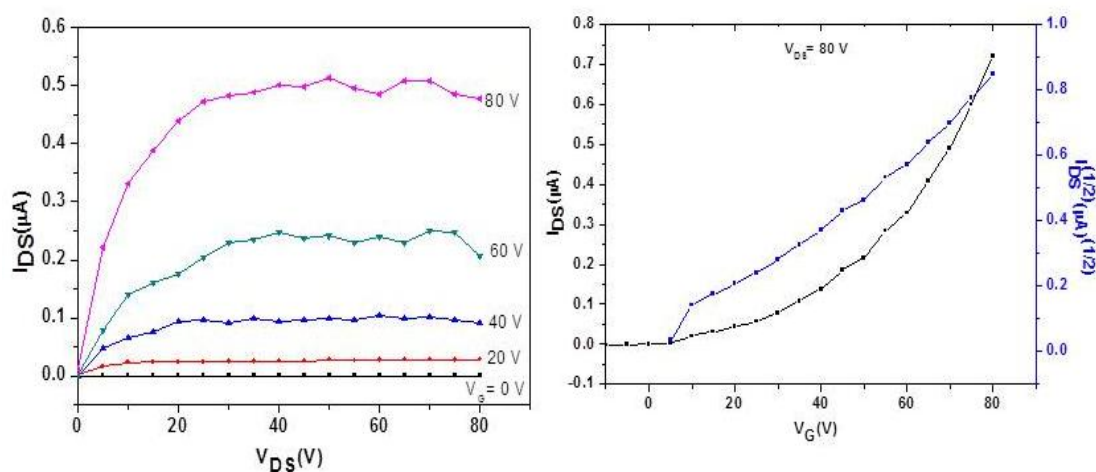


Figure 4.17 Typical output and transconductance curve for NDI-*alt*-BT.

The transition of charge transport from balanced ambipolar in NDI-*alt*-OPV to majority n-type in NDI-*r*-OPV/BBO was entirely attributed to small incorporation of benzobisoxazole comonomer. The HOMO energy level of NDI-*alt*-BT polymer was found to be -6.34 eV. This was the lowest HOMO energy level observed among all other polymers which lead to large barrier for hole transport in NDI-*alt*-BT. Interestingly, NDI-*alt*-BT showed only n-type charge transport (**Figure 4.17**) with electron mobility as high as $1.59 \times 10^{-3} \text{ cm}^2 \text{ V}^{-1} \text{ s}^{-1}$. Despite the high electron deficient nature, the twisted backbone of NDI-*alt*-BT as suggested by DFT and XRD limited the electron mobility in the range of $10^{-3} \text{ cm}^2 \text{ V}^{-1} \text{ s}^{-1}$.

4.3.7 Conclusions

The reports on rylene diimide based polymers for OFET applications are on the rise indicating their tremendous potential applicability. A deeper understanding of structure-property relationship in this class of polymers is an absolute necessity in order to be able to design the “ideal” polymer for device applications. Despite the large amount of literature available on the critical factors like increased π conjugation, conformation of donor comonomer, donor size and electron donating strength of donor etc which have to be taken into consideration while designing the polymer structure, there are still other parameters which makes the end result quite unpredictable. The donor strength is a design factor which can be fine-tuned to attain the ‘required’ energy level and band gap; however the packing and crystallinity are not so predictable features. For instance, although both NDI-*alt*-OPV and NDI-*alt*-BBO met one of the essential criteria i.e extended co planarity; the better crystallinity of the former was unexpected. The strong electron donating tendency of oligo(*p*-phenylenevinylene) compared to benzobisoxazole and benzthiadiazole comonomer had a considerable effect on the electrochemical and semiconducting properties of the corresponding polymers. The increased intramolecular charge transfer for NDI-*alt*-OPV as indicated by the smaller band gap along with fine-tuned energy level (HOMO/LUMO: -3.75 eV/-5.44 eV) resulted in ambipolar charge transport in OFETs with balanced electron and hole mobility up to (μ_e) $3.09 \times 10^{-3} \text{ cm}^2 \text{ V}^{-1} \text{ s}^{-1}$ and (μ_h) $2.1 \times 10^{-3} \text{ cm}^2 \text{ V}^{-1} \text{ s}^{-1}$ respectively. On the other hand, NDI-*r*-OPV/BBO having low-lying HOMO energy level (-5.86 eV) exhibited dominant n-type charge transport with a moderate electron mobility value of $4 \times 10^{-4} \text{ cm}^2 \text{ V}^{-1} \text{ s}^{-1}$ and negligible p-type charge transport. Furthermore, NDI-*alt*-BT having lowest HOMO energy level (-6.34 eV) exhibited only n-type charge transport with electron mobility value of $1.59 \times 10^{-3} \text{ cm}^2 \text{ V}^{-1} \text{ s}^{-1}$. The analysis of the thin film samples of both polymers using XRD and AFM once again highlighted the influence of solid state morphology and molecular packing in dictating the charge carrier mobility in an OFET device. Our results have demonstrated for the first time that a simple design of core substituted NDI-based polymer with OPV co monomer units are successful in producing device materials with ambipolar charge transport and most importantly, having balanced electron and hole mobility.

4.4. References

- (1) (a) Kolhe, N. B.; Asha, S. K.; Senanayak, S. P.; Narayan, K. S. *J. Phys. Chem. B* **2010**, *114*, 16694(b) Wang, Z. Y.; Qi, Y.; Gao, J. P.; Sacripante, G. G.; Sundararajan, P. R.; Duff, J. D. *Macromolecules* **1998**, *31*, 2075.
- (2) (a) Thalacker, C.; Röger, C.; Würthner, F. *J. Org. Chem.* **2006**, *71*, 8098(b) Suseela, Y. V.; Sasikumar, M.; Govindaraju, T. *Tetrahedron Lett.* **2013**, *54*, 6314(c) Bhosale, S. V.; Kalyankar, M. B.; Bhosale, S. V.; Langford, S. J.; Reid, E. F.; Hogan, C. F. *New. J. Chem.* **2009**, *33*, 2409.
- (3) (a) Zhou, W.; Wen, Y.; Ma, L.; Liu, Y.; Zhan, X. *Macromolecules* **2012**, *45*, 4115(b) Zhou, E.; Cong, J.; Zhao, M.; Zhang, L.; Hashimoto, K.; Tajima, K. *Chem. Commun.* **2012**, *48*, 5283.
- (4) (a) Guo, X.; Watson, M. D. *Org. Lett.* **2008**, *10*, 5333(b) Alvey, P. M.; Iverson, B. L. *Org. Lett.* **2012**, *14*, 2706.
- (5) Sakai, N.; Mareda, J.; Vauthey, E.; Matile, S. *Chem. Commun.* **2010**, *46*, 4225.
- (6) (a) Yan, H.; Chen, Z.; Zheng, Y.; Newman, C.; Quinn, J. R.; Dotz, F.; Kastler, M.; Facchetti, A. *Nature* **2009**, *457*, 679(b) Steyrlleuthner, R.; Schubert, M.; Howard, I.; Klaumünzer, B.; Schilling, K.; Chen, Z.; Saalfrank, P.; Laquai, F.; Facchetti, A.; Neher, D. *J. Am. Chem. Soc.* **2012**, *134*, 18303(c) Kang, H.; Kim, K.-H.; Choi, J.; Lee, C.; Kim, B. J. *ACS. Macro. Lett.* **2014**, *3*, 1009.
- (7) Chen, Z.; Zheng, Y.; Yan, H.; Facchetti, A. *J. Am. Chem. Soc.* **2009**, *131*, 8.
- (8) (a) Hwang, Y.-J.; Earmme, T.; Subramaniyan, S.; Jenekhe, S. A. *Chem. Commun.* **2014**, *50*, 10801(b) Earmme, T.; Hwang, Y.-J.; Murari, N. M.; Subramaniyan, S.; Jenekhe, S. A. *J. Am. Chem. Soc.* **2013**, *135*, 14960.
- (9) Shirota, Y.; Kageyama, H. *Chem. Rev.* **2007**, *107*, 953.
- (10) (a) Wen, Y.; Liu, Y. *Adv. Mater.* **2010**, *22*, 1331(b) Zhao, X.; Zhan, X. *Chem. Soc. Rev.* **2011**, *40*, 3728(c) Lee, J.; Han, A. R.; Yu, H.; Shin, T. J.; Yang, C.; Oh, J. H. *J. Am. Chem. Soc.* **2013**, *135*, 9540.
- (11) Zaumseil, J.; Sirringhaus, H. *Chem. Rev.* **2007**, *107*, 1296.
- (12) (a) Bijleveld, J. C.; Zoombelt, A. P.; Mathijssen, S. G. J.; Wienk, M. M.; Turbiez, M.; de Leeuw, D. M.; Janssen, R. A. J. *J. Am. Chem. Soc.* **2009**, *131*, 16616(b) Kim, F. S.; Guo, X.; Watson, M. D.; Jenekhe, S. A. *Adv. Mater.* **2010**, *22*, 478(c) Fan, J.; Yuen, J. D.; Wang, M.; Seifert, J.; Seo, J.-H.; Mohebbi, A. R.; Zakhidov, D.; Heeger, A.; Wudl, F. *Adv. Mater.* **2012**, *24*, 2186.

- (13) (a) Zaumseil, J.; Donley, C. L.; Kim, J. S.; Friend, R. H.; Sirringhaus, H. *Adv. Mater.* **2006**, *18*, 2708(b) Bürgi, L.; Turbiez, M.; Pfeiffer, R.; Bienewald, F.; Kirner, H.-J.; Winnewisser, C. *Adv. Mater.* **2008**, *20*, 2217(c) Gwinner, M. C.; Kabra, D.; Roberts, M.; Brenner, T. J. K.; Wallikewitz, B. H.; McNeill, C. R.; Friend, R. H.; Sirringhaus, H. *Adv. Mater.* **2012**, *24*, 2728.
- (14) Gu, C.; Hu, W.; Yao, J.; Fu, H. *Chem. Mater.* **2013**, *25*, 2178.
- (15) (a) Guo, X.; Kim, F. S.; Seger, M. J.; Jenekhe, S. A.; Watson, M. D. *Chem. Mater.* **2012**, *24*, 1434(b) Wu, P.-T.; Kim, F. S.; Jenekhe, S. A. *Chem. Mater.* **2011**, *23*, 4618.
- (16) Cao, Y.; Lei, T.; Yuan, J.; Wang, J.-Y.; Pei, J. *Polym. Chem.* **2013**, *4*, 5228.
- (17) Lei, T.; Dou, J.-H.; Ma, Z.-J.; Yao, C.-H.; Liu, C.-J.; Wang, J.-Y.; Pei, J. *J. Am. Chem. Soc.* **2012**, *134*, 20025.
- (18) (a) Yuen, J. D.; Fan, J.; Seifert, J.; Lim, B.; Hufschmid, R.; Heeger, A. J.; Wudl, F. *J. Am. Chem. Soc.* **2011**, *133*, 20799(b) Lee, J.; Han, A. R.; Kim, J.; Kim, Y.; Oh, J. H.; Yang, C. *J. Am. Chem. Soc.* **2012**, *134*, 20713(c) Chen, Z.; Lee, M. J.; Shahid Ashraf, R.; Gu, Y.; Albert-Seifried, S.; Meedom Nielsen, M.; Schroeder, B.; Anthopoulos, T. D.; Heeney, M.; McCulloch, I.; Sirringhaus, H. *Adv. Mater.* **2012**, *24*, 647(d) Kanimozhi, C.; Yaacobi-Gross, N.; Chou, K. W.; Amassian, A.; Anthopoulos, T. D.; Patil, S. *J. Am. Chem. Soc.* **2012**, *134*, 16532.
- (19) (a) Zhan, X.; Facchetti, A.; Barlow, S.; Marks, T. J.; Ratner, M. A.; Wasielewski, M. R.; Marder, S. R. *Adv. Mater.* **2011**, *23*, 268(b) Wurthner, F.; Stolte, M. *Chem. Commun.* **2011**, *47*, 5109.
- (20) Jones, B. A.; Facchetti, A.; Wasielewski, M. R.; Marks, T. J. *J. Am. Chem. Soc.* **2007**, *129*, 15259.
- (21) Durban, M. M.; Kazarinoff, P. D.; Luscombe, C. K. *Macromolecules* **2010**, *43*, 6348.
- (22) Hwang, Y.-J.; Ren, G.; Murari, N. M.; Jenekhe, S. A. *Macromolecules* **2012**, *45*, 9056.
- (23) Sajoto, T.; Tiwari, S. P.; Li, H.; Risko, C.; Barlow, S.; Zhang, Q.; Cho, J.-Y.; Brédas, J.-L.; Kippelen, B.; Marder, S. R. *Polymer* **2012**, *53*, 1072.
- (24) Heeger, A. J. *Chem. Soc. Rev.* **2010**, *39*, 2354.
- (25) Burroughes, J. H.; Bradley, D. D. C.; Brown, A. R.; Marks, R. N.; Mackay, K.; Friend, R. H.; Burns, P. L.; Holmes, A. B. *Nature* **1990**, *347*, 539.

- (26) Yu, G.; Gao, J.; Hummelen, J. C.; Wudl, F.; Heeger, A. J. *Science* **1995**, *270*, 1789.
- (27) Alam, M. M.; Jenekhe, S. A. *Chem. Mater.* **2004**, *16*, 4647.
- (28) (a) Neuteboom, E. E.; Meskers, S. C. J.; van Hal, P. A.; van Duren, J. K. J.; Meijer, E. W.; Janssen, R. A. J.; Dupin, H.; Pourtois, G.; Cornil, J.; Lazzaroni, R.; Brédas, J.-L.; Beljonne, D. *J. Am. Chem. Soc.* **2003**, *125*, 8625(b) Liu, Y.; Yang, C.; Li, Y.; Li, Y.; Wang, S.; Zhuang, J.; Liu, H.; Wang, N.; He, X.; Li, Y.; Zhu, D. *Macromolecules* **2005**, *38*, 716(c) Mikroyannidis, J. A.; Stylianakis, M. M.; Sharma, G. D.; Balraju, P.; Roy, M. S. *J. Phys. Chem. C* **2009**, *113*, 7904.
- (29) Grozema, F. C.; van Duijnen, P. T.; Berlin, Y. A.; Ratner, M. A.; Siebbeles, L. D. A. *J. Phys. Chem. B* **2002**, *106*, 7791.
- (30) (a) So, Y.-H. *Prog. Polym. Sci.* **2000**, *25*, 137(b) Kuroki, T.; Tanaka, Y.; Hokudoh, T.; Yabuki, K. *J. Appl. Polym. Sci.* **1997**, *65*, 1031.
- (31) (a) Ahmed, E.; Subramaniyan, S.; Kim, F. S.; Xin, H.; Jenekhe, S. A. *Macromolecules* **2011**, *44*, 7207(b) Intemann, J. J.; Mike, J. F.; Cai, M.; Bose, S.; Xiao, T.; Mauldin, T. C.; Roggers, R. A.; Shinar, J.; Shinar, R.; Jeffries-El, M. *Macromolecules* **2011**, *44*, 248.
- (32) (a) Subramaniyan, S.; Kim, F. S.; Ren, G.; Li, H.; Jenekhe, S. A. *Macromolecules* **2012**, *45*, 9029(b) Jenekhe, S. A.; de Paor, L. R.; Chen, X. L.; Tarkka, R. M. *Chem. Mater.* **1996**, *8*, 2401.
- (33) Alam, M. M.; Jenekhe, S. A. *Chem. Mater.* **2002**, *14*, 4775.
- (34) Mike, J. F.; Makowski, A. J.; Jeffries-El, M. *Org. Lett.* **2008**, *10*, 4915.
- (35) Drury, A.; Maier, S.; Ruther, M.; Blau, W. J. *J. Mater. Chem.* **2003**, *13*, 485.
- (36) Popere, B. C.; Della Pelle, A. M.; Thayumanavan, S. *Macromolecules* **2011**, *44*, 4767.
- (37) Li, Y.; Cao, Y.; Gao, J.; Wang, D.; Yu, G.; Heeger, A. J. *Synth. Met.* **1999**, *99*, 243.
- (38) Alvey, P. M.; Ono, R. J.; Bielawski, C. W.; Iverson, B. L. *Macromolecules* **2013**, *46*, 718.
- (39) Zhao, X.; Ma, L.; Zhang, L.; Wen, Y.; Chen, J.; Shuai, Z.; Liu, Y.; Zhan, X. *Macromolecules* **2013**, *46*, 2152.

Chapter 5

***Side-chain Engineering of Core Substituted
Naphthalenediimide Copolymer: Effect on Semiconducting
Properties***

5.1. Introduction

Solution-processable conjugated polymers (CPs) have been extensively utilized in the optoelectronic devices such as organic field effect transistors (OFETs), organic photovoltaic (OPV) and organic light emitting diode (OLEDs).¹⁻⁴ The solubility in conjugated polymers is often induced by substituting the rigid backbone with flexible side chains. However, the proper selection of side chain is a very important task while designing the structure of conjugated polymer because it has huge impact on the molecular packing, thin film morphology and optical and semiconducting properties of polymer.⁵ Additionally, the flexible side chain influences the crystalline nature and molecular orientation (edge-on or face-on) of the semiconducting backbone on a thin-film.⁶⁻¹⁰ Despite the decisive role of flexible side chain, the research on the side chain engineering of conjugated polymer has lagged behind the development of π -conjugated backbone and very little effort has been given to develop new solubilizing side chains.

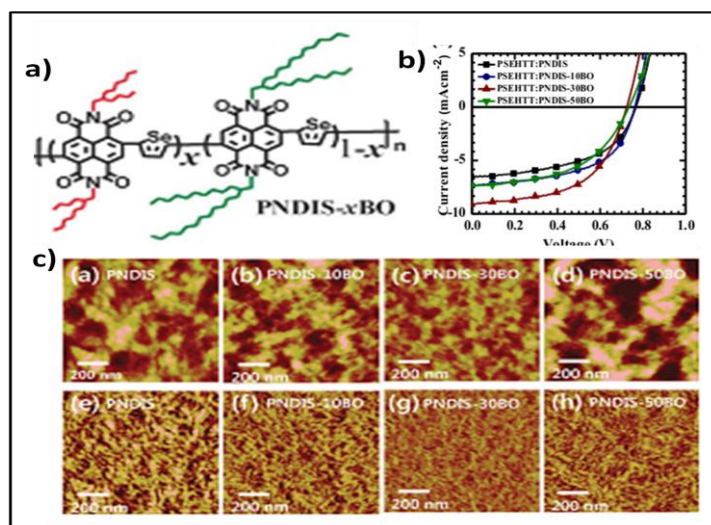


Figure 5.1 a) Molecular structures of the polymers PNDIS- xBO ($x=0, 10, 30, 50$) (b) J-V curves for solar cell (c) AFM images (*Adapted from ref⁸*)

Recent reports independently by Z. Bao and J. Pei give a brief overview of various side chains utilized in the conjugated polymer and their effect on the molecular packing and device performance.¹¹⁻¹² In most of the cases short branched alkyl chains are not sufficient to induce the solubility in polymer but they showed improved crystallinity.⁸ For example, Jenekhe et al. demonstrated the influence of side chain engineering in naphthalenediimide (NDI) copolymer on their crystallinity and device performance (**Figure 5.1**).⁸ They synthesized NDI-selenophene based alternating

copolymer by incorporating a different composition of NDI containing 2-butyloctyl/2-decyltetradecyl side chains. Higher incorporation of the short 2-butyloctyl alkyl substituted NDI (30/70) increased the crystallinity and electron mobility thereby enhancing the photocurrent in solar cell fabricated using them. This result showed that high density of longer alkyl chains is detrimental for the crystallinity and charge transport. Alternatively, a few reports are available on the use of linear hydrophilic oligo(ethyleneoxy) side chains which renders high solubility in polar solvent along with better charge transport properties in OFET device.^{6,9} For instance, Kim et al. reported the NDI based n-channel polymers with oligoethyleneoxy incorporated hybrid linear alkyl side chains which exhibited high electron mobility of $1.64 \text{ cm}^2 \text{ V}^{-1} \text{ s}^{-1}$ for thermally annealed OFET device (**Figure 5.2**).⁹ The high electron mobility was attributed to the improved crystallinity of polymer along with the thermodynamically favored edge-on texture obtained after thermal annealing.

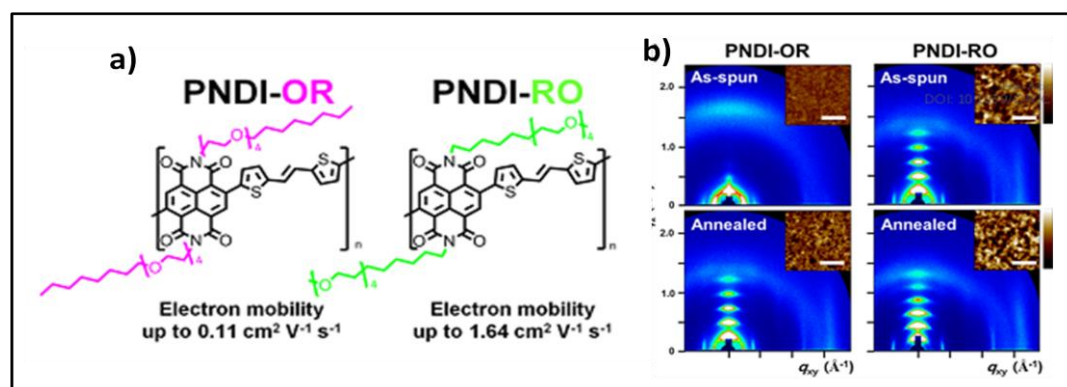


Figure 5.2 a) Molecular structures of the polymers (b) GIXRD patterns of thin film as-spun and after thermal annealing at $250 \text{ }^\circ\text{C}$. (Adapted from ref⁹)

Despite the several positive aspects, there is scarcity of conjugated polymer with oligoethyleneoxy side chain. Presumably these polymers have high affinity towards polar solvent including water and exhibited poor stability and performance in the device.¹¹ The copolymer having oligoethyleneoxy side chain combined with branched alkyl chain showed better performance in device. For example, S. Patil and coworkers reported the diketopyrrolopyrrole-diketopyrrolopyrrole (DPP–DPP) based conjugated copolymer where one DPP had a branched alkyl side chain and other had a triethylene glycol chain (**Figure 5.3**).⁷ This polymer adopted lamellar structure with lamellae parallel to the surface and exhibited unprecedented electron mobility of $\sim 3 \text{ cm}^2 \text{ V}^{-1} \text{ s}^{-1}$ in OFET device.

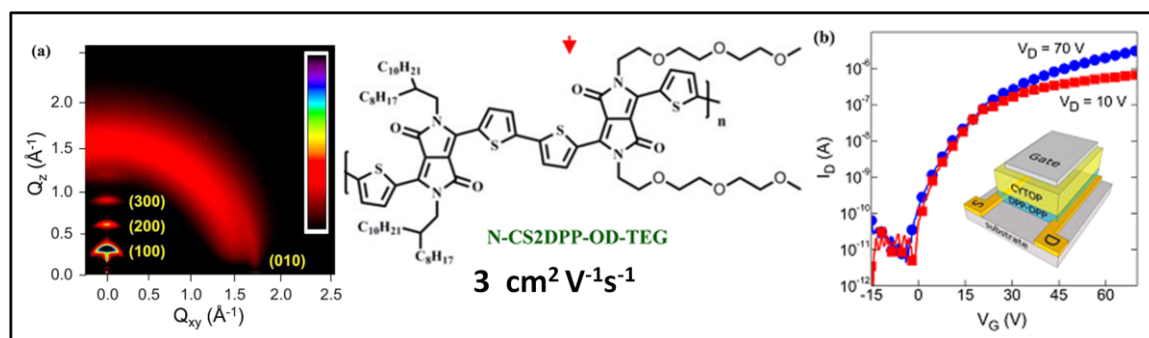


Figure 5.3 Molecular structures, GIXRD patterns of the as-spun thin film and transfer characteristics of DDP-DDP polymers. (Adapted from ref⁶)

Since the charge transfer in OFET occurs exclusively parallel to the substrate surface¹³⁻¹⁵, the edge-on arrangement of molecule proved to be helpful for improved charge transport.^{6-7,9,16-18} In this arrangement molecular planes are oriented perpendicular to the substrate surface whereas π -stacking direction is parallel to the surface; thus charge transport occurs at high rate resulting in good mobility.¹³⁻¹⁴ Aforementioned polymers which were mostly studied in OFETs exhibited high electron mobilities due to their preferred edge-on orientation on thin film.^{6-7,9} However, charge carrier mobilities measured by OFET may be insignificant when considering the bulk carrier transport at low carrier density e.g. organic photovoltaic (OPV) and (OLEDs).¹⁴ The electron or hole only current measurement is mostly utilized to study the perpendicular charge transport at low carrier density and it is more relevant to the bulk process.^{14,19-23} Unlike OFET mobility measurement, the effect of the oligoethyleneoxy side chain on the bulk charge carrier transport in polymer has remained an unexplored area and it is very interesting to study in NDI based polymers.

In this context, we have synthesized naphthalenediimide-oligophenylenevinylene based alternating copolymer (P1) where acceptor NDI unit was substituted with triethylene glycol chain and oligophenylenevinylene (OPV) moiety with 2-octyldodecyl branched chain. The NDI-OPV copolymer with 2-octyldodecyl chain on both the unit was also synthesized (P2) for comparison and their optical, electrochemical and semiconducting properties were studied. Both polymers exhibited identical UV-visible absorption spectra as well as HOMO and LUMO energy levels as observed from cyclic voltammetry. Molecular packing and crystalline nature of polymers were studied by thin film X-ray diffraction analysis

which suggested that thermal annealing had a huge impact on the crystallinity as well as molecular orientation of polymer on thin film. P1 exhibited predominant edge-on orientation on thin film upon thermal annealing which was confirmed by decrease in the SCLC electron mobility by four order ($\sim 10^{-9} \text{cm}^2 \text{V}^{-1} \text{s}^{-1}$) compared to as-spun thin film mobility ($\sim 10^{-5} \text{cm}^2 \text{V}^{-1} \text{s}^{-1}$). On the other hand, alkyl chain containing polymer P2 did not show significant change in the mobility after thermal annealing which confirmed that texture formed during active layer deposition was retained and exhibited majority of face-on arrangement.

5.2. Experimental Section

5.2.1 Materials

1,4,5,8-naphthalenetetracarboxylic dianhydride (NTCDA), 2-octyldodecanol, Triethylene glycol monomethyl ether, Lithium aluminium hydride (LAH), 4-toluenesulfonyl chloride, 1-4-hydroquinone, 4-formyl phenylboronic acid, Tetrakis(triphenyl-phosphine) palladium (0), Aliquat -336, Triethylphosphite, sodium azide, were purchased from Sigma Aldrich and used without further purification.

5.2.2 Instrumentations Details

^1H NMR and ^{13}C NMR spectra were recorded using 200 and 400 MHz Bruker NMR spectrophotometer in CDCl_3 containing small amounts of TMS as internal standard. Mass spectra were recorded on Voyager-De-STR MALDI-TOF (Applied Biosystems, Framingham, MA, USA) equipped with 337-nm pulsed nitrogen laser used for desorption and ionization. $1\mu\text{M}$ solution of sample was premixed with DHB (2,5 dihydroxy benzoic acid) matrix in CHCl_3 and mixed well before spotting on 96-well stainless steel MALDI plate by dried droplet method for MALDI-TOF analysis. The molecular weights of polymers were determined using gel permeation chromatography (GPC), which was performed by Viscotek VE 1122 pump, and Viscotek VE 3210 UV-Vis detector and tetrahydrofuran as solvent using polystyrene standards for the calibration. The flow rate of tetrahydrofuran was maintained as 1 mL/min throughout the experiments, and the polymer solutions at concentrations 2-3 mg/mL were filtered and injected for recording the chromatograms at 30 °C. FT-IR spectra were recorded with ATR mode using Bruker α -T spectrophotometer in the

range of 4000 to 400 cm^{-1} . Absorption spectra were recorded using Perkin Elmer Lambda -35 UV-Vis spectrophotometer. Thermo gravimetric analysis (TGA) was performed using a TGA Q 5000 thermogravimetric analyser. Samples were run from 40 to 900 $^{\circ}\text{C}$ with a heating rate of 10 $^{\circ}\text{C}/\text{min}$ under nitrogen. DSC (differential scanning calorimeter) measurements were performed on TA Q10 differential scanning calorimeter at a heating rate of 10 $^{\circ}\text{C}/\text{min}$ under nitrogen atmosphere. The thin film X-ray diffraction data were recorded using a Rigaku model Dmax-2500 diffractometer using Cu $K\alpha$ (1.54 \AA) emission, and the spectra were recorded in the range of (2θ) 2–50 $^{\circ}$. Electrochemical cyclic voltammetry behavior of NDI polymers were studied by using BAS-Epsilon potentiostat.

Sample preparation: For the UV-vis absorption studies, thin films were prepared by dissolving polymer in *o*-DCB (orthodichlorobenzene) and spin coated (1000 rpm/60sec) on quartz plates. For the XRD analysis, thin films were prepared by drop-casting the polymer solution on glass slide.

5.2.3 Device Fabrication

SCLC electron only devices were fabricated using the following structure: glass/ITO/ZnO/active layer/Al. The ITO coated glass substrates were cleaned using the following sequence in an ultrasonic bath: water, acetone, and 2-propanol. The substrates were then RCA treated. The solution of copolymer in ortho-dichlorobenzene were drop-casted on ZnO modified ITO substrates to get films of thickness 600 nm (P1) and 800 nm (P2). The thickness was determined using JPK AFM (Atomic force microscopy) used in contact mode. Aluminum counter electrode was evaporated through a shadow mask on top of the active layer to a thickness of 100 nm in a thermal evaporation chamber. The active device area was found to be in the range of 0.070 cm^2 . The mobility measurements were carried out by measuring the current– voltage characteristics with a Keithley 2400 source meter.

5.2.4 Synthesis

Synthesis of monomers

2-(2-(2-methoxyethoxy)ethoxy)ethyl- 4-methylbenzene sulfonate (TEG-tosylate): Sodium hydroxide (17.31 g, 432.9 mol) was dissolved in 150 mL of distilled water and added to a round bottom flask containing triethylene glycol monomethyl ether (50

g, 304 mol) in 150 mL tetrahydrofuran (THF) and stirred continuously. 4-toluene sulfonyl chloride (53.29 g, 280.48 mmol) in 150 mL THF was added drop wise to the reaction mixture over one hour at 5 °C. After complete addition, reaction mixture was stirred for additional two hours at 0-5 °C and poured in to ice cold water. The compound was extracted twice with chloroform and the combined organic layer was washed twice with water and brine and dried over sodium sulfate. The evaporation of chloroform gave colorless oil. Yield: 73 g (75 %) ¹H NMR (200 MHz), CDCl₃) δ ppm: 7.79-7.75 (d, 2H, aromatic), 7.34-7.30 (d, 2H, aromatic) 4.13 (t, 2H OCH₂), 3.68-3.50 (m, 10H OCH₂), 3.34 (s, 3H,-OCH₃), 2.42 (s, CH₃).

1-azido-triethylene glycol monomethylether (TEG-azide): In a 250 mL two neck round bottom flask containing TEG-tosylate (5 g, 15.70 mmol), 100 mL dimethylformamide (DMF) was added and the mixture was stirred for 10 minutes. This was followed by addition of sodium azide (10.20 g, 157 mmol) and the reaction mixture was stirred for 24 h at 60 °C. After completion of reaction DMF was removed by vacuum distillation. The crude compound was dissolved in 200 mL DCM and washed twice with brine and water. The organic layer was dried over sodium sulfate and passed through a short plug of silica. The solvent was evaporated by rotary evaporation to isolate product as oil. Yield: 2.2 g (74 %) ¹H NMR (200 MHz), CDCl₃) δ ppm: 3.65-3.59 (m, 8H -OCH₂-CH₂-O), 3.53-3.48 (m, 2H, -O-CH₂-CH₂-N₃), 3.31-3.36 (m, 5H, m, 5H, -O-CH₂-CH₂-N₃ and -OCH₃)

1-amino-triethylene glycol monomethylether (TEG-amine): In a 100 ml two neck round bottom flask, a solution of Lithium aluminium hydride (LAH) (1.27 g, 32.49 mmol) in 20 mL dry tetrahydrofuran (THF) was cooled in ice bath with stirring for 10 minutes. This was followed by drop wise addition of a solution of TEG azide (4.5 g, 16.24 mmol) in 20 mL THF over a period of one hour and stirred at room temperature for additional 6 hour. After completion of reaction, the excess of LAH was quenched by water and passed through plug of celite and washed with excess dichloromethane. The solvent was evaporated by rotary evaporation and the compound was extracted with dichloromethane, dried over sodium sulphate. The removal of DCM gave pure product. Yield: 1.5 g (80 %) ¹H NMR (200 MHz), CDCl₃) δ ppm: 3.61-3.47 (m, 10H OCH₂), 3.34 (t, 3H OCH₃), 2.82 (t, amine-CH₂), 1.45 (broad, NH₂)

N, N'-Bis (2-(2-(2-methoxyethoxy)ethoxy)ethyl)-2,6-dibromo-1,4,5,8-naphthalene diimide (NDI-TEG): The mixture of brominated NTCDA (synthesis is given in chapter 4) i.e NDI-Br₂ (1 g, 2.34 mmole) was suspended in 25 mL of glacial acetic

acid and stirred for a short period of time to get a homogeneous dispersion which was followed by addition of TEG-amine (1.53 g, 9.38 mmol). The reaction mixture was stirred and refluxed (at 120 °C) to complete dissolution for 3h. and cooled to room temperature. The reaction mixture was concentrated under reduced pressure to about 1/10th of original volume and then precipitated in to methanol to yield reddish brown powder that was filtered and dried under vacuum. The crude product was re-crystallized from acetone to get yellow powder of pure compound. Yield: 250 mg (15 %, by considering 2,6 isomer). Melting point (196-198 °C); ¹H NMR (200 MHz, CDCl₃) δ ppm: 8.96 (s, 2H, aromatic), 4.45 (t, 4H), 3.83 (t, 4H), 3.67-3.49 (m, 16H), 3.31 (2, 6H). ¹³C NMR (500 MHz, CDCl₃) δ ppm: 160.82, 160.73, 139.01, 128.32, 127.75, 125.32, 124.09, 71.86, 70.59, 70.49, 70.10, 67.57, 58.98, 40.02. FTIR (ATR, cm⁻¹): 3058, 2900, 1702, 1665, 1557, 1429, 1363, 1313, 1259, 1237, 1200, 1140, 1108, 1078, 1045, 989; MALDI-TOF MS (Calcd m/z 716.04); Found m/z = 738.85 [M+ Na+] 754.81 [M+ K+]. Anal. Calcd. for C₂₈ H₃₂ N₂ O₁₀ Br₂: C, 46.95; H, 4.50; N, 3.91. Found C, 46.50; H, 4.24; N, 3.57.

1, 4-di (2-otylododecyloxy) benzene (a): 1, 4-hydroquinone (2.5 g, 22.70 mmol) and potassium hydroxide (6.36 g, 113.5 mmol) was taken in a two neck round bottom flask and dry DMSO was added to it under nitrogen environment. The mixture was stirred for 30-45 min at room temperature. 2-octylododecyl bromide (20.5 g, 56.75 mmol) was added to the reaction mixture at room temperature and the reaction mixture was stirred for further two days at room temperature. The conversion was monitored by thin-layer chromatography (TLC). The reaction mixture was cooled and poured in crushed ice. The organic layer was extracted with chlorform, washed consecutively with water and brine. The organic layer was dried over Na₂SO₄ and solvent was evaporated by a vacuum rotary evaporator. The crude mixture was purified by silica column having pet ether as a mobile phase. Yield: 7.6 g (50 %). ¹H NMR (200 MHz), CDCl₃; δ: 6.81 (s, 4H), 3.77 (d, 4H), 1.71 (m, 2H), 1.25 (m, 64H), 0.86 (t, 12H).

2,5-bisbromomethyl 1,4-di-(2-otylododecyloxy) benzene (b): 1, 4-di (2-otylododecyloxy) benzene (8.4 g, 12.50 mmol) and p-formaldehyde (2.81 g, 93.75 mmol) was taken in a two neck round bottom flask, into which 175 mL glacial acetic acid was added. Hydrobromic acid (HBr) (3.75 g, 40.87 mmol) was then added to the reaction mixture under nitrogen atmosphere at room temperature. The reaction mixture was heated to 80-90 °C for 24 h, cooled and poured into a beaker containing

crushed ice and filtered to collect the precipitate. The crude compound was purified by column chromatography using pet ether/ethyl acetate solvent system (98:20 v/v). Yield: 6 g (56 %). ^1H NMR (200 MHz), CDCl_3 ; δ : 6.83 (s, 2H), 4.51 (s, 4H), 3.86 (d, 4H), 1.79 (m, 2H), 1.25 (m, 64H), 0.87 (t, 12H).

2,5-di-2-octylododecyloxy-1,4 xylenebis(diphosphonate) (c) : 2,5 bisbromomethyl 1,4 di-(2-octylododecyloxy) benzene (6 g, 7 mmol) and triethylphosphite (20 mL) was taken in a one neck round bottom flask. The reaction mixture was kept at 130-140 $^\circ\text{C}$ under nitrogen atmosphere and stirred for 24 h. The excess triethylphosphite and ethyl bromide was removed by vacuum distillation. A highly viscous liquid was obtained as product. Yield: 6.6 g (97 %). ^1H NMR (200 MHz), CDCl_3 ; δ : 6.90 (s, 2H), 3.99 (m, 8H), 3.79 (d, 4H), 3.26-3.15 (d, 4H), 1.73 (m, 2H), 1.24 (m, 64H), 0.86 (t, 12H).

OPV-diboronic acid pinacolester (OPV): 2,5-di-2-octylododecyloxy-1,4-xylenebis (diphosphonate) (5 g, 5.14 mmol) and 4-formyl phenyl (boronic acid pinacol ester) (2.98 g, 12.86 mmole) were dissolved in 60 mL dry THF under N_2 atmosphere. Potassium tertiary butoxide (2.88 g, 25.73 mmole) and 90 mL dry THF were taken in another 250 mL two neck round bottom flask. The mixture of diphosphonate and boronic ester was then added slowly to the round bottom flask containing potassium tertiary butoxide and THF at 0 $^\circ\text{C}$ and the reaction mixture was stirred for half an hour at the same temperature. Thereafter, the reaction mixture was stirred at room temperature overnight when the turned greenish. The reaction was quenched with 50 mL methanol and evaporation of the organic layer yielded a sticky greenish solid mass, which was added in 500 mL water and extracted with dichloromethane. The organic layer was dried over Na_2SO_4 and solvent was evaporated by a vacuum rotary evaporator. The crude compound was purified by column chromatography over silica gel with Petroleum ether / Ethyl acetate (98.5:2.5 v/v) as eluent. Yield: 2.1 g (35 %). Melting point (92-94 $^\circ\text{C}$); ^1H NMR (200 MHz, CDCl_3) δ ppm: 7.81-7.11 (m, aromatic and vinylic 14H), 3.94 (d, 4H), 1.85 (m, 2H), 1.34 (m, 24 H), 1.23 (m, 64H), 0.97 (m, 12H). ^{13}C NMR (400 MHz, CDCl_3) δ ppm: 14.11, 22.68, 24.87, 27.05, 29.34, 29.36, 29.63, 29.66, 29.69, 30.11, 31.75, 31.90, 38.31, 72.21, 83.71, 110.34, 124.48, 125.74, 126.83, 128.71, 135.13, 140.71, 151.28; FT-IR (ATR, cm^{-1}): 2959, 2925, 2858, 1603, 1494, 1462, 1416, 1396, 1355, 1321, 1261, 1198, 961; MALDI-TOF MS (Calcd m/z 1126.93); Found m/z = 1126.79, 1149.81 [$\text{M}+\text{Na}^+$], 1165.93 [$\text{M}+\text{K}^+$]. Anal. Calcd. for $\text{C}_{74}\text{H}_{120}\text{B}_2\text{O}_6$: C, 78.84; H, 10.73 Found C, 78.22; H, 10.95.

Synthesis of polymer

NDI(TEG)-alt-OPV (P1): NDI-TEG (0.4 g, 0.55 mmole) and OPV-diboronic pinacol ester (0.629 g, 0.55 mmole) were taken in air-free Schlenk tube and dissolved in 15 mL of dry toluene followed by purging with nitrogen for half-hour. Tetrakis (triphenylphosphine) palladium (0) (Pd (PPh₃)₄) (32 mg, 5 mole %) was added to the tube quickly by opening rubber septa and whole mixture was degassed by four freeze-vacuum-thaw cycles. In separate round bottom flask, 2 M aqueous solution of K₂CO₃ (1.7 mL, 3.34 mmol) along with Aliquat-336 (two drops) was purged with nitrogen for 20 minutes and added to the reaction mixture under nitrogen atmosphere. The reaction mixture was stirred at 90-95 °C for 3 days. Phenylboronic acid (31 mg, 0.255 mmole) was added under nitrogen and stirred at same temperature for 3 h followed by addition of bromobenzene (0.1 mL). The black reaction mixture was further stirred at 90-95 °C for 10 h. The polymer solution was precipitated in 300-400 mL methanol, stirred for 2h. and filtered on buchner funnel, washed with plenty of methanol and hexane. The polymer was dried in vacuum oven overnight and subjected to a soxhlet extraction with methanol and acetone. The polymer was obtained as a black solid, Yield: 0.7 g (87 %) ¹H NMR (400 MHz, CDCl₃) δ ppm: 8.70 (br s, 2H), 7.69-7.45 (br, 14H), 4.38 (br, 4H), 4.01 (br, 4H), 3.78 (br, 4H), 3.38 (br, 4H) 3.49-3.68 (br m, 16H), 3.32 (br s, 6H), 1.92 (broad, 4H), 1.22 (m), 0.85 (m). ¹³C NMR (500 MHz, CDCl₃) δ ppm: 162.57, 162.44, 151.33, 147.44, 139.22, 138.22, 135.89, 128.70, 128.21, 127.33, 126.89, 126.48, 125.56, 124.50, 122.72, 71.90, 70.51, 70.03, 67.81, 59.00, 39.51, 39.41, 38.34, 31.90, 31.73, 30.13, 29.71, 29.66, 29.36, 27.03, 14.11. (FTIR (ATR, cm⁻¹): 2918, 2852, 1704, 1667, 1558, 1436, 1377, 1313, 1261, 1203, 1104, 1028, 961; GPC: *M_n*, 12000; *M_w*, 27000 *M_w/M_n*, 2.25.

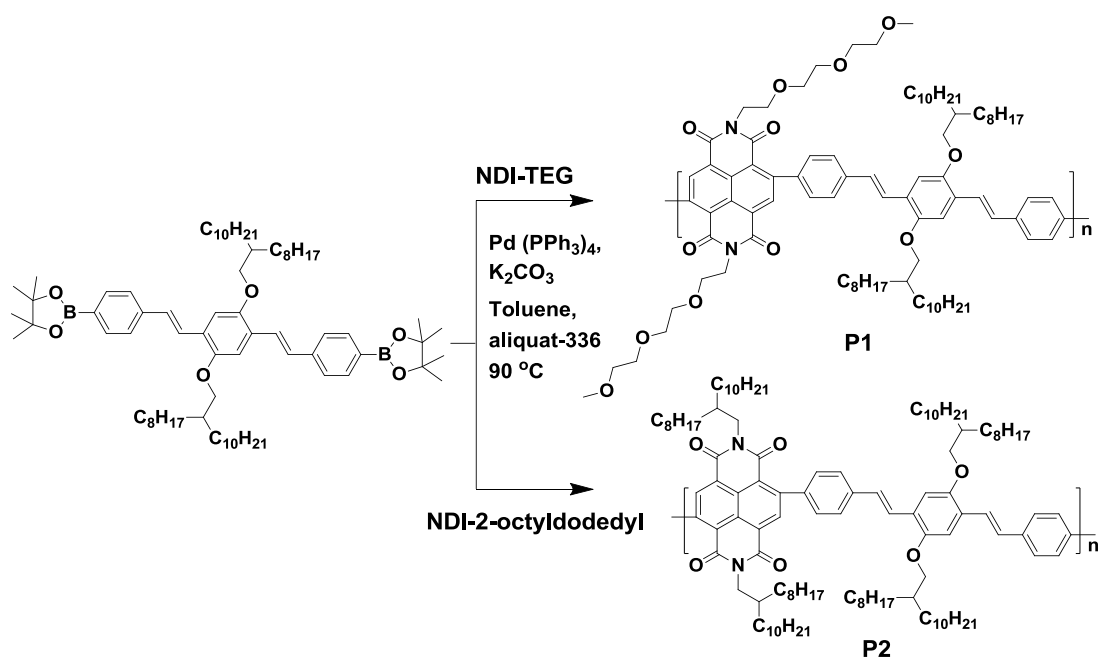
NDI(2-octyldodecyl)-alt-OPV (P2): P2 was synthesized using same procedure as that given for P1, but with NDI-2-O.D-Br₂ (0.5 g 0.51 mmole) and OPV-diboronic pinacol ester (0.571 g, 0.51 mmole) as the starting monomer. P2 was obtained as a black solid, Yield: 700 mg (81%) ¹H NMR (200 MHz, CDCl₃) δ ppm: 8.71 (s, 2H), 7.68-7.18 (br, 14H), 4.01 (br, 4H), 1.95 (broad, 4H), 1.23 (m), 0.85 (m). ¹³C NMR (500 MHz, CDCl₃) δ ppm: 162.90, 162.74, 151.34, 147.36, 139.35, 138.19, 128.78, 128.21, 127.32, 126.90, 126.53, 125.53, 124.49, 122.77, 110.33, 72.06, 44.81, 38.35, 36.43, 31.90, 31.74, 31.52, 30.14, 29.66, 29.36, 27.04, 26.36, 14.11. (FTIR (ATR, cm⁻¹):

2921, 2852, 1705, 1667, 1497, 1459, 1378, 1308, 1260, 1199, 1094, 1026, 963; GPC: M_n , 12500; M_w , 36600 M_w/M_n , 2.92.

5.3 Results and Discussion

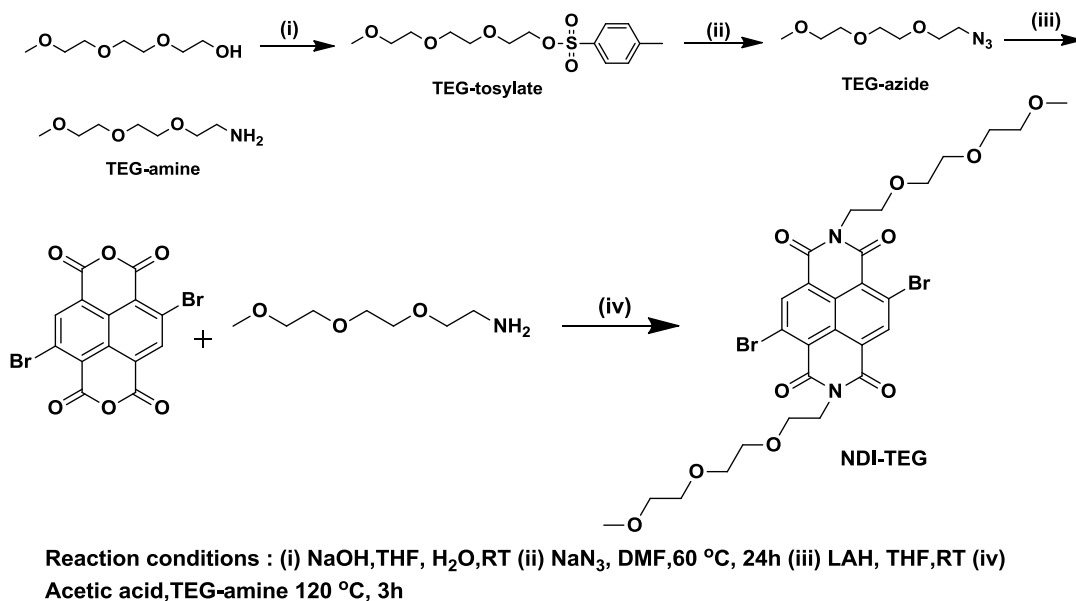
5.3.1 Synthesis and Characterization

Two types of naphthalenediimide (NDI) containing donor-acceptor copolymers (P1 and P2) were synthesized by Suzuki polycondensation and their synthesis is outlined in **Scheme 5.1**. Both the copolymer **P1** and **P2** had almost similar structure with oligo(phenylenevinylene) (OPV) as the identical donor count with NDI.



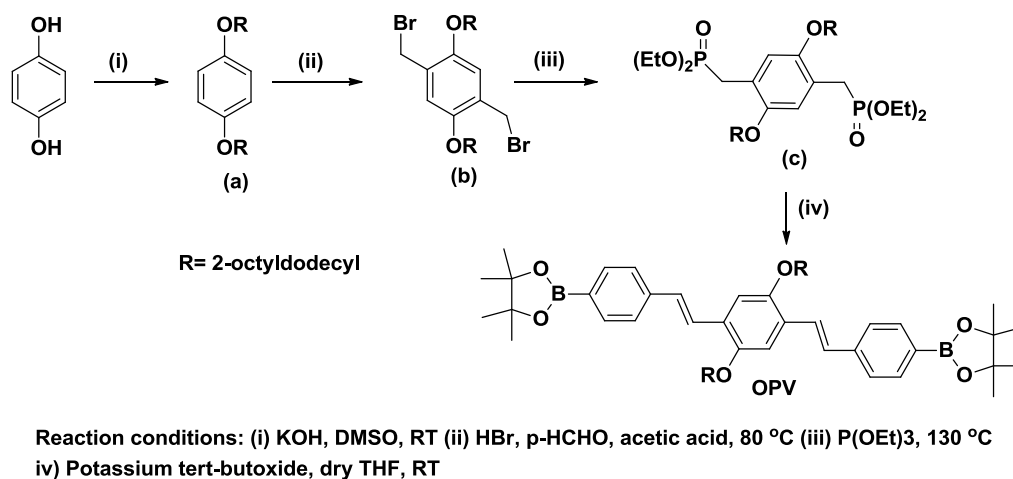
Scheme 5.1 Synthesis of copolymer P1 and P2.

However, they differed from one another by the side chain attachment to the imide nitrogen atom of NDI. Copolymer **P1** (NDITEG-*alt*-OPV) had (2-(2-(2-methoxyethoxy)ethoxy)ethyl) (TEG) side chain whereas, copolymer **P2** (NDI 2-octyldodecyl-*alt*-OPV) had 2-octyldodecyl chain. The synthesis of N,N-bis(2-octyldodecyl)-2,6-dibromonaphthalene-1,4:5,8 tetracarboxylicdiimide (NDI-2-O.D-Br₂) was carried out according to procedure reported in chapter 4. The monomer N, N'-Bis(2-(2-(2-methoxyethoxy) ethoxy) ethyl)-2, 6-dibromo-1, 4, 5, 8 naphthalenediimide (NDI-TEG) was obtained by imidization of 1-amino-triethylene glycol monomethylether (TEG-amine) with NTCDA-Br₂ (reported in chapter 4) in glacial acetic acid at $130\text{ }^\circ\text{C}$ (**Scheme 5.2**).



Scheme 5.2 Synthesis of NDI-TEG monomer.

The synthesis of TEG-amine was carried out in three steps (**Scheme 5.2**); starting from tosylation of hydroxyl group of triethylene glycol monomethyl ether (TEG) followed by converting tosyl group into azide using sodium azide in dimethylformamide (DMF) at 60 °C. Finally, the TEG-azide was reduced to amine in presence of Lithium aluminium hydride (LAH) to obtain TEG-amine.



Scheme 5.3 Synthesis of OPV monomer.

The oligo(phenylenevinylene) monomer (OPV) with boronic acid pinacol ester functionality required for Suzuki polymerization was synthesized from 2,5-di-2-

octyldodecyloxy-1,4 xylenebis(diphosphonate) (c) and 4-formylphenyl boronic acid pinacole ester by Wittig-Horner olefination (**Scheme 5.3**) to get exclusively the trans product. The structure of all monomers and polymers were characterized by ^1H NMR, ^{13}C NMR, FTIR and MADI-TOF spectra.

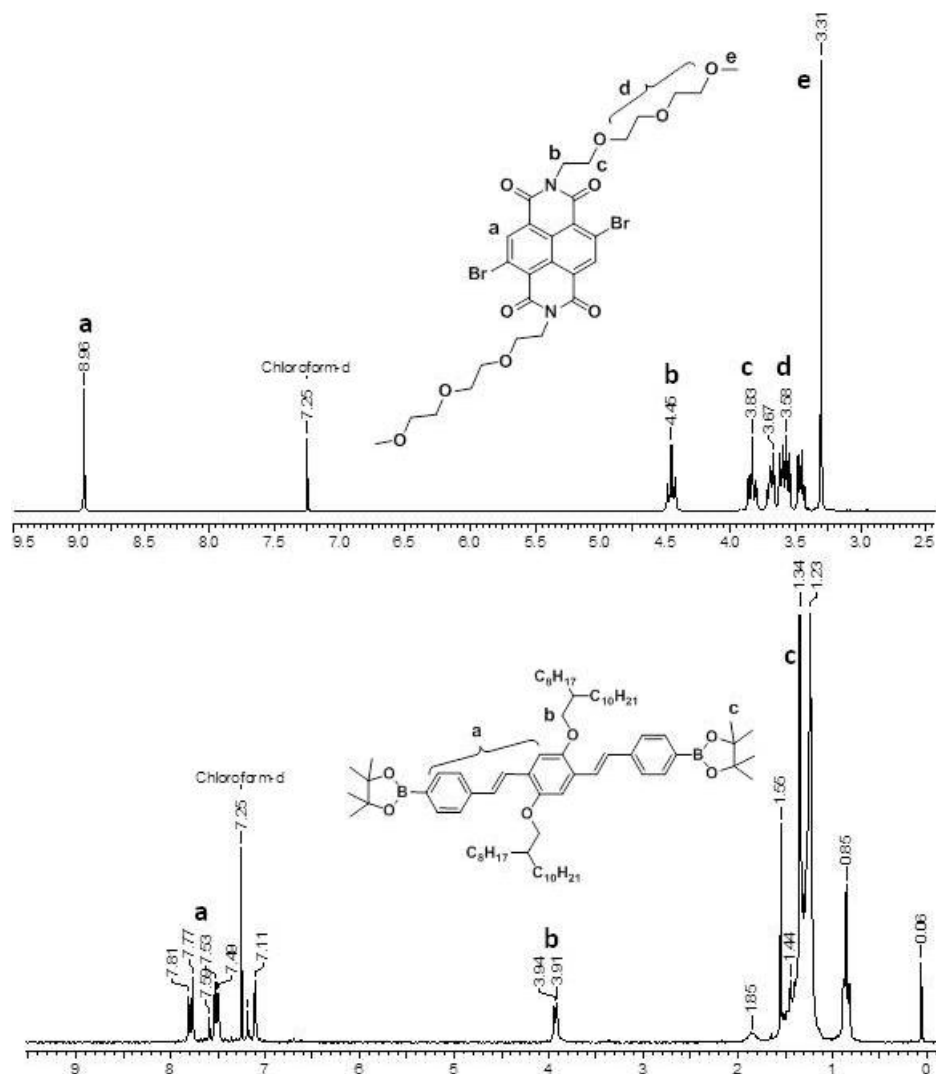


Figure 5.4 ^1H NMR spectra of NDI-TEG and OPV monomers.

The labeled ^1H NMR spectra of monomer (NDI-TEG and OPV) is given in **Figure 5.4**. Both the copolymer P1 and P2 showed noticeable peak broadening in their ^1H NMR spectra (**Figure 5.5**) which confirmed the formation of copolymer. The major difference in the structure of P1 and P2 was evident from their ^1H NMR spectra, which showed additional peaks for P1 in the range of 3.32-4.38 ppm corresponding to TEG side chain along with peaks for the 2-octyldodecyl chain on the OPV ring. Elemental analysis of the monomers was carried out to confirm the purity and the

observed CHN values were matching with the calculated values which are given in section 2.2.4 (experimental procedure).

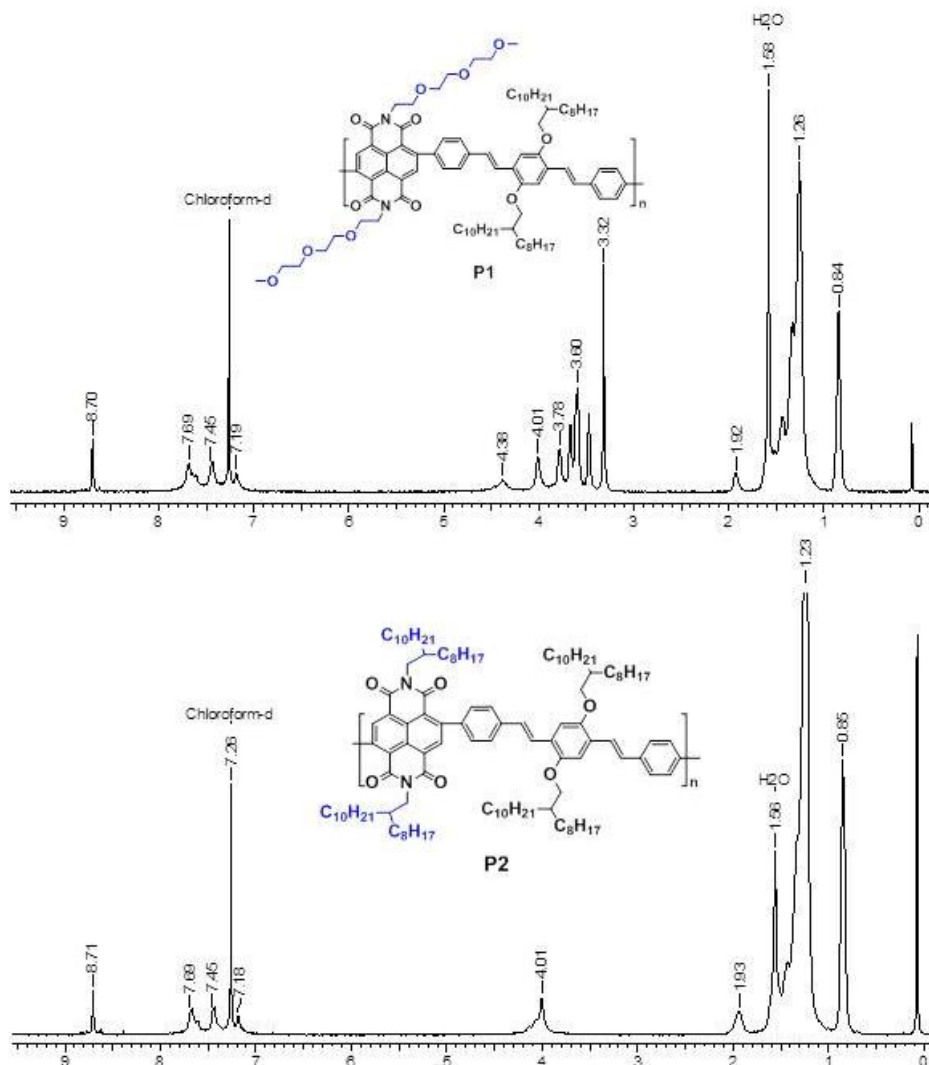


Figure 5.5 ¹H NMR spectra of copolymer P1 and P2.

The samples were subsequently subjected to MALDI-TOF analysis recorded using 2,5-dihydroxybenzoic acid as the matrix and molecular ion peaks were obtained for cationic species such as $[M+1]$, $[M+Na^+]$ and $[M+K^+]$. The MALDI spectra of the monomers are given **Figure 5.6**. Thus, the NMR, MALDI-TOF spectra and elemental analysis of the molecules confirmed the structure and high purity of the monomers. Both the copolymers P1 and P2 exhibited good solubility in common organic solvents such as chloroform, chlorobenzene, tetrahydrofuran and their molecular weights were determined by gel permeation chromatography (GPC), using polystyrene standards for the calibration with tetrahydrofuran as solvent and GPC traces are shown in **Figure 5.7**.

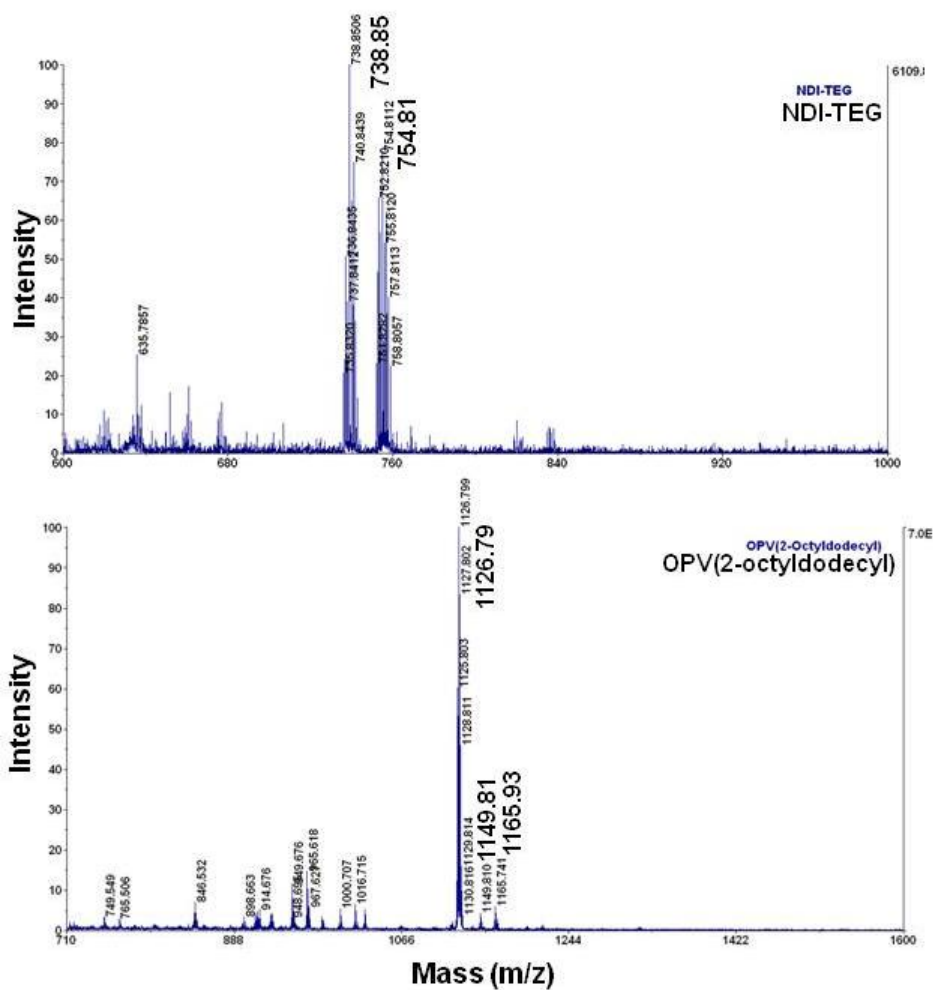


Figure 5.6 MALDI-TOF mass data for NDI-TEG and OPV monomers.

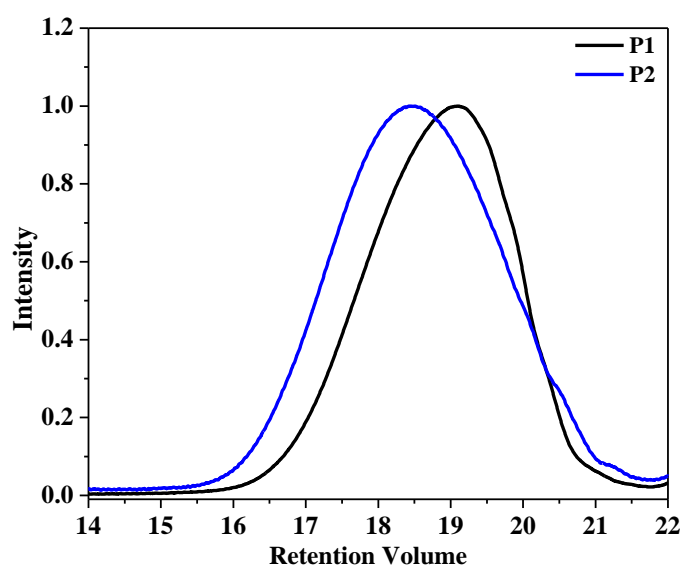


Figure 5.7 GPC traces for copolymers in THF using polystyrene as internal standard.

Almost similar value of number-average molecular weight was observed for P1 ($M_n = 12000$) and P2 ($M_n = 12500$) whereas, weight-average molecular weight for P2 ($M_w =$

36600) was higher than P1 ($M_w = 27000$) with polydispersity index (M_w/M_n) 2.25 and 2.95 respectively. These values are comparable with molecular weights reported for similar class of polymers in the literature.²⁴⁻²⁵

Table 5.1 Physical properties of polymers.

Polymer	M_n (kDa)	M_w (kDa)	PDI	E_g (eV)	E_{HOMO} (eV)	E_{LOMO} (eV)	T_d (°C)
P1	12.0	27.0	2.25	1.63	-5.47	-3.84	363
P2	12.5	36.6	2.92	1.68	-5.41	-3.73	383

Thermal properties of the polymers were determined by thermogravimetric analysis (TGA) as well as DSC measured under nitrogen atmosphere. TGA curves (**Figure 5.8**) showed thermal stability up to 350 °C for both polymers. The 5 % weight loss temperature (T_d) is shown in **Table 5.1**.

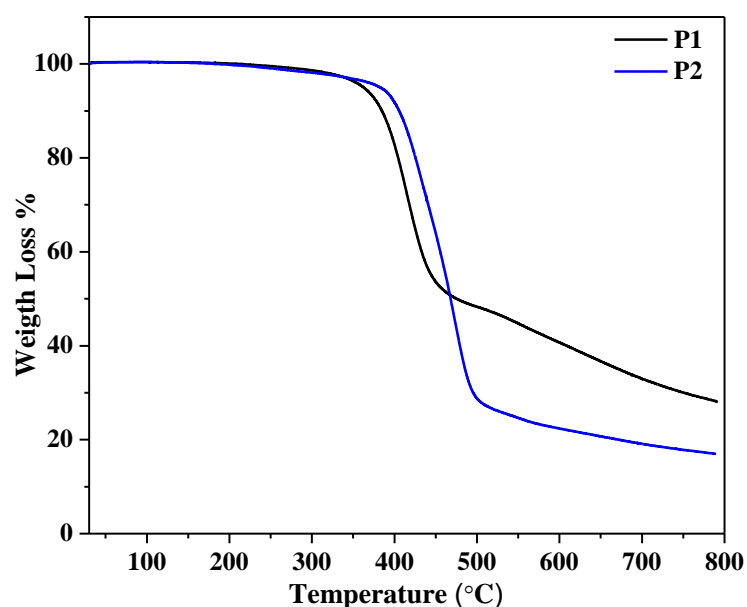


Figure 5.8 TGA curves for polymers.

DSC curves recorded for P1 (**Figure 5.9**) showed three low enthalpy endothermic transitions at $T_{m1} = 92$ °C, $T_{m2} = 130$ °C and $T_{m3} = 328$ °C during the second heating cycle and two exothermic peaks at $T_{c1} = 65$ °C and $T_{c2} = 313$ °C during second cooling cycle which indicated the possibility of presence of mesophase between T_{c1} and T_{c2} . In fact, the NDI-TEG monomer used for synthesis of P1 also exhibited multiple phase transitions in the heating cycle (**Figure 5.10**).

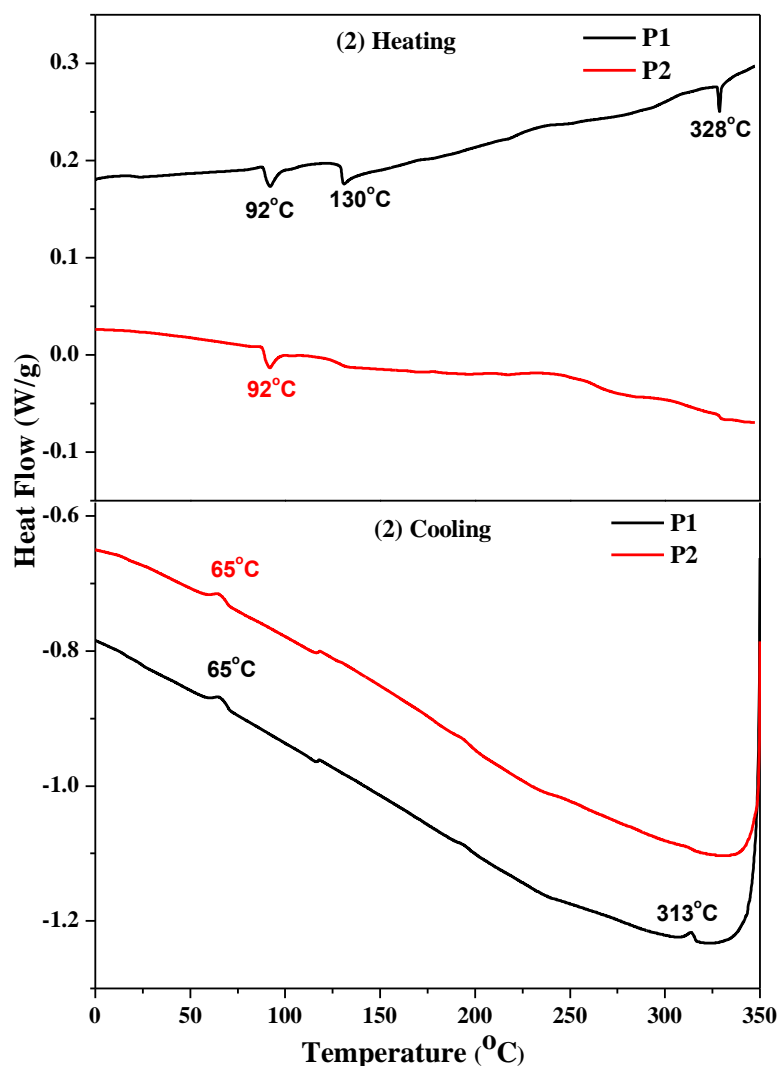


Figure 5.9 DSC curves for polymers during the second heating and cooling cycle.

In the cooling cycle it showed two exothermic transitions; the first at 194 °C for isotropic to LC (liquid crystal) transition which was confirmed by polarized optical microscope (PLM) and a second transition at 20 °C. **Figure 5.10** shows the PLM images for NDI-TEG taken during cooling from isotropic phase at a) 194 °C and at b) room temperature (25 °C). Although multiple transitions were observed both in the heating and cooling cycle for the polymer P1, prolonged heating up to 350 °C did not exhibit any mesophase under PLM. Nevertheless, the peaks in DSC during heating cycle suggested the crystalline nature of P1. On the other hand, P2 showed a single endothermic peak at 92 °C during heating and exothermic peak at 65 °C during cooling cycle.

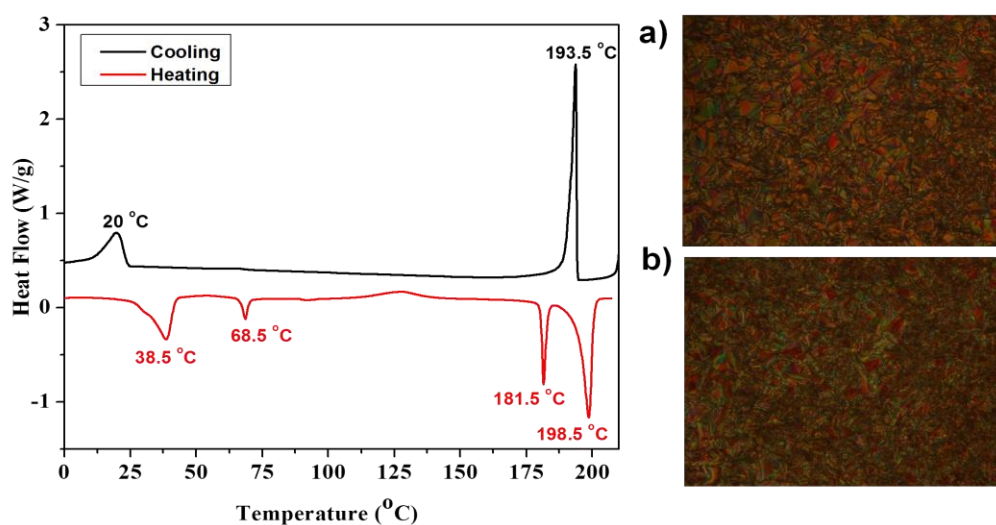


Figure 5.10 DSC curves for NDITEG during second heating and cooling cycle and polarized optical microscope images taken at a) 194 °C and b) RT (25 °C).

5.3.2 Optical and Electrochemical Properties

UV-Vis absorption spectra of polymers were recorded in both dilute chloroform solution as well as in thin-film spin coated from ODCB solution and are shown in **Figure 5.11**. Both the polymer P1 and P2 exhibited identical absorption spectra in solution and in thin film which contained two major absorption bands; the first high energy absorption band at $\sim 360\text{-}450$ nm was accounted for by $\pi\text{-}\pi^*$ transition and another low energy band at $\sim 480\text{-}750$ nm was assigned to intramolecular charge transfer (ICT) from OPV unit to NDI.²⁵⁻²⁶ Furthermore, broadening of the absorption band at ~ 410 nm occurred due to $\pi\text{-}\pi^*$ transition of the OPV conjugated backbone²⁷ which overlapped with the NDI absorption. Thin film of polymers showed red shifted absorption spectra compared to solution, which suggested the interchain aggregation and chain planarization in the solid state.²⁸ Particularly, the large red shifting for ICT absorption band (~ 40 nm) observed from solution to thin-film clearly indicated more ordered nature of thin film²⁸ of polymer, which was further substantiated by XRD. Electrochemical redox behavior and electronic energy levels of polymer were analyzed by cyclic voltammetry. Thin films of polymer were deposited on the platinum working electrode and their redox potential was measured against Ag/AgNO₃ reference electrode. The measurement was carried out in acetonitrile

solvent with ferrocene as an internal standard and tetrabutylammonium hexafluorophosphate ($n\text{-Bu}_4\text{NPF}_6$ 0.1M/ acetonitrile) as supporting electrolyte.

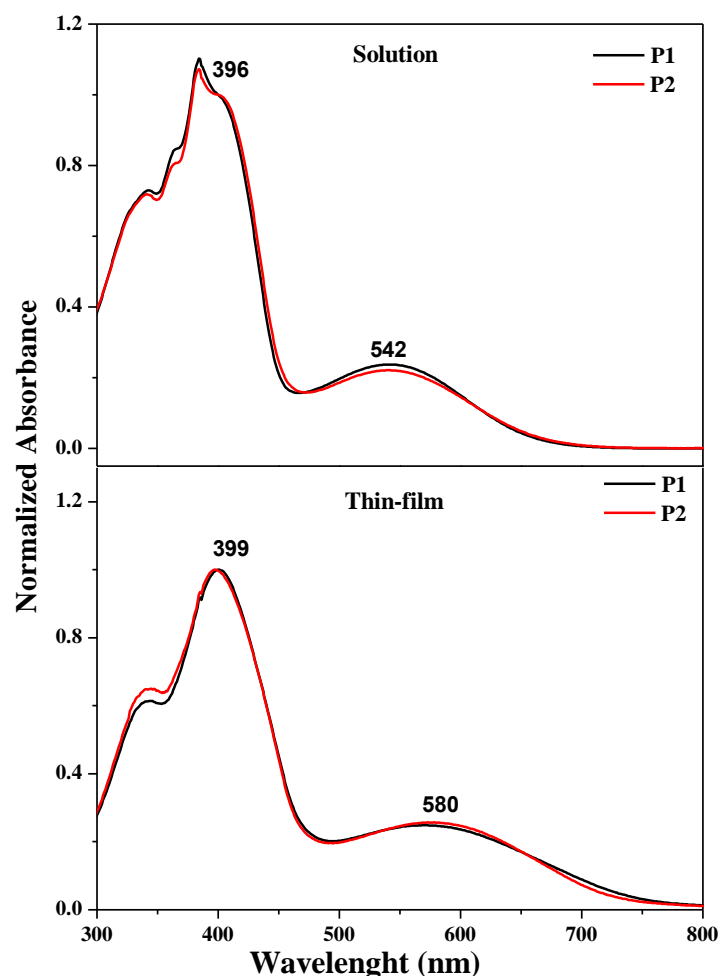


Figure 5.11 UV-Vis absorption spectra of dilute ($\sim 1 \times 10^{-5}$ M) solutions of NDI polymers in chloroform (top) and thin film (bottom).

Cyclic voltammogram for P1 and P2 are shown in **Figure 5.12** and the HOMO and LUMO energy levels are given in **Table 5.1**. Thin film of P1 exhibited perfect reversible reduction peaks with higher peak current compared to P2. However, almost similar values of electrochemical reduction were observed for both P1 and P2. The two reversible reduction peaks were attributed to the formation of radical anion and dianions of NDI in polymer.²⁵⁻²⁶ The lowest occupied molecular orbital (LUMO) energy levels were estimated based on the onset value of first reduction peak and reference energy level of ferrocene (4.8 eV below the vacuum level) according to $E_{\text{LUMO}} (\text{eV}) = -e \times (E^{\text{red}} \text{onset} + 4.8)$ below the vacuum level.²⁹ The highest occupied molecular orbital (HOMO) levels were calculated based on the optical band gap

obtained from the solid state absorption onset measurements. The LUMO and HOMO energy levels of P1 (-3.84 eV and -5.47 eV respectively) was found to be almost similar with P2 (-3.73 eV and -5.41 eV respectively) which suggested negligible effect of the side chain variation on the energy levels.

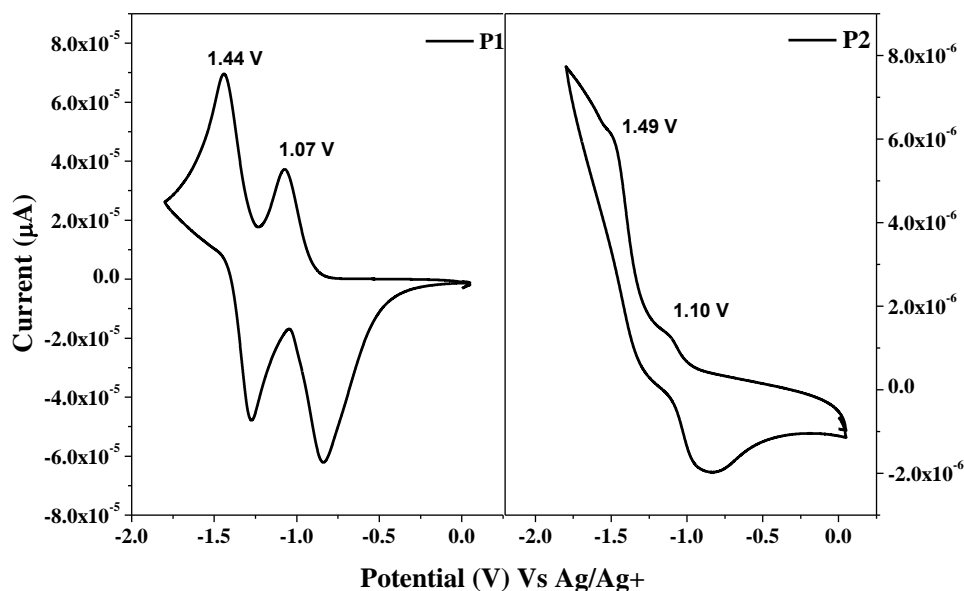


Figure 5.12 Cyclic voltammograms of P1 and P1 in acetonitrile at a scan rate 100 mV/s with Pt as the working and counter electrodes and the Ag/AgNO₃ electrode as the reference electrode and *n*-Bu₄NPF₆ (0.1 M) as the supporting electrolyte.

5.3.3 Thin-Film Morphology

The molecular packing and crystalline nature of polymers were analyzed using X-ray diffraction (XRD) measurement. **Figure 5.13** shows the X-ray diffraction pattern of as-spun and thermally annealed (at 180 °C) polymer thin-films on glass substrate and relevant data are given in **Table 5.2**. XRD pattern of as-spun thin films of P1 and P2 showed single broad peak at $2\theta = \sim 4.44^\circ$ (100) and 3.86° (100) respectively which corresponded to the interchain *d*-spacing.^{26,30} After thermal treatment of the thin films at 180 °C, the (*d*₁₀₀) peak of both the polymer P1 and P2 became more sharper and intense along with appearance of a new second order peak (*d*₂₀₀) which indicated the improved crystallinity and high structural lamellar ordering of the polymer.¹⁷ Annealed films of P1 showed *d*₁₀₀ peak at ($2\theta = \sim 4.45^\circ$) corresponding to the *d*-spacing of 19.84 Å which was found to be lower than as-spun *d*-spacing of 22.84 Å as observed for P2 ($2\theta = \sim 3.86^\circ$); this was accounted for by the difference in the chain length of TEG and 2-octyldodecyl respectively. Furthermore, P2 exhibited

relatively more intense second order peak d_{200} compared to P1 which suggested the different molecular orientation of P1 and P2 on thin film as discussed later on under device (SCLC mobility) section.^{7,20}

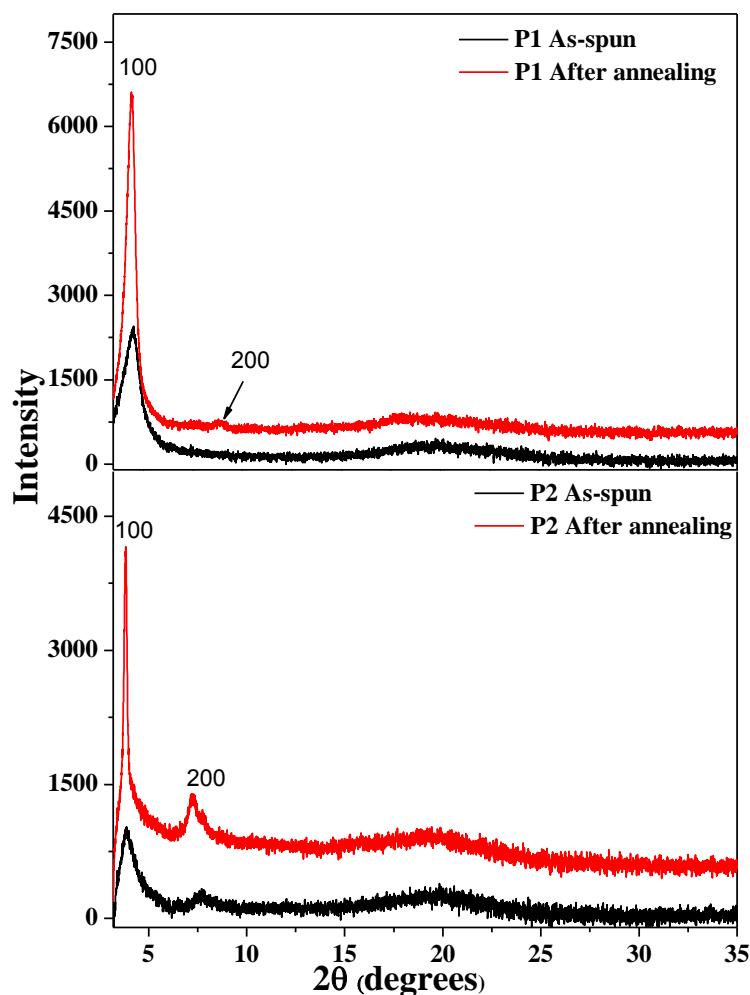


Figure 5.13 XRD patterns of polymer P1 (top) and P2 (bottom) for as-spun and after thermal annealing of thin film.

The effect of thermal annealing on the mean size of the crystalline domain (L) of the polymer was estimated from lamellar peak using the Scherrer formulae,⁸ $L = K\lambda / \beta \cos \theta$, where λ is the X-ray wavelength (1.54 \AA), β is the full width at half maxima in radian and K is the shape factor (0.9) and the values of (L) are given in **Table 5.2**. The crystalline domain size (L) increased from $\sim 8.2 \text{ nm}$ to $\sim 16 \text{ nm}$ for P1 and $\sim 10 \text{ nm}$ to $\sim 39 \text{ nm}$ for P2 after thermal annealing, which suggested the improved crystalline ordering with larger grain size.

Table 5.2 X-ray Diffraction data and the mean crystalline domain size (L) of Polymers.

Polymer	2 θ		<i>d</i> -spacing (Å)		(L) nm	
	100	200	<i>d</i> ₁₀₀	<i>d</i> ₂₀₀	Before annealing	After annealing
P1	4.45	8.85	19.84	9.98	8.2	16
P2	3.86	7.65	22.84	12.14	10	39.8

5.3.4 Device Characteristics (SCLC and solar cell)

The charge carrier transport characteristics of the polymers were analyzed by the space-charge limited current (SCLC) measurement which allowed determination of the microscopic bulk mobility of polymer in thin film.¹⁴ The electron-only device was fabricated by using ITO/ZnO/active layer/Al structure and the detailed fabrication procedure was given in the experimental section. The charge carrier mobilities were estimated by the current–voltage (*I*-*V*) measurement under inert atmosphere. The *J*-*V* curves showed two regimes: (i) low voltage ohmic region where the current is limited by traps (injection limited) (ii) high voltage trap-free SCLC region where charge transport is bulk limited. The electron mobilities were calculated from SCLC fittings to the *J*-*V* curve according to the Mott-Gurney equation¹⁴

$$J = (9/8) \epsilon \epsilon_0 \mu V^2/d^3$$

where *J* is the current density in SCLC region, *V* is the applied voltage, ϵ and ϵ_0 are the relative dielectric constant of the organic layer and permittivity of the free space respectively, μ is the charge carrier mobility, and *d* is the thickness of the film. **Figure 5.14** shows the *J*(*V*) responses corresponding to the P1 and P2 for as-spun and thermally annealed (at 180 °C) thin film device and the obtained values of electron mobilities are given in **Table 5.3**. Both the polymers P1 and P2 exhibited electron mobilities in the range of $\sim 10^{-5} \text{ cm}^2 \text{ V}^{-1} \text{ s}^{-1}$ for as-spun films. Interestingly, the thermal annealing at 180°C showed large decrease in the electron mobility for P1 ($\sim 10^{-9} \text{ cm}^2 \text{ V}^{-1} \text{ s}^{-1}$) whereas the polymer P2 showed only one order lower electron mobility ($0.84 \times 10^{-6} \text{ cm}^2 \text{ V}^{-1} \text{ s}^{-1}$) compared to as-spun film. This observation was consistent with the thin film XRD results where P1 showed very weak second order peak (*d*₂₀₀) after thermal annealing compared to P2. Noticeably, both the polymers did not have *d*₂₀₀

peak for as-spun films which, suggested the different molecular orientation of P1 and P2 on thin film after thermal annealing.

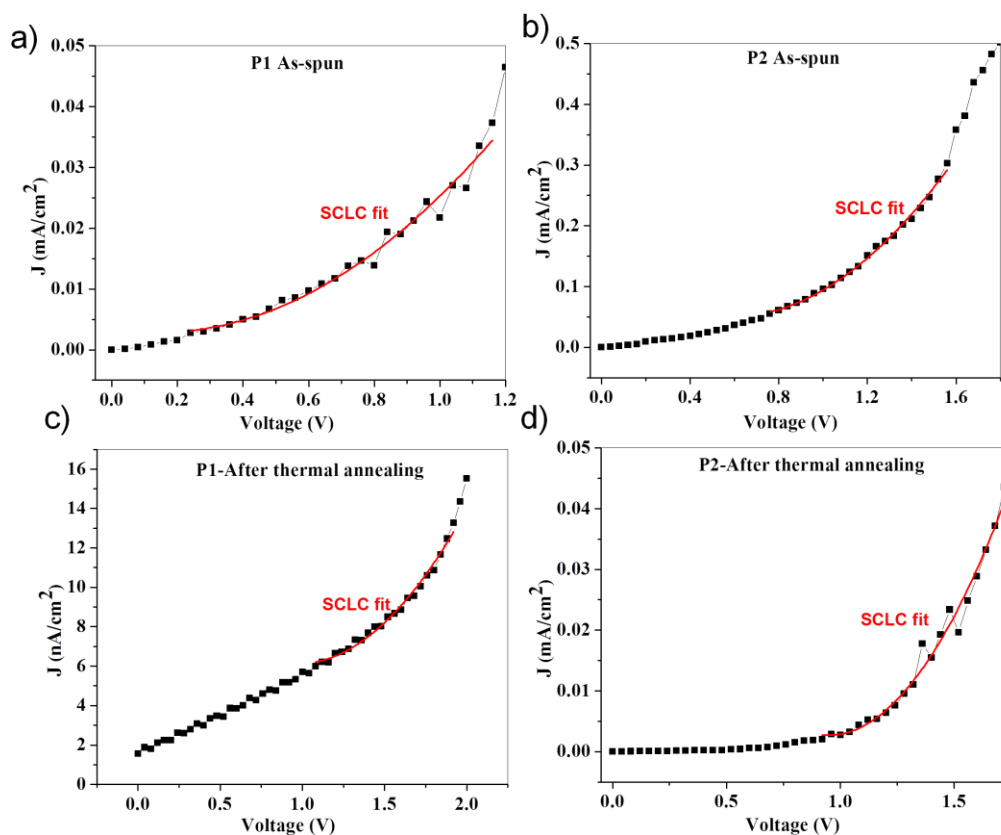


Figure 5.14 Current (J) - Voltage (V) characteristics as-spun thin film of polymer a) P1 and b) P2 and after thermal annealing at 180 °C c) P1 and d) P2 with red line indicating SCLC fit. (Device area of $\sim 0.70 \text{ cm}^2$ and thickness of 800 nm and 600 nm for P1 and P2 respectively)

A higher value of OFET electron mobility ($\sim 10^{-3} \text{ cm}^2 \text{ V}^{-1} \text{ s}^{-1}$) was observed for structurally similar polymer NDI-*alt*-OPV with 2-octyldodecyl side chain as reported in the previous chapter 4.²⁶ The lower SCLC bulk electron mobility observed for the polymers P1 and P2 is not surprising as similar observation was reported by A. Facchetti *et al.* in the case of NDI-bithiophene polymer where they found a low SCLC electron mobility ($\sim 10^{-3} \text{ cm}^2 \text{ V}^{-1} \text{ s}^{-1}$) compared to OFET ($\sim 0.85 \text{ cm}^2 \text{ V}^{-1} \text{ s}^{-1}$) mobility.¹⁴ We believe that the present polymers P1 and P2 would also exhibit high value of OFET mobility compared to SCLC. As explained earlier in the introduction section charge carrier mobility measured by OFET may not give the correct representation of mobility in bulk sample. On the other hand, mobility measured by SCLC method is more relevant to the bulk process e.g. OPV and OLED devices.¹⁴ Usually, in SCLC

measurement the charge transport occurs in perpendicular direction through the bulk of material at low carrier concentration. The SCLC electron mobility and thin film XRD inferred that both the polymer exhibited mixed face-on and edge-on texture. However, P1 showed thermodynamically favored predominant edge-on orientation on thin film after thermal annealing which did not support the perpendicular charge transport in SCLC device and eventually exhibited lower electron mobility ($\sim 10^{-9} \text{ cm}^2 \text{ V}^{-1} \text{ s}^{-1}$). On the other hand, predominant face-on texture was retained in P2 even after thermal annealing as a result of which it exhibited less decrease in the electron mobility ($0.84 \times 10^{-6} \text{ cm}^2 \text{ V}^{-1} \text{ s}^{-1}$). The possible molecular orientation of P1 on the thin film substrate after thermal annealing is shown by cartoon in **Figure 5.15**.

Table 5.3 SCLC mobility and photovoltaic properties of the polymers.

Polymer	$(\mu_e)^a$ cm^2/Vs	$(\mu_e)^b$ cm^2/Vs	J_{sc} (mA/cm^2)	V_{oc} (V)	FF	PCE_{avg} (%)
P1	2.9×10^{-5}	4.1×10^{-9}	0.23	0.81	26.13	0.050
P2	2.1×10^{-5}	8.4×10^{-7}	0.53	0.47	26.63	0.067

a) SCLC mobility measured for as-pun device b) SCLC mobility measured for thermally annealed devices (at 180 °C). Solar cell parameters are reported for thermally annealed device.

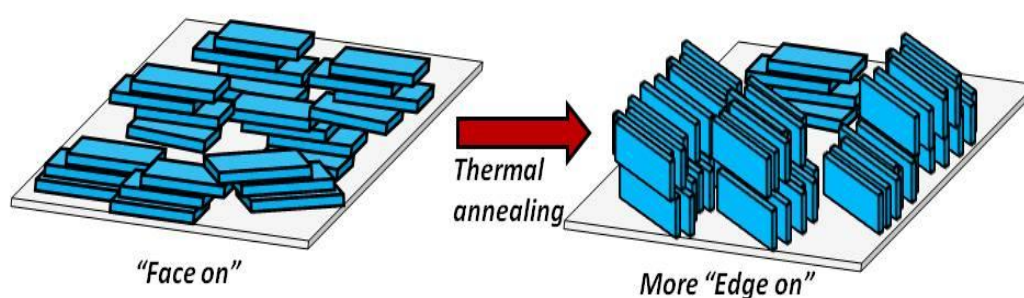


Figure 5.15 Molecular orientation of P1 on the thin-film substrate after thermal annealing.

As an additional experiment, all polymer bulk-hetero junction solar cells were fabricated using P1 and P2 as acceptor to validate the results obtained in SCLC measurement. The solar cells were fabricated using inverted device structure: ITO/ZnO/active layer/MoO₃/Ag, where active layer of PBDTTT-CT: P1 or PBDTTT-

CT: P2 blend with composition of 1:1.5 wt/wt was spin coated from dichlorobenzene. Both the polymer exhibited poor performances in solar cell. Thermally annealed solar cell devices of P1 exhibited relatively low current density and PCE ($J_{sc} = 0.23 \text{ mA cm}^{-2}$ and PCE = 0.050 %) as compared to P2 ($J_{sc} = 0.53 \text{ mA cm}^{-2}$ and PCE = 0.067 %) which was attributed to the lower SCLC electron mobility of P1.

5.3.5 Conclusions

In summary, the different flexible side chains in conjugated polymers are known to have a huge impact on their molecular packing, crystallinity and thin film orientation. Particularly, the linear hydrophilic oligoethyleneoxy side chain on the polymer backbone exhibited high charge carrier mobility due to their highly crystalline nature and preferred edge-on molecular orientation which supports the parallel charge transport in the OFETs. Here, we have demonstrated the effect of oligoethyleneoxy side chain of polymer on their bulk charge carrier transport. Two naphthalene diimide-oligo(phenylenevinylene) copolymers were synthesized by varying the two different side chains on the NDI acceptor unit. X-ray diffraction pattern of thermally annealed thin film of polymer P1 containing hydrophilic linear oligoethyleneoxy side chain showed different molecular orientation compared to polymer P2 with 2-octyldodecyl side chain. Moreover, the SCLC measurement of thermally annealed thin film of P1 showed four order of decrease in the bulk electron mobility ($\sim 10^{-9} \text{ cm}^2 \text{ V}^{-1} \text{ s}^{-1}$) as compared to mobility of as-spun thin film ($\sim 10^{-5} \text{ cm}^2 \text{ V}^{-1} \text{ s}^{-1}$) which gave clear evidence for predominant edge-on orientation of P1 on thermally annealed thin film. On the other hand, polymer P2 with 2-octyldodecyl side chain did not show significant lowering of electron mobility after thermal annealing which suggested that as-spun texture formed during active layer deposition was retained with majority of face-on arrangement. The difference in the charge transport properties of polymer was also reflected in the all-polymer solar cells fabricated using P1 or P2 as acceptor material. P1 showed low value of current density and PCE ($J_{sc} = 0.23 \text{ mA cm}^{-2}$ and PCE = 0.050 %) compared to P2 ($J_{sc} = 0.53 \text{ mA cm}^{-2}$ and PCE = 0.067 %). Although oligoethyleneoxy side chain showed negative impact on bulk carrier transport, the structure-property understanding obtained from the present study is expected to help establish material design guidelines required in this class of polymers.

5.4. References

- (1) Günes, S.; Neugebauer, H.; Sariciftci, N. S. *Chem. Rev.* **2007**, *107*, 1324.
- (2) Arias, A. C.; MacKenzie, J. D.; McCulloch, I.; Rivnay, J.; Salleo, A. *Chem. Rev.* **2010**, *110*, 3.
- (3) Facchetti, A. *Chem. Mater.* **2011**, *23*, 733.
- (4) Guo, X.; Facchetti, A.; Marks, T. J. *Chem. Rev.* **2014**, *114*, 8943.
- (5) Huang, Y.; Kramer, E. J.; Heeger, A. J.; Bazan, G. C. *Chem. Rev.* **2014**, *114*, 7006.
- (6) Kanimozhi, C.; Yaacobi-Gross, N.; Chou, K. W.; Amassian, A.; Anthopoulos, T. D.; Patil, S. *J. Am. Chem. Soc.* **2012**, *134*, 16532.
- (7) Kanimozhi, C.; Yaacobi-Gross, N.; Burnett, E. K.; Briseno, A. L.; Anthopoulos, T. D.; Salzner, U.; Patil, S. *Phys. Chem. Chem. Phys.* **2014**, *16*, 17253.
- (8) Hwang, Y.-J.; Earmme, T.; Subramaniyan, S.; Jenekhe, S. A. *Chem. Commun.* **2014**, *50*, 10801.
- (9) Kim, R.; Kang, B.; Sin, D. H.; Choi, H. H.; Kwon, S.-K.; Kim, Y.-H.; Cho, K. *Chem. Commun.* **2015**, *51*, 1524.
- (10) Lee, J.; Han, A. R.; Yu, H.; Shin, T. J.; Yang, C.; Oh, J. H. *J. Am. Chem. Soc.* **2013**, *135*, 9540.
- (11) Mei, J.; Bao, Z. *Chem. Mater.* **2014**, *26*, 604.
- (12) Lei, T.; Wang, J.-Y.; Pei, J. *Chem. Mater.* **2014**, *26*, 594.
- (13) Sun, Y.; Liu, Y.; Zhu, D. *J. Mater. Chem.* **2005**, *15*, 53.
- (14) Steyrleuthner, R.; Schubert, M.; Jaiser, F.; Blakesley, J. C.; Chen, Z.; Facchetti, A.; Neher, D. *Adv. Mater.* **2010**, *22*, 2799.
- (15) Dimitrakopoulos, C. D.; Malenfant, P. R. L. *Adv. Mater.* **2002**, *14*, 99.
- (16) Sirringhaus, H.; Brown, P. J.; Friend, R. H.; Nielsen, M. M.; Bechgaard, K.; Langeveld-Voss, B. M. W.; Spiering, A. J. H.; Janssen, R. A. J.; Meijer, E. W.; Herwig, P.; de Leeuw, D. M. *Nature* **1999**, *401*, 685.
- (17) Chen, C.-M.; Sharma, S.; Li, Y.-L.; Lee, J.-J.; Chen, S.-A. *J. Mater. Chem. C* **2015**, *3*, 33.
- (18) Zhang, X.; Richter, L. J.; DeLongchamp, D. M.; Kline, R. J.; Hammond, M. R.; McCulloch, I.; Heeney, M.; Ashraf, R. S.; Smith, J. N.; Anthopoulos, T. D.; Schroeder, B.; Geerts, Y. H.; Fischer, D. A.; Toney, M. F. *J. Am. Chem. Soc.* **2011**, *133*, 15073.

- (19) Zhou, N.; Lin, H.; Lou, S. J.; Yu, X.; Guo, P.; Manley, E. F.; Loser, S.; Hartnett, P.; Huang, H.; Wasielewski, M. R.; Chen, L. X.; Chang, R. P. H.; Facchetti, A.; Marks, T. J. *Adv. Ener. Mater.* **2014**, *4*, n/a.
- (20) Ma, J.; Hashimoto, K.; Koganezawa, T.; Tajima, K. *Chem. Commun.* **2014**, *50*, 3627.
- (21) Prajitha, K. P.; Chithiravel, S.; Krishnamoorthy, K.; Asha, S. K. *J. Mater. Chem. C* **2014**, *2*, 9882.
- (22) Ma, J.; Hashimoto, K.; Koganezawa, T.; Tajima, K. *J. Am. Chem. Soc.* **2013**, *135*, 9644.
- (23) Goh, C.; Kline, R. J.; McGehee, M. D.; Kadnikova, E. N.; Fréchet, J. M. J. *Appl. Phys. Lett.* **2005**, *86*, 122110.
- (24) Zhou, W.; Wen, Y.; Ma, L.; Liu, Y.; Zhan, X. *Macromolecules* **2012**, *45*, 4115.
- (25) Kim, Y.; Hong, J.; Oh, J. H.; Yang, C. *Chem. Mater.* **2013**, *25*, 3251.
- (26) Kolhe, N. B.; Ashar, A. Z.; Narayan, K. S.; Asha, S. K. *Macromolecules* **2014**, *47*, 2296.
- (27) Liu, Y.; Yang, C.; Li, Y.; Li, Y.; Wang, S.; Zhuang, J.; Liu, H.; Wang, N.; He, X.; Li, Y.; Zhu, D. *Macromolecules* **2005**, *38*, 716.
- (28) Steyrleuthner, R.; Schubert, M.; Howard, I.; Klaumünzer, B.; Schilling, K.; Chen, Z.; Saalfrank, P.; Laquai, F.; Facchetti, A.; Neher, D. *J. Am. Chem. Soc.* **2012**, *134*, 18303.
- (29) Kolhe, N. B.; Asha, S. K.; Senanayak, S. P.; Narayan, K. S. *J. Phys. Chem. B* **2010**, *114*, 16694.
- (30) Durban, M. M.; Kazarinoff, P. D.; Luscombe, C. K. *Macromolecules* **2010**, *43*, 6348.

Chapter 6

Summary and Conclusions

Very few choice is available in literature for good performing n-type and ambipolar organic semiconductors compared to their p-type counterpart. However, among the investigated organic semiconducting material, those based on naphthalene and perylenediimides (NDI and PDI) were found to be the most promising candidates which exhibited high performance under ambient condition. Despite the rapid development in NDI and PDI based small molecule and polymeric semiconductors, very few of them are able to reach satisfactory performance. Therefore, this area is still important and active which demands new design strategies to synthesize the novel material with desirable physical and semiconducting properties for organic electronics. In this context the present thesis entitled *“Design and Synthesis of Novel π -conjugated Molecules and Polymers based on Naphthalene and Perylene Diimides and their Application in Organic Electronics”* describes the design and synthesis of NDI/PDI based small molecules and polymers that finds application in the optoelectronics devices such as OFET. The NDI is the prime focus of this dissertation, most of the small molecules and polymers were synthesized using NDI building blocks.

In initial part of the work, two families of naphthalenediimide (NDI) derivatives were compared and contrasted for the effect of self-assembly on charge carrier transport. One series of NDI derivatives had a terminal phenyl ring attached to a hexyl spacer substituted naphthalene core either through an ester or an amide linkage (NDI-E and NDI-A respectively), while the other series had a 3,4,5-tridodecyloxy phenyl unit (NDI-E3, NDI-A3) instead of the terminal phenyl unit. The molecules were designed and synthesized in such a way that amide derivative would form self-assembly due to intermolecular hydrogen bonding and thereby differentiate them from non-hydrogen bondable ester derivative. Indeed, the amide linked NDI derivatives formed strong hydrogen bonded aggregates with pronounced red shifted emission both in solution and solid state. All the four NDI derivatives exhibited good n-type charge transport characteristics in an OFET device. The mobility values for the NDI ester and amide derivatives without terminal alkyl substitution (NDI-E and NDI-A) were one order higher in magnitude compared to their terminal alkyl substituted counter parts (NDI-E3 and NDI-A3). The comparison of mobility values of the ester versus amides revealed some interesting observations. Contrary to expectations, the hydrogen bonding in the amide derivatives did not facilitate better electron mobility. The ester derivatives exhibited better device performance compared to the amides.

Analyzing the packing in these molecules based on DFT energy minimized structures and powder XRD data, especially in the case of NDI-E and NDI-A, the NDI amide derivative showed a dihedral twist of the terminal phenyl unit with respect to the naphthyl aromatic core with a consequent shortening of the molecular length packing along the a axis. This small difference in the dihedral twist angle reduced the crystallinity and resulted in a more tilted orientation of the NDI-A molecules on the substrate surface. On the whole, the present studies thus demonstrated that self-organization of NDI molecules by restrictive directional hydrogen bonding interaction was not so favorable for efficient charge transport compared to the freedom in charge transport pathways offered by a three dimensional crystalline organization in ester.

Further, the similar building block NDI and its higher analogue PDI were used to develop the electron deficient polymeric material by synthesizing a novel n-type poly (imides) comprised of benzobisoxazole as an electron donor and NDI/ PDI as an electron acceptor. These poly (imide)s represented the unique combination of planar and robust heterocyclic aromatic molecule i.e benzobisoxazole with NDI and PDI. Unfortunately, these polymers exhibited solubility only in strong protic acid such as methane sulfonic acid (MSA) due to extremely rigid nature. Photoinduced energy transfer and charge separation were studied in MSA solution via absorption, excitation, and steady-state fluorescence studies. The perylenediimide-bisoxazole (PerPBO) copolymer showed interesting funneling behavior upon indirect excitation at the bisoxazole wavelength. Almost exclusive emission from PDI units was observed at 620 nm upon selective excitation of bisoxazole (345 nm) indicating highly efficient (> 90 %) energy transfer from bisoxazole to PDI as a result of FRET (Förster Resonance Energy Transfer). The emission at 620 nm was higher in intensity upon indirect excitation (345 nm) compared to the direct excitation of PDI moiety at 545 nm. The quenching of PDI fluorescence upon direct excitation showed that electron transfer also played an important role. There was complete quenching of fluorescence in spin coated films both upon direct as well as indirect excitation. The copolymer solution in MSA were protonated resulting in improved planarity leading to better electronic coupling and energy transfer from bisoxazole to PDI / NDI units. On the other hand, the geometry was different in the solid state resulting in total quenching of fluorescence of both bisoxazole and perylene units. Organic field effect transistors (OFETs) based on thermally annealed polymer films showed n-type charge transport. The maximum electron mobility of $2 \times 10^{-3} \text{ cm}^2 \text{ V}^{-1} \text{ s}^{-1}$ was observed for

random copolymer which contained both the PDI and NDI units with bisoxazole. Although, these poly (imides) showed better n-type performance in OFET device the inherent poor solubility in common organic solvent limited their use and device fabrication was possible only using harsh processing solvent like MSA.

To overcome this, solution-processable donor-acceptor polymers were synthesized using similar NDI building block but by changing the design strategy. Polymerization was carrying out at core position of NDI and the imide nitrogen atom was substituted with long branched alkyl chains for better solubility. Core-substituted NDI containing donor-acceptor copolymers were synthesized by systematically varying the different donors from oligo (phenylenevinylene) (OPV) NDI-*alt*-OPV to benzobisoxazole (BBO) NDI-*alt*-BBO to benzothiadiazole (BT) NDI-*alt*-BT. Random copolymer having maximum 30 % incorporation of BBO co monomer in NDI-*r*-OPV/BBO was also synthesized. A deeper understanding of structure-property relationships showed the noticeable effect of different donor strength of OPV, BBO and BT on the optical, electrochemical and semiconducting properties of the polymers. Fine-tuned energy level (HOMO/LUMO: -3.75 eV/-5.44 eV) of NDI-*alt*-OPV resulted in ambipolar charge transport in OFETs with balanced electron and hole mobility. On the other hand, NDI-*r*-OPV/BBO having low-lying HOMO energy level (-5.86 eV) exhibited dominating n-type charge transport and further lowering of HOMO energy level to (-6.34 eV) in NDI-*alt*-BT showed only n-type charge transport. The analysis of the thin film samples of polymers using XRD and AFM highlighted the influence of solid state morphology and molecular packing in dictating the charge carrier mobility in an OFET device. Our results have demonstrated that a simple design of core-substituted NDI-based polymer with OPV co monomer units are successful in producing device materials with ambipolar charge transport and most importantly, having balanced electron and hole mobility.

Structure-property relationship studies were extended to understand the effect of side-chain engineering in NDI-*alt*-OPV polymer on their bulk charge carrier transport. Two naphthalenediimide-oligo(phenylenevinylene) copolymers were synthesized by varying the two different side chains on the NDI acceptor unit viz., linear triethylene glycol (P1) and branched 2-octyldodecyl (P2). The analysis of thin film XRD and SCLC bulk electron mobility revealed that different flexible side chains on the NDI unit had huge impact on the molecular packing and device performance of polymer. The SCLC measurement of thermally annealed thin film of

P1 showed four order of decrease in the bulk electron mobility as compared to mobility of as-spun thin film which gave clear evidence for predominant edge-on orientation of P1 on thermally annealed thin film. On the other hand, polymer P2 with 2-octyldodecyl side chain did not show significant lowering of electron mobility after thermal annealing which suggested that as-spun texture formed during active layer deposition was retained with majority of face-on arrangement. The difference in the charge transport properties of polymer was also reflected in the all-polymer solar cells fabricated using P1 or P2 as acceptor material. P1 showed low value of current density and PCE ($J_{sc} = 0.23 \text{ mA cm}^{-2}$ and PCE = 0.050 %) compared to P2 ($J_{sc} = 0.53 \text{ mA cm}^{-2}$ and PCE = 0.067 %). Although oligoethyleneoxy side chain showed negative impact on the bulk carrier transport, the structure-property understanding obtained from the present study is expected to help establish material design guidelines required in this class of polymers.

To conclude, this dissertation is focused on the synthesis and structure-property studies of NDI/PDI based small molecules and donor-acceptor conjugated polymers. The important question of the effect of restricted self-assembly in NDI based small molecule on the charge carrier transport properties was addressed. Furthermore, the NDI/PDI containing n-type and ambipolar polymers with fine-tuned optical, electrochemical and semiconducting properties were synthesized by utilizing donor-acceptor strategy. The effect of various π -conjugated backbone and flexible side chain on the device performance of polymer was studied. In short the structure-property relationships reported in this thesis would help to design future generation NDI based material for optoelectronic application.

Publications in International Journals

- 1. Nagesh B. Kolhe**, Shekhar Shinde, B. Saibal, and S. K. Asha* “Novel Approaches in the Design of Donor-Acceptor Oligomeric and Polymeric Materials for Photovoltaic Applications: D/A Blend versus Self-assembly of D/A by Covalent or Non-Covalent Interaction.” *Organic Photonics and Photovoltaics*, **2015** (*Invited review accepted*)
- 2. Nagesh B. Kolhe**, A. Z. Ashar, K. S. Narayan* and S. K. Asha* “Naphthalene Diimide Copolymers with Oligo(p-phenylenevinylene) and Benzobisoxazole for Balanced Ambipolar Charge Transport” *Macromolecules* **2014**, **47**, 2296-2305.
- 3. Nagesh B. Kolhe**, R. N. Devi, S. P. Senanayak, B. Jancy, K. S. Narayan and S. K. Asha* “Structure engineering of naphthalene diimides for improved charge carrier mobility: self-assembly by hydrogen bonding, good or bad?” *J. Mater. Chem.* **2012**, **22**, 15235-15246.
- 4. Nagesh B. Kolhe**, S. P. Senanayak, K. S. Narayan* and S. K. Asha* “n-Type Field Effect Transistors Based on Rigid Rod and Liquid Crystalline Alternating Copoly (benzobisoxazole) Imides Containing Perylene and/or Naphthalene” *J. Phys. Chem. B*, **2010**, **114**, 16694–16704.
- 5. Nagesh B. Kolhe**, Sandeep Sharma and S. K. Asha* “All-Polymer Solar Cell Containing n-type Naphthalene / Perylene Diimide Copolymers: Tuning of Optical, Bulk and Semiconducting properties.” (*Manuscript under preparation*)
- 6. Saibal B., Nagesh B. Kolhe**, S. Chithiravel, and Asha S. K* “Poly(benzimidazole)/ Naphthalene Monoimide Semiconducting Composite by Complementary Hydrogen Bonding” (*Manuscript under preparation*)

Symposia Attended/Poster Presentation

- 1. Nagesh B. Kolhe** and S. K. Asha “Novel Perylene And Naphthalene Copoly(benzobisoxazole) Imides: Energy Transfer and Charge Carrier Mobility” **MACRO - International Conference on Frontiers of Polymers and Advanced Materials**, Indian Institute of Technology, New Delhi, 2010 (*Poster presentation*)
- 2. Nagesh B. Kolhe** and S. K. Asha “ n-type field Effect transistor based on Novel Copoly (benzobisoxazole) Imides containing Naphthalene and/or perylenediimide” **CRSI-National symposium in chemistry**, KIIT University, Bhubaneswar, 2011.(*Poster presentation*)
- 3. Nagesh B. Kolhe** and S. K. Asha “Novel Perylene And Naphthalene Copoly(benzobisoxazole) Imides: Energy Transfer and Charge Carrier Mobility” **National Science Day**, CSIR-NCL, Pune, 2011. (*Selected for Best poster award*)
- 4. Nagesh B. Kolhe** and S. K. Asha “Structure Engineering of Naphthalenediimides for improved Charge Carrier Mobility: Self-assembly by Hydrogen Bonding” **Raman Memorial conference**, University of Pune, 2013 (*Selected for best oral presentation*)
- 5. Nagesh B. Kolhe** and S. K. Asha “NDI-Donor Copolymers: Effect of varying Donor strength on Photophysical, Electrochemical and n-type Semiconducting Properties” **FAPS-MACRO, International Conference on Polymers**, Indian Institute of Science, Bangalore, 2013. (*Poster presentation*)
- 6. Nagesh B. Kolhe** and S. K. Asha “Effect of Different Donor Comonomer and Flexible Side Chain on Semiconducting Properties of Novel Naphthalenediimide Copolymers” **MACRO 2015 - International Conference on Polymers**, IACS, Kolkata, 2015. (*Selected for Best poster award*)
- 7. CRSI-National symposium in chemistry**, CSIR-National chemical Laboratory, Pune, 2009 (*Conference Attended*)